



HAL
open science

Impact of green roof plants on the removal of air pollutants (NO₂/O₃) and on the photochemical fate of pesticides

Yara Arbid

► **To cite this version:**

Yara Arbid. Impact of green roof plants on the removal of air pollutants (NO₂/O₃) and on the photochemical fate of pesticides. Analytical chemistry. Université Clermont Auvergne, 2021. English. NNT : 2021UCFAC095 . tel-03705687

HAL Id: tel-03705687

<https://theses.hal.science/tel-03705687>

Submitted on 27 Jun 2022

HAL is a multi-disciplinary open access archive for the deposit and dissemination of scientific research documents, whether they are published or not. The documents may come from teaching and research institutions in France or abroad, or from public or private research centers.

L'archive ouverte pluridisciplinaire **HAL**, est destinée au dépôt et à la diffusion de documents scientifiques de niveau recherche, publiés ou non, émanant des établissements d'enseignement et de recherche français ou étrangers, des laboratoires publics ou privés.



Impact of green roof plants on the removal of air pollutants (NO₂/O₃) and on the photochemical fate of pesticides

This dissertation is submitted to the:

University of Clermont Auvergne

For the degree of:

Doctor of Philosophy

By the candidate:

Yara Arbid

Faculty: **Fundamental Sciences**

Specialization: **Physical, theoretical, and analytical chemistry**

CHOVELON Jean-Marc, Pr, Université Lyon 1, IRCELYON UMR5256, reporter
VILLENAVE Eric, Pr, Université de Bordeaux, EPOC UMR5805, reporter
BEDOS Carole, CR, INRAe AgroParisTech, ECOSYS UMR1402, examiner
FERRONATO Corinne, MCF, Université Lyon 1, IRCELYON UMR5256, examiner
MAILHOT Gilles, DR CNRS, Université Clermont Auvergne, ICCF UMR6296, examiner
RICHARD Claire, DR CNRS, Université Clermont Auvergne, ICCF UMR6296, thesis co-director
SLEIMAN Mohamad, MCF, SIGMA Clermont, ICCF UMR6296, thesis director

Date of PhD defense: **December 13, 2021**

Table of contents

Abstract	1
Introduction	3
1. Bibliography	7
1.1 Air pollution increase	7
1.2 Air pollutants of vast importance	8
1.2.1 Ground-level Ozone (O ₃).....	8
1.2.2 Nitrogen oxides (NO _x)	9
1.2.3 Particulate matter (PM).....	11
1.3 Impact of air pollution	12
1.3.1 On the well-being.....	12
1.3.2 On the environment.....	13
1.4 Control strategies	17
1.4.1 Reduction strategies	18
1.4.2 Vegetation as a depollution strategy	20
1.5 Research questions/gaps	37
1.5.1 Uncertainty of models.....	37
1.5.2 Lack of studies concerning the interaction of VOCs and pollutants.....	39
1.5.3 Lack of studies regarding pesticides + VOCs/ pesticides + pollutants.....	40
1.5.4 Conclusion/scope of work.....	46
References:	49
2. Materials and Methods.....	71
2.1 Chemicals	71
2.2 Plants	72

2.3 Irradiation systems.....	75
2.4. Spectroscopic techniques.....	78
2.5 Chromatographic techniques	79
2.6 Microscopic techniques	83
2.7 Analyzers	84
2.8 Preparation of samples/experiments	85
2.8.1 Study of plants' depollution potential.....	85
2.8.2 Study of pesticides in the presence of thyme's volatiles	87
2.9 Toxicity estimation	88
2.10 Calculation of the compounds' concentrations	89
References	91
3. Results and discussion	93
3.1 Summary of the main results	93
3.2 Manuscripts	103
Manuscript 1.....	103
Supporting Information	113
Manuscript 2.....	125
Supporting Information	133
Manuscript 3.....	141
Supporting Information	153
4. General conclusions	163
Annex 1	167
Annex 2	168

Table of figures

Figure 1 Removal of air pollutants and the release of VOCs by plants.	8
Figure 2 O ₃ photolysis in the troposphere, source: [9][10].	9
Figure 3 NO ₂ photolysis in the troposphere, source: [13].	10
Figure 4 PM _{2.5} anthropogenic sources (according to the national emission inventory for 2001), source: [26].	11
Figure 5 Short-term and long-term air pollution exposure effects on humans.	13
Figure 6 Polluted air in Clermont-Ferrand and Riom (France), source: [41].	14
Figure 7 Temperature differences between urban and other areas due to the Urban Heat Island (UHI), source: [43].	15
Figure 8 The Photocatalysis mechanism, source: [64].	19
Figure 9 Absorption of air pollutants into a stoma, source of the leaf picture: [85].	21
Figure 10 The retention of particles on the abaxial and adaxial leaves surfaces of 8 different plants. Images obtained by the Scanning electron microscopy, source: [94].	22
Figure 11 Reaction of VOCs with O ₃	23
Figure 12 Reaction pathways of O ₃ with BVOCs, source: [114].	25
Figure 13 The different components of green roofs, source: [133].	28
Figure 14 A green-roofed school in France, source: [170].	33
Figure 15 A simplified diagram showing a photosensitized reaction where the photosensitizer produces a singlet oxygen species.	42
Figure 16 Simplified state energy diagram, source: [216], [217].	42
Figure 17 Chemical structures of the pesticides.	44
Figure 18 The reaction of a pesticide under sunlight [231].	45
Figure 19 Chemical structures of the studied pesticides	46
Figure 20 Chemical structures of Chlorothalonil and Imidacloprid.	47
Figure 21 Plants chosen for further experiments, from left to right: <i>Sedum sexangulare</i> , <i>Thymus vulgaris</i> , <i>Heuchera Americana L.</i>	75
Figure 22 Starlite tubes and their light spectrum.	76
Figure 23 Monochromator used with the spectral distribution of its Hg lamp.	76

Figure 24 The irradiation device used.....	77
Figure 25 Suntest device used and the spectral distribution of its lamp.	78
Figure 26 HPLC-DAD used.....	80
Figure 27 LC-MS apparatus.....	81
Figure 28 GC-MS instrument.....	81
Figure 29 HS vial with thyme.	82
Figure 30 ATD (automated thermal desorption) system.....	83
Figure 31 Thyme's adaxial surface seen by SEM.....	84
Figure 32 The NO _x (bottom) and the O ₃ (top) analyzers used in our experiments.	85
Figure 33 IMD solution in the glass reactor.....	86
Figure 34 3-carene stock solution.	87
Figure 35 Thyme twigs after extraction.	88
Figure 36 A scheme summarizing the PhD steps.....	93
Figure 37 A diagram of the setup used to demonstrate the formation of NO ₂ /NO from IMD.	94
Figure 38 A simplified diagram of the setup used to study the NO _x or O ₃ uptake by plants.	95
Figure 39 A diagram of the steps followed to study the interactions between volatiles and pesticides.	95
Figure 40 IMD degradation pathway and its possible nitration/nitrosation ability.....	96
Figure 41 Structures of IMD, nitrophenol, and nitrosophenol.....	97
Figure 42 A diagram of the steps followed to monitor NO _x and O ₃ uptakes of different plants...	97
Figure 43 The NO _x uptake of the 3 plants in the mall reactor.....	98
Figure 44 A succulent plant releasing water.	99
Figure 45 A diagram of the steps followed in manuscript 3.	100
Figure 46 Thyme oxidation products.	101
Figure 47 Photoproducts obtained in the mixture of thymol + IMD.	101
Figure A 1. Setup used to monitor NO _x formation upon irradiation of IMD solutions.....	167
Figure A 2. The NO _x (red) and O ₃ (blue) setups.....	168

Table of tables

Table 1 Air quality guidelines and standards of specific pollutants depending on the exposure time, source: [56] [57] [58].	17
Table 2 Differences between the 3 green roof types, source: [145].	30
Table 3 Amounts of pollutants mitigated by different studies.	35
Table 4 Chemical reagents used in this study.	71
Table 5 Plants chosen to be studied.	73
Table 6 HPLC conditions used for the CT/IMD experiments.....	79

Abstract

The green roof system is an environmentally friendly approach to help mitigate air pollution. Many studies estimate its removal capacity towards several air pollutants such as particulate matter (PM), nitrogen oxides (NO_x), ozone (O₃), etc. using dry-deposition models. In our studies, our aim was to quantitatively determine the depolluting potential of green roof plant species towards two prevalent air pollutants: NO₂ and O₃, and to examine the photochemical interactions possibly taking place on the surface of leaves. In chapter one, we built an experimental setup that enabled us to measure the NO₂/NO concentration produced by Imidacloprid (IMD), an insecticide. This served as the base of the main setup used to study the depollution ability of plants and helped to find a stable and continuous source of NO₂ using a chemical rather than pressurized gas cylinders. In chapter 2, screening of 13 plants species was done. Their capacity to remove NO₂ and O₃ was measured which further led to the selection of the 3 most performant species: *sedum sexangulare*, *thymus vulgaris*, and *heuchera Americana L.* The uptake/removal mechanisms were investigated using scanning electron microscopy (SEM), and Automated thermal desorption GC-MS (ATD-GC-MS) to inspect possible interactions between the pollutants and volatile organic compounds (VOCs). In chapter 3, photochemical processes occurring between volatiles emitted by green roof plant species and pesticides sprayed were studied. Two pesticides were selected: IMD, a nitrating/nitrosating agent, and chlorothalonil (CT), a strong oxidant. Possible photoproducts were detected with their acute/chronic toxicities predicted using an ECOlogical Structure-Activity Relationship approach (ECOSAR). This work is a step forward towards the development of experimental measurements of green roof depollution performance. By understanding the uptake mechanisms and the photochemical interactions taking place, the choice of appropriate green roof plant species/pesticides can become possible. Ultimately, this will facilitate the deployment of green roofs in urban environments.

La végétalisation des toits est une approche respectueuse de l'environnement pour aider à atténuer la pollution de l'air. De nombreuses études ont démontré, sur la base de modèles, la capacité de ce système à éliminer les polluants atmosphériques tels que les particules en suspension (PM), les oxydes d'azote (NO_x), l'ozone (O₃), etc. Dans cette thèse, l'objectif était de déterminer quantitativement le potentiel dépolluant de différentes espèces végétales utilisées sur les toits verts à l'égard de deux polluants atmosphériques prédominants : NO₂ et O₃ et d'examiner les réactions photochimiques entre les métabolites secondaires des plantes et les pesticides. Dans le premier chapitre, nous avons développé un dispositif expérimental qui nous a permis de mesurer les quantités de NO₂/NO produites par imidaclopride (IMD), un insecticide. Ce premier dispositif a servi de base à un deuxième système utilisé pour étudier la capacité de dépollution des plantes. IMD a pu être utilisé comme source stable et continue de NO₂. Dans le chapitre 2, le criblage de 13 espèces végétales a été effectué. Leur capacité à éliminer NO₂ et O₃ a été mesurée, ce qui a conduit à la sélection des 3 espèces les plus performantes : *sedum sexangulare*, *thymus vulgaris* et *heuchera americana* L. Les mécanismes d'absorption/élimination et les réactions possibles entre les polluants et les composés organiques volatils (COVs) ont été étudiés par microscopie électronique à balayage (MEB), piège à HONO, et par thermodésorption GC-MS (ATD-GC-MS). Dans le chapitre 3, les réactions photochimiques se produisant entre les substances volatiles émises par les espèces végétales utilisées sur les toits verts et les pesticides pulvérisés sur ces plantes ont été étudiés. Deux pesticides ont été sélectionnés : IMD, un agent nitrant/nitrosant et chlorothalonil (CT), un oxydant fort sous irradiation. Les principaux photoproduits ont été détectés et leurs toxicités aiguës/chroniques prédites à l'aide du logiciel ECOlogical Structure-Activity Relationship approach (ECOSAR). Ce travail constitue une avancée vers le développement de mesures expérimentales des performances de dépollution par les toits verts. La compréhension des mécanismes d'absorption et les réactions photochimiques doit permettre le choix d'espèces végétales/pesticides les plus appropriés pour les toits verts. À terme, cela facilitera le déploiement de toitures vertes en milieu urbain.

Introduction

This PhD fellowship was supported by the University Clermont Auvergne/French Ministry of Higher Education and Research and undertaken in the Institute of Chemistry of Clermont-Ferrand (Photochemistry group/ Université Clermont Auvergne/ France) with Dr. Claire Richard and Dr. Mohamad Sleiman as supervisors.

Our goal was to understand the role of certain green roof plants in depollution; especially those implemented in urban environments. The atmospheric composition is in a constant change due to the continuous release of hazardous air pollutants as carbon dioxide (CO₂), nitrogen oxides (NO_x), ozone (O₃), particulate matter (PM), etc. The excessive emission of pollutants is due to anthropogenic activities in urban areas as fossil fuels combustion, industries, incomplete fuel combustion in all transportation forms, etc. leading to the popular environmental problem: air pollution. This imposes a great threat to humans and the environment. For instance, millions of people die each year due to heart failures, central nervous system disorders, or cardiovascular diseases. This is all linked to the ambient air pollution which increases mortality and morbidity. In addition to that, the latter causes O₃ depletion, climate change, urban heat island, etc. which are then again related to the human health deterioration. Therefore, an approach using vegetation to decrease the concentration of harmful pollutants can be promising. Green roofs make use of the numerous impermeable roofs found in urban areas where they can uptake air pollutants.

Green roofs are roofs with plants in their final layer. They are a good compensation to the vegetation that has been cut or destroyed during the building's construction. Their benefits include lessening the urban heat island (UHI), improving the stormwater runoff's quality, reducing noise pollution, and most importantly decreasing air pollution. In general, extensive green roofs are more preferred where certain types of plants are implemented as herbaceous perennials, sedum species, as well as grass. Numerous studies deal with the depollution ability of vegetation but not of green roofs specifically. Published articles on green roofs reveal their capacity to reduce NO₂, CO₂, O₃, and PM. However, they were generally based on deposition models taking into consideration neither the possible interactions in the gaseous phase involving VOCs nor the latter's potential to

interact with pesticides sprayed on the plants. This renders experimental data a must to fully understand the green roof system.

In this research, we first constructed an experimental setup that allowed us to screen and quantify the uptakes of NO_x and O₃, two detrimental pollutants to the health and environment by different plant species. Besides of having adverse health effects, these two pollutants are regulated and contribute to the oxidative capacity of the atmosphere. It was comprised of flow controllers, pollutants sources, reactors, and analyzers. Special attention was given to find sources of the pollutants. O₃ was produced simply by the aid of an O₃ generator equipped with a UV pen-ray lamp while NO_x was produced via an Imidacloprid (IMD) solution. This insecticide was reported to have the ability of releasing the nitro group under irradiation. In our study, IMD dissolved in water with a small percentage of ACN was able to significantly produce NO₂ with a small concentration of NO without irradiation. This setup enabled us to determine quantitatively the uptake capacity of the 3 chosen plants often used on extensive green roofs: *sedum sexangulare*, *thymus vulgaris*, and *heuchera Americana L.* The effect of plants volatile organic compounds on the uptake was elucidated and the analysis of the products formed between the plants volatiles and pollutants was conducted. Although many studies show the important role of VOCs in the life of plants or crops, the information about the interaction that could happen between vegetation and the urban environment is still lacking.

Plants are sprayed with pesticides to protect them from harmful pests. Although several studies report the ability of certain pollutants –acting as oxidants- to degrade pesticides or their photolysis in solution or on supports, none or few studies -to our knowledge- focused on the probable interaction between certain pesticides and VOC-emitting plants. Different pesticides are usually sprayed on green roofs or greenery systems; hence, the possibility of an interaction to happen between the former and VOCs produced is high. In this regard, we investigated the interactions of two pesticides: the insecticide Imidacloprid and the fungicide Chlorothalonil with *Thymus Vulgaris* VOCs (a plant frequently used on green roofs) in solution and directly on its leaves. Different photoproducts were detected using different techniques such as HS-GC-MS, GC-MS, and LC-HR-MS.

In summary, our work intended to focus on experimental studies poorly available in the literature. We started by investigating the capacity of green roofs plants to lessen the concentration

of target pollutants. We took into account the different processes occurring responsible for the depollution ability. Afterwards, attention was given to the interaction of certain pesticides with the VOCs emitted by plants implemented on green roofs with the identification of possible formed photoproducts with their toxicities.

1. Bibliography

1.1 Air pollution increase

Economic developments and modernization have created a greater need of energy which in turn increased the use and combustion of fossil fuels. This is of a great concern since tremendous amounts of carbon dioxide (CO₂), nitrogen oxides (NO_x) particulate matter (PM), and ozone (O₃) are being produced, contributing to major health risks and climate changes. Ambient air pollution is a topic vastly studied due to the lack in the homogeneity of its environmental and health effects. In other words, the health effects inflicted in developing countries as China, India, or the Middle Eastern region vary from those in developed countries as United States of America or Europe. This is explained by the difference in the combustion sources used, energy use, lifestyle, etc. between countries which consequently affects the concentrations of the pollutants released [1]. Pollution in China is in general a result of coal combustion or coal burning [2][3]. However, heating and cooking, in other words- ‘residential energy demands’, are one of the main causes of air pollution in India or Bangladesh [1]. In 2013, almost 90 % of the world’s population lived in polluted zones that don’t meet the World Health Organization (WHO) guidelines [4].

Vegetation itself can affect the air quality by emitting Volatile Organic Compounds (VOCs) which can react with NO_x producing secondary pollutants thus changing the microclimate around it [5]. However, and fortunately, vegetation can also help reduce and remove gaseous air pollutants or PM. This topic has been subject of numerous studies [5] [6] where vegetation can directly uptake the pollutants by the absorption into their stomata or adsorption on their leaves where they might be further broken down (**Fig.1**). Vegetation can as well remove pollutants indirectly by cooling the surrounding air via transpiration and shading, hence limiting photochemical interactions that form secondary pollutants as O₃ [7]. Out of the numerous studies, a study in the USA showed that trees can eliminate up to 711,000 tons/year of air pollutants [7]. Another in London manifested that 2000 m² of uncut grass can remove about 4000 kg of PM [8]. Hence, vegetation can be a good sink to pollutants and a promising solution to air pollution.

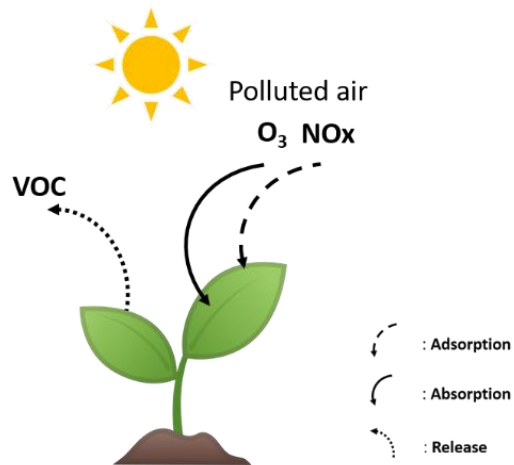


Figure 1 Removal of air pollutants and the release of VOCs by plants.

1.2 Air pollutants of vast importance

1.2.1 Ground-level Ozone (O₃)

O₃ is a trioxygen gas with a pale blue color which is beneficial in the stratosphere forming a protective layer towards harmful UV light. However, it is considered as a pollutant in the troposphere with high health risks and a cause to air pollution (ground-level ozone) [9]. The low level O₃ is not emitted directly from vehicle engines or industries, but it is rather a reaction between NO_x, VOC, and sunlight [10]. Its formation is totally dependent on the season; in summer for example, it shows the highest concentrations with huge traffic jam, slow wind movement, and high UV index. Sources of the tropospheric O₃ are fossil production, industries, transportation, smoking, chemical processes, etc.[10]. Nevertheless, a small amount of O₃ in the troposphere is considered essential; it undergo photolysis in the presence of UV light with a wavelength ≥ 290 nm to produce the excited oxygen where different reactions can further take place [11][12].

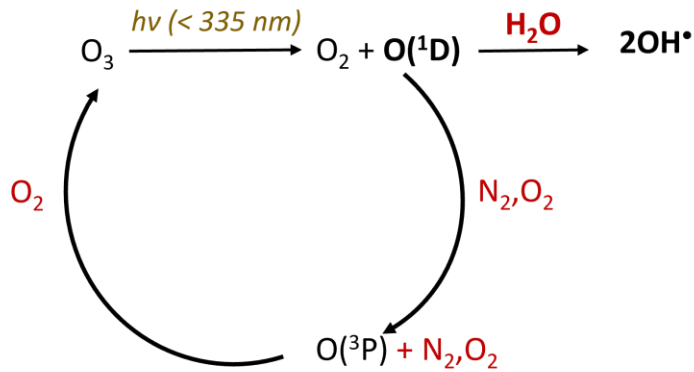


Figure 2 O_3 photolysis in the troposphere, source: [9][10].

$O(^1D)$ can be deactivated to $O(^3P)$ which regenerates the starting molecule (O_3) or it can react with water to produce hydroxyl radicals ($^\bullet OH$). $^\bullet OH$ reacts with almost all organic compounds; it is the key to initiate tropospheric reactions (**Fig.2**) [13].

Although it has been reported that plants remove pollutants, several studies show the threat that O_3 imposes on certain plants which can vary from visible foliar injuries to the negative effects regarding photosynthesis and stomatal conductance [14][15]. O_3 can enter the leaves through stomata and change the membrane properties leading to phototoxicity in the leaf tissues [16][17]. Since stomata are one of the ways that plants utilize to degrade or remove pollutants, the precision in choosing specific plants for a target pollutant becomes essential. Out of 473 plant species studied, 378 showed sensitivity towards O_3 . However, environmental stress can induce the production of VOCs which may contribute to air pollution through their interactions with NO_x [18][19] or may react with O_3 thus decreasing its ambient concentration .

1.2.2 Nitrogen oxides (NO_x)

The symbol ' NO_x ' mainly marks NO and NO_2 since they reach the troposphere in those forms- called as the fresh nitrogen oxides. Modernization created a high demand for fossil fuels; their combustion generates high amounts of pollutants especially nitrogen oxides. Their sources, particularly anthropogenic, are vast; they include incineration [20], the use of nitric acid [21],

industries. Out of the nitrogen oxides, NO and NO₂ are considered toxic [22]. NO_x can react with VOCs or sulfur dioxide (SO₂) producing tropospheric ozone, smog, or acid rain.

Fig.3 shows the photolysis of NO₂ giving NO and O(³P) where the latter further reacts with O₂ to produce O₃. But, NO can react with O₃ regenerating NO₂ and O₂ creating an equilibrium between the formation and destruction of O₃ (① in figure 3). However, this photo-equilibrium is disturbed by the presence of VOCs. The substituted alkyl peroxy radicals (RO₂[•]) and HO₂[•](hydroperoxyl) radicals formed due the degradation of VOCs can react with NO generating NO₂ which can undergo photolysis again and hence form O₃ (② in figure 3). If no NO or low concentrations of NO are present, the radicals might attack O₃ leading to O₃ loss. So, in this case, the formation or loss of O₃ is driven by the NO concentrations as well as the rate of the reaction between the radicals and NO. Nevertheless, the quantity of O₃ formed is limited and stopped by radical sinks, NO_x sinks, and other possible reaction pathways involving NO_x. They can influence the amount of NO converted to NO₂ and [•]OH concentrations; and since [•]OH initiates photochemical reactions, the system or cycle is fully interrupted. In addition to that, NO and NO₂ can directly react with O₃ forming NO₂ and NO₃ respectively where the latter can react together giving N₂O₅ (dinitrogen pentoxide) or with [•]OH radicals leading to HONO (nitrous acid) and HNO₃ (nitric acid) respectively.

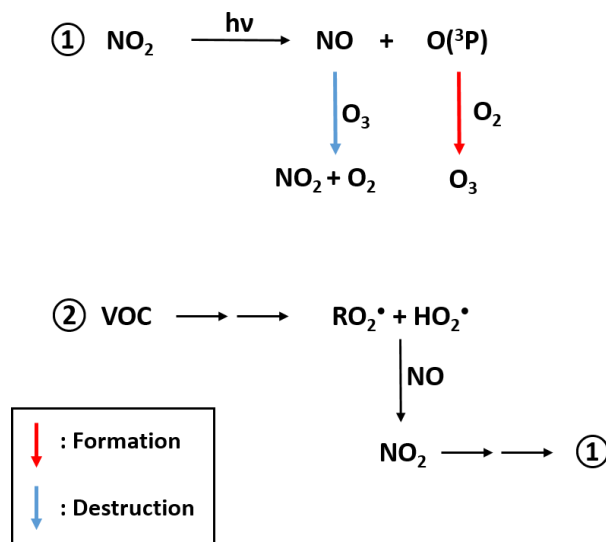


Figure 3 NO₂ photolysis in the troposphere, source: [13].

Vegetation or green roofs can help decrease the concentration of NO_x. For example, a study in Chicago using deposition models revealed that with a 19.8 ha of green roofs, around 1700 kg of pollutants was removed with the NO₂ percentage uptake being 27% [23]. Branches, twigs, and leaves provide a high surface area which is available as a sink for pollutants; and since NO₂ is soluble in water, it is expected that the NO₂ absorbed into the stomata is metabolized [24]. Hence, vegetation can rather degrade NO₂ than act as a temporary sink where pollutants are washed off by rain entering the soil and water system.

1.2.3 Particulate matter (PM)

PM consists of tiny particles or liquid droplets of soil, dust particles, chemicals, etc. [25] and categorized based on their diameter (size); those having a diameter of 10 μm or less, 2.5 μm or less, and 0.1 μm or less (PM₁₀ *coarse*, PM_{2.5} *fine*, and PM_{0.1} *ultrafine* respectively). The PM’s source and their behavior in human airways helps as well with this categorization. Sources include combustion, vehicle emissions, tobacco smoke, volcanoes, dust storms, etc. PM are considered dangerous since certain gases like O₃ can adsorb on their surface reaching the lungs after inhalation.

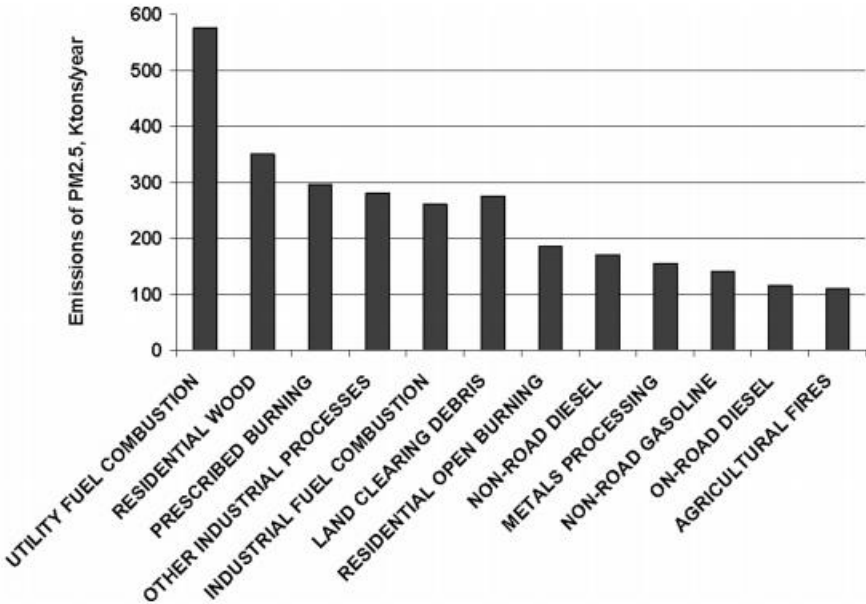


Figure 4 PM_{2.5} anthropogenic sources (according to the national emission inventory for 2001), source: [26].

In the USA, the major PM_{2.5} source is due to the coal burning to produce electricity (fuel combustion) followed by residential wood burning (**Fig.4**). This makes it difficult to avoid the exposure to PM_{2.5}; and since PM can be carried over large distances and secondary particles can be formed in the atmosphere (primary particles are those emitted directly from sources), having policies for reducing PM levels is tricky. However, there was a 23 % decrease in the PM_{2.5} national average from 2010 to 2019 [27]. A study in the winter of 1993-1994 showed low PM₁₀ concentration in the north of Europe (20 µg/m³ mean urban value) whereas higher concentrations were found in Amsterdam, Berlin, and central Europe (40-50 µg/m³). Concentrations were even more elevated in southern Europe. However, little to no difference was detected within the countries considering rural areas [28].

Vegetation is a promising approach to attenuate PM's health negative effects, in particular, that related to the decrease in the life expectancy especially concerning vulnerable people [29]. The size and structure of leaves is an important factor in determining the removal ability [30]. For example, trees are very efficient in offering a space for PM deposition due to the large leaf area. A study in the USA showed that urban trees and shrubs remove almost 220,000 tons of PM₁₀ each year [31] while another in China indicated the removal of 772 tons of PM₁₀ in the city center of Beijing [32]. Accumulation of PM is driven also by the leaf's surface hair density and wax quantity [33]. Vegetation targeting PM is able to remove as well polycyclic aromatic hydrocarbons (PAH) and heavy metals.

1.3 Impact of air pollution

1.3.1 On the well-being

Air pollution causes millions of deaths each year where 3.7 million people pass away due to ambient air pollution, and 4.3 million die from household pollution [34]. Its harmful effects are vast varying from the long-term exposure effects to the short-term ones; but it the long-term effects that matter the most [35].

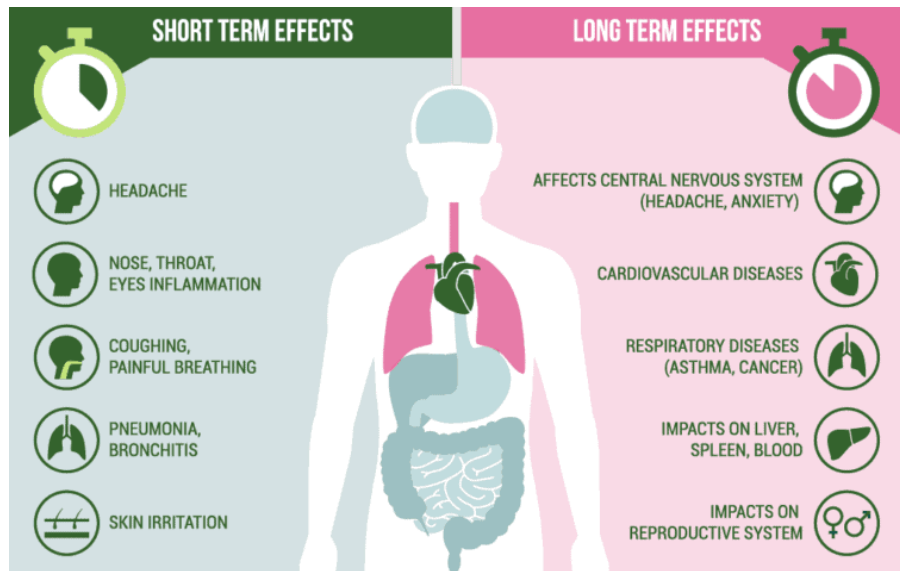


Figure 5 Short-term and long-term air pollution exposure effects on humans.

Short-term exposure effects are manifested by headaches, nose or throat inflammation, skin irritation, etc. while those of long-term are associated with heart failures, cardiovascular diseases, central nervous system disorders, hospital admission increase, and reproductive system failure (**Fig.5**). For example, a study showed the direct link between air pollution and male infertility [36]. Each pollutant, nevertheless, can undesirably affect the body in different ways. For instance, PM is known to be associated with cardiovascular morbidity and mortality which is responsible for almost 3 million deaths each year [37]. O₃, on the other hand, mostly causes lung impairments which affects the overall health, respiratory and cardiovascular diseases and acute exposures lead to headaches, wheezing, and breathing problems [38]. Also, short or long term exposure to NO₂ leads to problems such as respiratory/cardiovascular diseases and increased mortality [39]. NO_x is also a precursor to tropospheric ozone which has great impact on health. Air pollution, in general, increases mortality and morbidity.

1.3.2 On the environment

Numerous environmental effects exist due to air pollution. Some examples are climate change, ozone depletion, and acid rain.

Climate change

A noticeable change in the global and regional climates is present starting from mid to late 20th century onwards. This is connected to the increased emissions of greenhouse gases compared to pre-industrial period or in other words, 'enhanced greenhouse effect'. Major greenhouse gases are CO₂ and water alongside with CH₄, O₃, and N₂O. Increasing the amounts of these gases due to industrialization and human activities increases their role in the greenhouse effect thus leading to an enhanced greenhouse effect. Global average surface temperature is elevating which contribute to the melting of the Antarctic Sea ice and hence affecting sea levels [40]. Extreme weather/climate events (hurricanes, floods, droughts, etc.) have been happening changing precipitation. This all affects biological cycles, food production, health and economy.



Figure 6 Polluted air in Clermont-Ferrand and Riom (France), source: [41].

Fig.6 demonstrates the bad air quality in Clermont-Ferrand and Riom (2 cities in France, Puy-de Dôme department- Rhône-Alpes region) on a polluted day.

In addition to the global climate change, urban heat island (UHI) is an important consequence of air pollution. UHI is an urban area with a temperature higher than usual, or higher than rural areas due to human activities [42] as shown in **Fig.7**.

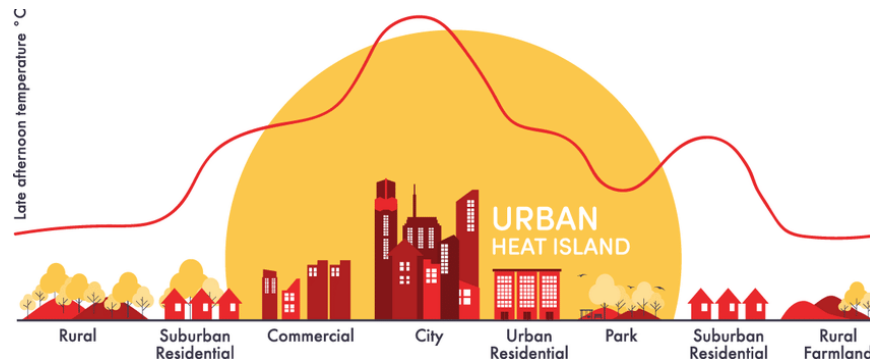


Figure 7 Temperature differences between urban and other areas due to the Urban Heat Island (UHI), source: [43].

During the day and by the mid-morning, heating starts to take place and the temperature can be warmer by 10°C compared to rural areas. This phenomenon is increasing and it is expected that by 2050, 2/3 of the world population will be living in urban areas [44]. Increased temperatures will also lead to higher energy demands thus elevating more the already present air pollution. This transformation of the natural surfaces into construction spaces has influenced the thermal balance. One solution to this is the use of roofs with high albedos like white roofs. Certain studies showed that increasing the albedo can mitigate the UHI. For example, the peak summertime temperatures were decreased by 1.5°C in Los Angeles [45] and by 1-2°C in Athens, Greece [46]. However, reflective surfaces may have some drawbacks manifested by the decrease in efficiency in terms of UHI mitigation in winter. Hence, an alternative solution can be vegetation or green facades. It doesn't only compensate the lost or destroyed vegetation when a certain building was being constructed but also by uptaking pollutants through their stomata, deposition on their surfaces of leaves, or by breaking down some contaminants in their plant tissues [47]. They can also indirectly decrease the production of secondary air pollutants by lowering the microclimate around them due to transpiration and shading properties. Green roofs, specifically, can reduce the heat transfer through the roof thus reducing the energy demands for cooling the building [48]. A study in Madrid showed the reduction of 6 % in the cooling demand in a big residential building [49].

Ozone depletion

In the stratosphere, O₃ forms a protective layer against harmful UV light coming from the sun. However, studies have shown that ODSs or ozone depleting substances have been getting emitted into the atmosphere the last couple of decades [50]. Compounds that have chlorine, fluorine, and carbons (CFCs) or those produced by industries or human activities lie in the ODSs category [50][51]. They are contained in the troposphere and then slowly carried to the stratosphere by air movements. Naturally, the ozone production and destruction rates in the stratosphere are equal but, when the destruction is favored over production, depletion arises [52]. This leads to a serious threat to human health indirectly due to the diminishing of the ozone layer leading to an increase in the UV radiation (cancer, weakened immune system, cataracts), or directly if some substances have accumulated in the troposphere [50]. It also affects plants and animals.

Catalytic processes of O₃ depletion:

Overall: O₃ + O → 2O₂ (middle and upper stratosphere)

Overall: 2O₃ → 3O₂ (lower stratosphere)

Acid rain

Pollutants involved in this process are NO_x and (SO_x) sulfur oxides; they undergo a series of reactions yielding harmful amounts of nitric and sulfuric acids. Escalated anthropogenic production of the acids responsible for acid rain is due mainly to industrialization and urbanization [53]. Pollutants principally react with oxygen and water-reactants found abundantly in the atmosphere- producing protons and lowering the pH [54]. Europe and north America are the biggest regions to receive acid rain [55], this is related to the economic and technological developments. Acid rain can influence plants' photosynthesis and transpiration [53]. It may speed the destruction of buildings, statues, and sculptures; or damage lakes, ponds, and soils; as well as decrease or cause the loss of biodiversity, or even affect humans indirectly because of the heavy metals liberated from soils and leached into underground waters consumed and used by humans [54].

1.4 Control strategies

Different strategies have been adopted to try to decrease air pollution or improve the air quality varying from source reduction strategies to depollution approaches. However, having regulations and air quality managements is an important step to understand the technique to be implemented based on the target pollutant and its accepted ambient concentration (**Table 1**). The purpose of air quality management is to preserve the human health as well as the environment from the unfavorable effects of air pollution. Air quality standards- the basis of air quality management- defines the limits on a pollutant atmospheric concentration or the allowable air pollution level in a specific country or region which are adopted by regulatory authorities [56].

Table 1 Air quality guidelines and standards of specific pollutants depending on the exposure time, source: [56] [57] [58].

Source	Nitrogen dioxide ($\mu\text{g}/\text{m}^3$)			PM _{2.5} ($\mu\text{g}/\text{m}^3$)		O ₃ ($\mu\text{g}/\text{m}^3$)	
	1 year	24 h	1 h	1 year	24 h	8 h	1 h
WHO	40	-	200	10	25	100	-
European Union	40	-	200	-	-	120	-
United States	100	-		15	65	157	-

Guidelines of a specific pollutant depend on diverse factors as the pollutants properties, its health effects, its acceptable risk level, the feasibility of compliance with the standards, and the decision uncertainty regarding the standards. In general, standards vary in their averaging times. For example, a 1 h average time is created to protect the population from peak concentrations (acute exposures) while the longer average times are suitable for chronic exposures and their irreversible adverse health effects [56]. PM_{2.5} is known to cause health effects after short or long exposures; hence, guidelines were formed to protect from acute and chronic exposures. A study showed that

in China and after implementing a policy or an air pollution regulation in 1998 that imposes strict regulations on emissions from power plants, infant mortality decreased by 20 % especially during the neonatal period [59]. Implementing guidelines is beneficial for the public health; however, inconsistency between them is an issue. For instance, the maximum exposure to NO₂ during 1 year is 40 µg/m³ according to the WHO standards but this concentration can be exceeded up to 100 µg/m³ in the USA; likewise, O₃ and PM_{2.5}. Those differences are due to the geographical locations, meteorological parameters, air pollution extent, the concentration of the target air pollutant, the health of a specific nation, etc. For that, some counties impose specific regulations based on their situation to protect their people.

1.4.1 Reduction strategies

Several interventions have been implemented to decrease ambient air pollution varying from source reduction strategies as decreasing the number of vehicles to depollution approaches. These strategies have been evaluated to assess their effectiveness. Some approaches are explained in detail in the following paragraphs: selective catalytic oxidation and photocatalysis.

Selective catalytic reduction

The gas exiting the exhaust of pipes in industries or power plants contains mainly water vapor, oxygen, NO_x, etc. The reaction to happen to abate NO_x is the transformation of NO into O₂ and N₂. However, in an oxidizing medium, NO reacts with O₂ producing NO₂, and hence this reaction

is marked unsuccessful [60]. A reductant such as anhydrous ammonia (NH₃) with a catalyst is required. The reduction catalyst should be active and selective towards N₂ and stable when unfavorable compounds are present. Some drawbacks of this technique as limited catalyst life duration, high costs of catalysts, and high temperature required are present; but its good efficiency and relatively simple installation makes it a good method for removing NO_x [60].

Photocatalysis

Building surfaces or walls can be covered with a photocatalytically active material which oxidizes/reduces pollutants in the presence of sunlight [61]. The covered surfaces, however, should be as close to the source of pollutants as possible. Titanium dioxide (TiO_2) is used as a catalyst which can transform NO_x to NO_3^- for example after being activated by UV light [62]. Recent studies show the possibility of using visible light which makes its application indoors or in tunnels more viable [63]. This heterogeneous photocatalysis is widely used and its efficiency is related to the catalyst ability to create free radicals which further reacts with the pollutants. The latter can be removed by washing the surface or by rain.

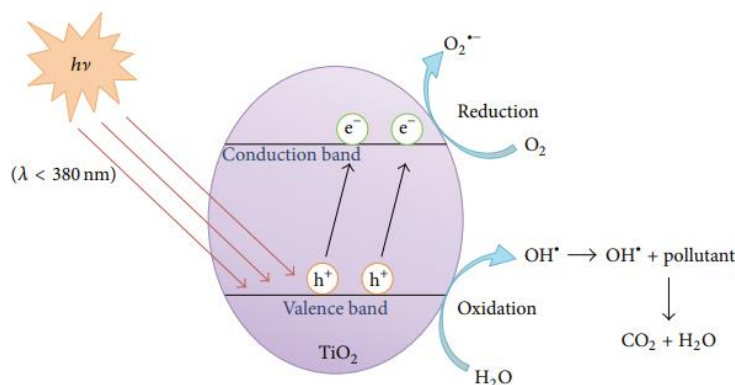


Figure 8 The Photocatalysis mechanism, source: [64].

Fig.8 shows the photocatalysis mechanism. The process starts after TiO_2 absorbs an energy greater than its band-gap energy and gets excited. This generates electrons and holes pairs that move to the TiO_2 surface and undergo redox reactions with a probable formation of superoxide radical anions and hydroxyl radical ($\text{O}_2^{\bullet -}$ and OH^{\bullet} respectively). The latter are the ones responsible for the degradation of organic pollutants in water which can further produce CO_2 and H_2O [65].

Other simple ways to reduce air pollution are to favor use of bikes or walking, taking buses or carpooling (BlaBlaCar in France which is an online marketplace for carpooling), turning off appliances when not in use, and most importantly raising awareness towards the deleterious effects of air pollution [66]. Nevertheless, it is worth to mention the emergence of the COVID-19 virus which froze all economic activities and social events during the past two years. Although the pandemic led to a fall in the economy [67][68], environmentalists call this pandemic a 'blessing in

disguise'. Lockdowns and strict regulations have given rise to a reduction in all pollutants emissions [69] since public mobility ceased and airlines shut down. This caused a significant decrease in greenhouse gases (GHGs) concentration and elucidated as well that outdoor air pollution and the cause of premature deaths each year are mainly due to human activities [70][71]. As an example, NO₂ emissions were reduced by 30 % in Wuhan comparing the periods of before and after the lockdown. Similarly, France encountered a 20-30 % decrease especially in Paris and other major cities [69]. In general, air pollution decreased worldwide. The pandemic has given nature a chance to recover, but this constructive effect is temporary since governments can't force people to be in an endless lockdown. So, strategies to decrease air pollution should remain in progress varying from source-reduction to depollution approaches.

1.4.2 Vegetation as a depollution strategy

Since source reduction strategies can be expensive or inefficient, depollution methods can be beneficial. An interesting ecological depollution approach can be the use of vegetation. Vegetation is a general broad term targeting all plant species without referring to a specific type or characteristic. Numerous studies reflect the ability of plants or trees to remove pollutants through various mechanisms which are described in the following paragraphs [47].

1.4.2.1 Mechanisms of pollutant uptake by vegetation

Absorption into stomata

Stomata are small openings found in plant tissues surrounded by certain cells which control the opening and closure of the pore. The latter regulates gas exchange between the plant and surrounding environment thus controlling the atmospheric environment [72]. Stomatal pores absorb CO₂ and transpire water, a process called photosynthesis [73]; they are necessary plant organs which help plants evolve according to the environment around or environmental stresses [74]. Since they control the absorbance and quantity of CO₂ entering leaf tissues, they can play a role in uptaking or removing air pollutants. Studies show that when pollutants as NO₂, O₃, or SO₂ are present, uptake takes place (**Fig.9**) but followed by a plant damage manifested by the closure

of stomata [75]. It has been concluded that NO_2 uptake is determined by the stomatal aperture and that cuticular deposition contributes not more than 5 % [76][77]. One study revealed that at high NO_2 concentrations, cuticular deposition was 2 times less than that into the stomata [78]; and another regarding tomato showed that it is 4 times less [79]. However, at high humidity, water films can form on the leaf surfaces acting as sinks to NO_2 [76][80][81]. NO_2 , in general is known to be less toxic to plants than O_3 or SO_2 [82]. O_3 can decline photosynthesis due to its direct effect on stomata [83]. A research conducted on seedlings where the latter was exposed to 0.3 ppm of NO_2 and a mixture of 0.3 ppm NO_2 and 0.1 ppm O_3 , showed that the grown trees that were exposed to NO_2 were healthy. However, those that were exposed to the mixture had visible injuries and smaller leaves [84].

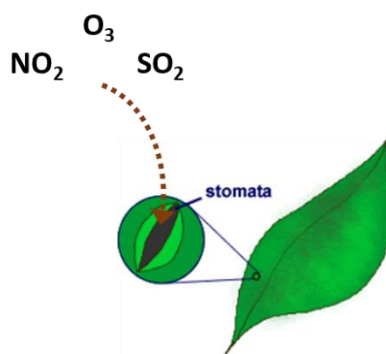


Figure 9 Absorption of air pollutants into a stoma, source of the leaf picture: [85].

Adsorption on leaf surface

Adsorption is the adhesion or deposition of certain molecules to a surface. Unlike absorption, adsorption is a surface phenomenon which creates an adsorbate film on the adsorbent. It can be either due to Van der Waals forces or covalent bonding. Plants or vegetation (adsorbent) intercept/adsorb pollutants (adsorbate) by their leaves, branches, barks, etc. due to the large surface area available. PM can be retained by vegetation surfaces for the moment before being washed out by rain or carried by wind to the soil or the atmosphere [86]. The deposited PM can be as well absorbed through the plant's external layer or penetrate the stomata [87]. Particles can be removed from the atmosphere by wet deposition (by precipitation), or dry deposition (settling of particles to be collected/intercepted). Since trees have large surface areas, they are capable of collecting particles more than any other form of vegetation [88]. It has been indicated that the deposition

velocity of aerosols in the woods is 3 times higher than that in a grassland [89]. A study in Chicago revealed that by increasing the tree cover from 19% to 24%, a 21% increase of PM₁₀ removal from the atmosphere can be attained [90]. Another in Philadelphia, using a model, displayed that the present tree cover can reduce PM₁₀ by 0.72%; however, it might reach 12% in woody areas [91]. In addition to that, O₃ can be deposited on the surfaces of plants. A study considering cuticles and O₃ showed that it can undergo deposition to be further destroyed or might enter the latter [92]. Hair present on plants with irregular surface features can augment the deposition velocity by providing a greater surface area. It is important to understand the dry deposition process since it is a way to remove pollutants from the air thus improving the air quality but at the same time, some plants can be harmed especially if the pollutant enters the stomata affecting photosynthesis [93]. So, vegetation can remove pollutants from polluted air by absorption or adsorption which might be followed by a series of reactions.

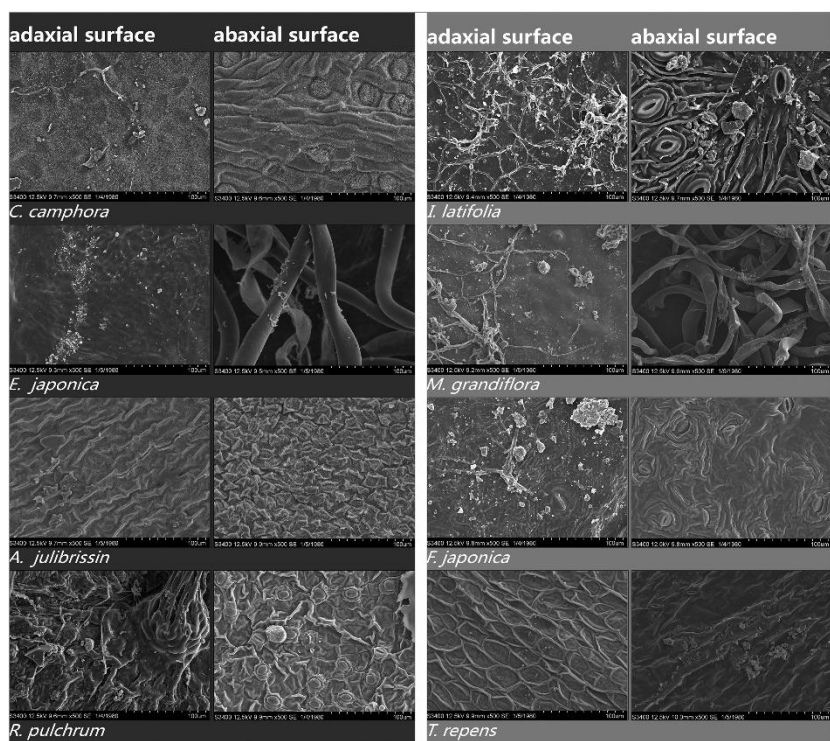


Figure 10 The retention of particles on the abaxial and adaxial leaves surfaces of 8 different plants. Images obtained by the Scanning electron microscopy, source: [94].

Fig.10 shows the adsorption of particles on 8 different studied plants. The images were obtained using Scanning electron microscopy (SEM).

Interaction of plant volatile metabolites with atmospheric pollutants

VOCs are principally present in the gas phase including a vast variety of compounds with boiling points ranging between less than 0 °C to 400 °C [93]. Plants use VOCs as a sort of communication among each other to transmit information in case of the presence of stress factors [95][96]. The latter are not only scents but rather warning signals to other plants or a source of attraction to pollinators [97][98]. Since vegetation emit VOCs and is known to remove pollutants, a certain interaction between VOCs and pollutants can occur. Thyme is a perennial plant used on green roofs and emits various VOCs such as thymol [7]. A study involving the catalytic ozonation of thymol reported the degradation of the latter where O₃ attacked the *para* and *ortho* positions of thymol followed by several reactions [99]. O₃ can react with terpenes indoors producing aldehydes and PM [100][101], this was in line with a study which indicated an increase in PM when O₃ and terpenes were concurrently present [102]. Cleaning events as well using a detergent containing VOCs, can form PM [103]. This reaction can form many radical species including [•]OH which might then react with other compounds or pollutants [104][105]. Hence, O₃ reacts with VOCs; this reaction leads to the formation of PM or other health-depleting pollutants. PM however, would deposit on the surface of leaves to be further followed by different reactions (**Fig.11**) [86][87].

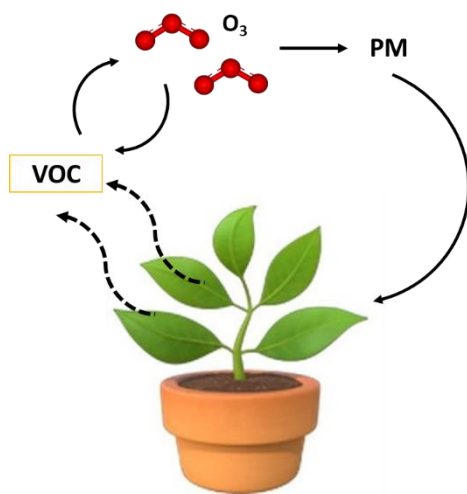


Figure 11 Reaction of VOCs with O₃.

As previously mentioned, plants emit VOCs due to environmental stress. An example is isoprene; its emission is widespread in plants. Its role is still unclear, but studies suggest its ability

to increase the thermotolerance of plants and hence, protects plants from environmental stress. Isoprene plays a role in atmospheric chemistry where it can either breakdown in the presence of NO_x and sunlight and produce O₃ or can directly react with O₃ [106]. This reaction can form formaldehydes or other oxidative species. Nevertheless, isoprene can contribute to the O₃ resistance in plants; it can scavenge O₃ in leaves yielding less toxic products [107]. To elucidate this, leaves of two ozone-sensitive genotypes of tobacco were exposed to O₃ with and without the presence of isoprene (these plants don't emit isoprene). Results showed that when no isoprene was present, acute and short exposures (300 ppb, 3h) to O₃ decreased photosynthesis which was worse 12 h after the treatment ended [108]. However, no important decrease in photosynthesis was reported when isoprene (3 ppm) was present at the end of exposure; but, a decrease was observed 12 h after ending the treatment but to a lesser extent. Hence, this study proves the protective effect isoprene has towards plants exposed to O₃. In order to fully understand the role of BVOCs, other types should be considered regarding their interactions with O₃.

A study involving the interaction between O₃ and selected terpenes (d-limonene, α -terpinene, and α -pinene) in an indoor environment showed that that the particle concentrations were the highest with d-limonene [102] followed by α -terpinene and α -pinene. D-limonene is often found indoors since it is used in cleaning products giving a citrus scent [109][110], and its interaction with O₃ was more significant than the one with α -terpinene even if it reacts 100 times slower than the latter [111]. This might be explained by the production of many condensable products in the case of limonene. In their experiments and in simulated O₃-terpene conditions, the formation of particles was as high as 95 $\mu\text{g}/\text{m}^3$. However, under typical indoor conditions, the production was between 2.5 and 5.5 $\mu\text{g}/\text{m}^3$. Nonetheless, it was necessary to understand the course of the interaction since terpenes are emitted abundantly indoors, especially limonene which was found in more than 50 % of monitored buildings according to the EPA's BASE study [112]. O₃, as well, can be present in the buildings due to the air exchange and other sources such as photocopiers, air purifiers, and electrostatic air cleaners [113]. Hence, all chemicals needed to form particles can be found indoors [114], the place where people spend more than 90 % of their time [115]. Nevertheless, another study confirmed this interaction which used the new state-of-the-art Vocus proton-transfer-reaction time-of-flight mass spectrometer (PTR-TOF) in the French Landes to identify gas-phase molecules emitted by the Landes forest [116]. The latter produces large quantities of monoterpenes and hence, can be a good site to study the Biogenic volatile organic

concentrations. In Paris particularly, an increase in NO₂ and PM increased the number of hospital admissions and consultations linked to asthma attacks [123]. Some research studies display that using new materials in constructing a building can reduce air pollution [61][124][125] while others reflect the importance of using vegetation to mitigate the negative air pollution effects [31][126].

Naturally, urban areas still have an ‘urban’ forest including all vegetation and soils already integrated into the roads, power lines, and infrastructure maintaining –to a certain extent- the quality of life [90]. However, planting more trees is beneficial due to the various advantages vegetation imposes varying from carbon sequestration, air pollution reduction (can remove SO₂, NO_x, O₃, etc.), temperature regulation (due to shading and evapotranspiration thus decreasing energy demands), and climate change diminution [31][32]. Vegetation can also serve recreational, cultural, and aesthetic needs.

Countless studies deal with the ability of vegetation, specifically trees, to remove air pollutants as O₃, NO₂, PM₁₀, and SO₂. A study in the USA approximated that urban trees remove 711,000 tons of pollutants with an annual economic benefit of 3.8 billion \$. They were able to remove 305,000 tons of O₃, 98,000 tons of NO₂, and 215,000 tons of PM₁₀ [31]. Their results were based on a modelling study consisting of meteorological and air pollution concentration data obtained. However, the pollution removal rates vary among different cities; this is due to the difference in the tree cover, pollution degree, meteorological variables, and leaf-off/leaf-on seasons which all affect deposition velocities. They, in general, uptake pollutants through their stomata, or by the pollutants deposition on the leaf surface. Once on the leaf surface, pollutants might enter the intercellular spaces reacting with the water present inside or might just be retained on the surface to be discharged again to the atmosphere [127]. Another research in Beijing [32], the capital of China and one of the top 10 most air polluted cities in the world, reflected that the urban forest can store around 225,000 tons of carbon in biomass thus decreasing the amount of CO₂ in the atmosphere which might reduce the global climate change. Older trees were bigger and able to store more carbon than younger ones; thus old ‘unchanged’ cities can remove more carbon as an overall. Trees were able to eliminate 1260 tons of pollutants from the atmosphere in one year with the PM₁₀ removal being 61 %. This might be due to the fact that PM₁₀ is a main pollutant in Beijing. Nevertheless, they also removed significant amount of O₃, NO₂, and SO₂. It is important to state that removal rates depend on the season; seasonal variations affect leaf expansion which in turn influences the total tree area available. Seasonal variations also mean a change in precipitation

patterns and the climate generally. The study also compared the pollution removal rates with those of different American cities and showed that the urban forest in Beijing had a higher rate which is explained by the higher concentration of air pollutants present. Nevertheless, trees can indirectly decrease air pollution by decreasing the temperatures leading to less air conditioning and energy demands; 16.4 % cover of trees/shrubs can decrease the temperature by 1.6°C.

In Europe, particularly in Strasbourg-France, a study highlighted that trees in public green spaces have the ability to remove around 88 tons/year (between 2012 and 2013) of pollutants varying from CO, NO₂, O₃, SO₂, and PM. The maximum uptake was for O₃ followed by PM (PM₁₀ and PM_{2.5}) and then NO₂ being 55.8 tons/year, 16.2 tons/year, and 13.8 tons/year respectively [128]. Hence, big polluted cities started integrating and planting more trees as seen in **Fig.13**. Pollutants mitigation was more efficient during the leaf-on season recording an 81 % of pollutant removal. This is explained by the greater surface area available, the warmer temperatures, the lower wind speed, as well as the more considerable stomatal conductance which all increase the concentrations and deposition velocities of pollutants. The tree species and their land use affect the removal potential. For example, in Strasbourg, forest lands were the most efficient in removing pollutants, followed by parks, industrial areas, and agricultural lands. On the other hand, the leaf area of a specific species can lead their depollution capacity. According to the study, the European beech was the best performant. They used a model called i-Tree model to assess their results which takes into consideration the forest structure and ecosystem services. This model was already used by other researchers in Spain and the United Kingdom (UK) [129][130]. In both Spain and the UK, the urban forest removed PM₁₀, NO₂, O₃, CO, and SO₂. The former eliminated 305.6 tons/year and 50 t/year of pollutants with PM₁₀ and O₃ having the highest removals respectively. The differences in tree cover, pollutants concentrations, leaf area, species present, and climate clarify the discrepancies obtained in all studies.

Trees then directly ameliorate air quality by decreasing the air temperature and by removing pollutants; and indirectly by reducing energy demands and consumption. However, at the same time, trees can be a source of pollutants. VOCs emitted can act as a precursor to O₃ and particles through their reaction with NO_x [131]. Also, the pollen and the particles produced can inflict serious health problems on allergic people [132]. In addition to that, toxic pollutants will eventually accumulate in the soil resulting in a contaminated one which affects water quality and future land use [133]. In urban sites and densely populated cities, there is little space to plant trees. For

example, in Midtown Manhattan, a district in New York, 94 % of the land is impervious surfaces like streets and rooftops. This makes it impossible to find a place to plant trees which also in turn take several years to grow to be able to mitigate air pollution. So, green roofs or greenery systems can make use of the available rooftops (40-50 % of the impermeable area in a city) and be a more appropriate solution to this perplexity as well as air pollution [134].

1.4.2.3 Greenery systems

Urbanization has created a pronounced construction demands where buildings, factories, and residential sectors are being constructed at the expense of green areas; turning our world into a densely populated place suffering from pollution [135]. By changing the already-present unused rooftops and by introducing different plant species to those rooftops, a compensation to the lost greens while the building was being constructed can be an outcome [7]. So, greenery systems are a way of ‘greening’ and at the same time mitigating air pollution. They are sorted as vertical greenery systems and green roofs. Green roofs or roofs with plants in their final layer are known as eco-roofs and are coated with green plants and growing media.

Components of green roofs

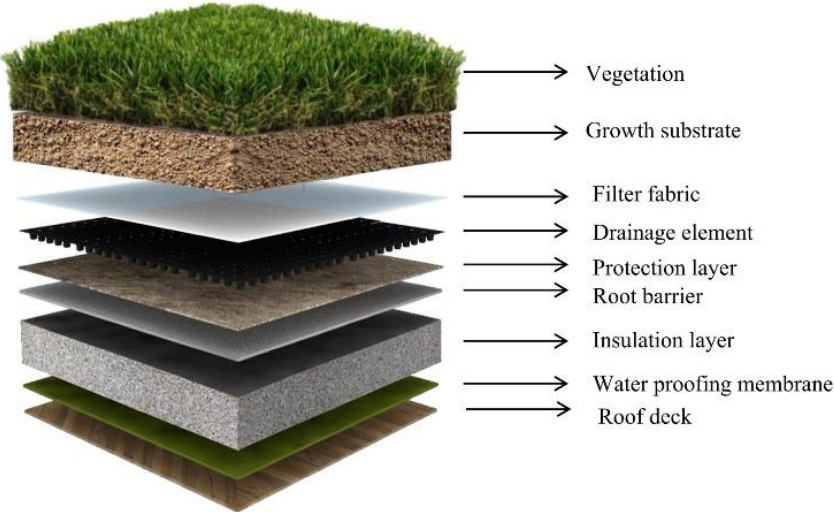


Figure 13 The different components of green roofs, source: [135].

Green roofs consist in general of vegetation with its substrate, filter fabric, root barrier, and the insulation layer (**Fig.14**). The layer holding the vegetation is the uppermost layer that adds life to the green roof and which can act as the air pollution mitigator. Those properties make the choice of plants a delicate factor. Since many limitations exist as water scarcity and building load restrictions, and since green roofs are not a favorable or a normal environment for plants to grow, the latter used should have specific properties to ease their implementation [7][136]. Plants should be drought-tolerant with little maintenance needs, have short roots, and be capable of removing contaminants from the soil or air. Preferable green roof vegetation is of the succulent type as the sedum species because they are able to limit transpiration and store water [137][138]. For instance, a study highlighted that sedum species were able to stay photosynthetically active even after lacking water for 4 months [139]. Another study indicated that sedum species survived 2 years without water [140]. This is due to their characteristic of storing water in their stems and leaves enabling them to survive drought conditions [141]. In addition to that, their shallow roots give them the advantage to be used excessively on extensive green roofs (with a small substrate depth) while also being healthy [142] Consequently, those properties decrease the cost of green roofs. Nonetheless, as sedum species are non-native for all countries in the world, research has been focusing on the use of native species since they are already evolved to adapt to the present weather conditions, thus resistant to local pests. Many studies dealt with native plant species to find the most suitable for green roofs and the closest to the qualities of sedum [143][144][145]. Nevertheless, using multiple types of plant species can yield a positive effect on the effectiveness of green roofs [146]. Some types of plants used on green roofs are: thymus vulgaris, sedum species, oregano, grasses, etc.

The growth substrate affects the performance of green roofs. It is related also to the thermal and sound insulation hence, it must have some unique properties as a low bulk density, high sorption capacity, good water holding capacity, and stable. On the other hand, the filter layer which separates the growth substrate and the drainage element should have high tensile strength, small pores to prevent particles from entering the drainage layer, and should act as a root barrier specially to plants that have soft or short roots. Those properties can improve the water retention capacity of green roofs. In general, all components should have specific compatible properties to ensure the most effectiveness possible [147].

Types of green roofs

Table 2 Differences between the 3 green roof types, source: [147].

Green roof type	Substrate layer thickness	Vegetation types	Maintenance recurrence	Cost
Intensive	Thick (20 – 200 cm)	Trees/shrubs (diverse)	Frequent	High
Semi-intensive	Moderate	Herbaceous plants/ grass/shrubs	Frequent	High
Extensive	Thin (< 15 cm)	Grass/ moss/ succulents	Minimal	Low

Table 2 shows that among the 3 types, extensive green roofs are the most common due to their low cost, maintenance demands, and weight meeting the building weight restrictions.

History of green roofs

The oldest example of a greenery system goes back to the city of Babylon 500 years BC where ‘hanging gardens’ were employed, as well as the Roman and Greek empires. Also, in the old Mediterranean area, vines were grown on pergolas providing shade or directly on the walls of the building lowering the indoor temperatures and providing more comfortable indoor conditions [148]. Years after, the use of ‘climbers’ increased as it became popular particularly in UK and Central Europe. In the 20th century, various studies especially in the botanical domain [149] were being done where they understood the significance of green facades towards ecology. Afterwards, green roofs were implemented in Germany. With passing years, more and more areas of green roofs were seen in Berlin where 10% of the buildings in Germany use green roof technology now [150] [151]. Lately, developed countries as USA, Canada, Japan, etc. started integrating new laws in the favor of green roofs and facades. Consequently, 15 % of roofs in Basel, a city in Switzerland, have been greened [152]; in Tokyo- Japan, a regulation was implemented that states that all newly built and enlarged buildings with land area $\geq 1000 \text{ m}^2$ must have green roofs [153]. Similarly, in Canada

where a law declares that if the floor area exceeds 2000 m², 20-60 % of the roof area should include green roofs [153]. It was approved in 2015 that in France, the new commercial constructions must at least partially cover their rooftops with plants or solar panels. This is a great step towards more sustainable cities [154].

Benefits of green roofs

Green roofs could promote biodiversity, reduce temperatures, mitigate the Urban Heat Island (UHI) effect, improve air quality, ameliorate the city image, and has many social and economic advantages as well [155][156][157][158]. Some benefits will be addressed in detail herein below.

Thermal performance enhancement

Enhancement in the thermal performances of a building positively affects and reduces its energy demands. This is due to the thermal insulation and shading properties as well as the thermal mass present [149]. A study in Greece showed that green roofs decrease the cooling energy demands by 2 to 48% (the percentage being related to the area covered by plants) with an indoor temperature decrease [159]. The growth medium helps in insulating the roof as well as the water content which can trap the heat; the vegetation layer plays a role in absorbing or reflecting the incoming solar radiation which limit the thermal loads. From the total incoming solar radiation, 27% was reflected, 60% absorbed by the plants, and 13% transferred to the growing medium [160]. According to the types of plants present and the thickness of the soil, the annual energy consumption savings can vary between 1-15% in a five-floor commercial building in Singapore [161]. Some authors claim that green roofs also have positive insulating properties during winter and hence on energy demands; however, others believe that it actually increases the latter [162][163]. Generally, green roofs decrease the ambient air temperature due to an increase in the albedo (fraction of light radiation reflected by a surface) of urban areas; for instance, the albedo of a green roof was shown to vary between 0.7 to 0.85 comparable to that of white roofs (0.8) while that of bitumen, tar, and gravel roofs range between 0.1 and 0.2 [146] which hence reduces the urban heat island effect.

Stormwater management

While raining, a fraction of the water will get absorbed by the growing medium; this water can be used by plants to be stored in their tissues/transpired back or retained in the pore spaces. However, the ‘unabsorbed or untrapped’ remaining water will percolate and reach the drainage system where it will be retained. Draining will happen with the saturation of the drainage space.

The retained water will either be absorbed again by the plant where part of it will be transpired or evaporated [135][164][165]. A study revealed that the runoff retention can reach 66 % on an intensive green roof which is much higher than that on a normal roof (34 %) [166]. Green roofs are recognized as a way to decrease the chances of flooding by retaining stormwater. Vegetation, the thickness and type of the growing medium, the drainage system present, slope of the roof, storage capacity, etc., all specify the retention potential of the roof with the growing medium playing the biggest role [143]. Some studies reflect that the runoff delay from green roofs is due to the high water holding capacity of the growing substrate [167]. Vegetation also plays a significant role in the runoff retention. Grasses were reported as being efficient for runoff control followed by sedum [165]. Sedum species transpire available water quickly and can retain rainwater by contributing to 40 % of the green roof capacity to retain stormwater [168].

Noise attenuation

Green roofs act as a cover separating or creating a boundary between indoors and outdoors. They can attenuate noise coming from the road or from traffic by absorbing sound waves or by increasing the road insulation [169] [170]. A study showed that the noise transmission loss of non-vegetative roofs is less than that of vegetative roofs by 10 to 20 dB [171]. The comparison of sound insulation between an extensive and an intensive green roof showed that an extensive roof is rather effective in reducing sound transmission however, an intensive roof showed no positive effects [169]. Not a lot of research focus on acoustical benefits but in general, noise pollution in urban spaces is reduced.

Green roofs can be viewed as a design for boring flat buildings. They enhance aesthetic values and act as a tool to restore biodiversity. For instance, **Fig.15** shows a green-roofed school in France which is more psychologically and aesthetically pleasing than a normal asphalt one. They,

as well, protect roofs from heat and ultra-violet radiation which decreases the daily expansion and contraction of conventional roofs [147]. The latter usually reaches 70°C of temperature compared to a 25°C of that of green roofs.



Figure 14 A green-roofed school in France, source: [172].

Air pollution mitigation: A literature review

Carbon sequestration

Green roofs also sequester carbon. The global warming and the enhanced greenhouse effect are facts that we have been living ever since the industrial revolution took place [173]. The increased demand for fossil fuels generated a great amount of CO₂ which is a by-product of combustion. CO₂ is one of the main gases that keeps our planet warm by trapping the received energy from the sun. Then, logically, an increase in CO₂ leads to an increase in the greenhouse effect. CO₂ concentrations increased by 32 % since 1750 and it is expected to escalate more since it has been proposed in 2010 to construct 100 new powerplants to support the expected energy demands [174] [175]. Green roofs can trap carbon naturally - a process called photosynthesis - hence sequestering carbon in their tissues. The latter can then reach the soil substrate due to the fall of dead organic material (plant litter) or due to the release of carbon by the roots. However, this phenomenon always reaches an equilibrium so, green roofs also decrease the emission of CO₂ by

mitigating the UHI and by decreasing the energy demands as seen in Fig.13. A study in Michigan quantified the sequestered carbon by sedum species on an extensive green roof and revealed that sedum and the substrate sequestered around 380 g/m² [176].

Modelling studies- Removal of adverse air pollutants

Vegetation as trees and shrubs is very efficient in mitigating the UHI and lowering pollution levels. But, due to limited availability of spaces especially in urban areas, the use of a vegetated roof or a green roof can be a good solution. They make use of impervious areas and at the same time, lower the pollutants concentration. Numerous researches tried to estimate the depollution capacities of green roofs. Starting with Toronto-Canada, a study revealed the ability of green roofs to reduce NO₂, SO₂, PM₁₀, and O₃ levels [126]. It dealt with a dry deposition model called Urban Forest Effects (UFORE) which quantifies the reduction in concentrations of the targeted pollutants by calculating the vegetation cover, weather data, and the pollutants concentrations. Their model estimated that intensive green roofs can play a big role in improving the air quality while an extensive roof plays a smaller one. However, due to the higher cost of intensive green roofs owing to the added structural loading requirements, an extensive roof is preferable. Another in Chicago-USA revealed the removal of 1675 kg of pollutants in one year by 19.8 ha of green roofs [23]. The latter comprised short grass, herbaceous plants, trees and shrubs, and other plants; which is the ensemble of all 71 green roofs studied varying from extensive, semi-intensive, and intensive green roofs. The O₃ uptake was the largest contributing to 52 % of the total uptake followed by NO₂, PM₁₀, and then SO₂. This is explained by the high concentration of O₃ present at that year which peaked in summer. This study used a dry-deposition model and indicated that if all green roofs were of the intensive type in Chicago, pollutants removal can reach up to 2047 metric tons. However, the installation cost is a great obstacle. As with normal vegetation, the most efficient pollutant removal was when the leaves were fully open and expanded. The annual removal rate per hectare of canopy cover was greater in the study in Chicago than in Toronto. This is due to the difference in plant cover, weather, and pollution severity. Also, the methods used in the modeling play a role. Similarly, a study on a 50 ha extensive green roof in UK holding 2 different grass types, a flowering plant, and sedum showed the ability of those species to capture PM₁₀ [166]. The grasses were more efficient than sedum in removing the particulate matter where both grass species

combined were able to mitigate around 2.5 metric tons/year of PM₁₀. Sedum removed 0.21 metric tons; this difference is due to the surfaces provided by the plant species.

Table 3 Amounts of pollutants mitigated by different studies.

Study	Plant species studied	Pollutants abolished (kg/year)
Currie & Bass [126]	Grass	1270 O ₃ 650 NO ₂
	Shrubs	1270 O ₃ 1240 NO ₂
Speak et al. [166]	Sedum	210 PM ₁₀
	Red Fescue	1605 PM ₁₀
Yang et al. [23]	Grass/ Herbaceous plants/ Shrubs	871 O ₃ 452 NO ₂
Johnson and Newton [8]	Grass	4000 PM
Clark et al. [177]	Sedum	800,000 NO ₂
Tan and Sia [179]	-	SO ₂

Table 3 shows the amount of pollutants removed by several studies. In all the previous studies [23] [126] [166], the plant species studied were able to remove PM₁₀, O₃, NO₂, and SO₂. For example, Currie & Bass [126] showed that grass can abolish 1270 kg of O₃ and 650 kg of NO₂; while shrubs can remove 1270 kg of the former and 1240 kg of the latter. Speak et al. [166] reported that sedum can capture 210 kg of PM₁₀ when Red Fescue (a grass species) trap 1605 kg. According to Yang et al. [23], a mixture of 63 % grass/14 % herbaceous plants/11 % shrubs/12 % hard surfaces mitigated 871 kg of O₃ and 452 kg of NO₂. The dissimilarities show the different effect each plant species has and the necessity to understand the mechanisms of each to help set the goals concerning air pollution mitigation.

Other studies showed that 2000 m² of grass on a green roof can abolish 4000 kg of PM [8]. So, if 0.1 kg of PM was released into the atmosphere in one year by one car, a 1 m² of uncut grass is sufficient to remove this pollutant. Similarly, it was reported that if only 20 % of industrial and commercial buildings in Detroit-USA were covered with extensive sedum green roofs, around 800,000 kg of NO₂ can be offset [177]; their estimation was achieved by assuming constant NO₂ removal rates by green roofs. In Singapore, the concentration of SO₂ was compared before and the installation of a 4000 m² green roof. Results show that a decrease of 37 % of SO₂ was attained above the roof [178].

In addition to the direct removal of pollutants and decreasing the pollution extremity, green roofs can as well indirectly remove pollutants by decreasing the emissions from powerplants. In Los Angeles, it was estimated that 350 tons/day of NO₂ can be eliminated by lessening the need for air conditioning which leads to a 10 % reduction in the formation of smog and a saving of 1 million dollars/day [6][179]. Due to evapotranspiration and shading properties, a green roof helps in bringing down indoor temperatures during summer which reduces cooling needs and insulates the building in winter hence decreases heating requirements [180][181]; therefore, mitigating the UHI (**Fig.16**).

Experimental studies

All previous studies show that green roofs are effective in removing pollutants, improving air quality, and mitigating the UHI. In addition to that, they can increase biodiversity, improve the building insulation, and increase the aesthetic value of a building with a boring standard roof. However, all those researches were based on modelling and few studies deal with laboratory or field measurements of green roofs depollution ability. A very recently published article compared the efficiencies of different ventilation filters (ventilation system) in removing O₃ [182]. One of the filters was installed on a white roof while the other on a vegetated one involving mostly succulents like sedum species. The ventilation system affects the quality of indoor air since it is usually installed on buildings and outdoor air can interact with the green or white roof prior to entering the building ventilation system. In their studies, they built a setup which enabled them to test the ozone removal efficiency (**Fig.17**). An air supply system was used followed by different filters and drying media to purify and condition the air. Purification and the removal of VOCs from the supplied air was done by 2 different filters and a drying medium while the control of humidity was achieved by

a glass impinger filled with distilled water. The temperature was also monitored and recorded using a temperature sensor. This process was then followed by a flow meter controlling the flow of the air entering the O₃ generator which produces O₃ to be fed to the filters under study. O₃ analyzers were found in the end of the setup monitoring the O₃ concentrations.

The results showed that green roof filters had a greater removal performance than white roof filters or even than an unused filter ranging from 10-25 % for green roof filters and from 5-15 % for white roof filters after 5 h of O₃ exposure (with a temperature of 21 °C and relative humidity being between 30 % and 70 %). This was explained by the help of the Scanning Electron Microscope (SEM) images that showed that non-ozonated green roof filters had an accumulation of deposits such as pollen or other biotic coatings. Contrary to that of white roof filters which had fewer deposits. Deposits offer a greater surfaces area which increases the amount of particles captured by the filter. The same group investigated the O₃ removal efficiency of the same filters present on a green roof as well as on a white roof with the variation of temperature and relative humidity [183]. They selected 3 temperatures and 3 relative humidity values: 15 °C, 23 °C, and 31 °C, and 20 %, 50%, and 80 % to cover all realistic conditions. The removal ability of all filters increased with the increase of relative humidity; however, the trend is uncertain regarding the temperature. Overall, they found that the best conditions were 23 °C temperature and 80 % relative humidity which suggests that O₃ removal by both roofs is relatively better in the winter season. This is in line with their previously reported work [182]. Green roofs hence directly improve the indoor air quality by removing O₃ or indirectly by affecting the effectiveness of ventilation/heating/air conditioning filters placed in the building ventilation system.

1.5 Research questions/gaps

1.5.1 Uncertainty of models

Since air pollution mitigation ability of green roofs was estimated or predicted using models rather than quantitatively calculated using field or laboratory research, many limitations and uncertainties can be an outcome. The study using UFORE model [126] held some unreliability

since in their data, grass was the plant species studied instead of sedum because data for other vegetation -usually used on extensive green roofs- were not available. The model predicted the leaf area index and evapotranspiration rates of grass in order to calculate the air pollution removal values and then compare the latter with those of trees and shrubs. The only model that was accessible in North America to estimate the vegetation effect on air pollutants was this one where its precision is unknown. Hence, plant selection to be studied was constrained. The economic benefits and analysis were also limited since they were related to values derived from a work done in New York [184]. Their data were based on the deduced cost of air pollution regarding its effects on the health and environment. This might pose a problem due to the probable differences in values between countries. The model acts mostly as a program where grass was chosen as a proxy unit.

Similarly, studies considering dry deposition/big-leaf models report various uncertainties. For example, the estimation of the air pollution removal by green roofs obtained from [23] is more an approximation than an accurate estimation. This is because the generalization of green roofs as continuous surfaces containing mostly grass, herbaceous plants, and deciduous trees with uniform heights was an obligation for implementing the big-leaf model at a big scale. Also, the air pollutants concentrations were deemed constant. However, the heights of green roofs, type of vegetation present, and the distances to the sources of emission (distance between the building having the green roof and the emission source) largely influence pollutants removal. Green roofs, for instance, located in a highly polluted area would uptake more pollutants than a roof situated in a clean area. Calibrating the dry deposition model and verifying the reported results is mandatory since the way that the deposition velocity on plants was modelled is also erroneous; they were taken from the literature without considering the differences among species.

Accurate laboratory and field studies are necessary to precisely measure and understand the depollution effect of green roofs. Starting from a small setup-to be extrapolated-, one can measure the uptake capacity of many plant species usually implemented on green roofs. Based on the uptake capacity of a certain plant species towards a target pollutant, the choice of green roofs, and plants to be installed in a region with an elevated concentration of this target pollutant would become easier.

1.5.2 Lack of studies concerning the interaction of VOCs and pollutants

VOCs emitted by plants play an important role in the plants life as in the chemical interaction occurring in the atmospheric compartment [185]. Being released by any type of vegetation, VOCs are usually a result of different stimuli. They are involved in the plant communication, pollinators attraction, stress adaptation, and defense from predators [186][187][188][189]. Nevertheless, the emission of VOCs is directly related to the plant species [190] and different plant species have different solutions to the same problem. For example, dissimilar flowers produce various odorous volatiles to face the problem of attracting the same pollinator [191]. Those biogenic volatile organic compounds (BVOCs) include isoprene, monoterpenes, and sesquiterpenes with alkanes, alkenes, alcohols, etc. as well [192].

The interactions between the urban vegetation and urban environment are rarely studied and since urban vegetation is always exposed to elevated pollutants concentrations and temperatures, it is important to understand the reactions taking place (**Fig.18**) [193].

For example, when vegetation is exposed to a change in the abiotic components (change in temperature, presence of high concentrations of pollutants, etc.), its ability to remove pollutants as well as its volatile emissions change. An augmentation of the latter leads to an increase in interactions between the VOCs and pollutants; this might provoke a boost in air pollution [194]. The production of isoprene is involved in the formation of ground-level O₃ while monoterpenes or sesquiterpenes are rather related to the increase in PM [195] [196]. In general, in the areas rich in NO_x, VOCs go through chemical interactions forming O₃ and PM [197]. This was in line with a study done in China showing that BVOCs affect the formation of O₃ and PM [198]. Out of the hundreds VOCs emitted by plants, only few impact the air quality [199]. However, some studies state a decrease in O₃ concentrations in the presence of plants. O₃, after being formed, can be captured by the vegetation (leaves, stomata, stems, etc.) or can react with NO and VOCs as monoterpenes and sesquiterpenes thus lowering its concentration [200] [201] [202]. In order to solve this complexity, laboratory or field studies should investigate the influence of a plant species emitting VOCs on O₃ concentrations. Also, to avoid the uncertainties carried by models, quantitative experimental work is needed.

1.5.3 Lack of studies regarding pesticides + VOCs/ pesticides + pollutants

Pesticides + pollutants

Pesticides are chemical agents that control pests and protect plants or crops; they include herbicides, insecticides, fungicides, etc., each having a role. Once on leaves, they can react with urban pollutants. Hence, understanding the fate of pesticides is necessary since their degradation can lead to an increase in doses applied or number of treatments. The formation of degradation products might lead sometimes to contamination of the environment as well. Numerous researches studied the interactions of pesticides and pollutants as O_3 in water, while others deal with their interaction on supports in the presence of O_3 (heterogeneous reactions).

In solution

Due to the industrial wastes, surface run-off owing to agricultural applications, domestic employments, etc., pesticides reach surface waters and pollute them [203]. According to a survey, surface and groundwaters were contaminated by different types of pesticides where concentrations up to $0.6 \mu\text{g/L}$ were detected in surface waters [204]. A review considering the ozonolysis of various types of pesticides in aqueous solutions showed that almost all pesticides were degraded in the presence of O_3 . For example, the insecticide called Aldrin- which is now banned - showed a consumption of around 90-100% when O_3 of a concentration between 1 and 4 mg/L was present [205] [206]. O_3 usually attacks the carbon-carbon double bond producing even more harmful and more toxic compounds. Dichlorodiphenyltrichloroethane (DDT) on the other hand, showed a low reactivity towards O_3 [206]. However, 94 % conversion was reported after prolonged ozonation [207]. Many factors affect this reaction such as the presence of humic substances, the solubility of pesticides in water, and the pH. This is important since pesticides in potable water poses a threat to the human health, thus ozonolysis can be applied only if complete mineralization is achieved or if the intermediate products are less toxic than the starting chemical.

On solid

Out of the various studies done on the heterogeneous phase, one involving 8 commonly used pesticides adsorbed on silica model particles and ozonolysis showed degradation concerning

4 pesticides while no effect was reported related to the others [208]. Ozonolysis was done for 26 h for 6 O₃ concentrations (0 to 997 ppb). The decay was proportional to the O₃ concentrations. In the absence of O₃, no effect was noted. However, the degradation increased with the O₃ concentration. In their experiments, they built a setup involving O₃ generator, O₃ analyzer, chambers, and a humidity system. This suggests a possible interaction taking place between pesticides and O₃ yielding products. Their results were in line with other studies that performed ozonolysis with many pesticides [209][210][211]. The same group also studied the heterogeneous degradation of the 8 commonly utilized pesticides by [•]OH radicals [212]. The latter was chosen since pesticides, in general, undergo photolysis and react with atmospheric oxidants like [•]OH, O₃, or nitrate radicals (NO₃). Pesticides were adsorbed on silica particles where a source of [•]OH was present. Similarly, 4 out of the 8 pesticides were degraded. The results concerning the 4 unreactive pesticides were unexpected since they are degraded in the gas phase according to some software calculations [213]. Hence, [•]OH can degrade the pesticides in the gaseous phase but the reactivity significantly decreases in the heterogeneous phase due to the probable steric hindrance and the absence of water on the solid surfaces rendering the diffusion of OH[•] or O₃ through solid the substrate limited. This reflects the complexity of this phase.

Pesticides photolysis

Pesticides, principally, undergo direct and indirect photolysis. Direct photolysis takes place via excited states when it has the ability to absorb a wavelength > 290 nm (UV-visible absorption) (**Fig.19**). Photoproducts different than the starting molecule are possibly formed; whereas indirect photolysis happens when the pesticide reacts with a photogenerated reactive oxygen species due to the presence of dissolved organic matter especially in water bodies. The singlet oxygen and [•]OH are important reactants in this process [214][215][216].

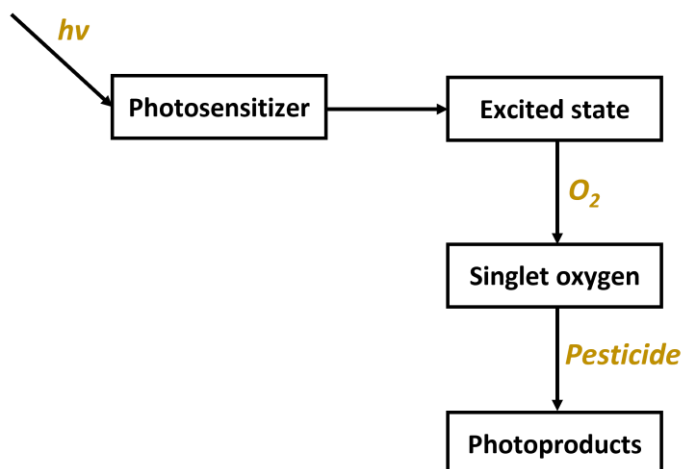


Figure 15 A simplified diagram showing a photosensitized reaction where the photosensitizer produces a singlet oxygen species.

Fig.20 shows that when a pesticide absorbs light, this molecule in the ground state (S_0) gets excited to the first excited singlet state (S_1) where several processes can further take place. S_1 can be deactivated through the nonradiative internal conversion (IC) to S_0 , through the emission of fluorescence (Fl), via an intersystem crossing (ISC) from S_1 to T_1 , or by undergoing further reactions forming photoproducts. T_1 is much long-lived than S_1 and has thus more time to undergo reactions with other reactants (O_2 , starting chemical, etc...).

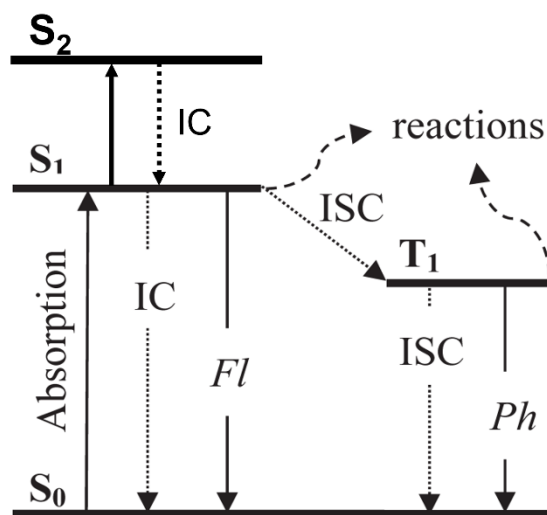


Figure 16 Simplified state energy diagram, source: [216], [217].

In solution

Leaching and run-off processes, for example, help pesticides reach waterbodies thus posing a threat to humans and the environment [218] [219]. Subsequently, they can be phototransformed in sunlit waters which can be the major transformation pathway for many pesticides besides hydrolysis and other biological reactions [220]. Bentazon didn't undergo any degradation in the dark but was phototransformed when irradiated by UV light in the collected lake/paddy water [221]. In general, photodegradation is mostly due to direct photolysis. Dissolved organic matter (DOM) that is ubiquitous in surface waters has a dual effect. It can inhibit the photolysis due to a competition for light between the pesticide itself and the chromophoric groups found in DOMs. Conversely, it can enhance the photodegradation because it generates reactive species such as excited states, $\cdot\text{OH}$, singlet oxygen radicals that are able to react with pesticides [222]. Many studies have been and are still undertaken to investigate these reactions.

On solid/leaves surfaces

Studies on solid surfaces mostly investigate the pesticides photodegradation on glass (simplest model) and silica gel to compare their photoreactivity. Pesticides degrade more slowly on glass since they form a thicker layer which causes light attenuation [223]. Usually, pesticides deposited on silica gel experience photoinduced homolytic cleavage that produces radicals, and photodegradation further takes place. A study involving benzyl phenylacetate concluded that radicals separated very well on silica gel surface via a translational motion [224]. Similarly, azobis(isobutyronitrile) under UV light and on silica surfaces was degraded with the formation of radicals according to another study [225]. These experiments demonstrate the degradation of pesticides on solid surfaces; however, they do not exactly represent the possible processes taking place on the surface of plants since the reaction environment is totally different from cuticular surface. Plant surfaces themselves are complex media influenced by several factors.

One study took into consideration the photodegradation of 2 herbicides (mesotrione and nicosulfuron) on thin wax films [222]. Previous studies on mesotrione show its photolysis in aquatic media as well as on wax films [226] [227]. Photoproducts of mesotrione were due to photohydrolysis since water molecules in the air/film interface can be present and involved in this

reaction, photocyclisation, or photoreduction; while those of nitrosulfuron were mainly because of hydroxylation, photoextrusion (loss of SO₂), and photohydrolysis [222]. These photochemical reactions were also reported with other herbicides on wax films [228][229]. The photoreactivity of both herbicides was faster when present as formulated molecules. This owes to the additives which facilitates their spreading and hence the absorption of light. In addition to that, the mixture of these 2 compounds leads to a further increase in photoreactivity due to the additive effect of additives or the photosensitizing effect. Experiments on wax films can be more representative of the cuticular surfaces than glass/silica; but the wax films still lack some characteristics or components naturally found in leaves. The structures of pesticides are present in **Fig.21**.

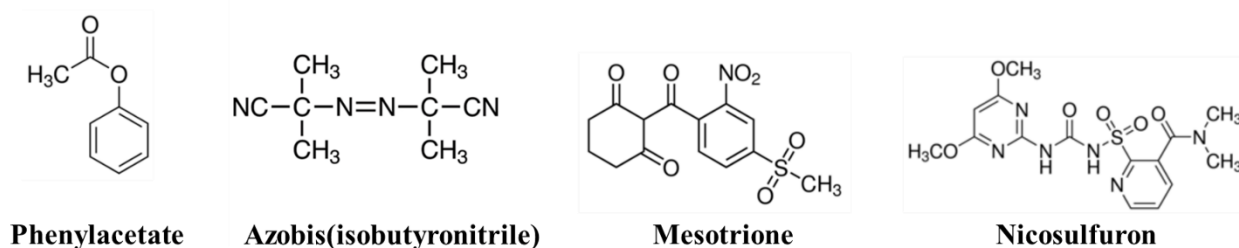


Figure 17 Chemical structures of the pesticides.

To have a better approach to cuticular surfaces, a study used the solution of soaked corn leaves as a deposit on Petri dishes. The solution was left to evaporate until a layer of plant wax remained on the surface. Dicamba, a herbicide, was then applied on the dishes and left to evaporate which thus created a solid layer [230]. Irradiating the dishes revealed dicamba photodegradation with the formation of photoproducts. The photochemical reaction is however slower on the solid/inert surfaces than in aqueous solutions; this is probably since dicamba is in the solid state. Nevertheless, when the solution of dicamba is applied as a formulation, faster photodegradation takes place. This is related to the presence of certain surfactants lowering the surface tension and other chemicals which helps the herbicide to spread on the surfaces. The matrix environment influences the photodegradation rates and photoproducts produced [231][232][233]. For instance, an experiment done with the same herbicide and irradiation conditions directly on glass Petri dishes showed that no degradation takes place. Epicuticular wax surfaces are a complex medium; pesticides deposited on them can undergo slow photolysis (screening effect) or a fast one

(photosensitization). They can be good candidates to represent the wax surfaces of plants but still lack some properties like the effect of volatiles or the real cuticular structure.

Plant surfaces, in other words leaves surfaces, are the first reaction site for pesticides. Sunlight can reach those surfaces provoking photodegradation [216]. For example, a study where bifenazate, an insecticide, was deposited on green pepper showed that bifenazate underwent photodegradation in dark and under irradiation [234]. The autoxidation was linked to the presence of water in the pepper or to transpiration. Various degradation products were detected with a major one formed by the elimination of 2H atoms. The photodegradation on green pepper skin needed water, oxygen, and a protic solvent. Another, demonstrated the phototransformation of Acibenzolar-S-methyl (BTH) when present on apple leaves and under irradiation (**Fig.22**) [231].

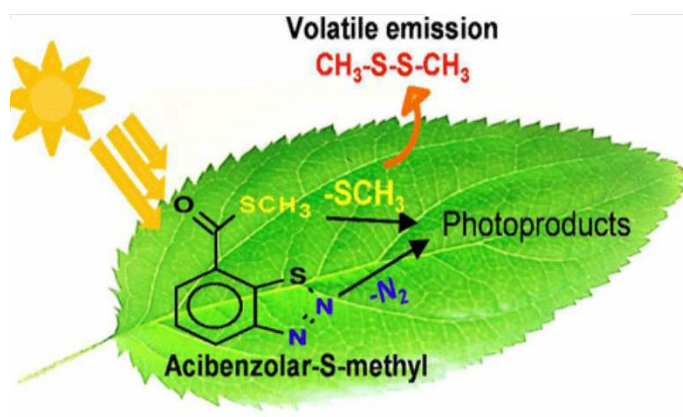
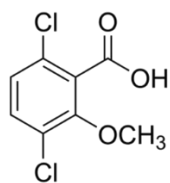
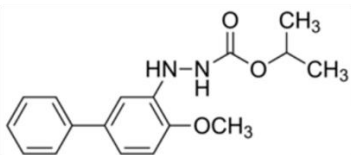


Figure 18 The reaction of a pesticide under sunlight [231].

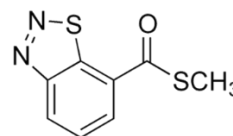
Around 75 % of BTH was degraded after 4 h; contrastingly to wax films which showed that only 10 % degradation was reported when BTH was deposited on them. The nature of the apple leaves was responsible for this difference i.e. the metabolism in the leaf, chemistry of the cuticle, formation of reactive species due to stress, and the emission of VOCs. Interestingly, volatile photoproducts arising from BTH were detected showing that pesticides can as well produce VOCs. Contrary to inert surfaces, ‘plants leaves’ is an ‘alive’ medium influenced by many factors such the anatomy of the leaf, wax, weather, etc. [216]. **Fig.23** shows the structures of studied pesticides.



Dicamba



Bifenazate



Acibenzolar-S-methyl

Figure 19 Chemical structures of the studied pesticides

Pesticides + VOCs

In addition to the previous interactions, it is necessary to investigate how pesticides would react with the VOCs naturally emitted by plants or crops. A research considered the interaction between an insecticide and BVOCs produced by orange trees [235]. The study was done under sunlight where results showed that this combination of BVOCs and pesticide formed O₃ and secondary organic aerosols (SOA). Those two highly contribute to the formation of smog. Having enough knowledge about atmospheric interactions involving pesticides facilitates the estimation of their impact on the environment as well as the selection of ‘environmentally friendly’ pesticides.

Since green roofs are ecofriendly, attention should be given to the interaction of the volatile metabolites of plants implemented and pesticides sprayed so that they don’t lose this beneficial characteristic. Hence, the necessity to understand this interaction is crucial especially with VOC-emitting green roof plants (since not all produce significant levels of VOCs).

1.5.4 Conclusion/scope of work

Holding many uncertainties, models should be carefully considered and more attention should be given to experimental/laboratory research in order to obtain quantitative results. In the first part of our study, we developed an experimental setup including flow meters, stainless steel reactors, an irradiation system, and analyzers to measure the uptake performances of certain plant species implemented on extensive green roofs. Two air pollutants with deleterious health and environmental effects were chosen to be studied: NO_x and O₃. Special attention was devoted to finding a long-lasting stable source of these 2 pollutants. An O₃ generator equipped with a UV pen-ray lamp was used as a source of O₃. However, the NO_x source used was based on a study done in

our team involving a solution of irradiated Imidacloprid which produced NO_x (NO + NO₂) with NO₂ being the major product [236].

In the second part, 13 different plants were selected for preliminary experiments. Their uptakes were noted by calculating the difference in the initial concentrations (coming from the source) and the ones read on the analyzers after passing through the reactors containing the plants. Following screening, the best performing species were selected: *Sedum sexangulare*, *Thymus vulgaris*, and *Heuchera Americana L.* Scanning electron microscopy was performed to characterize cuticular surfaces, headspace gas chromatography coupled with mass-selective detection (HS-GC-MS) was undertaken for the VOC analysis, Automated Thermal Desorption-Gas Chromatography coupled to Mass Spectrometry (ATD-GC-MS) analysis was done to identify possible reactions taking place in the gas phase, and a nitrous acid (HONO) trap was employed to detect the potential reaction between water and NO₂. All these factors were taken into consideration to deeply understand the uptake mechanisms. Nonetheless, experiments were done on both detached leaves and full size plant to test the feasibility of extrapolation; effect of soil was also evaluated.

The third part was dedicated to study the interactions between two abundantly used pesticides (Imidacloprid and Chlorothalonil, **Fig.24**) and *Thymus Vulgaris* volatiles after irradiation. Those pesticides have the potential to react with volatiles. Chlorothalonil, for example, has photooxidant properties due to the formation of its triplet excited state or singlet oxygen after irradiation; while Imidacloprid is a good nitrosating/nitrating chemical through the release of NO and NO₂. Experiments were conducted in solution to study the potential of the interaction, and then on *Thymus Vulgaris* leaves to approach realistic conditions. HS-GC-MS was performed to detect gaseous photoproducts, and GC-MS and liquid chromatography-high resolution mass spectrometry (LC-MS) to determine other formed photoproducts. The photochemical reactivity of these two pesticides in the presence of the volatiles was studied with the possible photooxidation or nitrosating/nitrating properties in case of Chlorothalonil and Imidacloprid respectively.

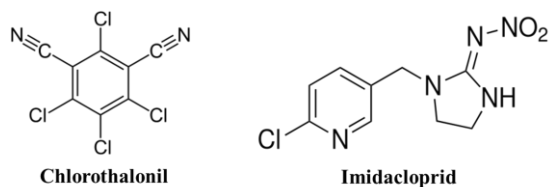


Figure 20 Chemical structures of Chlorothalonil and Imidacloprid.

References:

- [1] J. Lelieveld, J. S. Evans, M. Fnais, D. Giannadaki, and A. Pozzer, "The contribution of outdoor air pollution sources to premature mortality on a global scale," *Nature*, pp. 367–371, 2015.
- [2] S. Cai, Q. Ma, S. Wang, B. Zhao, M. Brauer, A. Cohen, R.V. Martin, Q. Zhang, Q. Li, Y. Wang, J. Hao, J. Frostad, M.H. Forouzanfar, R.T. Burnett, "Impact of air pollution control policies on future PM2.5 concentrations and their source contributions in China," *Journal of Environmental Management*, pp. 124–133, 2018.
- [3] Q. Ma S. Cai, S. Wang, B. Zhao, M. Brauer, A. Cohen, R.V. Martin, Q. Zhang, Q. Li, Y. Wang, J. Hao, J. Frostad, M.H. Forouzanfar, R.T. Burnett, "Impacts of coal burning on ambient PM2.5 pollution in China," *Atmospheric Chemistry and Physics*, pp. 4477–4491, 2017.
- [4] M. Brauer *et al.*, "Ambient Air Pollution Exposure Estimation for the Global Burden of Disease," *Environmental Science and Technology*, pp. 79–88, 2016, 2013.
- [5] C. Weber, "Ecosystem Services Provided by Urban Vegetation: A Literature Review," *Urban Environment*, pp. 119–131, 2013
- [6] H. Akbari, M. Pomerantz, and H. Taha, "Cool surfaces and shade trees to reduce energy use and improve air quality in urban areas," *Solar Energy*, pp. 295–310, 2001
- [7] D. B. Rowe, "Green roofs as a means of pollution abatement," *Environmental Pollution*, pp. 2100–2110, 2011.
- [8] J. Johnston, J. Newton, "A guide to using plants on roofs, walls and pavements," *Building green*, pp. 45-74, 2004.
- [9] Z. Tan, L. Keding, J. Meiqing, S. Rong, D. Huabin, Z. Limin, X. Shaodong, T. Qinwen, Z. Yaunhang, "Exploring ozone pollution in Chengdu, southwestern China: A case study from radical chemistry to O3-VOC-NOx sensitivity," *Science of the Total Environment*, pp. 775–786, 2018.
- [10] D. L. Mauzerall, B. Sultan, N. Kim, and D. F. Bradford, "NOx emissions from large point sources: Variability in ozone production, resulting health damages and economic costs," *Atmospheric Environment*, pp. 2851–2866, 2005.

- [11] Y. L. Yung, A. Y. T. Lee, F. W. Irion, W. B. DeMore, and J. Wen, "Carbon dioxide in the atmosphere: Isotopic exchange with ozone and its use as a tracer in the middle atmosphere," *Journal of Geophysical Research Atmospheres*, pp. 10857–10866, 1997.
- [12] R. Atkinson, "Atmospheric Reactions of Alkoxy and β -Hydroxyalkoxy Radicals," *International Journal of Chemical Kinetics*, pp. 99-111, 1997.
- [13] R. Atkinson, "Atmospheric chemistry of VOCs and NO_x," *Atmospheric Environment*, pp. 2063- 2101, 1998.
- [14] T. S. Fredericksen, J. M. Skelly, K. C. Steiner, T. E. Kolb, and K. B. Kousterick, "Size-mediated foliar response to ozone in black cherry trees," *Environmental pollution*, pp. 53-63, 1996.
- [15] Y. Hoshika, K. Omasa, and E. Paoletti, "Whole-tree water use efficiency is decreased by ambient ozone and not affected by O₃-induced stomatal sluggishness," *PLOS One*, pp. 1-8, 2012.
- [16] A. Calatayud, D. J. Iglesias, M. Talón, and E. Barreno, "Effects of 2-month ozone exposure in spinach leaves on photosynthesis, antioxidant systems and lipid peroxidation," *Plant Physiology and Biochemistry*, pp. 839–845, 2003.
- [17] G. Torsethaugen, E. J. Pell, and S. M. Assmann, "Ozone inhibits guard cell K⁺ channels implicated in stomatal opening," *Proceedings of the National Academy of Sciences of the United States of America*, pp. 13577-13582, 1999.
- [18] A. C. Heiden, T. Hoffmann, J. Kahl, D. Kley, D. Klockow, C. Langebartels, H. Mehlhorn, H. Sandermann, M. Schraudner, G. Schuh, J. Wildt, "Emission of volatile organic compounds from ozone-exposed plants," *Ecological applications*, pp. 1160-1167, 1999.
- [19] S. J. Roselle, "Effects of biogenic emission uncertainties on regional photochemical modeling of control strategies," *Atmospheric Environment*, pp. 1757-1772, 1994.
- [20] M. A. Gómez-García, V. Pitchon, and A. Kiennemann, "Pollution by nitrogen oxides: An approach to NO_x abatement by using sorbing catalytic materials," *Environment International*, pp. 445–467, 2005.
- [21] K. Skalska, J. S. Miller, S. Ledakowicz, "Effectiveness of nitric oxide ozonation," *Chemical Papers*, pp. 193–197, 2011.

- [22] K. Skalska, J. S. Miller, and S. Ledakowicz, "Trends in NO_x abatement: A review," *Science of the Total Environment*, pp. 3976–3989, 2010.
- [23] J. Yang, Q. Yu, P. Gong, "Quantifying air pollution removal by green roofs in Chicago," *Atmospheric Environment*, pp. 7266–7273, 2008.
- [24] A.C. Hill, "Vegetation: A Sink for Atmospheric Pollutants," *Journal of the Air Pollution Control Association*, pp. 341–346, 1971.
- [25] US Environmental Protection Agency, "Particulate Matter | Air & Radiation |", US EPA, 2011.
- [26] A. Middlebrook, J. Turner, P.A. Solomon, "Special issue of Atmospheric Environment for Particulate Matter: Atmospheric Sciences, Exposure, and the Fourth Colloquium on PM and Human Health," *Atmospheric Environment*, pp. 5179-5181, 2004.
- [27] US Environmental Protection Agency, "Particulate Matter (PM_{2.5}) Trends," <https://www.epa.gov/air-trends/particulate-matter-pm25-trends>.
- [28] World Health Organization, "Air quality guidelines. Global update 2005. Particulate matter, ozone, nitrogen dioxide and sulfur dioxide," 2006.
- [29] World Health Organization, "Health aspects of air pollution with particulate matter, ozone and nitrogen dioxide," 2003.
- [30] D. Fowler, J. N. Cape, M. H. Unsworth, "Deposition of atmospheric pollutants on forests," *Philosophical Transactions - Royal Society of London, B*, pp. 247–265, 1989.
- [31] D. J. Nowak, D. E. Crane, J. C. Stevens, "Air pollution removal by urban trees and shrubs in the United States," *Urban Forestry and Urban Greening*, pp. 115–123, 2006.
- [32] J. Yang, J. McBride, J. Zhou, Z. Sun, "The urban forest in Beijing and its role in air pollution reduction," *Urban Forestry and Urban Greening*, pp. 65–78, 2005.
- [33] A. Sæbø, R. Popek, B. Nawrot, H. M. Hanslin, H. Gawronska, and S. W. Gawronski, "Plant species differences in particulate matter accumulation on leaf surfaces," *Science of the Total Environment*, pp. 347–354, 2012.
- [34] "Air pollution: Consequences and actions for the UK, and beyond," *The Lancet*, pp. 817, 2016.

- [35] A. Ghorani-Azam, B. Riahi-Zanjani, M. Balali-Mood, "Effects of air pollution on human health and practical measures for prevention in Iran," *Journal of Research in Medical Sciences*, pp. 1-12, 2016.
- [36] N. Zhou, Z. Cui, S. Yang, X. Han, G. Chen, Z. Zhou, C. Zhai, M. Ma, L. Li, M. Cai, Y. Li, L. Ao, W. Shu, J. Liu, J. Cao, "Air pollution and decreased semen quality: A comparative study of Chongqing urban and rural areas," *Environmental Pollution*, pp. 145–152, 2014.
- [37] R. D. Brook, S. Rajagopalan, C.A. Pope, J.R. Brook, A. Bhatnagar, A.V. Diez-Roux, F. Holguin, Y. Hong, R.V. Luepker, M.A. Mittleman, A. Peters, D. Siscovick, S.C. Smith, L. Whitsel, J.D. Kaufman, "Particulate matter air pollution and cardiovascular disease: An update to the scientific statement from the american heart association," *Circulation*, pp. 2331–2378, 2010.
- [38] M. Zhong, F. Chen, E. Saikawa, "Sensitivity of projected PM_{2.5} and O₃-related health impacts to model inputs: A case study in mainland China," *Environment International*, pp. 256–264, 2019.
- [39] A. Chaloulakou, I. Mavroidis, I. Gavriil, "Compliance with the annual NO₂ air quality standard in Athens. Required NO_x levels and expected health implications," *Atmospheric Environment*, pp. 454–465, 2008.
- [40] Q. Chao, A. Feng, "Scientific basis of climate change and its response," *Global Energy Interconnection*, pp. 420–427, 2018.
- [41] A. Albert, "[Mise à jour] nuage pollution s'atténue sur Clermont-Ferrand et Riom", 2016.
- [42] H. H. Kim, "Urban heat island," *International Journal of Remote Sensing*, pp. 2319–2336, 1992.
- [43] K. Fuladlu, M. Riza, M. İlkan, "The effect of rapid urbanization on the physical modification of urban area," *5th International Conference S.ARCH*, 2018.
- [44] P.E.B. dos Santos, "Urbanization and climate change: buildings and GHG", *Academia.edu*, pp. 1-11, 2015."
- [45] D.J. Sailor, "Simulated urban climate response to modifications in surface albedo and vegetative cover," *Journal of Applied Meteorology*, pp. 1694-1704, 1995.
- [46] A. Synnefa, A. Dandou, M. Santamouris, M. Tombrou, N. Soulakellis, "On the use of cool materials as a heat island mitigation strategy," *Journal of Applied Meteorology and Climatology*, pp. 2846–2856, 2008.

- [47] A. J. M. Baker, "Terrestrial higher plants which hyperaccumulate metallic elements, A Review of their distribution, ecology, and Phytochemistry," *Biorecovery*, pp. 81-126, 1989.
- [48] E. Palomo, D. Barrio, "Analysis of the green roofs cooling potential in buildings," *Energy and Buildings*, pp. 179-193, 1998.
- [49] S. Saiz, C. Kennedy, B. Bass, K. Pressnail, "Comparative life cycle assessment of standard and green roofs," *Environmental Science and Technology*, pp. 4312–4316, 2006.
- [50] A. K. Singh and A. Bhargawa, "Atmospheric burden of ozone depleting substances (ODSs) and forecasting ozone layer recovery," *Atmospheric Pollution Research*, pp. 802–807, 2019.
- [51] S. Kellmann *et al.*, "Global CFC-11 (CCl₃F) and CFC-12 (CCl₂F₂) measurements with the Michelson Interferometer for Passive Atmospheric Sounding (MIPAS): Retrieval, climatologies and trends," *Atmospheric Chemistry and Physics*, pp. 11857–11875, 2012.
- [52] J. K. Angell, J. Korshover-Air, "Quasi-biennial and long-term fluctuations in total ozone," *Monthly Weather Review*, pp. 426-443, 1973.
- [53] E. Du, D. Dong, X. Zeng, Z. Sun, X. Jiang, and W. de Vries, "Direct effect of acid rain on leaf chlorophyll content of terrestrial plants in China," *Science of the Total Environment*, pp. 764–769, 2017.
- [54] A. Singh, M. Agrawal, "Acid rain and its ecological consequences," *Journal of Environmental Biology*, pp. 15-24, 2008.
- [55] H. Wei, W. Liu, J. Zhang, and Z. Qin, "Effects of simulated acid rain on soil fauna community composition and their ecological niches," *Environmental Pollution*, pp. 460–468, 2017.
- [56] World Health Organization, "Air quality guidelines. Global update 2005. Particulate matter, ozone, nitrogen dioxide and sulfur dioxide," 2006.
- [57] "Council directive 1999/30/EC of 22 April 1999 relating to limit values for sulphur dioxide, nitrogen dioxide and oxides of nitrogen, particulate matter and lead in ambient air," *Official Journal of the European Union*, pp. 41–60, 1999.
- [58] US Environmental protection agency, "Review of the National Ambient Air Quality Standards for Particulate Matter," *Federal Register*, pp. 24094-24144, 2005.

- [59] S. Tanaka, "Environmental regulations on air pollution in China and their impact on infant mortality," *Journal of Health Economics*, pp. 90–103, 2015.
- [60] B. Guan, R. Zhan, H. Lin, Z. Huang, "Review of state of the art technologies of selective catalytic reduction of NO_x from diesel engine exhaust," *Applied Thermal Engineering*, pp. 395–414, 2014.
- [61] J. Chen, C. sun Poon, "Photocatalytic construction and building materials: From fundamentals to applications," *Building and Environment*, pp. 1899–1906, 2009.
- [62] L. Cassar, A. Beeldens, N. Pimpinelli, G.L. Guerrini, "Photocatalysis of cementitious materials," *International RILEM Symposium on Photocatalysis, Environment and Construction Materials*, pp. 131-145, 2007.
- [63] A. Fujishima and X. Zhang, "Titanium dioxide photocatalysis: present situation and future approaches," *Comptes Rendus Chimie*, pp. 750–760, 2006.
- [64] M. Y. Ghaly, T. S. Jamil, I. E. El-Seesy, E. R. Souaya, R. A. Nasr, "Treatment of highly polluted paper mill wastewater by solar photocatalytic oxidation with synthesized nano TiO₂," *Chemical Engineering Journal*, pp. 446–454, 2011.
- [65] T. Feng, G.S. Feng, L. Yan, J.H. Pan, "One-dimensional nanostructured TiO₂ for photocatalytic degradation of organic pollutants in wastewater," *International Journal of Photoenergy*, pp. 1-14, 2014.
- [66] "Reducing Air Pollution." *Lumen*, <https://courses.lumenlearning.com/sanjac-earthscience/chapter/reducing-air-pollution/>.
- [67] B. Barua, S. Barua, "COVID-19 implications for banks: evidence from an emerging economy," *SN Business & Economics*, pp. 1-28, 2021.
- [68] S. Barua, "Understanding Coronanomics: The economic implications of the coronavirus (COVID-19) pandemic." *Social Science Research Network*, pp. 1-44, 2021.
- [69] S. Muhammad, X. Long, M. Salman, "COVID-19 pandemic and environmental pollution: A blessing in disguise?" *Science of the Total Environment*, pp. 1-5, 2020.
- [70] M. Wang, F. Liu, M. Zheng, "Air quality improvement from COVID-19 lockdown: evidence from - China," *Air Quality, Atmosphere, & Health*, pp. 591-604, 2021.

- [71] B. Lin, J. Zhu, "Changes in urban air quality during urbanization in China," *Journal of Cleaner Production*, pp. 312–321, 2018.
- [72] J.E. Gray, "Plant Development: Three Steps for Stomata," *Current Biology*, pp. 213-215, 2007.
- [73] I.R. Cowan, G.H. Troughton, "The Relative Role of Stomata in Transpiration and Assimilation," *Planta*, pp. 325-336, 1971.
- [74] T.A. Mansfield, P.H. Freer-Smith, "Chapter 10: The role of stomata in resistance mechanisms," pp. 131-146, 1984.
- [75] M.F. Robinson, J. Health, T.A. Mansfield, "Disturbances In stomatal behaviour caused by air pollutants," *Journal of Experimental Botany*, pp. 461-469, 1998.
- [76] B. Theone, P. Schröder, H. Papen, A. Egger, H. Rennenberg, "Absorption of atmospheric NO₂ by spruce (*Picea abies* L. Karst) trees. I. NO₂ influx and its correlation with nitrate reduction," *New Phytologist*, pp. 575-585, 1991.
- [77] A. Geßler, M. Rienks, H. Rennenberg, "NH₃ and NO₂ fluxes between beech trees and the atmosphere-correlation with climatic and physiological parameters," *New Phytologist*, pp. 539-560, 2000.
- [78] A. R. Wellburn, "Why are atmospheric oxides of nitrogen usually phytotoxic and not alternative fertilizers?," *New Phytologist*, pp. 395-429, 1990.
- [79] G. Kerstiens, R. Federholzner, K.J. Lenzian, "Dry deposition and cuticular uptake of pollutant gases," *Agriculture, Ecosystems and Environment*, pp. 239-253, 1992.
- [80] P. Weber, H. Rennenberg, "Dependency of nitrogen dioxide (NO₂) fluxes to wheat (*Triticum aestivum* L.) leaves from NO₂ concentration, light intensity, temperature and relative humidity determined from controlled dynamic chamber experiments," *Atmospheric Environment*, pp. 3001-3009, 1996.
- [81] J. Burkhardt, J. Gerchau, J. Burkhardt, R. Eiden, "Thin water films on coniferous needles (With an Appendix 'A new device for the study of water vapour condensation and gaseous deposition to plant surfaces and particle samples'," *Atmospheric Environment*, pp. 2001-2017, 1994.
- [82] P. A. Addison, S. S. Malhotra, A. A. Khan, "Effect of Sulfur Dioxide on Woody Boreal Forest Species Grown on Native Soils and Tailings," *Journal of Environmental Quality*, pp. 333-336, 1984.

- [83] T. Reichenauer, H.R. Bolhar-Nordenkamp, U. EHRlich, G. Soja, W.F. Postl, F. Halbwachs, "The influence of ambient and elevated ozone concentrations on photosynthesis in *Populus nigra*," *Plant, Cell, and Environment*, pp. 1061-1069, 1997.
- [84] K. Okano, T. Machida, T. Totsuka, "Differences in Ability of NO₂ Absorption in Various Broad-leaved Tree Species," *Environmental Pollution*, pp. 1-17 1989.
- [85] "What is Stomata?" <https://www.tech-faq.com/stomata.html>
- [86] A. Przybysz, A. Sæbø, H.M. Hanslin, S.W. Gawroński, "Accumulation of particulate matter and trace elements on vegetation as affected by pollution level, rainfall and the passage of time," *Science of the Total Environment*, pp. 360–369, 2014.
- [87] J. Burkhardt, S. Pariyar, "Particulate pollutants are capable to 'degrade' epicuticular waxes and to decrease the drought tolerance of Scots pine (*Pinus sylvestris* L.)," *Environmental Pollution*, pp. 659–667, 2014.
- [88] M.W. Gallagher, K.M. Beswick, J. Duyzer, H. Westrate, T.W. Choularton, P. Hummelshoj, "Measurements of aerosol fluxes to spruce forest using a micrometeorological technique," *Atmospheric Environment*, pp. 359-373, 1997.
- [89] D. Fowler, U. Skiba, E. Nemitz, F. Choubedar, "Measuring aerosol and heavy element deposition on urban woodland and grass using inventories of ²¹⁰Pb and element concentrations in soil," *Water Air and Soil Pollution*, pp. 483-499, 2004.
- [90] E.G. McPherson, D.J. Nowak, R.A. Rowntree, "Chicago's Urban Forest Ecosystem: Results of the Chicago Urban Forest Climate Project," General technical report NE-186, 1994.
- [91] D.J. Nowak, P.J. McHale, M. Ibarra, D. Crane, J. C. Stevens, and C.J. Luley, "Modeling the effects of urban vegetation on air pollution," *Air Pollution Modeling and Its Application XII*, pp. 399-407, 1998.
- [92] G. Kerstiens, K.J. Lenzian, "Interactions between ozone and plant cuticle I. Ozone deposition and permeability," *New Phytologist*, pp. 13-19, 1989.
- [93] O. Clifton, "Removal of Ozone Air Pollution by Terrestrial Ecosystems." 2020, <https://eos.org/editors-vox/removal-of-ozone-air-pollution-by-terrestrial-ecosystems>.

- [94] F. Shao, L. Wang, F. Sun, G. Li, L. Yu, Y. Wang, X. Zeng, H. Yan, L. Dong, Z. Bao, "Study on different particulate matter retention capacities of the leaf surfaces of eight common garden plants in Hangzhou, China," *Science of the Total Environment*, pp. 939–951, 2019.
- [95] C. E. Vickers, J. Gershenzon, M. T. Lerdau, F. Loreto, "A unified mechanism of action for volatile isoprenoids in plant abiotic stress," *Nature Chemical Biology*, pp. 283–291, 2009.
- [96] I.T. Baldwin, R. Halitschke, A. Paschold, C.C. von Dahl, C.A. Preston, "Volatile Signaling in Plant-Plant Interactions: "Talking Trees" in the Genomics Era," *Science*, pp. 812-815, 2006.
- [97] B.B. Simpson, J.L. Neff, "Floral Rewards: Alternatives to Pollen and Nectar," *Annals of the Missouri Botanical Garden*, pp. 301-322 1981.
- [98] C. Díaz-Castelazo, V. Rico-Gray, P.S. Oliveira, M. Cuautle, "Extrafloral nectary-mediated ant-plant interactions in the coastal vegetation of Veracruz, Mexico: Richness, occurrence, seasonality, and ant foraging patterns," *Ecoscience*, pp. 472–481, 2004.
- [99] L. Wang, A. Liu, Z. Zhang, B. Zhao, Y. Xia, and Y. Tan, "Catalytic ozonation of thymol in reverse osmosis concentrate with core/shell Fe₃O₄@SiO₂@Yb₂O₃ catalyst: Parameter optimization and degradation pathway," *Chinese Journal of Chemical Engineering*, pp. 665–670, 2017.
- [100] C.J. Weschler, H.C. Shields, "Production of the Hydroxyl Radical in Indoor Air," *Environmental Science & Technology*, pp. 3250-3258, 1996.
- [101] M. Skwarczyński, B. Poędnik, M. Dudzińska, P. Niewęglowski, "Determination of odor detection threshold for the mixtures of n-butanol, indoor air and ozone," *Proceedings of ECOpole*, pp. 107-111, 2008.
- [102] C.J. Weschler, H.C. Shields, "Indoor ozone/terpene reactions as a source of indoor particles," *Atmospheric environment*, pp. 2301-2312, 1999.
- [103] C. Chen, Y. Zhao, Y. Zhang, and B. Zhao, "Source strength of ultrafine and fine particle due to Chinese cooking," in *Procedia Engineering*, pp. 2231–2237, 2017.
- [104] K. Griesbau, V. Miclaus, I.C. Jung, "Isolation of Ozonides from Gas-Phase Ozonolyses of Terpenes," *Environmental Science and Technology*, pp. 647-649, 1998.
- [105] C.J. Weschler, H.C. Shields, "Measurements of the Hydroxyl Radical in a Manipulated but Realistic Indoor Environment," *Environmental Science and Technology*, pp. 3719-3721, 1997.

- [106] W.L. Chameides, R.W. Lindsay, J. Richardson, C.S. Kiang, "The role of biogenic hydrocarbons in urban photochemical smog: Atlanta as a case study," *Science*, pp. 1473-1475, 1988.
- [107] F. Sauer, C. Schafer, P. Neeb, O. Horie, G.K. Moortgat, "Formation of hydrogen peroxide in the ozonolysis of isoprene and simple alkenes under humid conditions," *Atmospheric Environment*, pp. 229-241, 1999.
- [108] H.E. Haggstad, "Origin of Bel-W3, Bel-C and Bel-B tobacco varieties and their use as indicators of ozone," *Environmental Pollution*, pp. 264-291, 1991.
- [109] S.K. Brown, M.R. Sim, M.J. Abramson, C.N. Gray, "Concentrations of Volatile Organic Compounds in Indoor Air-A Review," *Indoor Air*, pp. 123-134, 1994.
- [110] P. Wolkoff, "Volatile Organic Compounds Sources, Measurements, Emissions, and the Impact on Indoor Air Quality," *Indoor Air*, pp. 9-73, 1995.
- [111] Y. Shu, R. Atkinson, "Rate Constants for the Gas-Phase Reactions of O₃ with a Series of Terpenes and OH Radical Formation from the O₃ Reactions with Sesquiterpenes at 296 ± 2 K," *International Journal of Chemical Kinetics*, pp. 1193-120, 1994.
- [112] KWTham, SCSekhar, M. Amanullah, H.K. Lee, D. Cheong, "A detailed study of Volatile Organic compounds of 5-air conditioned building in Singapore," *Indoor Air*, pp. 561-566, 2002.
- [113] L.S. Sheldon, D.A. Whitaker, R.G. Hetes, J.A. Calcagni, K.W. Leovic, J.N. Baskir, "Measurement of Indoor Air Emissions from Dry-Process Photocopy Machines," *Journal of the Air and Waste Management Association*, pp. 821-829, Sep. 1996.
- [114] C.J. Weschler, H.C. Shields, "Potential interactions among indoor plants," *Atmospheric Environment*, pp. 3487-3495, 1997.
- [115] National Research Council, "Human Exposure Assessment for Airborne Pollutants: Advances and Opportunities," 1991.
- [116] H.Li, M.Riva, P.Rentala, L.Heikkinen, K.Daellenbach, J.E. Krechmer, P-M. Flaud, D. Wornsnop, M. Kulmala, E. Villenave, E. Pauraudin, M. Ehn, F. Bianchi, "Terpenes and their oxidation products in the French Landes forest: Insights from Vocus PTR-TOF measurements," *Atmospheric Chemistry and Physics*, pp. 1941-1959, 2020.

- [117] R. Atkinson, J. Arey, "Gas-phase tropospheric chemistry of biogenic volatile organic compounds: A review," in *Atmospheric Environment*, pp. 197–219, 2003.
- [118] S.E. Paulson, R.C. Flagan, J.H. Seinfeld, "Atmospheric Photooxidation of Isoprene Part 2: The Ozone-Isoprene Reaction," *International Journal of Chemical Kinetics*, pp. 103-125, 1992.
- [119] E.C. Tuazon, S.M. Aschmann, J. Arey, R. Atkinson, "Products of the Gas-Phase Reactions of O₃ with a Series of Methyl-Substituted Ethenes," *Environmental Science and Technology*, pp. 3004-3009, 1997.
- [120] S.E. Paulson, A.D. Sen, P. Liu, J.D. Fenske, M.J. Fox, "Evidence for formation of OH radicals from the reaction of O₃ with alkenes in the gas phase," *Geophysical Research Letters*, pp. 3193–3196, 1997.
- [121] T. Pfeiffer, O. Forberich, F.J. Comes, "The contribution of the ozonolysis of terpenes to tropospheric OH concentrations," *Canadian Journal of Physics*, pp. 351-358, 2001.
- [122] European Economic Area "Air quality in Europe - 2014 report (EEA Report No 5/2014)", <https://www.eea.europa.eu/publications/air-quality-in-europe-2014>.
- [123] É. Chatignoux, S. Host, "Expositions à la pollution atmosphérique et recours aux urgences pour pathologies respiratoires chez les enfants en Île-de-France," *Observatoire régional de santé Île-de-France*, ORS, pp. 1-8, 2013.
- [124] E. Boonen, A. Beeldens, "Recent photocatalytic applications for air purification in Belgium," *Coatings*, pp. 553–573, 2014.
- [125] J. Ângelo, L. Andrade, L.M. Madeira, A. Mendes, "An overview of photocatalysis phenomena applied to NO_x abatement," *Journal of Environmental Management*, pp. 522–539, 2013.
- [126] B.A. Currie, B. Bass, "Estimates of air pollution mitigation with green plants and green roofs using the UFORE model," *Urban Ecosystems*, pp. 409–422, 2008.
- [127] W.H. Smith, "Air pollution and forests: interactions between air contaminants and forest ecosystems," 1981 by Springer-Verlag New York inc.
- [128] W. Selmi, C. Weber, E. Rivière, N. Blond, L. Mehdi, D. Nowak, "Air pollution removal by trees in public green spaces in Strasbourg city, France," *Urban Forestry and Urban Greening*, pp. 192–201, 2016.

- [129] F. Baró, L. Chaparro, E. Gómez-Baggethun, J. Langemeyer, D.J. Nowak, J. Terradas, "Contribution of ecosystem services to air quality and climate change mitigation policies: The case of urban forests in Barcelona, Spain," *Ambio*, pp. 466–479, 2014.
- [130] K. Rogers, T. Jarratt, D. Hansford, "Torbay's urban forest : assessing urban forest effects and values : a report on the findings from the UK i-Tree Eco pilot project," *Treeconomics*, pp. 1-46, 2011.
- [131] M.T. Benjamin, A.M. Winert, "Estimating the ozone-forming potential of urban trees and shrubs," *Atmospheric Environment*, pp.53-68 1998.
- [132] K.P. Beckett, P.H. Freer-Smith, G. Taylor, "Urban woodlands: their role in reducing the effects of particulate pollution," *Environmental Pollution*, pp. 347-360, 1998.
- [133] D. Fowler, U. Skiba, E. Nemitz, F. Choubedar, "Measuring aerosol and heavy element deposition on urban woodland and grass using inventories of ²¹⁰Pb and element concentrations in soil," *Water Air and Soil Pollution*, pp. 483-499, 2004
- [134] N.W. Lepp, "Planting Green Roofs and Living Walls," *Journal of Environmental Quality*, pp. 2408–2408, 2008.
- [135] J.C. Berndtsson, "Green roof performance towards management of runoff water quantity and quality: A review," *Ecological Engineering*, pp. 351–360, 2010.
- [136] C. Farrell, R.E. Mitchell, C. Szota, J.P. Rayner, N.S.G. Williams, "Green roofs for hot and dry climates: Interacting effects of plant water use, succulence and substrate," *Ecological Engineering*, pp. 270–276, 2012.
- [137] B. Dvorak, A. Volder, "Green roof vegetation for North American ecoregions: A literature review," *Landscape and Urban Planning*, pp. 197–213, 2010.
- [138] C. Butler, C M. Orians, "Sedum cools soil and can improve neighboring plant performance during water deficit on a green roof," *Ecological Engineering*, pp. 1796–1803, 2011.
- [139] P.A. Brevis, D.S. Nesmith, H.Y. Wetzstein, "Flower Age Affects Fruit Set and Stigmatic Receptivity in Rabbiteye Blueberry," *Hortscience*, pp. 1656–1661, 2006.
- [140] J.A. Teeri, M. Turner, J. Gurevitch, "The response of leaf water potential and crassulacean acid metabolism to prolonged drought in *Sedum rubrotinctum*," *Plant Physiology*, pp. 678-680, 1986.

- [141] T. Emilsson, "Vegetation development on extensive vegetated green roofs: Influence of substrate composition, establishment method and species mix," *Ecological Engineering*, pp. 265–277, 2008.
- [142] K.L. Getter, D.B. Rowe, "Media depth influences Sedum green roof establishment," *Urban Ecosystems*, pp. 361–372, 2008.
- [143] K. Vijayaraghavan, U.M. Joshi, "Can green roof act as a sink for contaminants? A methodological study to evaluate runoff quality from green roofs," *Environmental Pollution*, pp. 121–129, 2014.
- [144] O. Schweitzer and E. Erell, "Evaluation of the energy performance and irrigation requirements of extensive green roofs in a water-scarce Mediterranean climate," *Energy and Buildings*, pp. 25–32, 2014.
- [145] M.A. Monterusso, D.B. Rowe, C.L. Rugh, "Establishment and Persistence of Sedum spp. and Native Taxa for Green Roof Applications," *Hortscience*, pp. 391–396, 2005.
- [146] U. Berardi, A.H. GhaffarianHoseini, and A. GhaffarianHoseini, "State-of-the-art analysis of the environmental benefits of green roofs," *Applied Energy*, pp. 411–428, 2014.
- [147] K. Vijayaraghavan, "Green roofs: A critical review on the role of components, benefits, limitations and trends," *Renewable and Sustainable Energy Reviews*, pp. 740–752, 2016.
- [148] Landscape Development and Landscaping Research Society, "Green Roof Guidelines for the Planning, construction and maintenance of green roofing – green roofing guideline," 2018, https://commons.bcit.ca/greenroof/files/2019/01/FLL_greenroofguidelines_2018.pdf.
- [149] M. Köhler, "Green facades-a view back and some visions," *Urban Ecosystems*, pp. 423–436, 2008.
- [150] E. Oberndorfer, J. Lundholm, B. Bass, R.R. Coffman, H. Doshi, N. Dunnett, S. Gaffin, M. Köhler, K.K.Y. Liu, B. Rowe, "Green roofs as urban ecosystems ecological structures, functions, and services," *BioScience*, pp. 823–833, 2007.
- [151] O. Saadatian, K. Sopian, E. Salleh, C.H. Lim, S. Riffat, E. Saadatian, A. Toudeshki, M.Y. Souleiman, "A review of energy aspects of green roofs," *Renewable and Sustainable Energy Reviews*, pp. 155–168, 2013.
- [152] D. Townshend, "Study on Green Roof Application in Hong Kong," Report, 2006.

- [153] C.F. Chen, "Performance evaluation and development strategies for green roofs in Taiwan: A review," *Ecological Engineering*, pp. 51–58, 2013.
- [154] K. Gloede, "France Mandates Green Roofs For All New Commercial Construction." 2015. https://www.architectmagazine.com/technology/france-mandates-green-roofs-for-all-new-commercial-construction_o.
- [155] J.T. Lundholm, "Green Roofs and Facades: A Habitat Template Approach," *Urban Habitats*, pp. 87-101, 2006.
- [156] M. Santamouris, "Cooling the cities - A review of reflective and green roof mitigation technologies to fight heat island and improve comfort in urban environments," *Solar Energy*, pp. 682–703, 2014.
- [157] E. Alexandri, P. Jones, "Temperature decreases in an urban canyon due to green walls and green roofs in diverse climates," *Building and Environment*, pp. 480–493, 2008.
- [158] I. Theodoridou, M. Karteris, G. Mallinis, A.M. Papadopoulos, M. Hegger, "Assessment of retrofitting measures and solar systems' potential in urban areas using Geographical Information Systems: Application to a Mediterranean city," *Renewable and Sustainable Energy Reviews*, pp. 6239–6261, 2012.
- [159] A. Niachou, K. Papakonstantinou, M. Santamouris, A. Tsangrassoulis, G. Mihalakakou, "Analysis of the green roof thermal properties and investigation of its energy performance," *Energy and Buildings*, pp. 719-729, 2001.
- [160] E. Eumorfopoulou, D. Aravantinos, "The contribution of a planted roof to the thermal protection of buildings in Greece," *Energy and Buildings*, pp. 29-36, 1998.
- [161] N.H. Wong, Y. Chen, C.L. Ong, A. Sia, "Investigation of thermal benefits of rooftop garden in the tropical environment," *Building and Environment*, pp. 261-270, 2003.
- [162] M. Zhao, J. Srebric, "Assessment of green roof performance for sustainable buildings under winter weather conditions," *Journal of Central South University of Technology*, pp. 639–644, 2012.
- [163] C.Y. Jim, S.W. Tsang, "Biophysical properties and thermal performance of an intensive green roof," *Building and Environment*, pp. 1263–1274, 2011.
- [164] J. Mentens, D. Raes, M. Hermy, "Green roofs as a tool for solving the rainwater runoff problem in the urbanized 21st century?" *Landscape and Urban Planning*, pp. 217–226, 2006.

- [165] A. Nagase, N. Dunnett, "Amount of water runoff from different vegetation types on extensive green roofs: Effects of plant species, diversity and plant structure," *Landscape and Urban Planning*, pp. 356–363, 2012.
- [166] A. F. Speak, J. J. Rothwell, S. J. Lindley, and C. L. Smith, "Urban particulate pollution reduction by four species of green roof vegetation in a UK city," *Atmospheric Environment*, pp. 283–293, 2012.
- [167] A. Graceson, M. Hare, J. Monaghan, N. Hall, "The water retention capabilities of growing media for green roofs," *Ecological Engineering*, pp. 328–334, 2013.
- [168] R. Berghage, A. Jarett, D. Beattie, K. Kelley, S. Husain, F. Rezai, B. Long, A. Negassi, R. Cameron, W. Hunt, "Quantifying evaporation and transpirational water losses from green roofs and green roof media capacity for neutralizing acid rain Report, National Decentralized Water Resources (NDWRCP) Research Project," Report, 2007.
- [169] T. van Renterghem, D. Botteldooren, "Numerical evaluation of sound propagating over green roofs," *Journal of Sound and Vibration*, pp. 781–799, 2008.
- [170] T. van Renterghem, D. Botteldooren, "In-situ measurements of sound propagating over extensive green roofs," *Building and Environment*, pp. 729–738, 2011.
- [171] M. Connelly, M. Hodgson, "Experimental investigation of the sound transmission of vegetated roofs," *Applied Acoustics*, pp. 1136–1143, 2013.
- [172] T. Laylin, "Former Renault Factory In France Becomes An Undulating Green-Roofed School," 2011, <https://inhabitat.com/former-renault-factory-in-france-becomes-an-undulating-green-roofed-school/>.
- [173] National research council, "Climate change science," *National Academies of Sciences, Engineering, and Medicine*, 2001.
- [174] E. Shuster, "Tracking New Coal-Fired Power Plants National Energy Technology Laboratory Office of Systems Analyses and Planning," report, 2010.
- [175] R. Alley, T. Berntsen, N.L. Bindoff, Z. Chen, A. Chidthaisong, P. Friedlingstein, J. Gregory, G. Hegerl, M. Heimann, B. Hewitson, B. Hoskins, F. Joos, J. Jouzel, V. Kattsov, U. Lohmann, M. Manning, T. Matsuno, M. Molina, N. Nicholls, J. Overpeck, D. Qin, G. Raga, V. Ramaswamy, J. Ren, M. Rusticucci,

- S. Solomon, R. Somerville, T.F. Stocker, P. Stott, R.J. Stouffer, P. Whetton, R.A. Wood, D. Wratt
 "Climate Change 2007: The Physical Science Basis," report, 2007.
- [176] K.L. Getter, D.B. Rowe, G.P. Robertson, B.M. Cregg, J.A. Andresen, "Carbon sequestration potential of extensive green roofs," *Environmental Science and Technology*, pp. 7564–7570, 2009.
- [177] C. Clark, B. Talbot, J. Bulkley, P. Adiaens, "Optimization of green roofs for air pollution mitigation," Conference, 2005.
- [178] P.Y. Tan, A. Sia, "A pilot green roof research project in Singapore," CiteSeerX, pp. 1-13.
- [179] A.H. Rosenfeld, H. Akbari, J. J. Romm, M. Pomerantz, "Cool communities: strategies for heat island mitigation and smog reduction," *Energy and Buildings*, pp. 51-62 1998.
- [180] M. Santamouris, Pavlou, C.P. Doukas, G. Mihalakakou, A. Synnefa, A.Hatzibiros, P. Patargias, "Investigating and analysing the energy and environmental performance of an experimental green roof system installed in a nursery school building in Athens, Greece," *Energy*, pp. 1781–1788, 2007.
- [181] D. J. Sailor, "A green roof model for building energy simulation programs," *Energy and Buildings*, pp. 1466–1478, 2008.
- [182] O.A. Abbass, D.J. Sailor, E.T. Gall, "Ozone removal efficiency and surface analysis of green and white roof HVAC filters," *Building and Environment*, pp. 118–127, 2018.
- [183] P. Ramasubramanian, I. Luhung, S.B.Y. Lim, S.C. Schuster, O. Starry, E.T. Gall, "Impact of green and white roofs on air handler filters and indoor ventilation air," *Building and Environment*, pp. 1-10, 2021.
- [184] S.E. Gryning, N. Chaumerliac, "Air pollution modelling and its application XII," Plunem Press, 1998.
- [185] M. Dicke, F. Loreto, "Induced plant volatiles: from genes to climate change," *Trends in Plant Science*, pp. 115–117, 2010.
- [186] I. T. Baldwin, R. Halitschke, A. Paschold, C.C. von Dahl, C.A. Preston, "Volatile Signaling in Plant-Plant Interactions: "Talking Trees" in the Genomics Era," *Science*, pp. 812-815, 2006.
- [187] N. Dudareva, E. Pichersky, "Biochemical and Molecular Genetic Aspects of Floral Scents," *Plant Physiology*, pp. 627–634, 2000.

- [188] J.K. Holopainen, J. Gershenzon, "Multiple stress factors and the emission of plant VOCs," *Trends in Plant Science*, pp. 176–184, 2010.
- [189] A.R. War, M.G. Paulraj, T. Ahmad, A.A. Buhroo, B. Hussain, S. Ignacimuthu, H.C. Sharma, "Mechanisms of plant defense against insect herbivores," *Plant Signaling and Behavior*, pp. 1306-1320, 2012.
- [190] J. Llusi, J. Pe, B.S. Gimeno, "Seasonal and species-specific response of VOC emissions by Mediterranean woody plant to elevated ozone concentrations," *Atmospheric Environment*, pp. 3931-3938, 2002.
- [191] E. Pichersky, D.R. Gang, "Genetics and biochemistry of secondary metabolites in plants: an evolutionary perspective," *Trends in Plant Science*, pp. 439-445, 2000.
- [192] J. Kesselmeier, M. Staudt, "Biogenic Volatile Organic Compounds (VOC): An Overview on Emission, Physiology and Ecology," *Journal of Atmospheric Chemistry*, pp. 23–88, 1999.
- [193] C. Calfapietra, J. Peñuelas, Ü. Niinemets, "Urban plant physiology: Adaptation-mitigation strategies under permanent stress," *Trends in Plant Science*, pp. 72–75, 2015.
- [194] G. Churkina, R. Grote, T. M. Butler, M. Lawrence, "Natural selection? Picking the right trees for urban greening," *Environmental Science and Policy*, pp. 12–17, 2015.
- [195] W.L. Chameides, R.W. Lindsay, J. Richardson, C.S. Klang, "The Role of Biogenic Hydrocarbons in Urban Photochemical Smog: Atlanta as a Case Study," *Science*, pp. 1473-1475, 1988
- [196] T. Hoffmann, J.R. Odum, F. Bowman, D. Collins, D. Klockow, R.C. Flagan, J.H. Seinfeld, "Formation of Organic Aerosols from the Oxidation of Biogenic Hydrocarbons," *Journal of Atmospheric Chemistry*, pp. 189–222, 1997.
- [197] J.I. Steinfeld, "Atmospheric Chemistry and Physics: From Air Pollution to Climate Change," *Environment: Science and Policy for Sustainable Development*, pp. 26–26, 1998.
- [198] A. Ghirardo, J. Xie X. Zheng, Y. Wang, R. Grote, K. Block, J. Wildt, T. Mentel, A. Kiendler-Scharr, M. Hallquist, K. Butterbach-Bahl, J.P. Schnitzler, "Urban stress-induced biogenic VOC emissions and SOA-forming potentials in Beijing," *Atmospheric Chemistry and Physics*, pp. 2901–2920, 2016.

- [199] J.-H. Park, A.H. Golstein, J. Timkovsky, S. Fares, R. Weber, J. Karlik R. Holzinger, "Active atmosphere-ecosystem exchange of the vast majority of detected Volatile Organic Compounds," *Science*, vol. 341, no. 6146, pp. 640–643, 2013.
- [200] S. Fares, M. McKay, R. Holzinger, A.H. Goldstein, "Ozone fluxes in a *Pinus ponderosa* ecosystem are dominated by non-stomatal processes: Evidence from long-term continuous measurements," *Agricultural and Forest Meteorology*, pp. 420–431, 2010.
- [201] S. Fares, R. Weber, J.H. Park, D. Gentner, J. Karlik, A.H. Goldstein, "Ozone deposition to an orange orchard: Partitioning between stomatal and non-stomatal sinks," *Environmental Pollution*, pp. 258–266, 2012.
- [202] G. Gerosa, M. Vitale, A. Finco, F. Manes, A.B. Denti, S. Cieslik, "Ozone uptake by an evergreen Mediterranean Forest (*Quercus ilex*) in Italy. Part I: Micrometeorological flux measurements and flux partitioning," *Atmospheric Environment*, pp. 3255–3266, 2005.
- [203] N.D. Bedding, A.E. McIntyre, R. Perry, J.N. Lester, "Organic Contaminants in the Aquatic Environment. I. Sources and Occurrence," *Science of The Total Environment*, pp. 143-167, 1982.
- [204] B.T. Croll, "Pesticides in Surface Waters and Groundwaters," *Water and Environment Journal*, pp. 389- 395, 1991.
- [205] C.A. Buescher, J.H. Dougherty, and R.T. Skrinde, "Chemical Oxidation of Selected Organic Pesticides," *Water Pollution Control Federation*, pp. 1005-1014 , 1964.
- [206] Kuehn, W. Ing, H. Sontheimer, "Oxidation techniques in Drinking water treatment. Drinking water pilot project. Report IIa. Advanced treatment technology," Final report, 1979.
- [207] F.J. Beltrán, J.F. García-Araya, B. Acedo, "Advanced oxidation of atrazine in water—II. Ozonation combined with ultraviolet radiation," *Water Research*, pp. 2165-2174, 1994.
- [208] J. Socorro, S. Gligorovski, H. Wortham, E. Quivet, "Heterogeneous reactions of ozone with commonly used pesticides adsorbed on silica particles," *Atmospheric Environment*, pp. 66–73, 2015.
- [209] M. Pflieger, A. Monod, H. Wortham, "Kinetic study of heterogeneous ozonolysis of alachlor, trifluralin and terbuthylazine adsorbed on silica particles under atmospheric conditions," *Atmospheric Environment*, pp. 5597–5603, 2009.

- [210] B. Yang, Y. Wang, W. Zhang, C. Liu, X. Shu, and J. Shu, "Heterogeneous ozonolysis of pirimicarb and isopropalin: Mechanism of ozone-induced N-dealkylation and carbonylation reactions," *Environmental Chemistry*, pp. 521–528, 2012.
- [211] M. Pflieger, I. Grgić, Z. Kitanovski, L. Nieto, H. Wortham, "The heterogeneous ozonation of pesticides adsorbed on mineral particles: Validation of the experimental setup with trifluralin," *Atmospheric Environment*, pp. 7127–7134, 2011.
- [212] C. Mattei, H. Wortham, E. Quivet, "Heterogeneous degradation of pesticides by OH radicals in the atmosphere: Influence of humidity and particle type on the kinetics," *Sciences of the Total Environment*, pp. 1084-1094, 2019.
- [213] W.M. Meylan, P.H. Howard, "Computer estimation of the Atmospheric gas-phase reaction rate of organic compounds with hydroxyl radicals and ozone," *Chemosphere*, pp. 2293-2299, 1993.
- [214] H.D. Burrows, M. Canle, J.A. Santaballa, S. Steenken, "Reaction pathways and mechanisms of photodegradation of pesticides," *Journal of Photochemistry and Photobiology B: Biology*, pp. 71-108, 2002.
- [215] C.K. Remucal, "The role of indirect photochemical degradation in the environmental fate of pesticides: A review," *Environmental Sciences: Processes and Impacts*, pp. 628–653, 2014.
- [216] Toshiyuki Katagi, "Photodegradation of Pesticides on Plant and Soil Surfaces Toshiyuki Katagi Contents," *Reviews of Environmental Contamination and Toxicology*, pp. 1-78, 2004.
- [217] N.L. Turro, "Modern Molecular Photochemistry," 1978.
- [218] M. Milan, A. Ferrero, S. Fogliatto, S. Piano, F. Vidotto, "Leaching of S-metolachlor, terbuthylazine, desethyl-terbuthylazine, mesotrione, flufenacet, isoxaflutole, and diketonitrile in field lysimeters as affected by the time elapsed between spraying and first leaching event," *Journal of Environmental Science and Health - Part B Pesticides, Food Contaminants, and Agricultural Wastes*, pp. 851–861, 2015.
- [219] G. Riise, H. Lundekvam, Q. L. Wu, L.E. Haugen, J. Mulder, "Loss of pesticides from agricultural fields in SE Norway-runoff through surface and drainage water," *Environmental Geochemistry and Health*, pp. 269–276, 2004.

- [220] K. Fenner, S. Canonica, L.P. Wackett, M. Elsner, "Evaluating Pesticide Degradation in the Environment: Blind Spots and Emerging Opportunities," *Science*, pp. 752-758, 2013.
- [221] L. Carena, D. Fabbri, M. Passananti, M. Minella, M. Pazzi, D. Vione, "The role of direct photolysis in the photodegradation of the herbicide bentazone in natural surface waters," *Chemosphere*, 2020.
- [222] A. ter Halle, D. Lavieille, C. Richard, "The effect of mixing two herbicides mesotrione and nicosulfuron on their photochemical reactivity on cuticular wax film," *Chemosphere*, pp. 482-487, 2010.
- [223] Z. Chen, M.J. Zabik, R.A. Leavitt, "Comparative study of thin film photodegradative rates for 36 pesticides," *Industrial & Engineering Chemistry Product Research and Development*, pp. 5-11, 1984.
- [224] B. David Avnir, L.J. Johnston, P. de Mayo, S. King Wong, "Surface Photochemistry: Radical Pair Combination on a Silica Gel Surface and in Micelles," *Journal of the Chemical Society, Chemical Communications*, pp. 933-972, 1981.
- [225] L.J. Johnston, P. de Mayo, and S.K. Wong, "Surface Photochemistry: Decomposition of Azobis(isobutyronitrile) on Dry Silica Gel," *Journal of Organic Chemistry*, pp. 20-26, 1984.
- [226] A. ter Halle, C. Richard, "Simulated solar light irradiation of mesotrione in natural waters," *Environmental Science and Technology*, pp. 3842-3847, 2006.
- [227] D. Lavieille, A. ter Halle, C. Richard, "Understanding mesotrione photochemistry when applied on leaves," *Environmental Chemistry*, pp. 420-425, 2008.
- [228] B. Eyheraguibel, A. ter Halle, and C. Richard, "Photodegradation of Bentazon, clopyralid, and triclopyr on model leaves: Importance of a systematic evaluation of pesticide photostability on crops," *Journal of Agricultural and Food Chemistry*, pp. 1960-1966, 2009.
- [229] D. Hainzl, J.E. Casida, "Fipronil Insecticide: Novel Photochemical Desulfinylation with Retention of Neurotoxicity," *National Academy of Sciences*, pp. 12764-12767, 1996.
- [230] A. ter Halle, D. Drncova, C. Richard, "Phototransformation of the herbicide sulcotrione on maize cuticular wax," *Environmental Science and Technology*, pp. 2989-2995, 2006.
- [231] M. Sleiman, P. de Sainte Claire, C. Richard, "Heterogeneous Photochemistry of Agrochemicals at the Leaf Surface: A Case Study of Plant Activator Acibenzolar-S-methyl," *Journal of Agricultural and Food Chemistry*, pp. 7653-7660, 2017.

- [232] S. Monadjemi, A. ter Halle, and C. Richard, "Reactivity of cycloxydim toward singlet oxygen in solution and on wax film," *Chemosphere*, pp. 269–273, 2012.
- [233] A.S. Trivella, S. Monadjemi, D.R. Worrall, I. Kirkpatrick, E. Arzoumanian, C. Richard, "Perinaphthenone phototransformation in a model of leaf epicuticular waxes," *Journal of Photochemistry and Photobiology B: Biology*, pp. 93–101, 2014.
- [234] S. Hamdache, M. Sleiman, P. de Sainte-Claire, F. Jaber, C. Richard, "Unravelling the reactivity of bifenazate in water and on vegetables: Kinetics and byproducts," *Science of the Total Environment*, pp. 107–114, 2018.
- [235] E. Borrás, M. Ródenas, T. Vera, A. Muñoz, "Ozone and secondary organic aerosol production by interaction between organophosphorous pesticide and biogenic VOCs mixture," Conference, 2017.
- [236] D. Palma, Y. Arbid, M. Sleiman, P. de Sainte-Claire, C. Richard, "New Route to Toxic Nitro and Nitroso Products upon Irradiation of Micropollutant Mixtures Containing Imidacloprid: Role of NO_x and Effect of Natural Organic Matter," *Environmental Science and Technology*, pp. 3325–3333, 2020.

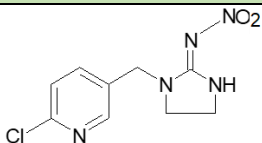
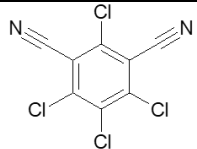
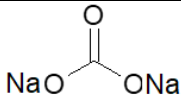
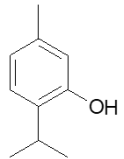
2. Materials and Methods

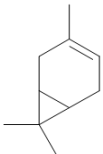
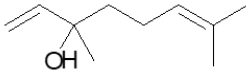
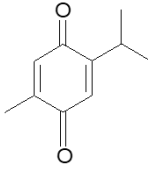
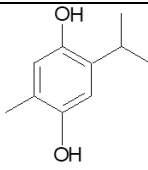
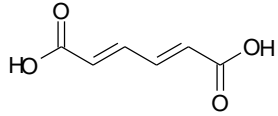
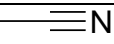
In this section, the different chemicals, plants, instruments, and the process of sample preparation are described. Experiments related to the uptakes of plants are marked with a green color while those concerning the interactions of pesticides with the plants' volatiles are distinguished by a blue color (in solution) and a brown color (on thyme leaves).

2.1 Chemicals

The chemical reagents used are listed in **Table 4** below.

Table 4 Chemical reagents used in this study.

Name	Structure	Purity (%)	Supplier
Imidacloprid (IMD) C ₉ H ₁₀ ClN ₅ O ₂		≥ 98.0	Sigma Aldrich
Chlorothalonil (CT) C ₈ Cl ₄ N ₂		≥ 98.0	Sigma Aldrich
Sodium carbonate anhydrous Na ₂ CO ₃		≥ 99.5	Fluka
Thymol C ₁₀ H ₁₄ O		≥ 98.5	Sigma Aldrich
α-pinene C ₁₀ H ₁₆		98	Sigma Aldrich

3-carene C ₁₀ H ₁₆		90	Sigma Aldrich
Linalool C ₁₀ H ₁₈ O		≥ 97.0	Sigma Aldrich
Thymoquinone C ₁₀ H ₁₂ O ₂		≥ 98	Sigma Aldrich
Thymohydroquinone C ₁₀ H ₁₄ O ₂		95	Enamine
Synperonic Polyoxyethylene C ₉ - C ₁₁ alcohol 10/6	-	-	Uniquema
Trans,trans muconic acid C ₆ H ₆ O ₄		> 97.0	Fluka
Acetonitrile CH ₃ CN		HPLC Plus Gradient grade	Carlo Erba Reagents

All chemicals were used without further purification. Water was produced using a reverse osmosis RIOS 5 and Synergy (Millipore) device (resistivity 18 MΩ cm, DOC < 0.1 mg L⁻¹). Prepared solutions were stored in a fridge at 4 °C.

2.2 Plants

Thirteen different plant species were selected and purchased for screening experiments (**Table 5**). They vary in shape, leaf size, emission of volatile organic carbons (VOCs), tolerance, rooting depth, etc.

Table 5 Plants chosen to be studied.

Plant	Picture
Achillée millefeuille paprika	
Achillea umbellate à feuillage gris	
Alchemille jaune	
Aster des alpes rose	
Heuchera americana L.	
Joubarbe calcareum	
Joubarbe rubin	
Thymus nummularius	

Sedum floriferum jaune			
Sedum reflexum jaune			
Sedum sexangulare			
Sedum spurium			
Thymus vulgaris			

The preliminary experiments studying the plants' uptakes helped us to choose 3 plants among 13 for further experiments: *Sedum sexangulare*, *Thymus vulgaris*, and *Heuchera Americana L* (**Fig.25**). One of the sedum species was selected since the latter are known to be drought tolerant and suitable to be implemented on green roofs. *Sedum sexangulare*, specifically, had the best removal capacity of NO_x among the sedum species in our preliminary experiments; it also has a good performance under severe climate conditions according to literature. The second chosen plant was *Thymus vulgaris* which is a perennial plant emitting various VOCs having the possibility to remove pollutants such as O₃ through possible reactions with volatile metabolites; while *Heuchera Americana L*. is an aesthetically-pleasing plant often used on green roofs due to its beautiful colors, and can in turn retain particulate matter (PM) due to its hairy leaves.



Figure 21 Plants chosen for further experiments, from left to right: *Sedum sexangulare*, *Thymus vulgaris*, *Heuchera Americana L.*

Plants were purchased from a plant nursery (Botanic®, Beaumont, France) and stored in an indoor greenhouse. They were stored indoors in the laboratory near a large window where they received sufficient sunlight and were watered every 2 days. The plants leaves were cut prior to the experiment using scissors and weighed (0.9-1.2 g) or were used directly as a full-size plant having a pot size varying between 9-15 cm and containing soil.

2.3 Irradiation systems

Irradiation of plants

- a. For visible light irradiation, 2x55W Starlite tubes ($\lambda = 400-800$ nm) were used (**Fig.26**). Usually, these lamps emit light necessary for photosynthesis. They were used for irradiation in the experiments concerning plants with their uptakes. Two air-tight cylindrical stainless steel reactors were used. Their volume ranged from 0.6 L (small reactor) to 12 L (big reactor). The distance between the leaves/ full plant and the lamps was 30 cm.

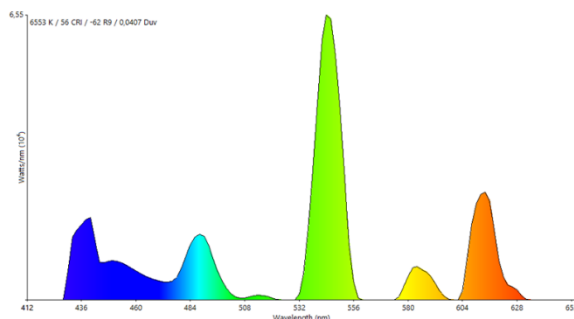


Figure 22 Starlite tubes and their light spectrum.

Irradiation of solutions

b. For calculating the quantum yields of solutions (CT + volatiles), a high-pressure mercury lamp equipped with an Oriel monochromator was used (**Fig.27**). A radiometer QE65000 from Ocean optics was utilized to measure the photon flux. Since the photon beam is homogeneous and parallel, I_0 measurement becomes possible as well as the absorbed light intensity (I_a). The lamp is connected to a cooling system; both the monochromator and the lamp are switched on 20 min before their use. This ensures a stable and homogeneous photon flow for the solution to be irradiated. Solutions of CT + volatiles were placed in a 1 cm thick cuvette equipped with Teflon caps and irradiated at 313 nm.

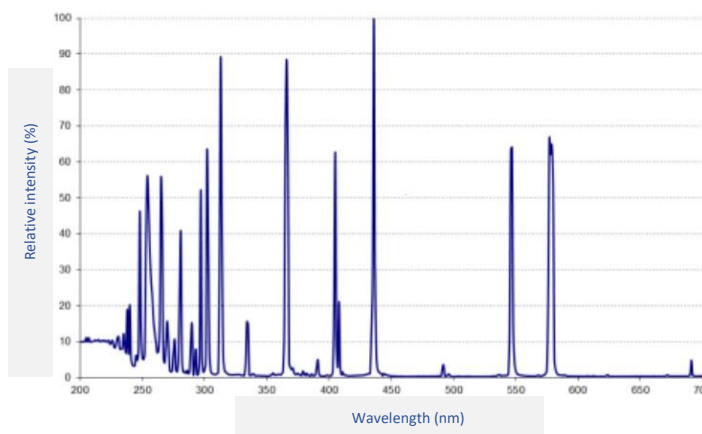


Figure 23 Monochromator used with the spectral distribution of its Hg lamp.

c. For monitoring the disappearance of molecules, 3 polychromatic tubes (Philips, TL20W/01-RS, $\lambda_{\text{max}} = 310 \text{ nm}$) installed inside a custom-made cylindrical irradiation device were used (**Fig.28**). Solutions of CT/IMD alone or CT/IMD + volatiles were placed in a cylindrical Pyrex reactor (1.4 cm internal diameter) sealed with an air-tight silicon cap and surrounded by these tubes. Cooling was provided by a ventilator maintaining the temperature at around 23°C. Aliquots were sampled at chosen irradiation times.

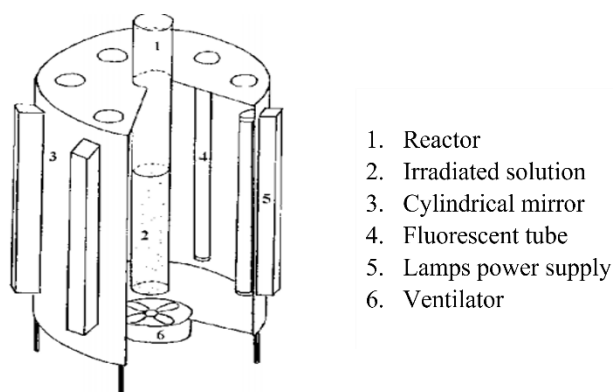


Figure 24 The irradiation device used.

Irradiation of leaves

d. For irradiating thyme twigs alone or covered with CT/IMD, a solar simulator CPS Atlas equipped with a xenon arc lamp and a filter cutting off wavelengths shorter than 290 nm was used with its power set at 500 W m^{-2} in our experiments (**Fig.29**). This light source has a spectral distribution very close to that of solar radiation. It included a cooling system maintaining the bottom of the device at 10 °C. The twigs were put in headspace vials which were placed inside the device. This system uses ventilation to ensure the cooling of lamps; hence, a cover made of quartz (plate) was used to protect the vials from the air flow caused by ventilation during irradiation.

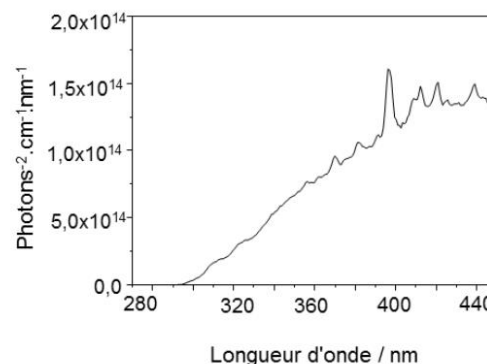


Figure 25 Suntest device used and the spectral distribution of its lamp.

Actinometry

e. The photon flux, I_0 , was measured using a radiometer QE65000 from Ocean optics. It measures the number of photons emitted by the light used. I_0 =number of photons emitted by each light was measured in photons $\text{cm}^{-2} \text{sec}^{-1}$ which is directly related to the degradation capacity. The higher the number of photons emitted, the higher will be the number of photons absorbed (I_a) and hence, a higher rate of photolysis.

2.4. Spectroscopic techniques

UV-Visible absorbance of solutions was measured by a Varian Cary 3 UV-Visible spectrophotometer in a 1 cm-thick quartz cell (**Fig.30**). The absorbance spectra of thymol, linalool, 3-carene, α -pinene, chlorothalonil, imidacloprid, thymoquinone, and thymohydroquinone were recorded, all having a concentration of 10^{-4} M. The absorbance precision is of ± 0.002 .

A baseline correction was necessary before every analysis. For this, the solvent used, which was ACN in our experiments, was put in a cuvette and its absorption reported. The latter serves as a baseline. Baseline correction is a pre-processing technique that enhances the precision of the spectroscopic signal by separating it from interference and background effects.

2.5 Chromatographic techniques

- a. High performance liquid chromatography coupled to a diode array detector (HPLC-DAD, **Fig.31**)

Disappearance of thymol

To monitor the disappearance of thymol after bubbling O₃, HPLC analyses were carried out. They were performed using a NEXERA XR HPLC equipped with an auto-sampler, a pump, and coupled to a UV/Vis DAD apparatus. The analysis was done in the reverse phase using a phenomenex -kinetex C₁₈ column (100 mm × 2.1 mm, 2.6 μm particle size) analytical column. An identical pre-column was added. The flow rate was set at 0.2 mL/min and the eluent was a mixture of ACN and water. It was an isocratic elution with 10 % ACN maintained for 10 min. The retention time of thymol was 1.3 min (λ= 274 nm). The injection volume was 10 μL.

Degradation of the pesticides (CT and IMD)

HPLC analyses were as well performed to monitor the degradation profiles of CT and IMD in solution with and without the presence of volatiles. Regarding CT experiments, the analytical column was a Phenomenex-kinetex C₁₈ (100 mm × 2.1 mm, 2.6 μm particle size); the flow rate was set at 0.2 mL min⁻¹; while for the IMD experiments, the analytical column was EC 150/4.6 NUCLEODUR C₁₈ endcapped column with a flow rate of 1 mL min⁻¹ (an identical pre-column was also present). The injection volume was 10 μL in all the analyses.

Table 6 HPLC conditions used for the CT/IMD experiments.

CT	Time (min)	% ACN	IMD	Time (min)	% ACN
	0.01	30		0	30
	2	50			
	4	60			
	8	60			
	15	80			
	15.1	30		10	30
	21	30			



Figure 26 HPLC-DAD used.

Purging was performed prior to every experiment. In the HPLC system, a certain percentage of ACN with water was used depending on the method. Its aim is to flush through the lines any remaining solvent or air bubbles from previous analysis to be replaced by the new mobile phase.

b. High performance liquid chromatography coupled to mass spectrometry (LC-MS, **Fig.32**)

Photoproducts of the reaction between pesticides and volatiles in solution and on leaves

Photoproducts obtained in solution and on thyme leaves due to the interaction between volatiles and pesticides under irradiation were identified by high resolution mass spectrometer (HRMS) on an Orbitrap Q-Exactive (ThermoScientific) coupled to an ultra-high performance liquid chromatography (UHPLC) instrument Ultimate 3000 RSLC (ThermoScientific) equipped with a UV/Vis detector. The sample to be analyzed is introduced into the mass spectrometer from the HPLC by direct vaporization in a nebulization chamber. In this chamber, the molecules are ionized by electrospray (or electrospray ionization ESI). The column used in our experiments was a Kinetec EVO C18 (100 × 2.1 mm), particle size of 1.7 μm (Phenomenex). The elution gradient started with 15% acetonitrile maintained for 5 min, then the percentage of acetonitrile was linearly increased to reach 55% after 5 min. The flow was set at 0.45 mL min⁻¹. Analyses were made in positive (M+H⁺/M+Na⁺) and negative (M-H⁺) electrospray modes (ESI⁺/ESI⁻). Mass accuracy was less than 5 ppm.



Figure 27 LC-MS apparatus.

c. Gas chromatography coupled to mass spectrometry (GC-MS, **Fig.33**)

Photoproducts of the reaction between pesticides and volatiles in solution and on leaves

Photoproducts were also analyzed using an Agilent 6890 gas chromatograph coupled to an Agilent 5973 mass spectrometry detector. The separation was carried out using a HP-5 μs column ($25\text{ m} \times 0.25\text{ mm} \times 0.25\text{ }\mu\text{m}$) operating initially at 80°C over 1 min, followed by a $10^\circ\text{C min}^{-1}$ ramp to reach to reach 200°C and then a $30^\circ\text{C min}^{-1}$ ramp to reach 260°C maintained for 1 min (to calculate the degradation of volatiles) in the case of CT + volatiles experiments, while the analysis was operated initially at 70°C followed by a $10^\circ\text{C min}^{-1}$ ramp to reach 160°C for 5 min and then a $30^\circ\text{C min}^{-1}$ ramp to reach 250°C maintained for 2 min in the case of IMD + volatiles. The flow rate was 1 mL min^{-1} with an injection volume of $1\text{ }\mu\text{L}$ in both cases.



Figure 28 GC-MS instrument.

In the GC system, purging with the carrier gas removes traces of O₂ and moisture from the injection port and hence column. Pressure stability in the column before running the analysis should be ensured in all cases.

d. Headspace gas chromatography coupled to mass spectrometry (HS-GCMS)

Volatile metabolites of the reaction between pesticides and volatiles on leaves

The volatile metabolites produced by thyme when found alone or after being dipped in CT before and after irradiation were detected using HS-GC/MS (Shimadzu HS-20 coupled with QP2010SE). Twigs (0.2 g) were transferred into a 20 mL headspace glass vial (**Fig.34**) and incubated for 5 min at 80°C. The analytical column (Mega 5-MS 30 m × 0.25 mm) was operated initially at 50°C for 1 min, followed by an 8°C min⁻¹ ramp to reach 170°C and held for 4 min, and then a 15°C min⁻¹ ramp to reach 275°C maintained for 1 min. The mass spectrometer source was heated to 200°C, and signals were detected between mass to charge ratios (m/z) of 50 and 350. Identification of the major constituents was carried out using the NIST 17 database and when necessary using authentic standards.



Figure 29 HS vial with thyme.

e. Automated thermal desorption gas chromatography couple to mass spectrometry (ATD-GC-MS, **Fig.35**)

Products formed between O₃ and thyme's volatiles

To detect the volatile compounds collected in a cartridge after air sampling formed due to the reaction between thyme leaves (put in a reactor) and O₃, ATD-GC-MS was used. The reactor's gas phase was sampled for 3 min at a sampling rate of 100 mL min⁻¹ into the Tenax sorbent tubes. After sampling, the tubes were thermally desorbed using TurboMatrix thermal desorption unit (ATD 150, Perkin Elmer) equipped with a cold trap (Carbotrap 300) and coupled to an Agilent 6890 gas chromatograph and an Agilent 5973 mass spectrometry detector. The separation of desorbed volatiles was carried out using a HP-5 μ s column (25 m \times 0.25 mm \times 0.25 μ m) operated initially at 50°C over 1 min, followed by a 10°C/min ramp to reach 230°C. Mass spectra were scanned between m/z 35 and m/z 350 with the source temperature set at 20°C.



Figure 30 ATD (automated thermal desorption) system.

2.6 Microscopic techniques

Scanning electron microscopy (SEM)

Thyme's surface

Thyme's abaxial and adaxial cuticular surfaces were examined by SEM (**Fig.36**). Leaves were mounted on aluminum stubs using double-sided adhesive tape and sputter-coated with 10-15 nm gold-palladium (20 s, 25 mA, partial argon pressure 60 mTorr, Denton Desk V. The samples

were investigated with a field-emission scanning electron microscope (SH 4000 M) using a 20 kV acceleration voltage and a 10 mm working distance.

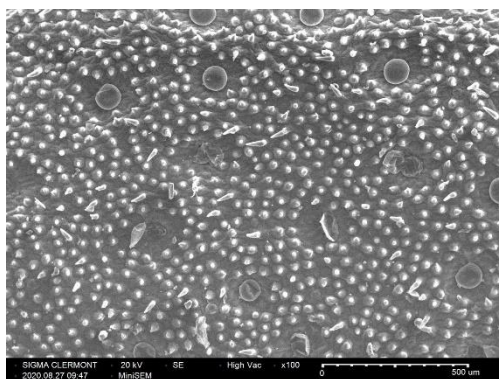


Figure 31 Thyme's adaxial surface seen by SEM.

2.7 Analyzers

a. NO_x analyzer

A NO_x Thermo scientific 42i model-NO NO₂ NO_x analyzer (chemiluminescence analyzer) was utilized to measure the uptake capacity of *Sedum sexangulare*, *Thymus vulgaris*, *Heuchera Americana L.* The detection technique is based on the reaction of nitric oxide (NO) with O₃ to produce nitrogen dioxide (NO₂). Following the NO-O₃ reaction, the NO₂ molecules immediately revert to NO₂. This process creates a light emission directly proportional to the NO concentration in the sample. The intensity of the resulting light emission is then measured by photomultiplier tube and associated electronics. An NO₂ to NO converter is used for NO_x (NO + NO₂) analysis.

b. O₃ analyzer

An O342e ozone analyzer O₃ (Environnement S.A) was used to note the uptake potential of *Sedum sexangulare*, *Thymus vulgaris*, *Heuchera Americana L.* The detector measures the UV absorption of O₃ molecules. The O₃ concentration is calculated by measuring the difference between UV absorption of the gas sample and the sample without O₃ after a filtration performed by a catalytic convertor.

Both analyzers (**Fig.37**) were turned on 30 min prior to uptake experiments to allow their lamps to heat up. The background concentrations of NO_x and O₃ were always noted to correct any

interference coming from the laboratory room air. Each analyzer needed at least a flow rate of 0.6 L min^{-1} ; hence when the flow was not sufficient, a T shaped tube fitting was installed to allow the analyzer to suck air from the room. This was taken into consideration in our calculations.



Figure 32 The NO_x (bottom) and the O₃ (top) analyzers used in our experiments.

2.8 Preparation of samples/experiments

2.8.1 Study of plants' depollution potential

Plants

Plants were either used directly as a full size plant or their leaves cut using scissors prior to experiments in order to obtain a mass ranging between 0.9-1.2 g. They were then put in stainless steel chambers having a volume of 0.6 L (case of detached leaves) and 12 L (case of the full size plant) to be further irradiated and their uptakes noted. 13 plants species were first carefully chosen and studied to compare their uptake capacities. This screening allowed the selection of 3 plants to carry on with the experiments.

Preparation and storage of IMD solution (source of NO₂)

200ml of IMD (10^{-5} M) was prepared in a cylindrical glass Pyrex gas flow-reactor (0.65 L, length 27 cm and diameter 5.7 cm, **Fig.38**); the solvent was mainly water with a small percentage of ACN to ensure IMD's total dissolving. Values of NO_x read on the analyzer were 50-60 ppbv NO₂ and 0.1-0.5 ppbv NO under dark conditions. The solution was stored in a fridge and used for several months. Before performing each experiment, the amount of NO₂ produced by IMD was

noted; if a decrease in values was noticed, IMD powder was added to the already prepared solution in order to attain the needed NO_2 concentration. A previous study helped us with the choice of the source which showed that the irradiation of IMD solution produced significant amount of NO_2 due to the homolytic cleavage of RN-NO_2 [1].

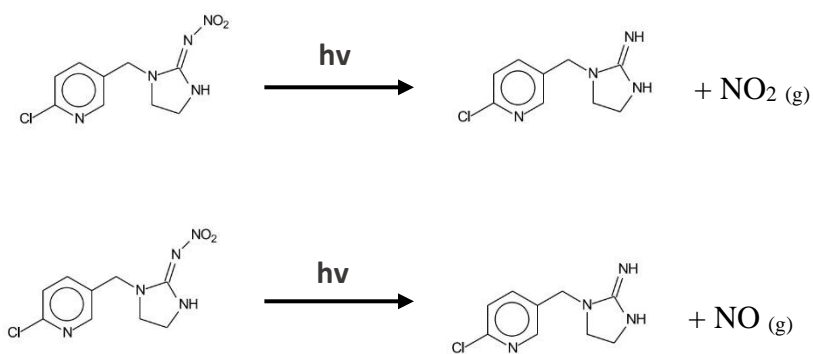


Figure 33 IMD solution in the glass reactor.

Nitrous acid (HONO) trap

The trap was prepared by placing Na_2CO_3 in a 6 cm Teflon tube sealed with glass wool on both sides and put before the NO_x analyzer. Sodium carbonate covered only about $\frac{1}{4}$ of the tube. It trapped the HONO that might have been generated. The trap acts as a denuder [2]. The concentration of HONO was calculated by subtracting the concentration of NO_2 from IMD with the trap from that without the trap.

2.8.2 Study of pesticides in the presence of thyme's volatiles

In solution

All stock solutions were prepared in a volumetric flask by adding a certain amount of the chemical and a specific volume of a solvent, and then transferred into a bottle and kept in the dark at 4°C (**Fig.39**). The solvent used in our experiments was ACN due to the compounds' high solubility in it. Prior to experiments, the stock or mother solution was diluted by ACN or water. Dilution was achieved by adding a specific volume of the mother solution-by the aid of a micropipette (100-1000 μl or 20-200 μl) - into a labeled glass bottle; the solvent was then added using a 500-5000 μl micropipette to reach the desired final volume. The prepared solutions were directly used after their preparation. Water was produced by a reverse osmosis RIOS 5 and Synergy (Millipore) device (resistivity 18 M Ω cm, DOC<0.1 mg L⁻¹). This water had a very low dissolved organic carbon content.

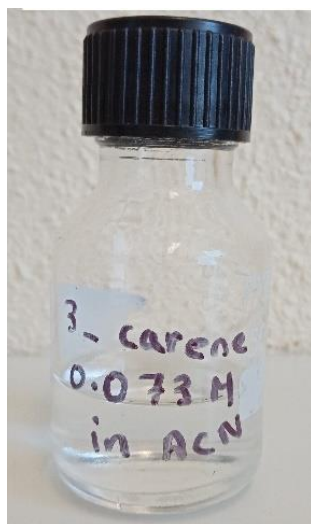


Figure 34 3-carene stock solution.

On thyme leaves

Two thyme twigs were cut using scissors, their leaves counted, and then dipped into a 7.5×10^{-4} M solution of either CT or IMD for 30 s. They were then left freely to dry for 1h and transferred into a hermetically sealed head space vials to be left in the dark or irradiated (**Fig.40**). Possible products were directly analyzed by HS-GCMS or extracted by 2 ml ACN (immersed and agitated) to be analyzed by GC-MS, LC-MS, or HPLC-DAD.



Figure 35 Thyme twigs after extraction.

2.9 Toxicity estimation

ECOSAR (ECOLOGICAL Structure-Activity Relationship) computer program

The toxicity of certain compounds was estimated using this software by using a structure-activity approach. LC50 (Acute toxicity, the concentration that is lethal to half of fish after 96 h of exposure to a certain molecule), ChV (Chronic toxicity), and logKow were obtained. The reported toxicities are those of the compounds on fish in fresh waters. The program (v 2.0) is available on the website: epa.gov/tsca-screening-tools/ecological-structure-activity-relationships-ecosar-predictive-model.

2.10 Calculation of the compounds' concentrations

Quantification of thymol after bubbling O₃, of CT/IMD, and of the volatiles analyzed by HPLC-DAD was done by the calibration method. In this method, a sample of a known concentration is analyzed (using the same method) serving as a reference. This helps us calculate the concentration of our target molecule by using the following equations:

$$A_0 = \varepsilon \times \ell \times C_0 \text{ Eq1}$$

$$A_t = \varepsilon \times \ell \times C_t \text{ Eq2}$$

Where A₀ and A_t are the absorbance of the reference and that of the molecule at any time t respectively, ε is the molar absorptivity coefficient (L mol⁻¹ cm⁻¹), ℓ is the path length (1 cm), and C₀ and C_t are the molar concentrations of the reference molecule and the studied molecule at any time t respectively.

By dividing Eq1 by Eq2, we get:

$$\frac{A_0}{A_t} = \frac{C_0}{C_t} \text{ Eq3}$$

A₀ and A_t are obtained after the HPLC analysis, C₀ is given; hence, C_t can be calculated using Eq3 by cross multiplication. Note that ε and ℓ in both equations cancel each other.

Same calculations (Eq3) were followed after LC-MS analysis by using the surface area.

References

- [1] D. Palma, Y. Arbid, M. Sleiman, P. De Sainte-claire, C. Richard, "New Route to Toxic Nitro and Nitroso Products upon Irradiation of Micropollutant Mixtures Containing Imidacloprid: Role of NO," *Environmental Science & Technology*, pp. 3325-3333, 2020.
- [2] J.D. Spengler, G.J. Keeler, J.L. Slater, "Determination of aerosol strong acidity losses due to interactions of collected particles: Results from laboratory and field studies," *Atmospheric Environment. Part A. General Topics*, pp. 987-995, 1992.

3. Results and discussion

3.1 Summary of the main results

The objectives of this PhD thesis were to study the depollution mechanism and performances of plant species implemented on green roofs towards two prevalent air pollutants: NO_x and O₃ (Fig 41, B), as well as to investigate the possible photochemical interactions taking place between secondary metabolites and pesticides sprayed on plants (Fig 41, C). In both cases, the leaves surface is the site of reactions involving the plants constituents and chemicals.

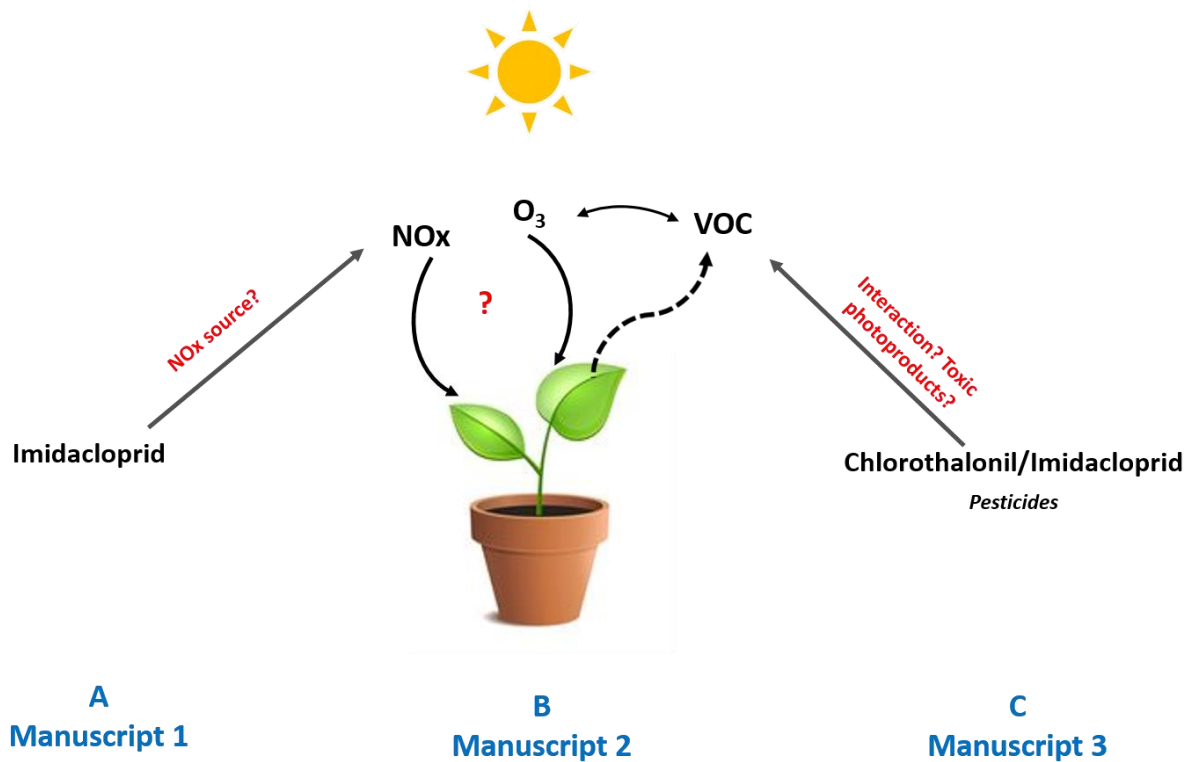


Figure 36 A scheme summarizing the PhD steps.

To achieve the experiments with air pollutants, we needed to get an O₃ and a NO_x source. Our laboratory was equipped with an UVP ozone generator having a UV-pen ray lamp; however, a stable and continuous NO_x source was necessary. NO₂ cylinders could be used for this purpose but they are potentially harmful and hazardous due to the high pressure stored inside. Moreover, they do not last long which makes them costly due to the need of using often a new one. Hence, the idea was to use a chemical as a source of NO₂. Our choice fell on Imidacloprid (IMD) as a candidate that possibly produces NO₂/NO (Fig 41, A). A setup was first developed to monitor and evidence the NO_x production from aqueous solutions of IMD (**Manuscript 1**). In this manuscript, I performed experiments on IMD by irradiating it first to monitor NO₂/NO values via the developed setup as well as experiments regarding its nitrating/nitrosating effect. The setup consisted of flow controllers, a reactor, an irradiation system, and an NO_x analyzer as seen in **Fig.42**. It is fully described in Annex 1. This first set-up served as a base to the more complicated setup used to monitor the ability of plants to retain pollutants.

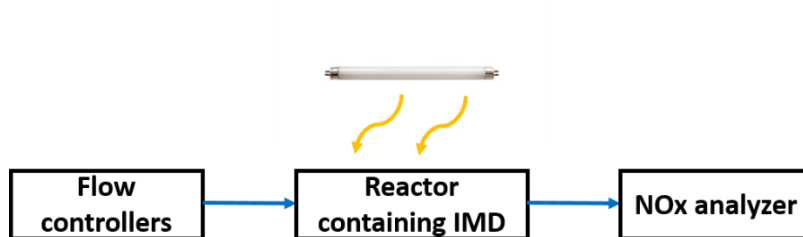


Figure 37 A diagram of the setup used to demonstrate the formation of NO₂/NO from IMD.

Since one of our main objective during the PhD was to present a solution to pollution via an environmentally friendly approach, special attention was given to the plants and their uptake mechanisms (**Manuscript 2**). The simplified diagram of the setup is shown **Fig.43**. Plants were put in a reactor where air was passed carrying either NO_x or O₃, and their ability to remove those 2 pollutants was studied by monitoring the time evolution of concentrations using NO_x and O₃ online analyzers. A full description of the setup is given in Annex 2.

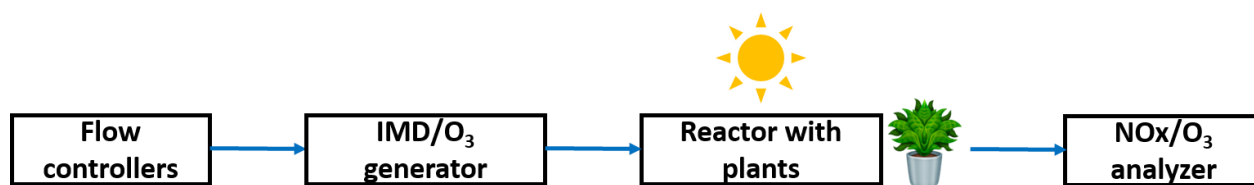


Figure 38 A simplified diagram of the setup used to study the NO_x or O₃ uptake by plants.

Then, we investigated the ability of VOCs emitted by plants to possibly react with the pesticides sprayed on them (Fig.42, C). Pesticides are used to protect the plants from pests. However, they can be toxic to humans or other living species, and it is therefore important to get insight into their fate to assess and estimate their (or their degradation products) risks. Solar light can induce reactions involving pesticides deposited on leaves, and the presence of VOCs in the close vicinity of pesticides could provoke cross reactions. The last part of the thesis was thus dedicated to study the photochemical interactions between VOCs emitted by a fragrant plant and two pesticides: Chlorothalonil (CT) and IMD (**Manuscript 3**). The diagram of the different steps followed in this case is given in **Fig.44**.

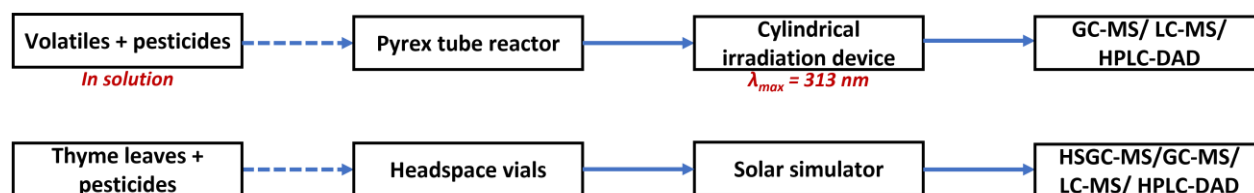


Figure 39 A diagram of the steps followed to study the interactions between volatiles and pesticides.

Manuscript 1:

In this manuscript, we studied the ability of IMD to generate NO_x (gaseous phase) and NO₂⁻/NO₃⁻ ions (aqueous phase) as well as the latter's ability to produce nitro/nitroso compounds (**Fig.45**).

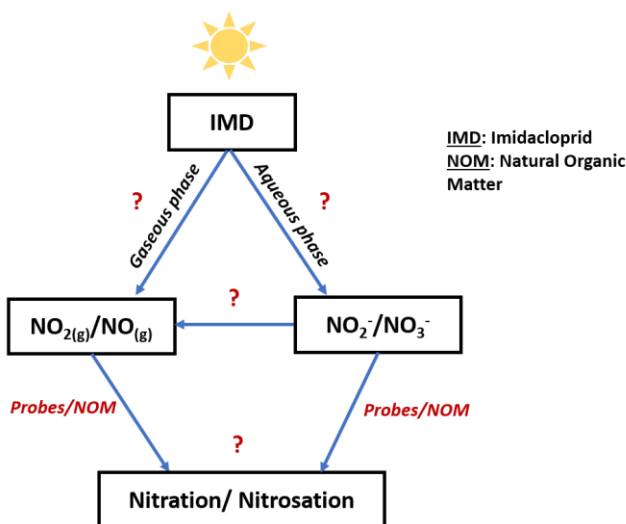


Figure 40 IMD degradation pathway and its possible nitration/nitrosation ability.

Aqueous solutions of IMD were irradiated within the wavelength range of 300-450 nm. Results showed that IMD underwent photodegradation. Although other photoproducts were detected, HPLC and LC-MS analyses showed the main formation of desnitro-IMD in accordance with the release of NO_2 . This formation is due to the cleavage of the N- NO_2 bond present in IMD (**Fig.46**). Both NO_2 and NO were detected with NO_2 production much higher than that of NO ; 1 h of IMD irradiation was enough to produce around 800 ppbv and 350 ppbv of NO_2 and NO respectively. Quantum calculations showed that IMD photolysis takes place in the triplet state and the dissociation of N- NO_2 is mainly homolytic. NO , on the other hand, could be produced by the photodecomposition of the nitroso derivative (IMD-O). In addition to that, NO_2^- and NO_3^- ions were detected in solution. Their photolysis should also form NO_2 and NO but their contribution to the total amount of NO_x detected was found to be minor. An experiment where IMD was deposited on glass petri dishes and irradiated was performed. In this case, lower concentrations of NO (23 ppbv) and NO_2 (297 ppbv) compared to the ones produced by IMD solution were detected in solid probably because IMD is much less dispersed than in water, and the absorption of light is lower.

We also showed that the irradiation of IMD photoinduced the nitration and nitrosation of phenolic probes representing water NOM moieties. It is supposed that phenols were oxidized by NO_2 into phenoxy radicals which could further react with NO_2 or NO to yield nitro or nitroso compounds (**Fig.46**).

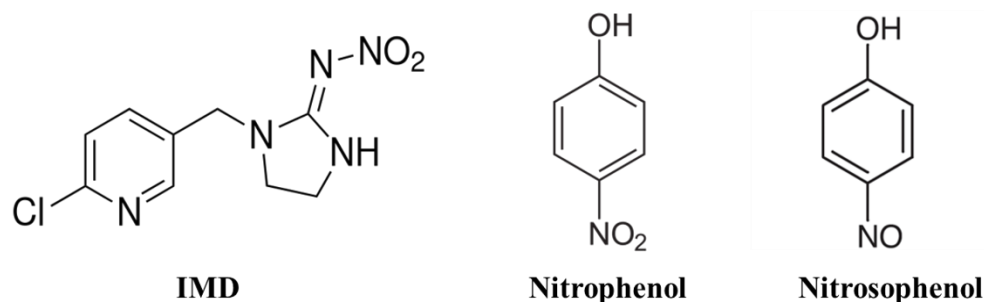


Figure 41 Structures of IMD, nitrophenol, and nitrosophenol.

To conclude, IMD, a neonicotinoid insecticide, produces a continuous and stable flow of NO_2/NO ; hence, for further experiments with plants, it was used as a source of NO_x .

Manuscript 2 (B):

Manuscript 2 took into consideration the NO_x and O_3 uptakes of different plants used on green roofs. For this, we started by modifying the base setup by adding new parts enabling us to study the pollutants uptakes in addition to the reactions taking place. Then, preliminary experiments were done which led to the selection of 3 plants for further experiments (**Fig.47**).

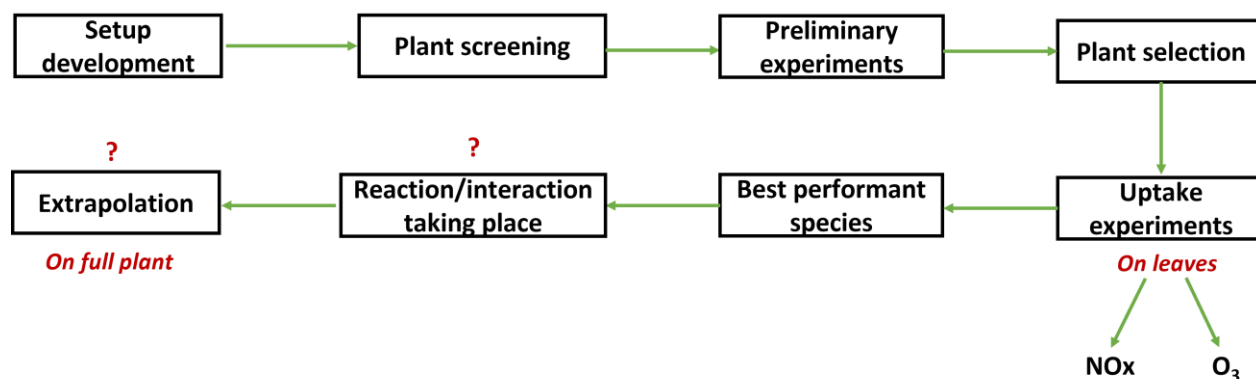


Figure 42 A diagram of the steps followed to monitor NO_x and O_3 uptakes of different plants.

The uptakes of the 13 plants were measured using their leaves. This allowed us to finally select 3 plants for further experiments: *sedum sexangulare* (sedum), *thymus vulgaris* (thyme), and *heuchera Americana L.* (heuchera). The choice was based on the frequency of their usage on green

roofs, emission of VOCs, and aesthetic values besides their uptakes. Nevertheless, the NO_x/O_3 backgrounds of the plants were investigated. Plants showed a negligible production of NO_x/O_3 . The reactor's NO_x/O_3 uptakes were also taken into consideration (**Fig.48**).

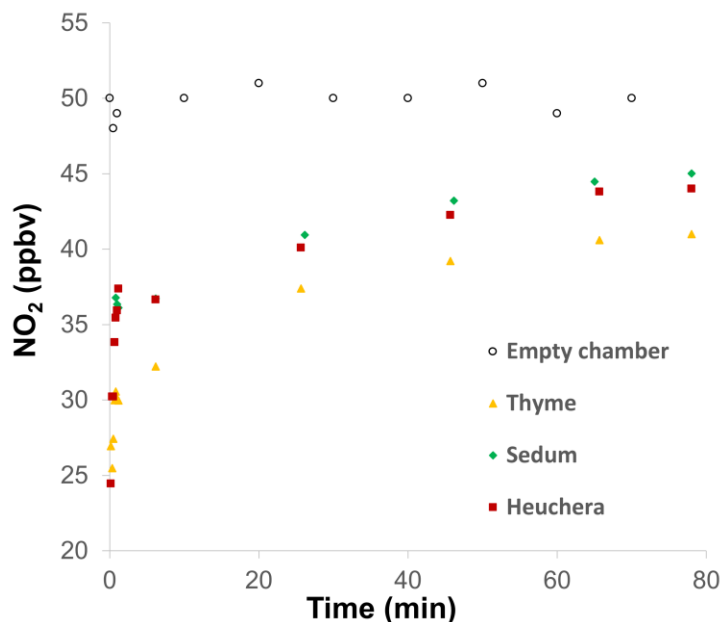


Figure 43 The NO_x uptake of the 3 plants in the mall reactor.

Thyme showed the highest uptake followed by sedum and then heuchera (**Fig.48**). To understand the reasons behind the uptakes and their mechanisms, additional experiments were performed. Using SEM, we observed that thyme exhibited the largest stomatal area and the second highest stomatal density. This explains thyme's good performance towards NO_2 and its removal mechanism.

In addition to that, the surface reaction between NO_2 and water potentially released by plants was investigated by using a nitrous acid (HONO) trap. Although the uptake is directly related to stomata, a surface reaction between NO_2 and H_2O potentially released by the plant due to the irradiation heat is possible. This reaction forms HONO. Among the 3 plants tested, sedum showed that more than half of the NO_2 uptake is due to this reaction. Hence, its uptake is because of stomata and the fact that it is a succulent plant that stores water in its leaves which might be released and react with NO_2 (**Fig.49**).

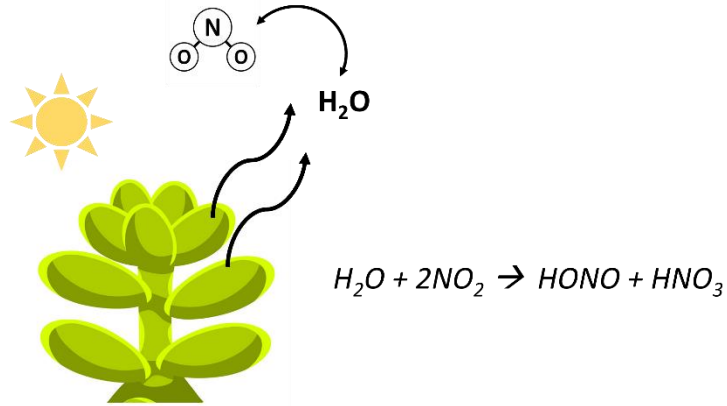


Figure 44 A succulent plant releasing water.

The same calculation was done as with NO_x to find out the most effective plants in removing O₃. The order was the same as for NO_x with thyme being the most performant followed by sedum and then heuchera. Thyme emits volatile compounds that might react with O₃. An experiment was performed in solution by bubbling O₃ into thymol (a major volatile emitted by thyme leaves) and directly on thyme leaves + O₃. Results showed that an interaction between volatiles and the pollutant takes place. Therefore, NO_x and O₃ are removed by the plants through different mechanisms; thyme removes O₃ by a reaction involving its VOCs, sedum removes NO₂ through a surface reaction involving water, while heuchera adsorbs both on its big hairy leaves making them a good adsorbent in addition to stomatal absorption which occur for all three studied plants.

The uptake coefficients and deposition velocities were calculated to understand the performance and to confirm our obtained results. The uptake coefficient shows the reactive uptake after a gas collides with a surface while the deposition velocity reflects the deposition rate of the gas on the surface. Values were in this order thyme > sedum > heuchera.

Extrapolation was tested by performing experiments on whole plants. The values obtained in both cases (NO_x and O₃ uptakes) were similar to those with detached leaves. Therefore, extrapolation is possible, and the uptake depends on the area exposed, as it can be expected.

Manuscript 3 (C):

Pesticides are regularly sprayed on plants to protect them from harmful pests and their presence on the leaves makes possible interactions, in particular photochemical ones, with plant constituents. For instance, an odorous plant like thyme can emit volatiles which might react with the sprayed pesticides. In this manuscript, the interaction of thyme's volatiles and 2 pesticides (the fungicide CT, and the insecticide IMD) was studied as well as the toxicity of photoproducts (**Fig.50**).

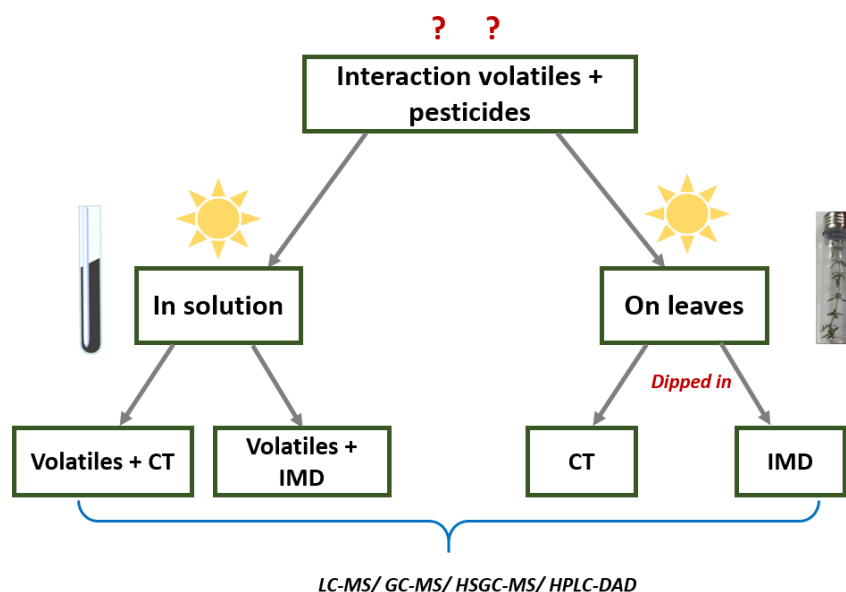


Figure 45 A diagram of the steps followed in manuscript 3.

We first determined what are the products of thyme emitted in the dark and under irradiation. The HSGC-MS analyses showed the production of thymol, linalool, 3-carene, and α -pinene confirming previous analyses of ATD-GCMS (**Manuscript 2**). Non-volatile compounds were also detected by LC-MS and GC-MS: several oxidation products, TO, the most concentrated, TQ, TQO, and dimers (**Fig.51**). Under irradiation, their production increased; for example, that of TO was 20-fold higher.

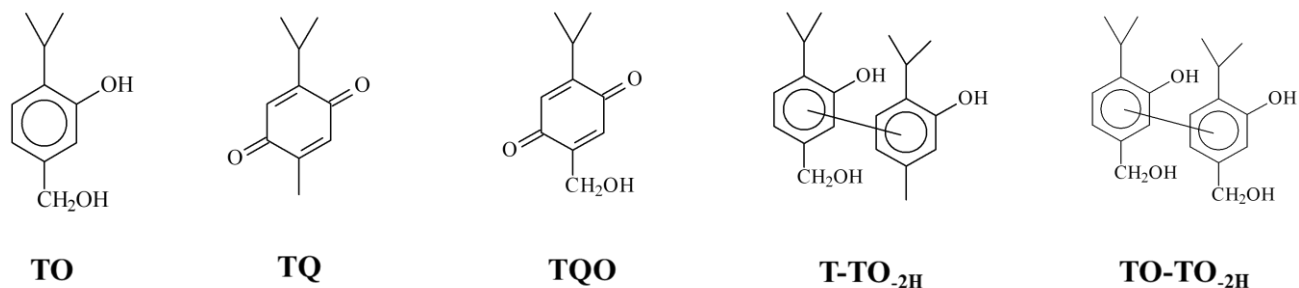


Figure 46 Thyme oxidation products.

The photochemical interactions between thymol (a phenolic derivative), linalool, 3-carene, and α -pinene (terpenes) with CT was first studied in acetonitrile solutions. They all significantly enhanced the rate of phototransformation of CT that was photoreduced. Laser flash photolysis experiments confirmed the ability of the triplet excited state of CT to react with thyme's volatiles and allowed to determine the reaction rate constants. Then, CT was irradiated on thyme's leaves directly. Again, CT underwent photoreduction. This result is in line with those obtained in solution and suggests the involvement of thyme's volatiles in the process.

Similarly, experiments were conducted with IMD and thymol in solution. In this case, thymol partly inhibited the photolysis of IMD and new photoproducts derived from thymol were detected (**Fig.52**). Some of them were nitrated in accordance with the capacity of IMD to release NO_2 under irradiation (**Manuscript 1**). It is supposed that NO_2 oxidizes thymol and TO leading to TNO_2 and TONO_2 respectively. The inhibiting effect of thymol on the IMD photolysis strongly suggests that NO_2 also oxidizes IMD.

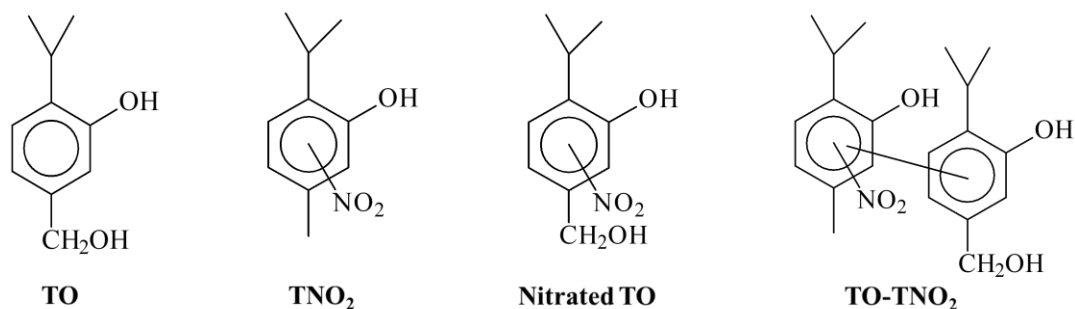


Figure 47 Photoproducts obtained in the mixture of thymol + IMD.

Thyme's twigs dipped in IMD, and either left in the dark or irradiated in the solar simulator produced these nitrated compounds. However, in the presence of light, the formation of TO and TONO₂ was drastically increased. These experiments demonstrate that nitrated compounds can be formed on plants treated with this insecticide. The ECOSAR (ECOLOGICAL Structure-Activity Relationship) computer program was used to estimate the toxicity of the starting and formed compounds. Thymol is moderately toxic; however, its oxidation products (TQ, T-TO-_{2H}, TO-TO-_{2H}) are more toxic. Also, the nitrated oxidation products of thymol (TNO₂ and TONO₂) are considered toxic especially TNO₂. Therefore, formed photoproducts are in general more toxic than the starting one rendering the choice of pesticides on plants important and the study of chemicals in real conditions necessary for a better assessment of their fates and toxicities.

3.2 Manuscripts

In this part, the 3 manuscripts will be presented.

Manuscript 1

New Route to Toxic Nitro and Nitroso Products upon Irradiation of Micropollutant Mixtures Containing Imidacloprid: Role of NO_x and Effect of Natural Organic Matter

Date of acceptance: February 15, 2020

New Route to Toxic Nitro and Nitroso Products upon Irradiation of Micropollutant Mixtures Containing Imidacloprid: Role of NO_x and Effect of Natural Organic Matter

Davide Palma, Yara Arbid, Mohamad Sleiman,* Pascal de Sainte-Claire, and Claire Richard*

Cite This: *Environ. Sci. Technol.* 2020, 54, 3325–3333

Read Online

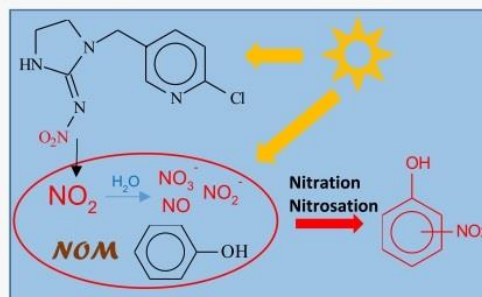
ACCESS |

Metrics & More

Article Recommendations

Supporting Information

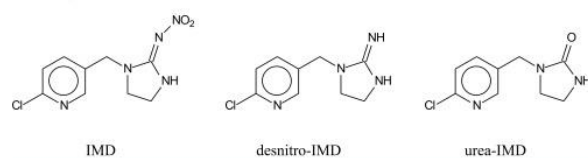
ABSTRACT: In this study, we reveal the capacity of imidacloprid (a neonicotinoid insecticide) to photoinduce the nitration and nitrosation of three aromatic probes (phenol, resorcinol, and tryptophan) in water. Using a gas-flow reactor and a NO_x analyzer, the production of gaseous NO/NO₂ was demonstrated during irradiation (300–450 nm) of imidacloprid (10^{−4} M). Quantum calculations showed that the formation of NO_x proceeds via homolytic cleavage of the RN–NO₂ bond in the triplet state. In addition to gaseous NO/NO₂, nitrite and nitrate were also detected in water, with the following mass balance: 40 ± 8% for NO₂, 2 ± 0.5% for NO, 52 ± 5% for NO₃[−], and 16 ± 2% for NO₂[−]. The formation of nitro/nitroso probe derivatives was evidenced by high-resolution mass spectrometry, and their yields were found to range between 0.08 and 5.1%. The contribution of NO₃[−]/NO₂[−] to the nitration and nitrosation processes was found to be minor under our experimental conditions. In contrast, the addition of natural organic matter (NOM) significantly enhanced the yields of nitro/nitroso derivatives, likely via the production of triplet excited states (³NOM*) and HO•. These findings reveal the importance of investigating the photochemical reactivity of water contaminants in a mixture to better understand the cocktail effects on their fate and toxicity.



INTRODUCTION

Imidacloprid (1-[(6-chloropyridin-3-yl)methyl]-N-nitro-imidazolidin-2-imine, IMD, Scheme 1) is a widely used and effective

Scheme 1. Molecular Structure of IMD and Its Main Photoproducts



neonicotinoid insecticide.¹ IMD, like other neonicotinoids, is used in a variety of crops, and its applications have been recently extended to the domestic sector and animal health.¹ Once released into the environment, it can reach the aquatic, atmospheric, and terrestrial compartments and be in contact with a lot of living organisms.^{2–4} IMD affects the central nervous system of insects,⁵ and there are increasing concerns about its deleterious effects with confirmed toxicity for pollinators, especially bees.⁶ Toxicity or adverse effects in other species have also been reported.^{7–9}

Several studies have been performed to investigate the fate of IMD under solar light, mainly in aqueous solutions,^{1,10–13} on plant leaves and cuticles,^{14–16} and more recently on solid

thin films.¹⁷ Desnitro-IMD (1-[(6-chloropyridin-3-yl)methyl]-imidazolidin-2-imine) was reported to be the main photoproduct and the urea-IMD (1-[(6-chloropyridin-3-yl)methyl]-imidazolidin-2-one) is a minor photoproduct (Scheme 1).¹⁶ The formation of these byproducts seems to imply the cleavage of the N–NO₂ bond; however, the fate of NO₂ is not yet clear. Recently, the formation of gaseous nitrogen oxides during the irradiation of IMD at the surface of a germanium attenuated total reflectance crystal was investigated.¹⁷ The authors detected nitrous oxide (N₂O), which was proposed to be formed by the recombination of detached NO₂ with the IMD fragments, in the electronic ground state.

In previous studies, we showed that the fungicides chlorothalonil and thiophanate-methyl can photoinduce the degradation of other pesticides during irradiation.^{18,19} These reactions can take place in surface waters, where fungicides are present together with a wide range of other chemicals, and on solid supports such as the surface of leaves, where pesticides are often applied in combination. However, the effect that a

Received: December 11, 2019

Revised: February 10, 2020

Accepted: February 15, 2020

Published: February 15, 2020

pollutant can have on another pollutant remains largely overlooked in photochemical studies, and little is known about the transformation of photostable pollutants via light-induced reactive intermediates of other co-pollutants. The ability of IMD to release NO_2 upon irradiation makes this compound important to study in this context because nitration of chemicals has been reported in a lot of systems generating NO_2 .^{20–28}

The goal of this study was thus to explore the formation of reactive NO_x via IMD photolysis and their reactivity toward surrogates of water contaminants and typical moieties of natural organic matter (NOM; phenol, resorcinol, and tryptophan). In particular, we investigated the formation of nitro- and nitroso-derivatives, two potentially toxic categories of compounds, from the three selected probes under polychromatic irradiation (300–450 nm) in the presence of IMD. Experiments were carried out using a flow-tube reactor equipped with a NO_x analyzer, whereas the formation of byproducts was characterized by high-resolution ultrahigh-performance liquid chromatography system–electrospray ionization-mass spectrometry (UHPLC–ESI-MS). Theoretical calculations were also performed to elucidate the mechanisms of NO_x formation. To the best of our knowledge, this is the first study reporting on the measurement of NO_x during irradiation of IMD in water and on their role in nitrosation/nitration of other water pollutants. Environmental implications of this light-induced indirect degradation are discussed.

MATERIALS AND METHODS

Chemicals and Materials. Imidacloprid (PESTANAL, analytical standard), resorcinol (purity 99%), phenol (purity $\geq 99.5\%$), L-tryptophan (purity $\geq 98\%$), and 2,4-dinitrophenylhydrazine (DNPH, purity 97%) were purchased from Sigma-Aldrich and used as received. Sodium nitrite (Rectapur 98%), sodium nitrate (Fluka, purity 99%), 2- and 4-nitrophenol (Fluka, purity $\geq 99\%$), and 4-nitrosophenol (Aldrich-Chemie, purity 60% due to the water content of 40%) were also used without further purification. Suwannee River NOM (2R101N) was purchased from IHSS. Water was purified using a reverse osmosis RiOs 5 and Synergy (Millipore) device (resistivity 18 $\text{M}\Omega$ cm, DOC < 0.1 $\text{mg}\cdot\text{L}^{-1}$). All solvents or other reactants were of the highest grade available.

Irradiation. Two different irradiation devices were used. To monitor NO_x formation in the gas phase, device 1 was designed with a cylindrical Pyrex gas flow reactor (0.65 L, length 27 cm, and diameter 5.7 cm) containing 200 mL of IMD solution (10^{-4} M or 25.6 $\text{mg}\cdot\text{L}^{-1}$) and irradiated from the top with two fluorescent tubes (Sylvania F15W/BL 368, 438 mm \times 26 mm, 300–450 nm, and λ_{max} at 365 nm, see Figure S1) placed at a distance of 5 cm. The rate of incident light entering the solution was measured using a QE65000 radiometer (Ocean Optics); it was equal to 1.3×10^{16} $\text{photon}\cdot\text{cm}^{-2}\cdot\text{s}^{-1}$. The gas flow reactor was connected to a NO_x chemiluminescence analyzer (Thermo Scientific i-42 NO_x analyzer), as shown in Figure 1. Experiments were carried out under a continuous flow of clean air to reduce the residence time of NO_x and minimize NO_2 photolysis. The gaseous inlet of the reactor was connected to flow controllers for N_2 and O_2 (model Brooks 4800 Series), allowing the selection of the atmosphere under which irradiation was performed (pure N_2 , pure O_2 , or a 80/20 O_2/N_2 mixture) and to adjust the flow rate to 0.7 $\text{L}\cdot\text{min}^{-1}$. Background levels of NO_x in the gas inlet were negligible (< 0.4 ppbv). Before irradiation, the levels of NO_x in

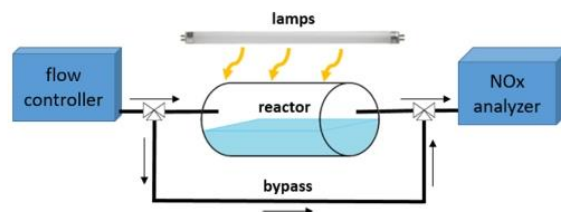


Figure 1. Schematic representation of device 1 used to monitor NO_x formation upon irradiation of IMD solutions.

the gas phase of the reactor were monitored continuously every 10 s until they reached a steady state within a few minutes (Figure S2). Despite the fact that NO_2 concentrations of up to 40 ppbv were detected initially (first 30 s), a background level of NO_x (< 5 ppbv) was quickly reached. This production of NO_2 might possibly be due to IMD photolysis under indoor lighting during the preparation and handling of the solutions. During IMD irradiation, we have chosen to monitor NO_x levels in the gas phase of the reactor at selected times and not continuously. After selected irradiation times, the light was turned off, and the outlet of the reactor was connected to the NO_x analyzer. NO_x levels were measured every 10 s for a period of 1–2 min at a flow rate of 0.7 $\text{L}\cdot\text{min}^{-1}$. The time profile of NO_x concentrations shown in Figure S2 corresponds to the decay of the NO_x level in the reactor due to dilution with clean air. The level of NO_x measured was relatively constant at 1, 2, 4, and 6 h of IMD irradiation, in accordance with a steady-state regime. The levels of NO_x generated were then obtained by integrating the time profiles of NO_x concentrations. For calculating the yields of NO_x , the ratio of NO_x concentrations (ppbv) was converted into molar by taking into account the gas phase volume of the reactor (450 mL). By measuring the converted quantity (in moles) of IMD during the irradiation period, it was possible to calculate the molar yield for NO and NO_2 .

A second device, device 2, was used to monitor the formation of nitro- and nitroso-derivatives. Fifteen milliliters of solutions was placed in a cylindrical Pyrex reactor sealed with an air-tight silicon cap and surrounded by six fluorescent tubes (Sylvania F15W/BL 368), installed inside a custom-made cylindrical irradiation device. Solutions were not buffered, but pH was controlled during the reactions. The initial pH was 6.5 ± 0.3 , and in the course of the reactions, the pH was set to above 5. In the case of IMD + resorcinol mixtures, aliquots were sampled after several selected irradiation times, and the consumption profiles of IMD and nitro- and nitroso-resorcinol were obtained. For IMD + phenol and IMD + tryptophan mixtures and experiments with nitrate/nitrite and NOM, aliquots were only sampled after 16 h of irradiation. Samples were analyzed by HPLC to monitor the loss of IMD and the probes and by UHPLC–high-resolution mass spectrometry (HRMS) to characterize the photoproducts and estimate their levels. For the experiment with 10^{-5} M IMD and 10^{-4} M resorcinol, 75 mL was irradiated in portions of 25 mL, and water was evaporated up to 6 mL using a rotavapor before further analyses. Experiments were done in duplicate or triplicate.

Analytical methods. Absorption spectra were recorded using a Varian Cary 3 spectrophotometer. IMD, phenol, resorcinol, and L-tryptophan concentrations were monitored by HPLC (Waters Alliance 2695) equipped with a photodiode

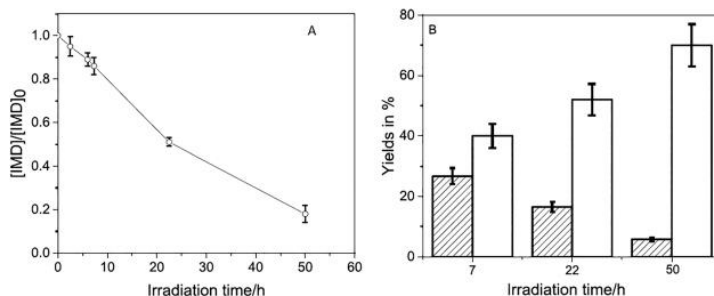


Figure 2. Consumption profile of aqueous IMD (10^{-4} M) irradiated in device 1 (A) and yields of NO_3^- (white bars) and NO_2^- (shaded bars) (B). Error bars are standard deviations.

array detector (Waters 2996) and an EC150/4.6 Nucleodur 100-5 C_8 endcapped column. The HPLC conditions are presented in Table S1. Photoproducts were quantified using the same instrument after derivatization with DNP. The derivatizing solution (15 mL) was prepared by mixing concentrated HCl, ultrapure water, and acetonitrile at a ratio of 2.5:1. Fifty microliters of this solution was added to 5 mL of sample solution. The derivatization reaction was completed in 5 min, and HPLC analyses were run shortly after. Calibration used derivatized NO_2^- solutions in the concentration range 10^{-6} to 10^{-5} M. All the HPLC analyses were done in triplicate, and the presented data are the mean values obtained.

NO_3^- was measured by ionic chromatography on a Dionex ICS-5000⁺ using a column model Dionex Ion Pack AS11 2 mm \times 250 mm; the flow was $0.25 \text{ mL} \cdot \text{min}^{-1}$; and the mobile phase was an aqueous solution of KOH at the concentration of 0.43 mM for the first 4.5 min followed by linear gradient for up to 18 min of runtime by increasing the KOH concentration up to 11.70 mM. The injection volume was $750 \mu\text{L}$, and the temperature of the column oven was set to 30°C . External standards were prepared using NaNO_3 in the concentration range $50\text{--}200 \mu\text{g} \cdot \text{L}^{-1}$. Nitro- and nitroso-derivatives of phenol, resorcinol, and L-tryptophan were characterized, and their concentrations were estimated by HRMS performed on an Orbitrap Q-Exactive (Thermo Scientific) coupled to an UHPLC system, Ultimate 3000 RSLC (Thermo Scientific). Because of the lack of available standards, desnitro-IMD and the minor photoproducts were tentatively identified by HRMS, but quantification was not possible. Analyses were carried out in both negative (ESI^-) and positive (ESI^+) electrospray modes. The column used was the same column used for HPLC-UV. The binary solvent system was composed of acetonitrile and acidified water using formic acid at 40 and 60%, respectively, with a flow rate of $1.0 \text{ mL} \cdot \text{min}^{-1}$. Nitro- and nitroso-phenols were quantified by the injection of external standards of 4-nitro- and 4-nitroso-phenols at concentrations varying from 5×10^{-7} to 4×10^{-6} M (Figure S3). Because of commercial unavailability of nitrated derivatives, the concentrations of nitro- and nitroso-resorcinols were estimated using the calibration curves of 4-nitro- and 4-nitroso-phenols. The concentrations of nitro-tryptophan and nitroso-tryptophan were estimated using L-tryptophan at the concentration of 10^{-6} M as a reference. Yields were obtained by dividing the photoproducts' concentrations by the loss of IMD in concentration and by multiplying these ratios by 100.

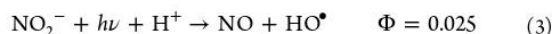
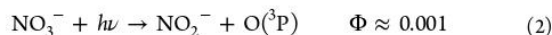
Computational Method. Potential energy surfaces (PESs) were investigated with the Gaussian series of programs.³⁰ Density functional theory (DFT) calculations

(optimizations, frequency calculations, identification of transition states, and IRC calculations) were performed at the MN12SX/6-311++G(d,p)//MN12SX/6-31+G(d,p) level of calculation. Among the large set of hybrid range-separated functionals that we tested, MN12SX³¹ gave the best agreement between the experimental and theoretical absorption spectra. Finally, the time-dependent-DFT (TD-DFT) method was used to compute singlet excited states. The triplet state was explored with conventional self-consistent field calculations. The solvent was modeled implicitly with the polarizable continuum model (PCM). Electronic energies are reported throughout (Gibbs free energies are not provided here because low vibrational modes may introduce large uncertainties in this calculation).

RESULTS AND DISCUSSION

Photolysis of IMD. The degradation profile of neutral aqueous IMD (10^{-4} M) irradiated in device 1 is shown in Figure 2A. HPLC-UV and UHPLC-HRMS analyses indicated that the main photoproduct was desnitro-IMD (Figure S4). Three minor photoproducts were also found: a compound produced by addition of an oxygen atom on IMD (IMD + O), another one produced by addition of two oxygen atoms on desnitro-IMD (desnitro-IMD + 2O), and the nitroso derivative of IMD (IMD-O) as traces (Table S2).

NO_3^- and NO_2^- were detected in the aqueous phase (Figure S4). The yield of NO_3^- increased constantly to reach $72 \pm 5\%$ after 50 h of irradiation (Figure 2B, white bars). In contrast, the yield of NO_2^- decreased from 27% after 7 h of irradiation to 6% after 50 h (Figure 2B, shaded bars). The higher accumulation of NO_3^- compared to that of NO_2^- is consistent with the spectral properties and the known photoreactivity of these ions. NO_3^- ($\lambda_{\text{max}} = 300 \text{ nm}$ and $\epsilon = 8 \text{ M}^{-1} \cdot \text{cm}^{-1}$) absorbs much less solar light than NO_2^- ($\lambda_{\text{max}} = 355 \text{ nm}$ and $\epsilon = 22 \text{ M}^{-1} \cdot \text{cm}^{-1}$), and its quantum yield of photolysis is also lower (reactions 1–4) leading to a smaller photolysis rate³²



The detection of IMD + O and of desnitro-IMD + 2O appears to be consistent with the formation of hydroxyl radicals through reactions 1 and 3.

Table 1. Formation of NO_x after 2 h of Irradiation of IMD (10⁻⁴ M) or NO₃⁻/NO₂⁻ Mixtures in Device 1

conditions	quantity of IMD converted	quantity of NO ₂ formed (molar yield)	quantity of NO formed (molar yield)
IMD (10 ⁻⁴ M)	380 ± 20 μg	24 ± 5 μg (40 ± 8%)	0.88 ± 0.20 μg (2 ± 0.5%)
NO ₃ ⁻ (1.8 × 10 ⁻⁶ M) + NO ₂ ⁻ (1.7 × 10 ⁻⁶ M)		1.6 ± 0.3 μg	3.9 ± 0.8 μg
NO ₃ ⁻ (2 × 10 ⁻⁵ M) + NO ₂ ⁻ (5 × 10 ⁻⁶ M)		4.8 ± 1.0 μg	11.6 ± 2.3 μg

NO_x Formation upon Irradiation of IMD. We also measured the NO_x formation in the gaseous phase above the solutions. NO and NO₂ were successfully detected upon irradiation of IMD (10⁻⁴ M) in device 1. Examples of collected data are shown in Figure S2. During the first 2 h of reaction of irradiation, 24 μg of NO₂ and 0.88 μg of NO were produced, whereas the IMD loss was around 380 μg (see Table 1). After integrating the nitrite and nitrate levels produced and considering the volume of gas (200 mL) and of water (450 mL), an overall mass balance of IMD conversion into inorganic N-containing products was determined: 40 ± 8% for NO₂, 2 ± 0.5% for NO, 52 ± 5% for nitrate, and 16 ± 2% for nitrite.

As the presence of NO₃⁻/NO₂⁻ in the aqueous solution could potentially generate NO_x,³³ we irradiated these ions independently to estimate their contribution to the pool of NO_x detected upon irradiation of IMD. We chose to perform these comparative experiments with NO₃⁻ = 1.8 × 10⁻⁶ M and NO₂⁻ = 1.7 × 10⁻⁶ M corresponding to the concentrations estimated after 2 h of irradiation in device 1 (Figure S4). The irradiation of this mixture for 2 h yielded 15-fold less NO₂ and 4.4-fold more NO than the irradiation of IMD (10⁻⁴ M) (Table 1). The amount of NO_x formed above the IMD solution was 4.5-fold higher than that above the NO₃⁻/NO₂⁻ solution, showing that IMD was the main contributor. Moreover, the higher yield of NO in the latter system confirmed that the NO_x precursor in the NO₃⁻/NO₂⁻ mixture was NO₂⁻, through reaction 3. At higher concentrations of NO₃⁻/NO₂⁻ (2.0 × 10⁻⁵ M and 5 × 10⁻⁶ M, respectively), not far from those reached after 16 h of IMD irradiation, NO and NO₂ levels were 3-fold higher than in the previous case, respectively, showing that, in this concentration range, the NO and NO₂ amounts accumulated in proportion to NO₂⁻ concentration. Again, the amount of NO_x generated from NO₂⁻ (2.0 × 10⁻⁵ M) was still below the one formed upon irradiation of IMD solution.

As previously shown, the bond N–NO₂ was cleaved when IMD was irradiated in the solid phase at 305 and 254 nm.¹⁷ However, some questions remain unanswered: would the proposed mechanism in the solid phase and at short wavelengths be still valid in solution and at longer wavelengths, and thus at lower excitation energies? How is NO formed and how the oxygen atom is eliminated? In an attempt to answer these questions, we performed quantum calculations.

Theoretical Calculations. Several conformers were found for the solvated imidacloprid system. The structure of the global minimum was similar to that found from the recent first-principles^{17,34} and crystallographic investigations³⁴ (see the Supporting Information section for all structures reported in this work). Moreover, the DFT method used here was able to reproduce accurately the experimental absorption spectrum (see Figure 3).

A detailed investigation of the ground state (S₀), the first triplet state (T₁), and the first singlet excited state (S₁) was performed. Some of the key results are shown in Figure 4 and discussed below. The minima and transition state structures are given in the Supporting Information section. The

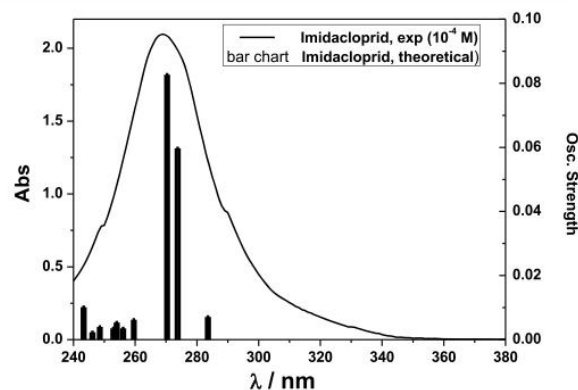


Figure 3. Experimental (Abs, left axis) and theoretical (oscillator strengths, right axis) absorption spectra of imidacloprid (theoretical spectrum for the most stable conformer (Figure S5a)) at the TD-MN12SX/6-311++G(d,p),PCM//MN12SX/6-31+G(d,p),PCM level. The oscillator strength is the probability of absorption. It is related to the dipole strength of the transition and is proportional to the molar absorptivity maximum for this transition. The S₁–S₀ transition is optically active (284 nm). The oscillator strength of this transition is 0.02, which is significant (an ε of about 6000 L·mol⁻¹·cm⁻¹ can be estimated from this value, when a UV-vis half-width at half-height of 0.333 eV is used to model the absorption spectrum).

dissociation pathways of interest are depicted in this figure: NO₂ is shown on the left-hand side of Figure 4, and triplet atomic oxygen (a reaction that is precursor to the production of NO) is shown on the right-hand side of Figure 4. The minimum energy path was followed to investigate the formation of NO₂ in S₁ by performing partial optimizations of imidacloprid for fixed RN–NO₂ bond distances. The MEP maximum is indicated by a dashed level in Figure 4.

S₀ and S₁ States. Our results show that the departure of atomic triplet oxygen is not favored in the ground state because the predissociated intermediate ¹RNNO–O (R(O–O) = 1.523 Å; 56.4 kcal·mol⁻¹) cannot be reached because of very large activation energy (106.1 kcal·mol⁻¹). Similarly, the formation of NO₂ is not expected in the ground state because the respective electronic dissociation energy in S₀ is large (64.4 kcal·mol⁻¹; RN + NO₂). A transition state could not be found between imidacloprid (¹RNNO₂) and separated radicals in S₀. This is expected for homolytic dissociations in the ground state. In S₁, the dissociation of the RN–NO₂ bond required 14.0 kcal·mol⁻¹ (MEP maximum). In addition, the in-cage dissociation complex ¹RN···NO₂ is less stable (85.3 kcal·mol⁻¹) than the respective reactant (79.3 kcal·mol⁻¹). Thus, dissociation in S₁ is less favored than that in the triplet state (an activation energy of 6.1 kcal·mol⁻¹ was found in T₁, and the reaction is now exothermic; see Figure 4). Moreover, our results show that the heterolytic dissociation mechanism would lead to RN⁺/NO₂⁻ species, which are slightly less stable (see also Supporting Information) than the respective separated radicals (RN/NO₂). Thus, it seems reasonable to consider that

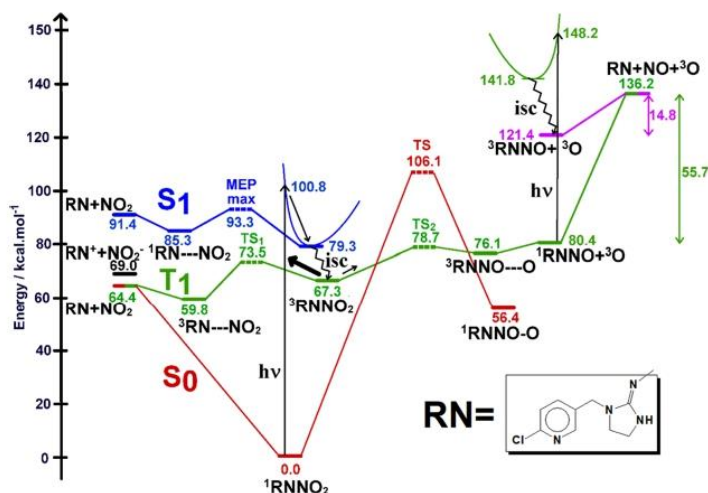


Figure 4. Electronic energies of stationary points in the ground state (S_0 , red), first triplet (T_1 , green), and first singlet (S_1 , blue) excited states of imidacloprid ($^1\text{RNNNO}_2$). Calculations were performed by the MN12SX/6-311++G(d,p),PCM//MN12SX/6-31+G(d,p),PCM method. Transition states and the MEP maximum are represented by dashed levels. Dashed bonds represent long-range separations. The energies of separated fragments $\text{RN} + \text{NO}_2$ and $^1\text{RNNNO} + ^3\text{O}$ are also given in the figure. The energies of the heterolytic dissociation products (left-hand side, black) and the triplet state of RNNNO (right-hand side, purple) are also indicated. The separated fragments RN and NO_2 in S_1 are, respectively, in the first doublet excited state (RN) and the doublet ground state (NO_2).

it is these radicals that are eventually obtained in the liquid phase. However, considering the small energy difference between heterolytic and homolytic dissociation energies, a mixture of homolytic and heterolytic dissociation products might not be completely ruled out. Implicit solvation models underestimate the solvation free energy of small ions, the cases of the proton and hydroxide being emblematic of this issue. In order to address this point, we computed $\Delta G_{r,\text{calc}}^{*m}$ the dissociation Gibbs free energy for both heterolytic and homolytic NO_2 cleavage. In this calculation, $RT \times \ln(24.46)$ was added to $\Delta G_{r,\text{calc}}^*$ to account for the free energy change of 1 mol of an ideal gas from 1 atm to 1 M.³⁵ $\Delta G_{r,\text{calc}}^0 = \Delta G_{r,\text{calc}}^* + RT \times \ln(24.46)$ was 58.6 and 49.2 $\text{kcal}\cdot\text{mol}^{-1}$, respectively, for the heterolytic and homolytic dissociation reactions, thus a difference of 9.4 $\text{kcal}\cdot\text{mol}^{-1}$ (recall that the respective difference in electronic energies was smaller, i.e., 4.6 $\text{kcal}\cdot\text{mol}^{-1}$). Considering the implicit solvation model may underestimate the solvation free energy for NO_2^- by as much as 10 $\text{kcal}\cdot\text{mol}^{-1}$, the radical dissociated species are still more stable than the heterolytic dissociation fragments, in agreement with our results.

Triplet State T_1 . Second, S_1/T_1 intersystem-crossing (isc) is favored because minimum energy geometries in S_1 and T_1 are very similar for RNNNO_2 , and the energy gap is small (less than 0.1 $\text{kcal}\cdot\text{mol}^{-1}$ at the Franck–Condon geometry). In addition, in the triplet state, the barrier for NO_2 dissociation (6.1 $\text{kcal}\cdot\text{mol}^{-1}$) is significantly smaller than that for dissociation into a triplet atomic oxygen and a singlet fragment ($^1\text{RNNNO} + ^3\text{O}$; 11.4 $\text{kcal}\cdot\text{mol}^{-1}$), in agreement with our experimental findings. Moreover, the in-cage dissociation complex $^3\text{RNNNO}\cdots\text{O}$ is thermodynamically less stable than the respective reactant $^3\text{RNNNO}_2$, and this reaction is displaced toward the reactant. Nevertheless, this pathway is investigated below to see if this reaction could play a role, even minor, in the formation of NO radicals.

NO Formation, A Minor Pathway. The mechanism of production of nitric oxide from $^1\text{RNNNO}$ is also shown in

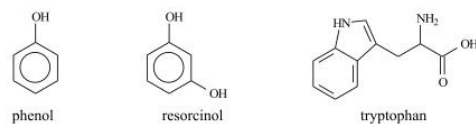
Figure 4. NO bond dissociation energy was 55.7 $\text{kcal}\cdot\text{mol}^{-1}$ for $^1\text{RNNNO}$ in the ground state, whereas cleavage in the triplet state (reached through S_1 followed by isc) required only 14.8 $\text{kcal}\cdot\text{mol}^{-1}$ (RN is obtained). A transition state could not be found in T_1 , and the energy of activation may be identified with the dissociation energy in that case. Thus, the formation of NO as a primary product from RNNNO is probably a minor pathway.

Thus, our quantum calculations provide strong evidence that photolysis of IMD mainly leads to NO_2 formation in the overall triplet state's PES, while NO formation is a minor pathway.

Evidence for Nitro-/Nitroso-Derivative Formation.

Nitrate and nitrite ions which generate HO^\bullet radicals simultaneously with NO or NO_2 have been reported to photoinduce the nitration and/or the nitrosation of phenolic derivatives.^{20–24} Whether the photolysis of IMD could also contribute to the formation of such toxic products was a hypothesis that we aimed to verify in this study. Thus, IMD was irradiated with each of the three probes, shown in Scheme 2, in a small reactor (device 2) for 16 h. Under these

Scheme 2. Selected Probes



conditions, the loss of IMD irradiated alone reached 60% (Figure S7). We first compared the probes' consumption (10^{-4} M) in the absence and in the presence of IMD (10^{-4} M) to quantify the photoinductive effect (Table S4). The disappearance of phenol and resorcinol was drastically faster in the presence of IMD, evidencing a strong effect. Only in the case

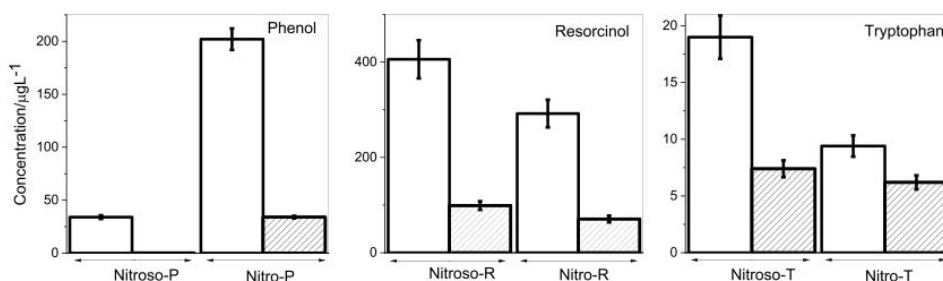


Figure 5. Concentrations of nitro- and nitroso-derivatives of phenol, resorcinol, and tryptophan detected after 16 h of irradiation of the probes (10^{-4} M) in device 2 in the presence of IMD (10^{-4} M) (white bars) and in the presence of the mixture of NO_3^- (2×10^{-5} M) and NO_2^- (5×10^{-6} M) (shaded bars). Error bars are standard deviations.

Table 2. Effect of NOM ($11 \text{ mg}\cdot\text{L}^{-1}$) on the Photo-Nitration/Photo-Nitrosation of Resorcinol (10^{-4} M) after 2 h of Irradiation in Device 2 in the Presence of IMD (10^{-4} M) or NO_2^- (5×10^{-6} M)^a

conditions	% resorcinol converted	nitroso-derivatives formed ($\mu\text{g}\cdot\text{L}^{-1}$)	nitro-derivatives formed ($\mu\text{g}\cdot\text{L}^{-1}$)
IMD + resorcinol	7.0 ± 0.3	83 ± 8	44 ± 4
IMD + resorcinol + NOM	18 ± 1	110 ± 10	88 ± 9
NO_2^- + resorcinol	<1	20 ± 2	1 ± 0.1
NO_2^- + resorcinol + NOM	<1	55 ± 5	35 ± 3

^aThe light screening effect of NOM (10%) is taken into account.

of tryptophan, the acceleration effect was small because of the fast photolysis of the probe under the studied conditions.

Then, we monitored the formation of nitro-/nitroso-derivatives by UHPLC–HRMS analyses. Figure S8 shows the formation profile of nitroso- and nitro-resorcinols upon irradiation of IMD (10^{-4} M) and resorcinol (10^{-4} M). The concentration of the two photoproducts increased linearly up to 7 h of irradiation before reaching a plateau value after 16 h. Nitro- and nitroso-derivatives were also detected with phenol and tryptophan. The detected levels after 16 h of irradiation are given in Figure 5 (white bars) and Table S4. The estimated yields of nitro-resorcinols reached 3.3% of converted IMD and those of nitroso-resorcinols 5.1%. The yield of nitro-phenols (ortho + para derivatives)²¹ was equal to 2.6%, but that of nitroso-phenols (ortho + para derivatives) was smaller (0.5%). For tryptophan, both yields were very small, reaching only 0.08% (nitro-derivatives) and 0.14% (nitroso-derivatives) of tryptophan converted because of the fast-direct photolysis of tryptophan.

Experiments were also performed at lower reactant concentrations to determine the impact of this parameter on the rates. A 10-fold decrease of the concentration of IMD for a concentration of resorcinol kept constant at 10^{-4} M reduced the amount of nitro-resorcinols by 18-fold and that of nitroso-resorcinols by 9-fold, while the sum of the two photoproducts was reduced by about 10-fold (Table S4). A 10-fold decrease of the concentration of resorcinol for a concentration of IMD kept constant at 10^{-4} M decreased 3-fold the amount of nitro-resorcinols and 100-fold that of nitroso-resorcinols, and their sum (nitro + nitroso) was reduced by about 5-fold (Table S4). These results indicate that the reaction rate was proportional to the concentrations of reactants. The decay rate of resorcinol followed a first-order kinetic with a rate constant k that can be expressed as: $k = 5.9 \times 10^{-3} [\text{IMD}] \text{ s}^{-1}$.

We also studied the nitro/nitrosation capacity of the $\text{NO}_3^-/\text{NO}_2^-$ mixture to quantify their contributions in these reactions (shaded bars in Figure 5 and Table S4). For these comparisons, we fixed $\text{NO}_3^-/\text{NO}_2^-$ concentrations to those

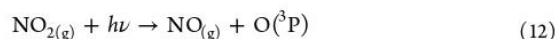
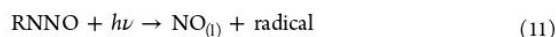
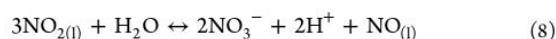
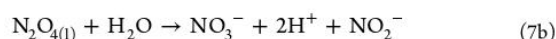
measured in the IMD solution after 16 h of irradiation in device 2 (2×10^{-5} and 5×10^{-6} M, respectively), and the mixtures of $\text{NO}_3^-/\text{NO}_2^-$ and probes were irradiated for 16 h in device 2. Nitrosation was 121-fold lower in the case of phenol, 4.1-fold in the case of resorcinol, and 2.6-fold in the case of tryptophan than in the presence of IMD, while nitration was 5.9-fold lower for phenol, 4.1-fold for resorcinol, and 1.5-fold for tryptophan. One concludes that the contributions of $\text{NO}_3^-/\text{NO}_2^-$ to the nitration/nitrosation processes observed in irradiated IMD solutions were minor, especially for phenol and resorcinol, even though we acknowledge that the conditions chosen for the comparative experiments (fixed $\text{NO}_3^-/\text{NO}_2^-$ concentrations) cannot perfectly reproduce the dynamic and complex evolution of $\text{NO}_3^-/\text{NO}_2^-$ during IMD irradiation.

Effect of NOM on Nitration/Nitrosation of Probes. Another important aspect we attempted to explore is the effect of NOM on these photochemical nitration/nitrosation reactions. The experimental conditions and results are reported in Table 2. NOM ($11 \text{ mg}\cdot\text{L}^{-1}$) increased the percentage of resorcinol loss in the presence of IMD by a factor of 2.6, after correction for the light screening effects (10%). The formation of nitroso- and nitro-resorcinols in IMD solutions was increased by a factor of 1.3 and 2.0, respectively, and the formation of nitro- and nitroso-resorcinols in NO_2^- solutions by factors of 35 and 2.8, respectively. The very low formation of nitro-resorcinols in the system NO_2^- + resorcinol was already shown.²⁰ These data highlight the significant effect of NOM on the nitro-/nitroso-derivative formation.

Reaction Mechanism. Many reactions are expected to take place in this complex system. The main ones are summarized below. The photolysis of IMD in water generates NO_2 in the liquid phase ($\text{NO}_{2(l)}$) together with the radical RN, as shown by the quantum calculations, and the latter mainly gives rise to desnitro-IMD (reaction 5). The radicals $\text{O}(^3\text{P})$ and RNNO are also produced, but in much lower amounts (reaction 6). The reactivity of NO_2 in water is very high. It is reported in the literature that NO_3^- and NO_2^- are generated according to reactions 7a and 7b through the intermediary

dimerization of $\text{NO}_{2(l)}$.^{36,37} NO_3^- and $\text{NO}_{(l)}$ can also be produced through reaction 8.^{37,38} In our experiments, $\text{N}_2\text{O}_{4(g)}$ cannot be distinguished from $\text{NO}_{2(g)}$. Reaction 8 is probably the major NO formation pathway, but the photolysis of RNNO (reaction 11), of $\text{NO}_{2(g)}$ (reaction 12), and of NO_2^- (reaction 3) is the alternative pathway for NO formation. NO is stable in water and volatilizes in the gaseous phase (reaction 9).³⁷ It generates $\text{NO}_{2(g)}$ by reacting with oxygen (reaction 10).

In this scheme, we did not take into account the oxidation of IMD by HO^\bullet formed in reaction 3 because the formation of oxidation products (IMD + O) was small. NO_2^- and NO_3^- could also be oxidized by HO^\bullet .³⁹ However, because of the high concentration of IMD compared to those of NO_2^- and NO_3^- in the first half of the reaction, IMD and its main photoproduct desnitro-IMD are expected to be the main sinks of HO^\bullet .



The nitration/nitrosation of phenolic/aromatic compounds in the presence of NO_2^- or NO_3^- has already been studied.^{26–25,39–41} NO_2 is recognized as having a key role in these reactions, even though the mechanisms are not fully understood. Several studies attributed the formation of phenoxyl radicals to the reaction of phenols with NO_2 ,^{20,25,39,41} while others to their reaction with HO^\bullet .⁴⁰ Once formed, the phenoxyl radicals further react with NO_2 to yield the ortho- and para-derivatives of nitro-phenols. Similarly, the reaction of phenoxyl radicals with NO is expected to generate nitroso-phenols. The effect of NOM on these reactions is difficult to predict because of the existence of opposite reactions. Indeed, on the first hand, NOM can potentially favor the nitro/nitrosation reactions by generating photooxidants, such as the triplet excited states (${}^3\text{NOM}^*$), singlet oxygen, or HO^\bullet , that are expected to induce the formation of phenoxyl radicals, as shown in the literature.³⁹ In addition, ${}^3\text{NOM}^*$ or HO^\bullet could be able to oxidize NO_2^- and NO_3^- into NO_x ³⁹ (see process 13 related to NO_2^-)



On the other hand, NOM could also be a sink for NO_x because of the presence of aromatic moieties in its structure and therefore could inhibit the nitration/nitrosation reaction to some extent.^{26,42} The overall effect of NOM will thus depend on the experimental conditions, and in particular on the relative concentrations of reactants. In our set-up, the presence of NOM (11 mg·L⁻¹) in IMD or NO_2^- solutions containing resorcinol (10⁻⁴ M) increased the amounts of nitro-

and nitroso-resorcinols, showing that in this case, NOM favors the formation of the phenoxyl radical and of NO_2 . Because Suwannee River NOM contains 68% of fulvic acids and fulvic acids contain ~3 mmol oxidizable phenol per g of carbon,⁴³ there are about 20 μM of oxidizable phenols originating from NOM in a solution containing 11 mg/L. Under these conditions, where the quenching molecule is in large excess over phenolic moieties in NOM, it can be expected that the majority of NOM-derived photooxidants will be quenched by the probe compounds to form phenoxyl radicals, which can then further react with NO_x to produce nitro-/nitroso-phenol/resorcinol, enhancing the yields of these products as it is observed.

Environmental Significance. Our study showed that NO_x (NO and NO_2) could be generated by irradiation of IMD, and that these NO_x were capable of reacting with phenolic probes to produce nitro- and nitroso-derivatives. This suggests that in surface water, IMD could induce the formation of nitro and nitroso derivatives of other contaminants that could be toxicants in the aquatic environment. The importance of the phenomenon will depend on the level of IMD present in surface waters. The frequency of IMD detection in surface waters is high, and the concentration of IMD varies in a large range reaching 1 μg·L⁻¹ in agricultural areas.^{3,4} Based on this work and on the light absorption capacities of IMD and NO_2^- , one can calculate that at 1 μg·L⁻¹, IMD could generate as much as nitroso-/nitro-derivatives as NO_2^- at 0.1 μg·L⁻¹. The relative contributions of NO_2^- and IMD to nitroso-/nitro-derivative formation depend therefore on their levels in water. NO_2^- is present in surface waters at a maximal concentration of 0.1 mg·L⁻¹.⁴⁴ In many cases, the NO_2^- concentration will be high enough to make negligible the contribution of IMD in nitro/nitrosation reactions. However, in waters containing very low levels of NO_2^- and high levels of IMD, IMD might play a role in the nitro/nitrosation reactions.

On the other hand, we observed that NOM (11 mg·L⁻¹) enhanced the nitro and nitrosation reactions of phenols (10⁻⁴ M). The yield of nitro-resorcinol was multiplied by 2, whereas that of nitroso-resorcinol by 1.3, and when NO_2^- was used instead of IMD, the yields of nitro-resorcinol and of nitroso-resorcinol were increased by 35-fold and 2.8-fold, respectively. This can be explained by the enhanced formation of phenoxyl radicals in the quenching of NOM deriving photooxidants by phenols. However, this effect might be concentration-dependent. The level of NOM used in this study falls in the range of typical NOM levels found in rivers and eutrophic lakes,⁴⁵ but those of probes are high. At environmentally relevant concentrations of the probe compounds (<1 μM), phenolic moieties in NOM are in excess, and it might be possible that the NOM-bound phenoxyl radicals, at higher concentrations than the probe-derived phenoxyl radicals, might outcompete the latter for reaction with NO_x . In other words, under environmentally relevant conditions, a shift toward nitration/nitrosation of NOM seems possible, and the yield of nitro-/nitroso-derivatives of probes could then be lower compared to the ones in the absence of NOM. The incorporation of N inorganic nitrogen (N) into NOM via photolysis of nitrate/nitrite and/or in advanced oxidation process treatments was already reported and were also shown to generate potentially toxic compounds.^{26–28} Therefore, such reactions might also have environmentally negative consequences. We could not detect any significant structural changes in NOM using HRMS analyses. Nevertheless, further experiments using N-labeled

IMD or nitrite/nitrate and other hyphenated techniques may provide evidence for NOM nitration/nitrosation. Therefore, consistent monitoring of nitro/nitroso byproducts is highly recommended to verify their potential formation.

Our study confirms the capacity of water contaminants to interact with each other under irradiation and to induce mutual degradation. Mutual effects can involve reactions between excited- and ground-state contaminants or the intermediary formation of reactive species like NO_x in the case of IMD. Up to now, they have been poorly investigated in photochemical studies and would deserve more attention. Thus, future studies should further consider the investigation of the “cocktail effect” on the environmental fate of contaminants and more specifically the reactivity of intermediates in order to enable a more reliable monitoring of nontarget pollutants and assessment of potential risks.

■ ASSOCIATED CONTENT

Supporting Information

The Supporting Information is available free of charge at <https://pubs.acs.org/doi/10.1021/acs.est.9b07304>.

Spectrum of light received by the solutions in devices 1 and 2, NO_x formation in device 1 upon photolysis of IMD (10^{-4} M), calibration curve for nitroso-phenol and nitro-phenol, profiles of NO_x , NO_3^- , NO_2^- , nitroso-resorcinol, and nitro-resorcinol formation and of IMD consumption, structure and Cartesian coordinates of the minimum energy structures of IMD in S_0 (a), S_1 (b), and T_1 (c), of TS (d), of intermediate $\text{RNNO}-\text{O}$ (e) in S_0 , of TS_1 in T_1 (f), of TS_2 in T_1 (g), of ${}^3\text{RN}-\text{NO}_2$ (h) and ${}^3\text{RN}-\text{NO}_2$ in T_1 (i), of ${}^1\text{RNNO}$ (j) and ${}^3\text{RNNO}$ (k) at the B3LYP/6-311++G(d,p)/B3LYP/6-31+G(d,p) level, minima and transition state structures with Cartesian coordinates, photo-nitration and photo-nitrosation of the probes after 16 h of irradiation in the presence of IMD (10^{-5} or 10^{-4} M) or a mixture of NO_3^- (2×10^{-5} M) and NO_2^- (5×10^{-6} M), and the effect of NOM (11 mg L^{-1}) on the photo-nitration/photo-nitrosation of resorcinol (10^{-4} M) after 2 h of irradiation in device 2 in the presence of IMD (10^{-4} M) or NO_2^- (5×10^{-6} M) (PDF)

■ AUTHOR INFORMATION

Corresponding Authors

Mohamad Sleiman – Université Clermont Auvergne, CNRS, SIGMA Clermont, Institut de Chimie de Clermont-Ferrand F-63000 Clermont-Ferrand, France; orcid.org/0000-0002-2273-1053; Email: Mohamad.sleiman@sigma-clermont.fr

Claire Richard – Université Clermont Auvergne, CNRS, SIGMA Clermont, Institut de Chimie de Clermont-Ferrand F-63000 Clermont-Ferrand, France; orcid.org/0000-0001-6520-5494; Phone: +33 (0)4 73 40 71 42; Email: Claire.richard@uca.fr; Fax: +33 (0)4 73 40 77 00

Authors

Davide Palma – Université Clermont Auvergne, CNRS, SIGMA Clermont, Institut de Chimie de Clermont-Ferrand F-63000 Clermont-Ferrand, France

Yara Arbid – Université Clermont Auvergne, CNRS, SIGMA Clermont, Institut de Chimie de Clermont-Ferrand F-63000 Clermont-Ferrand, France

Pascal de Sainte-Claire – Université Clermont Auvergne, CNRS, SIGMA Clermont, Institut de Chimie de Clermont-Ferrand F-63000 Clermont-Ferrand, France

Complete contact information is available at: <https://pubs.acs.org/doi/10.1021/acs.est.9b07304>

Notes

The authors declare no competing financial interest. The paper reflects only the author's view, and the Agency is not responsible for any use that may be made from the information it contains.

■ ACKNOWLEDGMENTS

This paper is part of a project that received funding from the European Union's Horizon 2020 research and innovation programme under the Marie Skłodowska-Curie grant agreement no. 765860 (Aquality). The authors also thank the European Regional Development Fund of the European Union and the Région Auvergne-Rhône-Alpes for financial support under the Program “Nouveau Chercheur” (no. AV0004494), which allowed the acquisition of the NO_x analyzer. We thank Martin Lereboure and Guillaume Voyard (CNRS engineers), for assistance with chromatographic and mass spectrometry analyses, and the anonymous reviewers who helped to improve the manuscript.

■ REFERENCES

- Jeschke, P.; Nauen, R.; Schindler, M.; Elbert, A. Overview of the status and global strategy for neonicotinoids. *J. Agric. Food Chem.* **2011**, *59*, 2897–2908.
- Désert, M.; Ravier, S.; Gille, G.; Quinapallo, A.; Armengaud, A.; Pochet, G.; Savelli, J.-L.; Wortham, H.; Quivet, E. Spatial and temporal distribution of current-use pesticides in ambient air of Provence-Alpes-Côte-d'Azur Region and Corsica, France. *Atmos. Environ.* **2018**, *192*, 241–256.
- Struger, J.; Grabuski, J.; Cagampan, S.; Sverko, E.; Mcgoldrick, D.; Marvin, C. H. Factors influencing the occurrence and distribution of neonicotinoid insecticides in surface waters of southern Ontario, Canada. *Chemosphere* **2017**, *169*, 516–523.
- Hladik, M. L.; Kolpin, D. W.; Kuivila, K. M. Widespread occurrence of neonicotinoid insecticides in streams in a high corn and soybean producing region, USA. *Environ. Pollut.* **2014**, *193*, 189–196.
- Abou-Donia, M. B.; Goldstein, L. B.; Bullman, S.; Tu, T.; Khan, W. A.; Dechkovskaia, A. M.; Abdel-Rahman, A. A. Imidacloprid induces neurobehavioral deficits and increases expression of glial fibrillary acidic protein in the motor cortex and hippocampus in offspring rats following in utero exposure. *J. Toxicol. Environ. Health. A* **2008**, *71*, 119–130.
- Laycock, I.; Lenthall, K. M.; Barratt, A. T.; Cresswell, J. E. Effects of imidacloprid, a neonicotinoid pesticide, on reproduction in worker bumble bees (*Bombus terrestris*). *Ecotoxicology* **2012**, *21*, 1937–1945.
- Woodcock, B. A.; Isaac, N. J. B.; Bullock, J. M.; Roy, D. B.; Garthwaite, D. G.; Crowe, A.; Pywell, R. F. Impacts of neonicotinoid use on long-term population changes in wild bees in England. *Nat. Commun.* **2016**, *7*, 12459.
- Berheim, E. H.; Jenks, J. A.; Lundgren, J. G.; Michel, E. S.; Grove, D.; Jensen, W. F. Effects of Neonicotinoid Insecticides on Physiology and Reproductive Characteristics of Captive Female and Fawn White-tailed Deer. *Sci. Rep.* **2019**, *9*, 1–10.
- Duzguner, D.; Erdogan, E. Acute oxidant and inflammatory effects of imidacloprid on the mammalian central nervous system. *Pestic. Biochem. Physiol.* **2010**, *97*, 13–18.
- Moza, P. N.; Hustert, K.; Feicht, E.; Kettrup, A. Photolysis of imidacloprid in aqueous solution. *Chemosphere* **1998**, *36*, 497–502.

- (11) Redlich, D.; Shahin, N.; Ekici, P.; Friess, A.; Parlar, H. Kinetic study of the photoinduced degradation of imidacloprid in aquatic media. *Clean: Soil, Air, Water* **2007**, *35*, 452–458.
- (12) Wamhoff, H.; Schneider, V. Photodegradation of imidacloprid. *J. Agric. Food Chem.* **1999**, *47*, 1730–1734.
- (13) Zheng, W.; Liu, W. P.; Wen, Y. Z.; Lee, S.-J. Photochemistry of insecticide imidacloprid: direct and sensitized photolysis in aqueous medium. *J. Environ. Sci.* **2004**, *16*, 539–542.
- (14) Schippers, N.; Schwack, W. Photochemistry of imidacloprid in model systems. *J. Agric. Food Chem.* **2008**, *56*, 8023–8029.
- (15) Scholz, K.; Reinhard, F. Photolysis of imidacloprid (NTN 33893) on the leaf surface of tomato plants. *Pestic. Sci.* **1999**, *55*, 652–654.
- (16) Schippers, N.; Schwack, W. Phototransformation of imidacloprid on isolated tomato fruit cuticles and on tomato fruits. *J. Photochem. Photobiol. B* **2010**, *98*, 57–60.
- (17) Aregahegn, K. Z.; Shemesh, D.; Gerber, R. B.; Finlayson-Pitts, B. J. Photochemistry of thin solid films of the neonicotinoid imidacloprid on surfaces. *Environ. Sci. Technol.* **2017**, *51*, 2660–2668.
- (18) Monadjemi, S.; ter Halle, A.; Richard, C. Accelerated dissipation of the herbicide cycloxydim on wax films in the presence of the fungicide chlorothalonil and under the action of solar light. *J. Agric. Food Chem.* **2014**, *62*, 4846–4851.
- (19) Kouras-Hadef, S.; Hamdache, S.; de Sainte-Claire, P.; Sleiman, M.; Jaber, F.; Richard, C. Light induced degradation of the fungicide Thiophanate-methyl in water: Formation of a sensitizing photoproduct. *J. Photochem. Photobiol. A* **2018**, *360*, 262–269.
- (20) Machado, F.; Boule, P. Photonitration and photonitrosation of phenolic derivatives induced in aqueous solution by excitation of nitrite and nitrate ions. *J. Photochem. Photobiol. A: Chem.* **1995**, *86*, 73–80.
- (21) Vione, D.; Maurino, V.; Pelizzetti, E.; Minero, C. Phenol Photonitration and Photonitrosation upon Nitrite Photolysis in basic solution. *Int. J. Environ. Anal. Chem.* **2004**, *84*, 493–504.
- (22) Suzuki, J.; Yagi, N.; Suzuki, S. Photochemical nitrosation of phenol in aqueous nitrite solution. *Chem. Pharm. Bull.* **1984**, *32*, 2803–2808.
- (23) De Laurentiis, E.; Minella, M.; Berto, S.; Maurino, V.; Minero, C.; Vione, D. The fate of nitrogen upon nitrite irradiation: Formation of dissolved vs. gas-phase species. *J. Photochem. Photobiol. A: Chem.* **2015**, *307–308*, 30–34.
- (24) Scholes, R. C.; Prasse, C.; Sedlak, D. L. The Role of Reactive Nitrogen Species in Sensitized Photolysis of Wastewater-Derived Trace Organic Contaminants. *Environ. Sci. Technol.* **2019**, *53*, 6483–6491.
- (25) Vione, D.; Maurino, V.; Minero, C.; Pelizzetti, E. New processes in the environmental chemistry of nitrite: nitration of phenol upon nitrite photoinduced oxidation. *Environ. Sci. Technol.* **2002**, *36*, 669–676.
- (26) Thorn, K. A.; Cox, L. G. Ultraviolet irradiation effects incorporation of nitrate and nitrite nitrogen into aquatic natural organic matter. *J. Environ. Qual.* **2012**, *41*, 865–881.
- (27) Yang, P.; Ji, Y.; Lu, J.; Huang, Q. Formation of nitrophenolic byproducts during heat-activated peroxydisulfate oxidation in the presence of natural organic matter and nitrite. *Environ. Sci. Technol.* **2019**, *53*, 4255–4264.
- (28) Ji, Y.; Wang, L.; Jiang, M.; Lu, J.; Ferronato, C.; Chovelon, J.-M. The role of nitrite in sulfate radical-based degradation of phenolic compounds: An unexpected nitration process relevant to groundwater remediation by in-situ chemical oxidation (ISCO). *Water Res.* **2017**, *123*, 249–257.
- (29) Kieber, R. J.; Seaton, P. J. Determination of Subnanomolar Concentrations of Nitrite in Natural Waters. *Anal. Chem.* **1995**, *67*, 3261–3264.
- (30) Frisch, M. J.; Trucks, G. W.; Schlegel, H. B.; Scuseria, G. E.; Robb, M. A.; Cheeseman, J. R.; Scalmani, G.; Barone, V.; Mennucci, B.; Petersson, G. A.; Nakatsuji, H.; Caricato, M.; Li, X.; Hratchian, H. P.; Izmaylov, A. F.; Bloino, J.; Zheng, G.; Sonnenberg, J. L.; Hada, M.; Ehara, M.; Toyota, K.; Fukuda, R.; Hasegawa, J.; Ishida, M.; Nakajima, T.; Honda, Y.; Kitao, O.; Nakai, H.; Vreven, T.; Montgomery, J. A., Jr.; Peralta, J. E.; Ogliaro, F.; Bearpark, M.; Heyd, J. J.; Brothers, E.; Kudin, K. N.; Staroverov, V. N.; Keith, T.; Kobayashi, R.; Normand, J.; Raghavachari, K.; Rendell, A.; Burant, J. C.; Iyengar, S. S.; Tomasi, J.; Cossi, M.; Rega, N.; Millam, J. M.; Klene, M.; Knox, J. E.; Cross, J. B.; Bakken, V.; Adamo, C.; Jaramillo, J.; Gomperts, R.; Stratmann, R. E.; Yazyev, O.; Austin, A. J.; Cammi, R.; Pomelli, C.; Ochterski, J. W.; Martin, R. L.; Morokuma, K.; Zakrzewski, V. G.; Voth, G. A.; Salvador, P.; Dannenberg, J. J.; Dapprich, S.; Daniels, A. D.; Farkas, O.; Foresman, J. B.; Ortiz, J. V.; Cioslowski, J.; Fox, D. J. *Gaussian 09*, Revision C.01; Gaussian, Inc.: Wallingford CT, 2010.
- (31) Peverati, R.; Truhlar, D. G. Screened-exchange density functionals with broad accuracy for chemistry and solid-state physics. *Phys. Chem. Chem. Phys.* **2012**, *14*, 16187–16191.
- (32) Vione, D.; Maurino, V.; Minero, C.; Pelizzetti, E. Reactions induced in natural waters by irradiation of nitrate and nitrite ions. *Environmental Photochemistry*; Springer-Verlag Berlin, 2005; Vol. 2, Part M, pp 221–253.
- (33) Richards-Henderson, N. K.; Anderson, C.; Anastasio, C.; Finlayson-Pitts, B. J. The effect of cations on NO₂ production from the photolysis of aqueous thin water films of nitrate salts. *Phys. Chem. Chem. Phys.* **2015**, *17*, 32211–32218.
- (34) Le Questel, J.-Y.; Graton, J.; Cerón-Carrasco, J. P.; Jacquemin, D.; Planchat, A.; Thany, S. H. New insights on the molecular features and electrophysiological properties of dinotefuran, imidacloprid and acetamiprid neonicotinoid insecticides. *Bioorg. Med. Chem.* **2011**, *19*, 7623–7634.
- (35) Bryantsev, V. S.; Diallo, M. S.; Goddard, W. A., III Calculation of Solvation Free Energies of Charged Solutes Using Mixed Cluster/Continuum Models. *J. Phys. Chem. B* **2008**, *112*, 9709–9719.
- (36) Grätzel, M.; Henglein, A.; Lilie, J.; Beck, G. Pulsradiolytische untersuchung einiger elementarprozesse der oxydation und reduktion des nitritions. *Ber. Bunsenges. Phys. Chem.* **1969**, *73*, 646–653.
- (37) Tan, S. P.; Piri, M. Modeling the Solubility of Nitrogen Dioxide in Water Using Perturbed-Chain Statistical Associating Fluid Theory. *Ind. Eng. Chem. Res.* **2013**, *52*, 16032–16043.
- (38) Burdick, C. L.; Freed, E. S. The equilibrium between nitric oxide, nitrogen peroxide and aqueous solution of nitric acid. *J. Am. Chem. Soc.* **1921**, *43*, 518–530.
- (39) Vione, D.; Minella, M.; Maurino, V.; Minero, C. Indirect Photochemistry in Sunlit Surface Waters: Photoinduced Production of Reactive Transient Species. *Chem.—Eur. J.* **2014**, *20*, 10590–10606.
- (40) Barzaghi, P.; Herrmann, H. A mechanistic study of the oxidation of phenol by OH/NO₂/NO₃ in aqueous solution. *Phys. Chem. Chem. Phys.* **2002**, *4*, 3669–3675.
- (41) Alfassi, Z. B.; Huie, R. E.; Neta, P. Substituent effects on rates of one-electron oxidation of phenols by the radicals ClO₂, NO₂, SO₃^{•-}. *J. Phys. Chem.* **1986**, *90*, 4156–4158.
- (42) Semitsoglou-Tsiapou, S.; Templeton, M. R.; Graham, N. J. D.; Mandal, S.; Hernández Leal, L.; Kruithof, J. C. Potential formation of mutagenicity by low pressure-UV/H₂O₂ during the treatment of nitrate-rich source waters. *Environ. Sci.: Wat. Res. Technol.* **2018**, *4*, 1252–1261.
- (43) Ma, H.; Allen, H.; Yin, Y. Characterization of isolated fractions of dissolved organic matter from natural waters and a wastewater effluent. *Wat. Res.* **2001**, *35*, 985–996.
- (44) Keeney, D.; Olson, R. A. Sources of nitrate to ground water. *Crit. Rev. Environ. Control.* **1986**, *16*, 257–304.
- (45) Perdue, E. M. Natural Organic Matter. In *Biogeochemistry of Inland Waters*; Likens, G. E., Ed.; Academic Press, 2009; pp 503–516.

Supporting Information

New Route to Toxic Nitro and Nitroso Products upon Irradiation of Micropollutant Mixtures Containing Imidacloprid: Role of NO_x and Effect of Natural Organic Matter

Davide Palma, Yara Arbid, Mohamad Sleiman*, Pascal de Sainte-Claire, Claire Richard*

Université Clermont Auvergne, CNRS, SIGMA Clermont, Institut de Chimie de Clermont-Ferrand, F-63000 Clermont-Ferrand, France

Mohamad.sleiman@sigma-clermont.fr

Claire.richard@uca.fr

Figure SI-1 . Irradiance of the fluorescent tubes Sylvania F15W/BL 368S used in devices 1 and 2.

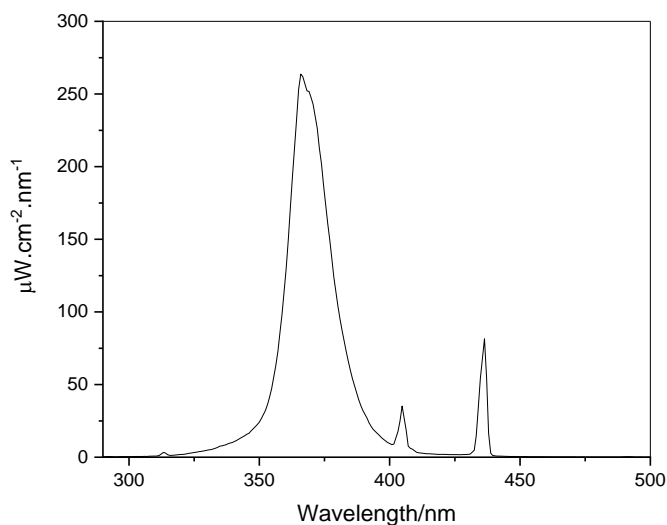


Figure SI-2. Background level of NO_x formation (A) and NO_x formation upon irradiation of IMD (10^{-4} M) for 1 h in device 1 (B). After selected irradiation times, the light was turned off and the outlet of the reactor connected to the NO_x analyzer. NO_x were measured every 10 seconds for a period of 1-2 min at a flow rate of 0.7 L min^{-1} . The time profile of NO_x concentrations corresponds to the decay of NO_x level in the reactor due to the dilution with clean air.

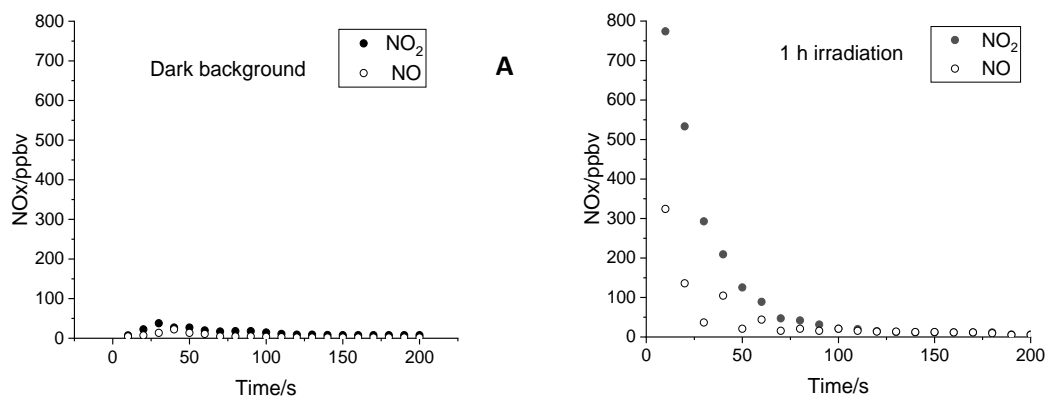


Table SI-7. HPLC conditions used for separation and analysis of the different compounds.

Compound	H ₂ O (%)	ACN	Detection wavelength/nm
IMD	60	40	270
Phenol	60	40	270
L-tryptophan	85	15	280
Resorcinol	70	30	274
NO ₂ ⁻ (derivatized)	60	40	307

Figure SI-3. Calibration curve for nitroso-phenol (open circles) and for nitro-phenol (black circles). Area were obtained by UPLC-HR-MS analyses in electrospray negative mode. For nitrosophenol $m/z=122.0237$ (5 ppm) and for nitrophenol $m/z=138.0186$ (5 ppm).

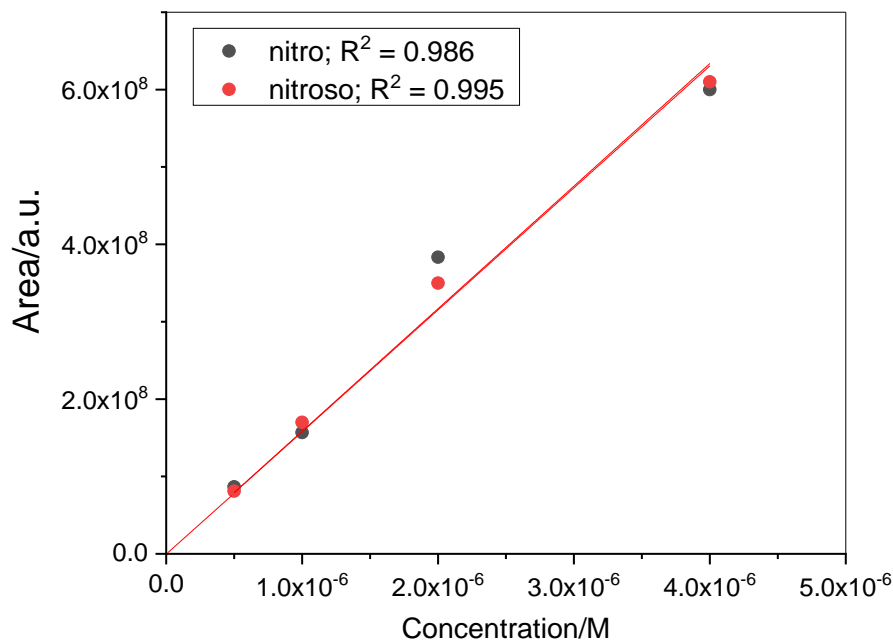
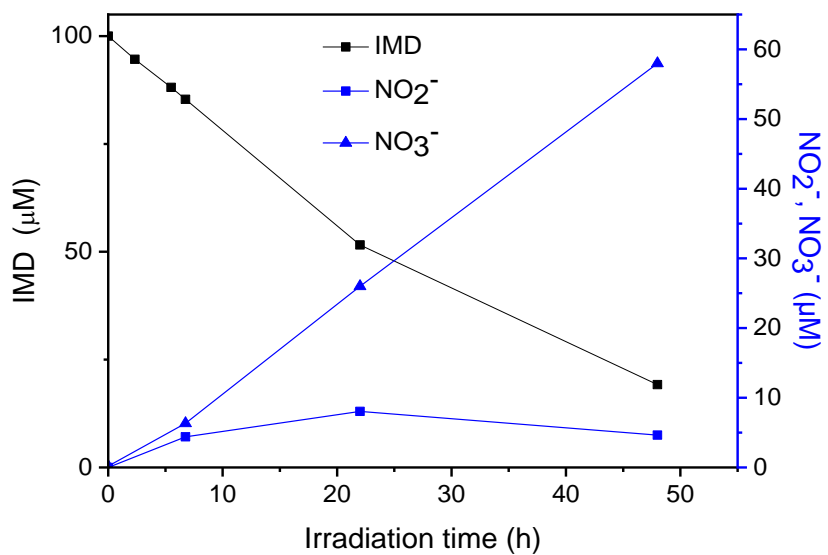


Figure SI-4. Consumption profile of aqueous IMD (10^{-4} M) irradiated in device 1, formation of NO_3^- and NO_2^- (A) and area UPLC-HRMS of desnitro-IMD (B). IMD was analyzed by HPLC-UV, NO_3^- by ionic chromatography, NO_2^- by HPLC-UV after derivatization by DNPH. Desnitro-IMD was identified by UPLC-HRMS ($m/z = 22.0740/213.0709$, $\square = 2.2$ ppm).

A)



B)

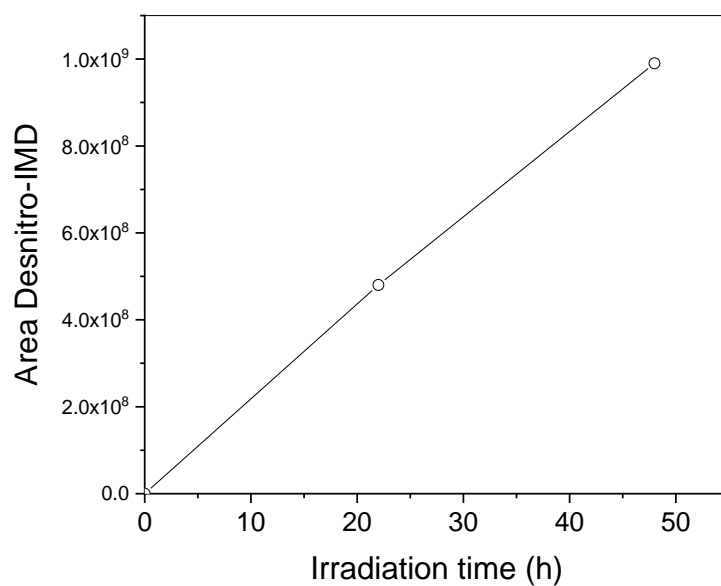
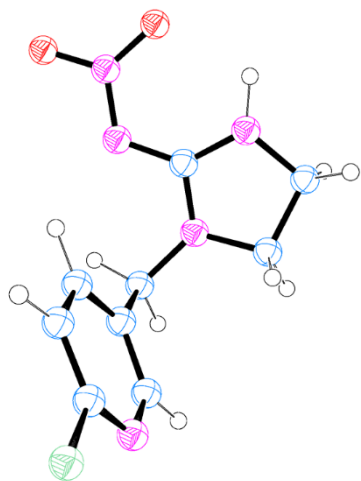


Table SI-2: UPLC-HMRS of IMD and photoproducts.

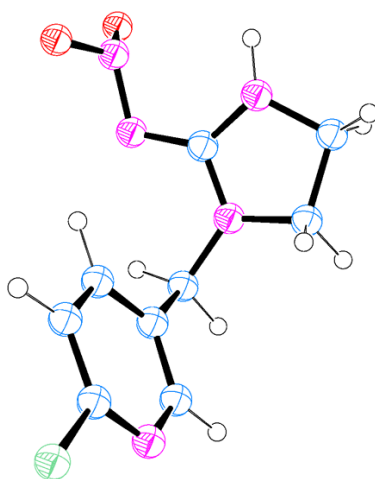
Name	m/z exp. in ES ⁺	m/z theor. in ES ⁺	Δ ppm	Formula of the neutral molecule
IMD	256.0603/ 258.0571	256.0596/ 258.0566	2.82	C ₉ H ₁₀ ClN ₅ O ₂
IMD+O	272.0549/ 274.0517	272.0545/ 274.0515	1.38	C ₉ H ₁₀ ClN ₅ O ₃
IMD-O	240.0650/ 242.0620	240.0647/ 242.0617	1.52	C ₉ H ₁₀ ClN ₅ O
Desnitro-IMD	211.0746/ 213.0717	211.0745/ 213.0716	0.33	C ₉ H ₁₁ ClN ₄
Desnitro- IMD+2O	243.0650/ 245.0619	243.0643/ 245.0614	2.84	C ₉ H ₁₁ ClN ₄ O ₂

Figure SI-5. Structures (a)-(k) of the minimum energy structures and TSs at the MN12SX/6-311++G(d,p),PCM/MN12SX/6-31+G(d,p),PCM level. Energies are given relatively to the global minimum (see Figure 4). Specific bond distances (Å) are also indicated.



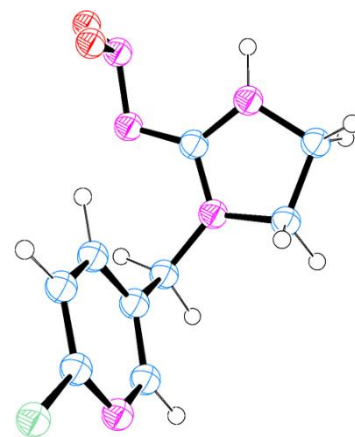
**Global min in S₀,
¹RNNNO₂ (a)**

0.0 kcal mol⁻¹



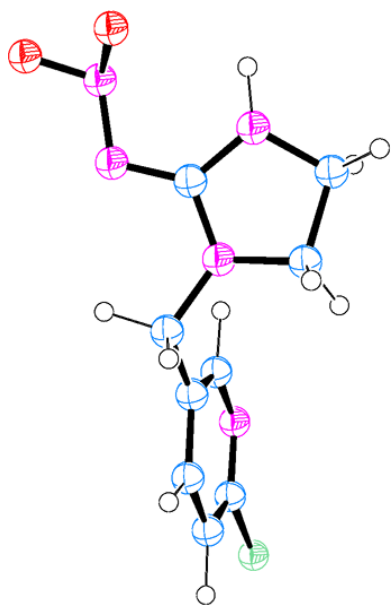
Min in S₁ (b)

79.3 kcal mol⁻¹



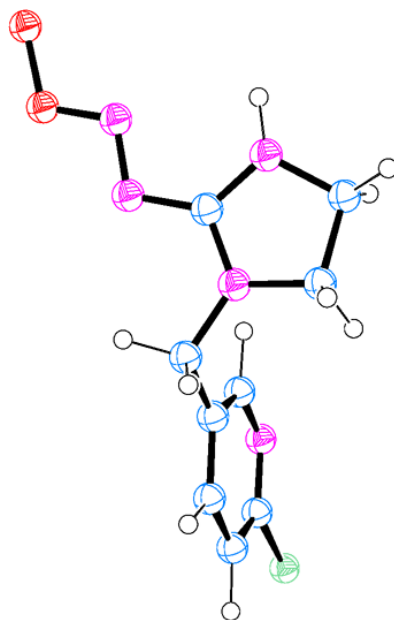
Min in T₁, ³RNNNO₂ (c)

67.3 kcal mol⁻¹



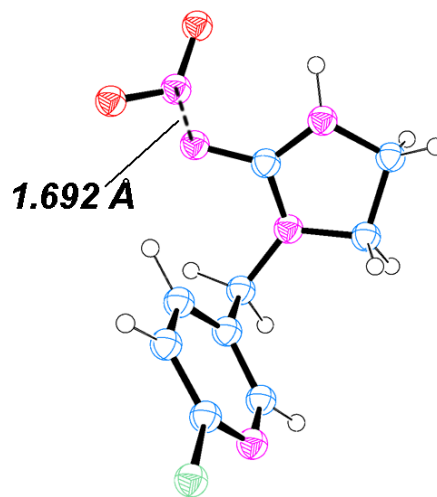
TS in S₀ (d)

106.1 kcal mol⁻¹



¹RNNNO-O (e)

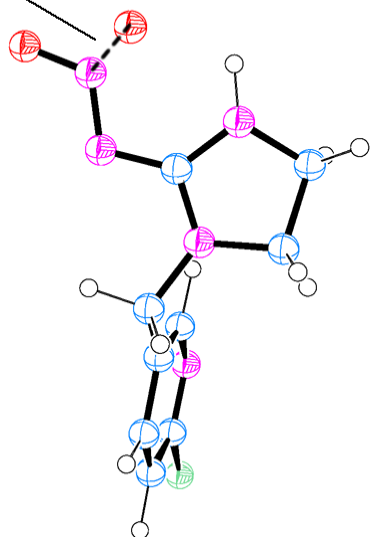
56.4 kcal mol⁻¹



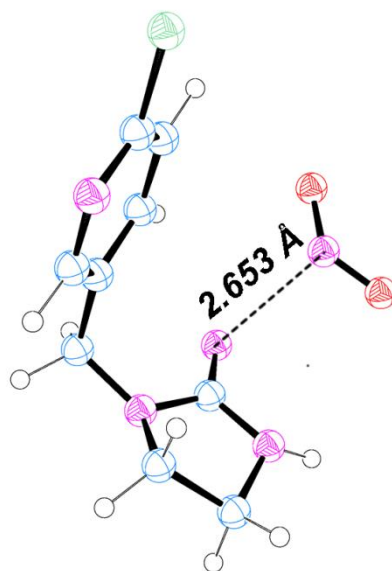
TS₁ in T₁ (f)

73.4 kcal mol⁻¹

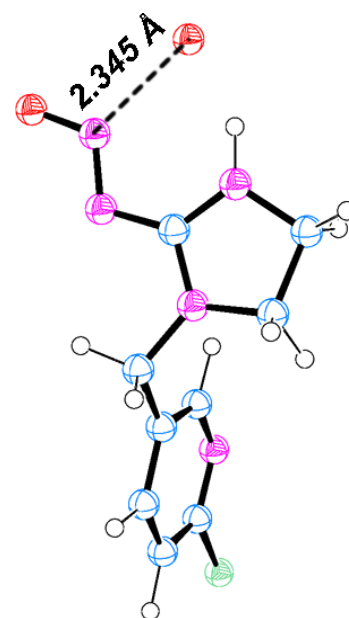
1.746 Å



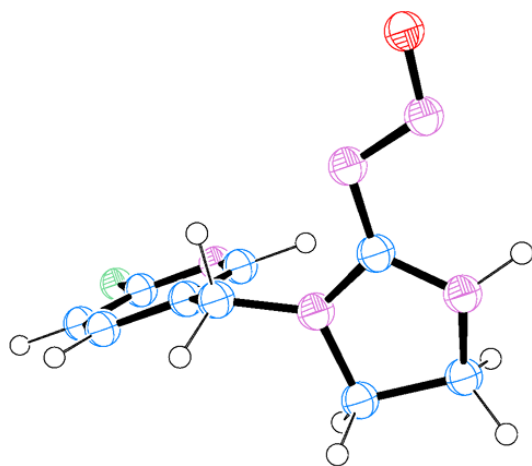
TS₂ in T₁ (g)
78.7 kcal mol⁻¹



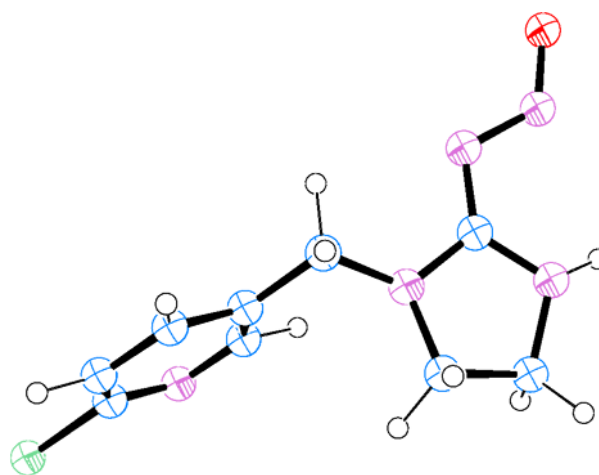
³RN---NO₂ (h)
59.8 kcal mol⁻¹



³RNNO-O in T₁ (i)
76.1 kcal mol⁻¹



¹RNNO (j)
80.4 kcal/mol



³RNNO (k)
121.4 kcal/mol

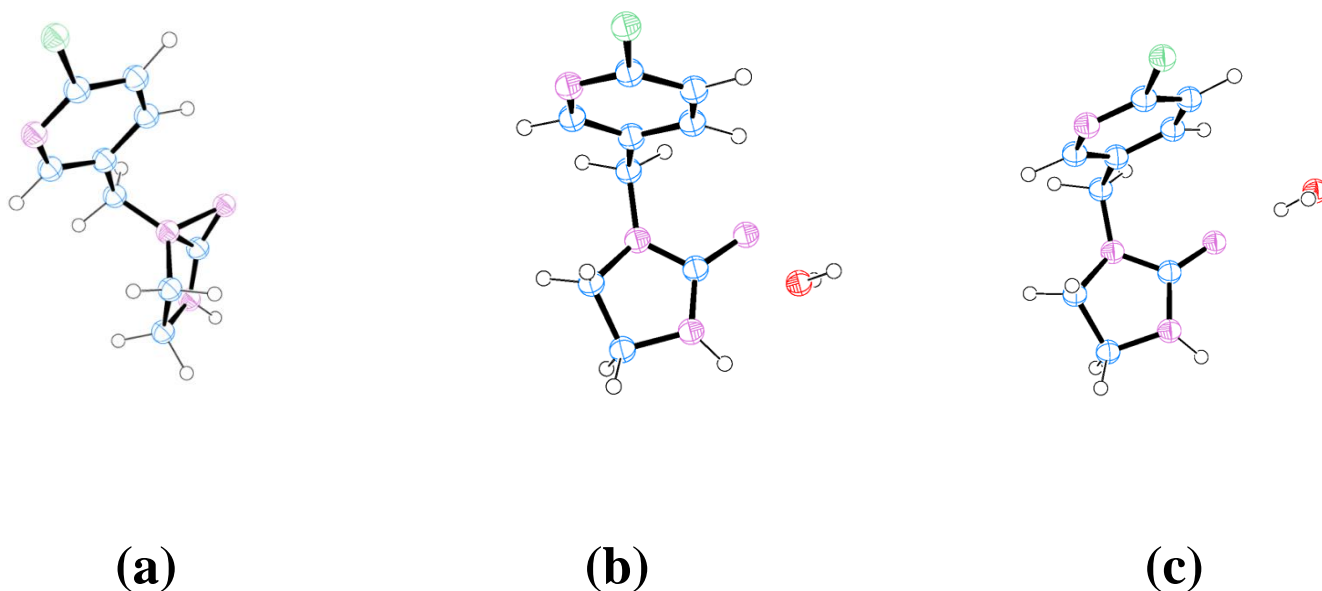
Table SI-3: Cartesian coordinates of the minimum energy structures and TSs at the MN12SX/6-311++G(d,p),PCM/MN12SX/6-31+G(d,p),PCM level.

Min S ₀ , ¹ RNNO ₂ (a)		Min S ₁ (b)		Min T ₁ , ³ RNNO ₂ (c)			TS S ₀ (d)		¹ RNNO-O (e)									
C	-3.904635	0.765039	C	-3.398081	0.341802	C	-3.362675	-0.347631	-	C	-0.203027	-0.349078	C	-0.154117	0.191187			
0.032387			0.079196			0.074888				1.121773			1.381299					
C	-2.651975	1.265986	-	C	-2.294923	1.176317	C	-2.232460	-1.117072	-	H	-0.281192	-0.106962	H	-0.106941	0.737387		
0.317873			0.255215			0.347477				2.195510			2.336454					
C	-1.771163	0.388254	-	C	-1.082502	0.731770	-	C	-1.023506	-0.662472	C	-0.927867	1.995016	C	-0.739471	2.341866		
0.933223			0.248795			0.141601				0.156625			0.147460					
C	-2.166764	-0.931261	-	C	-1.017011	-0.505420	-	C	-0.987178	0.524124	C	-2.038247	2.499264	-	C	-1.809222	2.629975	
1.177332			0.896764			0.897419				0.402607			0.911387					
C	-3.448748	-1.301054	-	C	-2.191008	-1.246366	-	C	-2.187175	1.202458	H	0.065289	2.357516	H	0.281189	2.492397		
0.779059			0.998624			1.087676				0.229170			0.221553					
N	-4.312703	-0.469965	-	N	-3.370853	-0.830912	-	N	-3.364975	0.775416	H	-1.113855	2.266057	H	-0.881746	2.940803		
0.181967			0.522588			0.614761				1.571397			1.060570					
H	-0.776932	0.727778	-	H	-0.190402	1.353466	-	H	-0.110339	-1.235334	-	H	-1.666108	2.679980	-	H	-1.412985	2.518630
1.229275			0.141601			0.023647				1.422076			1.930749					
H	-2.387350	2.301614	-	H	-2.391683	2.132733	-	H	-2.306763	-2.033495	-	H	-2.521117	3.407213	-	H	-2.254452	3.623066
0.116328			0.763368			0.928024				0.029650			0.803036					
H	-3.809069	-2.319038	-	H	-2.192201	-2.220737	-	H	-2.212382	2.137059	N	-1.031695	0.548155	N	-0.982752	0.931296		
0.948182			1.492300			1.652683				0.348818			0.453497					
Cl	-5.046843	1.828429	-	Cl	-4.947854	0.860345	-	Cl	-4.909736	-0.885948	-	N	-2.954805	1.363624	-	N	-2.783146	1.578648
0.817110			0.690667			0.680589				0.384090			0.630835					
C	-1.232405	-1.933964	-	C	0.284558	-1.025771	-	C	0.307430	1.054822	H	-3.762834	1.318289	-	H	-3.601560	1.412056	
1.814625			1.465310			1.468931				0.997301			1.206440					
H	-1.798679	-2.809084	-	H	0.121930	-1.973713	-	H	0.132063	1.999553	C	-2.283558	0.237601	-	C	-2.199555	0.582978	
2.160279			1.994034			1.999723				0.063034			0.040735					
H	-0.725483	-1.498193	-	H	0.717191	-0.308883	-	H	0.737372	0.344379	N	-2.734621	-1.004600	-	N	-2.702912	-0.649266	
2.682400			2.173030			2.185474				0.084846			0.324821					
C	-0.574092	-3.204168	-	C	1.131843	-2.341972	-	C	1.135361	2.343184	-	N	-3.959398	-1.067285	-	N	-3.874881	-0.779031
0.277229			0.556493			0.572120				0.660242			0.195123					
C	0.789058	-3.429027	-	C	2.423456	-2.204268	-	C	2.415193	2.194510	-	O	-4.611643	-2.141095	-	O	-4.346713	-1.939414
0.931785			1.370553			1.400977				0.408242			0.072304					
H	-1.068425	-4.135321	-	H	1.028070	-3.311187	-	H	1.036222	3.327626	-	O	-5.110203	-0.465414	-	O	-5.621750	-2.141845
0.020573			0.056855			0.102311				0.134532			0.462369					
H	-1.253750	-2.632790	-	H	0.232750	-2.158848	-	H	0.230410	2.138675	-	H	-0.594941	-1.366250	-	H	-0.644501	-0.770714
0.931988			1.167751			1.167309				0.989337			1.576793					
H	1.249157	-4.371466	-	H	3.217372	-2.862363	-	H	3.203420	2.879828	-	C	1.242504	-0.290799	-	C	1.240908	-0.022062
0.600354			0.989606			1.057836				0.691388			0.843308					
H	0.746251	-3.415572	-	H	2.272044	-2.399108	-	H	2.245955	2.346043	-	C	1.593661	-0.164240	-	C	1.469772	-0.258065
2.024795			2.435751			2.470799				0.652341			0.511323					
N	-0.214848	-2.410322	-	N	1.268626	-1.268798	-	N	1.301086	1.300108	C	2.279394	-0.394872	-	C	2.348739	-0.015140	
0.893377			0.425800			0.439606				1.619394			1.691979					
N	1.544992	-2.291783	-	N	2.767602	-0.804712	-	N	2.786811	0.811780	-	H	0.821427	-0.066346	-	H	0.640957	-0.266019
0.421331			1.131045			1.113668				1.418580			1.222977					
H	2.526684	-2.126330	-	H	3.643477	-0.393806	-	H	3.658194	0.398663	-	C	3.598640	-0.382619	-	C	3.615398	-0.245686
0.609672			1.439213			1.430265				1.185131			1.172933					
C	0.977749	-1.810901	-	C	2.172605	-0.379626	-	C	2.210014	0.409620	H	2.059851	-0.483432	-	H	2.226772	0.173523	
0.690410			0.008438			0.025425				2.684555			2.759720					
N	1.360434	-0.869752	-	N	2.361218	0.770849	-	N	2.440532	-0.712142	C	3.810872	-0.256142	-	C	3.706360	-0.466007	
1.568602			0.659494			0.738625				0.184742			0.198603					
N	2.579242	-0.334902	-	N	3.279295	1.593014	-	N	3.347063	-1.548856	H	4.433881	-0.460282	-	H	4.503037	-0.245919	
1.426154			0.010847			0.067730				1.877288			1.801116					
O	2.875910	0.546229	-	O	4.420065	1.561650	-	O	4.205043	-2.174075	Cl	5.450699	-0.230562	-	Cl	5.279412	-0.743932	
2.242636			0.596315			0.755423				0.787984			0.906833					
O	3.377159	-0.691010	-	O	2.747453	2.691061	-	O	2.498420	-2.230334	-	N	2.857413	-0.145456	-	N	2.682984	-0.474873
0.533892			0.409641			0.725516				1.090040			1.031162					

TS ₁ , T ₁ (f)		TS ₂ , T ₁ (g)		³ RN---NO ₂ (h)			³ RNNO-O in T ₁ (i)							
C	3.187194	0.227055	-	C	-0.205293	-0.060599	C	2.814838	-0.330504	-	C	-0.119348	0.059714	
0.124355			1.314892			0.104796					1.469669			
C	2.151026	1.138337	H	-0.225749	0.396895	C	2.114040	0.556284	H	-0.069546	0.605839			
0.074237			2.317390			0.708377				2.425420				
C	0.975015	0.646553	C	-1.037432	2.128770	C	0.901175	0.115662	C	-1.011961	2.155277			
0.621106			0.331767			1.220359				0.347300				
C	0.879107	-0.711259	C	-2.129584	2.411617	-	C	0.436348	-1.163967	C	-2.178567	2.355329		
0.943283			0.703288			0.903215				0.625482				
C	1.988973	-1.514046	H	-0.045765	2.465962	C	1.243134	-1.952450	H	-0.044390	2.445562			
0.692219			0.008335			0.083372				0.078388				
N	3.132100	-1.057506	H	-1.264221	2.578975	N	2.416805	-1.548618	-	H	-1.158771	2.696668		
0.166573			1.311582			0.417693				1.295427				
H	0.138042	1.327863	H	-1.716339	2.479670	-	H	0.313353	0.770053	H	-1.840656	2.350273		
0.800686			1.720069			1.867321				1.672011				
H	2.270553	2.187294	-	H	-2.695331	3.321754	-	H	-2.507230	1.545953	H	-2.733398	3.278748	
0.186483			0.483212			0.930126				0.434443				
H	1.966680	-2.580645	N	-1.088372	0.671828	H	0.939235	-2.968736	-	N	-1.065274	0.715845		
0.929145			0.437138			0.181882				0.595987				
Cl	4.689901	0.800493	-	N	-2.966371	1.222997	-	Cl	4.350410	0.173373	-	N	-2.997235	1.179441
0.804530			0.571628			0.772346				0.350447				

C	-0.389542	-1.299857	H	-3.745817	1.032188	-	C	-0.908128	-1.653261	H	-3.826097	0.923517	-		
1.516466			1.193510				1.387958			0.890056					
H	-0.200563	-2.300278	C	-2.262716	0.219044	-	H	-0.902819	-2.744665	C	-2.262662	0.235823			
1.925345			0.023736				1.506130			0.242243					
H	-0.778435	-0.671310	N	-2.607783	-1.069180		H	-1.139081	-1.213097	N	-2.592191	-1.049179			
2.328589			0.109505				2.368362			0.519810					
C	-1.356164	-2.374792	-	N	-3.779593	-1.321407	-	C	-2.131166	-1.961989	-	N	-3.771921	-1.362575	
0.593330			0.472256				0.816481			0.037006					
C	-2.639341	-2.062339	-	O	-4.195045	-2.471112	-	C	-3.316312	-1.199517	-	O	-4.181012	-2.488907	
1.370850			0.504790				1.397255			0.271856					
H	-1.313314	-3.403713	-	O	-5.077016	-0.351132	-	H	-2.317457	-3.035770	-	O	-5.042584	-0.382344	-
0.220838			0.178466				0.700481			1.673348					
H	-0.452574	-2.169155	-	H	-0.599483	-1.080291	-	H	-1.226612	-1.815491	-	H	-0.503267	-0.945154	
1.190489			1.416376				1.433860			1.687434					
H	-3.477316	-2.694880	-	C	1.214956	-0.100755	-	H	-4.270264	-1.631624	-	C	1.260847	-0.028331	
1.044078			0.803031				1.055222			0.862984					
H	-2.515145	-2.155929	-	C	1.507667	-0.062886	-	H	-3.306916	-1.162074	-	C	1.450728	-0.180374	-
2.453515			0.559029				2.491041			0.509285					
N	-1.441694	-1.426608	C	2.288934	-0.215521		N	-1.997941	-1.317254	C	2.399265	0.002449			
0.518570			1.688497				0.485603			1.670371					
N	-2.871707	-0.672843	-	H	0.708298	0.036117	-	N	-3.085288	0.122779	-	H	0.597108	-0.199956	-
0.985360			1.296650				0.824530			1.190479					
H	-3.677759	-0.121158	-	C	3.583197	-0.300980	-	H	-3.789700	0.848562	-	C	3.655784	-0.128373	
1.268011			1.195184				0.910140			1.096183					
C	-2.250335	-0.412582	H	2.116853	-0.238813		C	-2.443143	-0.018085	H	2.307632	0.129040			
0.167004			2.765821				0.379887			2.750445					
N	-2.366870	0.699289	C	3.736657	-0.256583	-	N	-2.271254	0.910898	C	3.706095	-0.278963	-		
0.925083			0.188209				1.266655			0.287035					
N	-2.480190	2.017349	-	H	4.444850	-0.392440	-	N	-0.783212	2.567466	-	H	4.565384	-0.108351	
0.129050			1.852223				0.175823			1.691679					
O	-3.713558	2.017662	-	Cl	5.345353	-0.362644	-	O	-1.580424	2.968442	-	Cl	5.264756	-0.448675	-
0.435706			0.862800				0.977686			1.059718					
O	-1.882135	3.011505	N	2.749246	-0.137062	-	O	-0.042379	3.151509	N	2.654169	-0.302675	-		
0.314613			1.053440				0.565595			1.082295					

Figure SI-6. Structures of RN^+ (a), $\text{RN}^+\cdot\text{H}_2\text{O}$ (b) and $\text{RN}\cdot\text{H}_2\text{O}$ (c) obtained at the MN12SX/6-31+G(d,p),PCM level and calculation of RN^+ energy:



Calculation of RN^+ energy:

Optimization of RN^+ at the MN12SX/6-31+G(d,p),PCM level gave rise to the high energy cyclized species in Fig SI-6a. This structure is similar to that found in the gas phase (MN12SX/6-31+G(d,p)) and it became clear that the PCM model was not sufficient to account for solvent effects here. It was thus decided to optimize RN^+ at the MN12SX/6-31+G(d,p),PCM level in the presence of one water molecule (implicit + explicit solvation model). The obtained geometry is shown below in Figure SI-6b (no spurious cyclization). Thus, the more accurate energy of RN^+ ($\text{RN}^+/\text{NO}_2^-$ at 69.0 kcal/mol in Figure 4) was that of RN^+ obtained at the MN12SX/6-31+G(d,p),PCM level and corrected with the energy difference below, i.e:

$$E_{\text{text}}(\text{RN}^+) = E(\text{RN}^+) + \underbrace{[E(\text{RN}^+\cdot\text{H}_2\text{O}) - E(\text{RN}\cdot\text{H}_2\text{O})] - [E(\text{RN}^+) - E(\text{RN})]}_{\text{These species computed at the MN12SX/6-311++G(d,p),PCM // MN12SX/6-31+G(d,p),PCM level}}$$

i.e:

$$E_{\text{text}}(\text{RN}^+) = E(\text{RN}) + [E(\text{RN}^+\cdot\text{H}_2\text{O}) - E(\text{RN}\cdot\text{H}_2\text{O})]$$

Figure SI-7. Consumption profile of IMD (10^{-4} M) upon irradiation in device 2. The concentrations of IMD were determined by HPLC-UV.

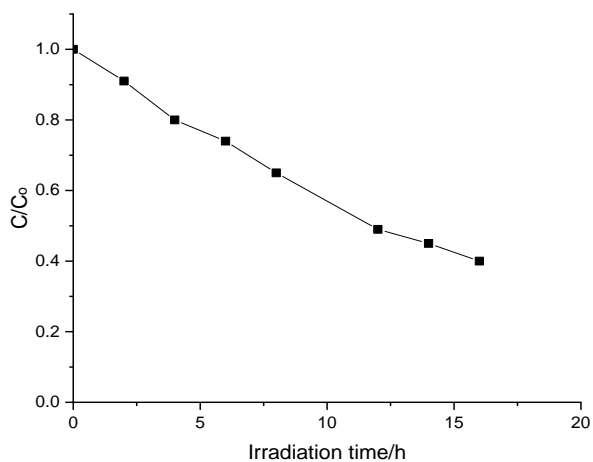


Figure SI-8: Formation of nitroso-resorcinol (open circles) and nitro-resorcinol (full circles) upon irradiation in device 2 of IMD (10^{-4} M) and resorcinol (10^{-4} M). The concentrations of nitroso and nitro-resorcinols were estimated using calibration curves of Figure SI-3.

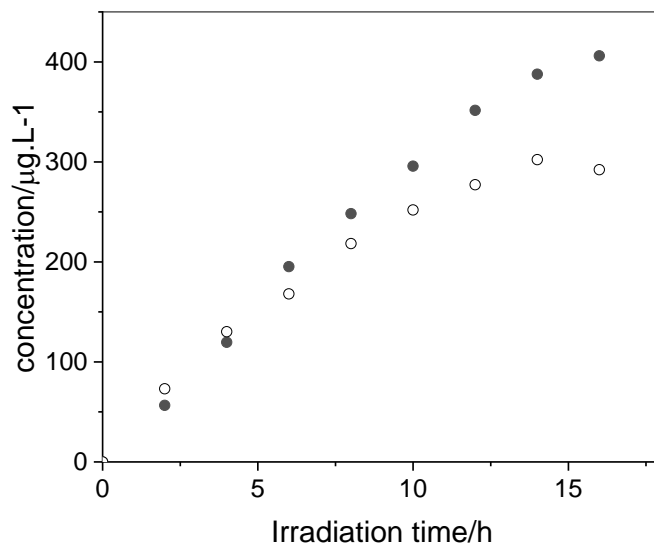


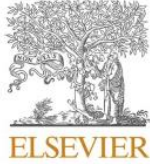
Table SI-4: Photonitration and photonitrosation of the probes after 16 h of irradiation in device 2 in presence of IMD (10^{-5} or 10^{-4} M) or a mixture of NO_3^- (2×10^{-5} M) and NO_2^- (5×10^{-6} M). The concentrations of IMD and of the probes were obtained by HPLC-UV while the amounts of nitro and nitro-derivatives by UPLC-HRMS.

Conditions	% of converted IMD	% of converted probe	Nitroso derivative formed ($\mu\text{g.L}^{-1}$)	Nitro derivative formed ($\mu\text{g.L}^{-1}$)	Sum ($\mu\text{g.L}^{-1}$)
Phenol (10^{-4} M)	-	< 0.5	-	-	-
Phenol (10^{-4} M)+ IMD (10^{-4} M)	56±3	14±1	34±2	202±10	236±12
Phenol (10^{-4} M)+ $\text{NO}_2^-/\text{NO}_3^-$	-	3.4±0.1	0.28±0.02	34±2	34±2
Resorcinol (10^{-4} M)	-	< 0.5	-	-	-
Resorcinol (10^{-4} M)+IMD (10^{-4} M)	58±3	29±1	406±40	292±29	498±69
Resorcinol (10^{-4} M)+IMD (10^{-5} M)	61±3	46±5	43±4	16±2	59±6
Resorcinol (10^{-5} M)+IMD (10^{-4} M)	62±3	58±5	3.6±0.8	100±20	104±21
Resorcinol (10^{-4} M)+ $\text{NO}_2^-/\text{NO}_3^-$	-	6.2±0.3	99±9	70.8±7	170±16
Tryptophan (10^{-4} M)	-	91±5	-	-	-
Tryptophan (10^{-4} M)+IMD (10^{-4} M)	60±3	95±5	19±2	9.4±0.9	28±3
Tryptophan (10^{-4} M)+ $\text{NO}_2^-/\text{NO}_3^-$	-	96±5	7.4±0.7	6.2±0.6	14±2

Manuscript 2

Towards an experimental approach for measuring the removal of urban air pollutants by green roofs

Date of acceptance: August 23, 2021



Towards an experimental approach for measuring the removal of urban air pollutants by green roofs

Yara Arbid, Claire Richard, Mohamad Sleiman*

Université Clermont Auvergne, CNRS, INP Clermont Auvergne, SIGMA Clermont, Institut de Chimie de Clermont-Ferrand, F-63000, Clermont-Ferrand, France

ARTICLE INFO

Keywords:
Green roofs
Air pollution
NO_x
O₃

ABSTRACT

Green roofs are a promising approach to mitigate air pollution in urban environments, but limited experimental data is yet available. In this study, we developed a laboratory-scale setup to measure the removal nitrogen dioxide (NO₂) and ozone (O₃) using a variety of common green roof species. Experiments were conducted on detached leaves and whole plants using two chambers (0.6 L and 12 L), visible lighting, NO_x/O₃ sources and online analyzers. Three species were the best performant (*Thymus vulgaris*, *Sedum sexangulare* and *Heuchera Americana* L.) with deposition velocities (v_d) ranging from 1.6 to 4.82 m/h for NO₂, and 1.7–5.56 m/h for O₃. In both cases, thyme was the most effective plant likely due to its higher stomatal area and the reactivity of its volatile metabolites with O₃ leading to several oxidized by-products. Furthermore, NO₂ uptake was found to be enhanced by surface water released by leaf transpiration leading to the production of nitrous acid (HONO). Similar values of (v_d) were observed (3.84–4.65 m/h) when whole thyme plant was used. The soil was also found to be competitive in removing O₃ but less performant in capturing NO₂. Using a dry deposition model, we estimated that the three plant species can uptake up to 9 kg/ha/year of NO₂ and 13.6 kg/ha/year, which fall in agreement with previously reported modeling data. Our experimental approach can be a rapid tool for screening the depollution performances of green roof species enabling an effective prioritization for deployment in urban environments.

1. Introduction

Outdoor air pollution causes up to 10 million deaths annually, and around 90% of the world population live in urban environments where air pollution exceeds the World Health Organization (WHO) limits [1]. Air pollution mitigation strategies such as source reduction (electrical vehicles [2], fuel and traffic regulations [3], renewable energy resources [4], etc.), and depollution technologies have been increasingly adopted in the recent years. Among depollution methods, the use of highly reflective photocatalytic roofs and walls [5] have been shown to be effective in reducing the urban heat island effect, and in the removal of Volatile Organic Compounds (VOCs) and Nitrogen Oxides (NO_x) [6,7]. However, photocatalytic oxidation process can lead to the formation of toxic intermediates and the VOC removal performance can decrease over time [8]. Another promising alternative is the use of natural walls and roofs such as vertical greening systems or green roofs which can be a replacement to conventional roofs especially in crowded urbanized areas [9]. Green roofs have been receiving attention recently as effective nature-based solution to eco-environmental problems arising from

climate change and rapid urbanization [10]. They can retain storm water via absorption into the substrate [11,12], reduce the building energy demand by improving the thermal insulation [13], lower noise pollution [14], in addition to improving the roof aesthetic values.

Plants used in such green roofs are able to mitigate air pollution [15] by absorbing the pollutants through their stomata via dry deposition on the surfaces of leaves [16]. Urban trees and shrubs are known to remove efficiently air pollutants [17]. Reactive pollutants (O₃, NO_x, SO₂) can be removed by absorption via stomata or by surface uptake via potential chemical reactions with volatile metabolites such as terpenes. On the other hand, the formed particulate matter (PM) can be removed via deposition on the leaf surface. The performance depends on various factors such as the proximity of the vegetation to the road and its height [18]. Although trees are a very effective strategy in controlling pollution, planting trees in crowded cities with high percentages of impervious areas is challenging. Thus, in metropolitan cities, green roofs can be an alternative solution to make use of rooftops [19]. Several modelling studies showed that green roofs can be efficient in removing various prevalent air pollutants. According to Yang et al., 22.8

* Corresponding author.

E-mail addresses: Yara.arbid@etu.uca.fr (Y. Arbid), Claire.richard@uca.fr (C. Richard), Mohamad.sleiman@sigma-clermont.fr (M. Sleiman).

<https://doi.org/10.1016/j.buildenv.2021.108286>

Received 8 June 2021; Received in revised form 18 August 2021; Accepted 23 August 2021

Available online 24 August 2021

0360-1323/© 2021 Elsevier Ltd. All rights reserved.

kg/ha/year of NO₂ and around 44 kg/ha/year of O₃ can be eliminated using green roofs [16]. Grass was found effective in removing O₃ (5.2 kg/ha/year) whereas, shrubs have the potential to eliminate 18 kg/ha/year of PM₁₀ [20]. Speak et al. [21] showed that sedum, a widely used plant species on extensive green roofs, could remove 4.2 kg/ha/year of PM₁₀. However, most aforementioned studies were based solely on modelling using estimated deposition velocities (v_d) which can vary significantly depending on the plant species, seasonality, climate, etc.

To the best of our knowledge, the air depollution performance of green roofs species has been very little investigated, and only limited recent data exist on their efficiency in the laboratory and in the field [22, 23]. Performance-based laboratory screening measurements –in combination with field campaigns—are thus needed to improve the precision of models and to provide a valuable tool for implementing the best performing species as a function of target pollutants. In this study, we developed an experimental setup to measure the NO_x/O₃ uptakes of 13 plants commonly used on green roofs. After initial screening, 3 species were selected (*Sedum sexangulare*, *Thymus vulgaris*, and *Heuchera Americana* L.). The removal rates of these plants were investigated using detached leaves as well as full size plants. This work aimed to guide in the choice of plants to be used on green roofs according to the need of targeting a specific pollutant in an urbanized area, and to get insight into the mechanisms taking place.

2. Materials and methods

2.1. Chemicals and materials

Imidacloprid (IMD) was purchased from Sigma Aldrich, Switzerland (Pestanal™, analytical standard, ≥98.0% purity HPLC area %). Sodium carbonate anhydrous was purchased from Fluka, Germany (≥99.5% purity ACS). Both were used without further purification. Water was produced using a reverse osmosis RIOS 5 and Synergy (Millipore) device (resistivity 18 MΩ cm, DOC < 0.1 mg L⁻¹). Acetonitrile (ACN) was purchased from Carlo Erba Reagents (HPLC Plus Gradient grade-ACS-Reag).

Process of plant selection: Green roofs vary from intensive to extensive roofs differing in the maintenance needs, substrate depth, plants implemented, etc. Contrarily to intensive ones where shrubs or even trees may be implemented, extensive green roofs use shallow root plants and thus are more commonly used due to their low maintenance needs and lightweight. Hence, in this study, we solely focused on extensive green roof species which are drought tolerant such as grasses, perennials, and succulents. Based on literature review, and after careful consideration of weather conditions in central France, 13 species were selected for screening: *Achille millefeuille paprika*, *Achillea umbellata à feuillage gris*, *Alchemille jaune*, *Aster des alpes rose*, *Heuchera americana* L., *Joubarbe calcareum*, *Joubarbe rubin*, *Thymus nummularius*, *Sedum floriferum jaune*, *Sedum reflexum jaune*, *Sedum sexangulare*, *Sedum spurium*, and *Thymus vulgaris*. After pre-screening, three species were chosen to further investigate their performance for the removal of O₃ and NO₂: *Sedum sexangulare*, *Thymus vulgaris*, *Heuchera americana* L.

Conditions for plant storage and care: Plants were stored in an indoor greenhouse exposed to outdoor sunlight through a large window and were watered every two days. Temperature was between 20 and 25 °C in the greenhouse during storage and around 23° ± 2 C when used in the laboratory. Relative humidity (RH) was ranged between 30 and 55%.

Sedum sexangulare, *Thymus vulgaris*, and *Heuchera Americana* L. were purchased from a plant nursery (Botanic®, Beaumont, France) and watered every two days. These species are used on green roofs and different studies report their performance towards different air pollutants [24–26].

Sedum sexangulare (sedum): Sedum species are considered as appropriate plants to be applied on extensive green roofs. They are drought tolerant and can survive in harsh climate conditions. In the literature, *Sedum sexangulare* showed a good performance under severe climate conditions and that it is suitable to be implemented in a

Mediterranean climate [24].

Thymus vulgaris (thyme): Thyme is an odorous perennial plant used on green roofs. It emits different VOCs (Fig. SI-1.) which can react with air pollutants [25].

Heuchera Americana L. (heuchera): Heuchera species are used in vertical greenery systems and green roofs because their colorful glossy leaves give them important aesthetics values. Heuchera retains different elements and particulate matter (PM) due to its hairy undersides [26].

Plants were stored in an indoor greenhouse with direct solar light. They were either used directly as a full-size plant (pot size: 9–15 cm) or their leaves cut using scissors into pieces of 0.9–1.2 g prior to the experiment.

To avoid changes induced by diurnal cycles, all experiments using plants were performed during the day from 10 a.m. to 3 p.m. The planting soil was a universal soil with a water retention capacity of 75%, pH = 6.5, and N, P, K values of 5.5, 2.5, and 1.5 for 2 kg/m³ respectively (Fig. 1).

2.2. Experimental setup

A new experimental setup was designed to measure the uptakes of leaves and the full-size plant under irradiation with NO_x and O₃ configurations.

NO_x/O₃ setup The setup includes:

1. Two flow meters (Brooks 4800 series/50–500 mL/min) to regulate the flow of O₂ and N₂ simultaneously mimicking the ratio of these gases in ambient air.
2. An NO_x source via a 200 mL solution of IMD (10⁻⁵ M) producing 40–50 ppbv of NO₂ and 0.1–0.5 ppbv of NO contained in a cylindrical Pyrex glass flow-reactor (0.65 L, length 27 cm and internal diameter 5.7 cm). This was based on our previous study showing that irradiating a solution of IMD with a polychromatic light ($\lambda_{max} = 365$ nm) leads to the production of NO_x (NO + NO₂) with NO₂ being the major product [27].
A UVP ozone generator equipped with a UV pen-ray lamp that uses the photochemical reaction of O₂ under UVC (185 nm) to produce the continuous flow of O₃.
3. Two air-tight stainless-steel reactors (see Fig. SI-2.) that are cylindrical with a Pyrex glass top window for irradiation. A small one (Reactor S- 0.6 L) for leaves and a big reactor (Reactor B- 12 L) for the full-size plant.
4. 2 × 55W Starlite tubes ($\lambda = 400$ –800 nm) that were placed at a distance of ≈30 cm above the reactors for irradiation. Absolute Irradiance at this distance was 6–7 μW/cm²/nm @ 610 nm. This lamp is commonly used for growing plants indoors where it covers the light range needed for photosynthesis (see spectrum Fig. SI-3).
5. A NO_x Thermo scientific 42i model-NO NO₂ NO_x analyzer (chemiluminescence analyzer). To measure the nitrous acid (HONO) and estimate its contribution to the NO₂ measured levels, a Na₂CO₃-impregnated quartz filter was installed upstream of the NO_x monitor, to trap HONO. Its concentration was then calculated by measuring the difference between measured NO₂ values with and without the HONO scrubber.

An O342e ozone analyzer O₃ (Environnement S.A). Both analyzers were online real-time analyzers with a 10 s temporal resolution.

The tubes used were PTFE (Teflon) to minimize secondary reactions, the fitting and valves were stainless steel from Swagelok (Lyon-France), and the temperature was regulated to 23 °C by an air conditioner.

2.3. Calculation of deposition velocities and plant uptake coefficients

For the plants tested in this study, transient deposition velocities (v_d) for NO₂ and O₃ were calculated, similar to Poppendieck et al. [28] and Abbass et al. [29], based on a mass balance that is shown in equation (1):



Fig. 1. Pictures of the 3 studied plants: *Sedum sexangulare*, *Thymus vulgaris*, and *Heuchera Americana* L. (left to right).

$$\frac{dC_{out}}{dt} = \lambda(C_{in} - C_{out}) - v_{d(p)}C_{out}\frac{A_{(p)}}{V} - v_{d(c)}C_{out}\frac{A_{(c)}}{V} \quad (1)$$

where $\frac{dC_{out}}{dt}$ represents the change in the outlet O₃ or NO₂ concentration (ppb h⁻¹), C_{in} and C_{out} are the inlet and the outlet concentration of NO₂ or O₃, in the inlet and the outlet of the exposure chamber (ppbv), respectively, λ is the air exchange rate for the chamber (h⁻¹), $v_{d(p)}$ and $v_{d(c)}$ are the deposition velocities for a plant and chamber (m/h), respectively, $A_{(p)}$ and $A_{(c)}$ are the exposed area of the plant and chamber walls (m²), respectively. Equation (1) was solved for the transient deposition velocity shown in equation (2):

$$v'_{d(p)} = \frac{V}{A_{(p)}} \frac{1}{C_{out}} \left[\lambda (C'_{in} - C'_{out}) - v_{d(c)} C_{out} \frac{A_{(c)}}{V} - \frac{C'_{out} - C'_{out+1}}{\Delta t} \right] \quad (2)$$

where $v'_{d(p)}$ is the time varying deposition velocity for a plant, t and t indicate consecutive data points (h), V is the volume of the test chamber. The deposition velocity associated with chamber walls $v_{d(c)}$ was observed to be negligible for all experiments. To facilitate comparison across plants, the near steady-state deposition velocity was calculated when the rate of change in exit concentration was less than 2 ppb over 15 min. The uptake coefficients U'_p were then calculated by multiplying the deposition velocity $v'_{d(p)}$ by the inlet concentration of NO₂ or O₃ (C'_{in}) after its conversion from ppbv to $\mu\text{g}/\text{m}^3$ (eq. (3)).

$$U'_p = v'_{d(p)} (C'_{in}) \quad (3)$$

2.4. Analytical methods

VOC analysis. The composition of VOC produced by the three plant species was determined using headspace gas chromatography coupled with mass spectrometry detection (HS-GC/MS; Shimadzu HS-20 coupled with QP2010SE). 1 g of leaves from each species was transferred into a 20 mL headspace glass vial and incubated for 10 min at 80 °C. The analytical column (Mega 5-MS 30 m × 0.25 mm) was operated initially at 60 °C for 1 min, followed by an 8 °C min⁻¹ ramp to reach 240 °C and held for 4 min. The mass spectrometer source was heated to 200 °C, and signals were detected between mass to charge ratios (m/z) of 50 and 350. Identification of the major constituents was carried out using the NIST 17 database and when necessary, using authentic standards.

ATD-GC-MS. After the ozonation of thyme leaves, the reactor gas phase was sampled for 3 min at a sampling rate of 100 mL min⁻¹ into the Tenax sorbent tubes. After sampling, the tubes were thermally desorbed using TurboMatrix thermal desorption unit (ATD 150, PerkinElmer) equipped with a cold trap (Carbotrap 300) and coupled to an Agilent 6890 gas chromatograph and an Agilent 5973 mass spectrometry detector. The separation of desorbed volatiles was carried out using a HP-5 μs column (25 m × 0.25 mm × 0.25 μm) operated initially at 50 °C for 1 min, followed by a 10 °C/min ramp to reach 230 °C. Mass spectra were scanned between m/z 35 and m/z 350 with the source temperature set at 20 °C.

HPLC-DAD. HPLC analyses were performed using a NEXERA XR HPLC/DAD apparatus. Separation was conducted using a phenomenex reversed phase C18 column (100 mm × 2.1 mm, 2.6 μm particle size) and a binary solvent system composed of 10% acetonitrile and 90% water at a flow of 0.2 mL/min. Analysis time was 10 min. HPLC analyses allowed the monitoring of thymol disappearance as well as its absorption spectrum.

Scanning electron microscopy (SEM). The structure of thyme cuticular surfaces before and after ozonation were characterized using scanning electron microscope. Leaves were mounted on aluminum stubs using double-sided adhesive tape and sputter-coated with 10–15 nm gold-palladium (20 s, 25 mA, partial argon pressure 60 mTorr, Denton Desk V. The samples were investigated with a field-emission scanning electron microscope (SH 4000 M) using a 20 kV acceleration voltage and a 10 mm working distance. Pictures were taken from adaxial and abaxial leaf surfaces.

3. Results and discussion

3.1. Depollution capacity of detached leaves

3.1.1. NO₂ uptake

A maximum of 1 g of leaves was irradiated in the reactor for 1 h while being ventilated with pure synthetic air at a flow rate of 0.8 L/min (green line in Fig. 2) under visible light allowing the plant to adapt to the conditions given before measuring the uptake. During this period, NO₂ generated by IMD was directly monitored and its average concentration was found to be relatively stable around 50 ± 2 ppbv. Following the 1 h pre-conditioning of the plant, NO₂ gas flow was introduced into the reactor containing the detached leaves and the NO₂ concentration was monitored initially every 10 s and then regularly until reaching a steady-state to calculate the NO₂ uptake. In control experiment, NO₂ flow was passed through empty chamber (no leaves) and its concentration showed negligible drop suggesting a negligible background removal of NO₂ due to chamber walls (See Fig. 3). In the presence of detached leaves of green roof species, the chamber exit concentration of NO₂ concentration increases quickly in the first minute as the chamber is filled with constant level NO₂ followed by a slower and progressive increases until approaching a steady-state after 1 h of exposure. At the end of the experiment, thyme showed the highest NO₂ uptake with a reduction of about 9 ppbv in NO₂ concentration followed by sedum and heuchera with a reduction of about 5–6 ppbv. The near steady-state deposition velocities for the three plants were calculated by averaging the last 15 min of the exposure.

Table 1 shows the near steady-state NO₂ deposition velocities and corresponding uptake coefficients for the three plant species tested. While Heuchera seems to perform as good as sedum according to Fig. 3, the exposed surface of its leaves was twice higher than that for Sedum and Thyme due to its large leaves. Yang et al. [16] estimated the removal capacity of 71 green roofs using a big leaf dry deposition model and reported an average uptake coefficient of 260 $\mu\text{g}/\text{m}^2/\text{h}$ for NO₂ which is

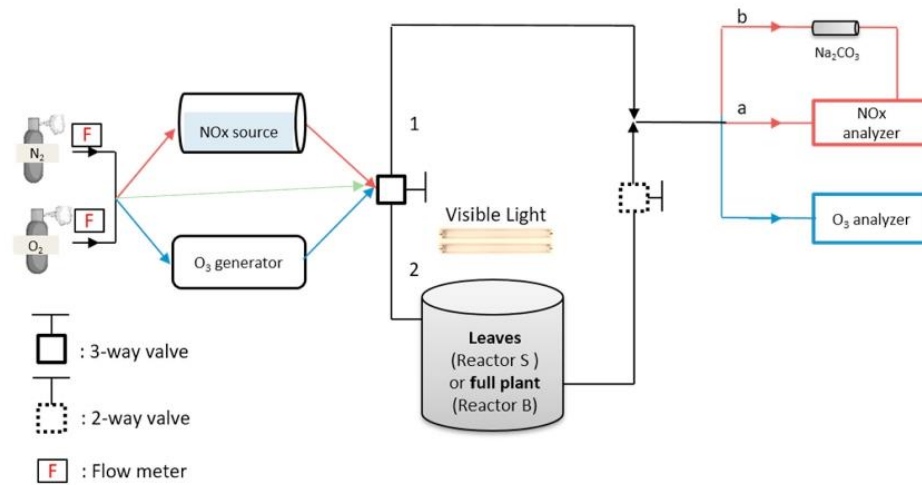


Fig. 2. Experimental setup used for measuring the uptake of NO₂ (red) and O₃ (blue). (For interpretation of the references to color in this figure legend, the reader is referred to the Web version of this article.)

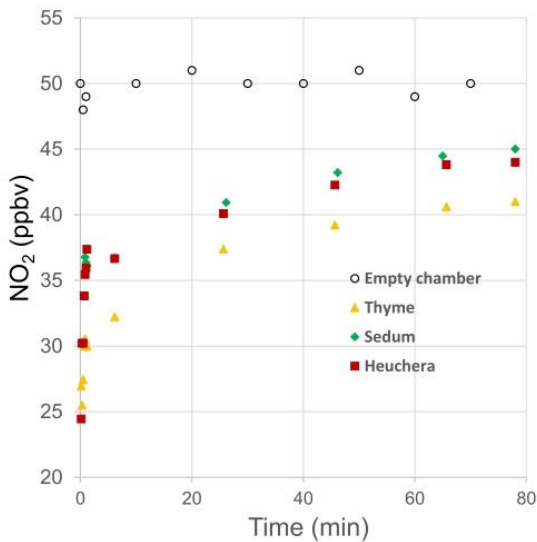


Fig. 3. Empty chamber and outlet NO₂ concentration for sedum, thyme, and heuchera.

Table 1
Near steady-state NO₂ deposition velocities and plant uptake coefficients.

Plant	$v'_{d(p)}$ (m/h)	U_p ($\mu\text{g}/\text{m}^2/\text{h}$)
Sedum	2.99	282
Thyme	5.56	523
Heuchera	1.70	160

comparable to the values reported in this study. In addition, the calculated $v'_{d(p)}$ (1.70–5.56) fall also within the range of v_d in their model (0.36–21.6 m/h). Our values are also in agreement with those reported by Currie and Bass [20] who used the UFORE model (urban forest effects model) and grass as a proxy unit for green roofs and reported an NO₂ uptake of 300 $\mu\text{g}/\text{m}^2/\text{h}$.

To better understand the uptake mechanisms and the difference

between studied species, several experimental factors such as the stomata, water and chemical reactions were investigated.

- Effect of stomata

Leaf stomates are very important organs on the leaf surface as they control exchange of plants with the environment. In general, green plants affect air pollutants by taking up gaseous pollutants primarily through leaf stomates. The higher the density, the more CO₂ and gaseous pollutants can be absorbed or released [30].

Using SEM, we observed the stomates on each leaf and estimated the stomatal density and average stomatal areas by taking into consideration abaxial and adaxial sides (See Fig. 4). Highest stomata density was seen with heuchera followed by thyme and sedum (40 mm⁻² ± 2, 6 mm⁻² ± 2, and 4 mm⁻² ± 2 respectively). However, thyme exhibited the largest stomatal area (8400 ± 150 μm^2) while those of sedum and heuchera were equal to 5700 ± 150 μm^2 and 1400 ± 150 respectively. This finding suggests that the higher stomatal area for thyme could be responsible for its better performance in removing NO₂.

- Effect of transpiration (surface reaction)

A fraction of the consumption of NO₂ could be due to reactions with VOCs emitted by the plants. In general, NO₂ has a low reactivity towards VOCs. However, NOx might generate O₃ by photolysis under UV. As UV was not present, this pathway should be negligible. An alternative possibility is the decay of NO₂ through reaction with water leading to the formation of nitrous acid or HONO (process 1).



Such reaction is possible in the case of sedum particularly as it is an evergreen plant with moist leaves and transpiration can occur. In our experiments, sedum might release moisture after being irradiated and its water might react with NO₂ to yield HONO. We checked this hypothesis by performing experiments aiming to monitor the formation of HONO. This was done by including Na₂CO₃ trap to sample HONO as described in the experimental section. In the same conditions as before, 1 g of leaves was irradiated under visible light for 1 h and the NO₂ uptake was monitored using sodium carbonate as a trap. The difference in the NO₂ uptake in the presence and absence of the trap reveals the uptake due to the reaction between NO₂ and water. Comparing the NO₂ values with and without the trap, we conclude that 55% of the uptake capacity was

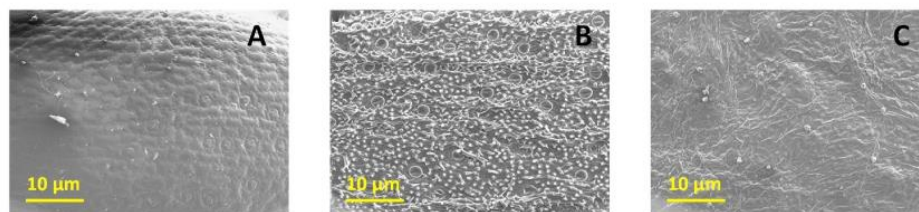


Fig. 4. SEM Images of the three studied plants: sedum (A), thyme (B), and heuchera (C).

due to the reaction as shown in **process 1**. In the case of other species, no significant HONO production was observed, confirming that NO₂ uptake in the case of sedum is enhanced by surface water and its reaction with NO₂. This finding highlights the importance of chemical reaction in addition to stomatal uptake in the overall performance of plant species and could have implication on the photochemistry of air pollutants since HONO can undergo direct photolysis to produce hydroxyl radicals (OH[•]).

3.1.2. O₃ uptake

Fig. 5 illustrates the time evolution of the outlet concentration of O₃ in the case of an empty chamber and in presence of the three studied plants. The same steps were followed as the ones in part 2.1 using same plants, irradiation system, and duration (1 h of pre-conditioning in the chamber). As for the experiment with NO₂, thyme showed the highest O₃ uptake with a reduction of about 10 ppbv followed by sedum and heuchera with a reduction of about 6–7 ppbv. Table 2 shows the near steady-state O₃ deposition velocities and plant uptake coefficients for the three studied plants calculated by averaging the last 20 min of the exposure.

The calculated values in our study are in agreement with those reported by Yang et al. [16] whereas the study of Curie et Bass [20] showed lower values compared to those found here.

- Effect of thyme volatile metabolites

While the higher stomatal area can be responsible for the better performance of thyme in removing O₃, O₃ can potentially react with plant volatile metabolites particularly in the case of thyme which is

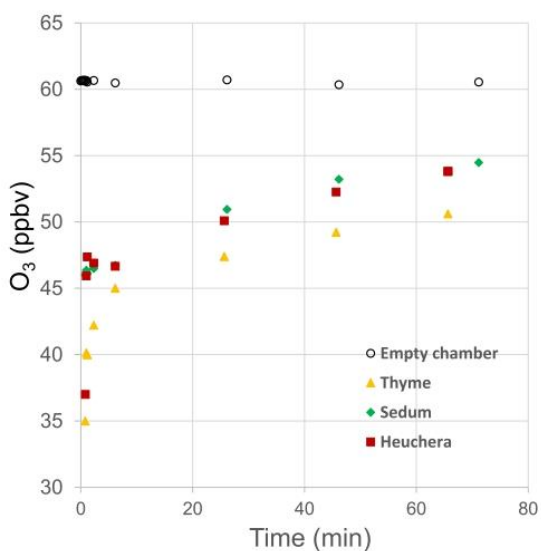


Fig. 5. Empty chamber and outlet O₃ concentration for sedum, thyme, and heuchera.

Table 2

Near steady-state O₃ deposition velocities and plant uptake coefficients.

Plant	$v'_{d(p)}$ (m/h)	U'_p ($\mu\text{g}/\text{m}^2/\text{h}$)
Sedum	2.69	317
Thyme	4.82	569
Heuchera	1.60	189
Yang et al. [10]	1.8	100–6500
Curie et Bass [11]	0.18	–

known to release several terpenes in addition to thymol. For these reasons, thyme was selected as the main species to study in the following experiments. For a simpler approach, experiments were undertaken with one of the major emitted VOC, thymol (a phenolic derivative), first in solution to examine the feasibility of thymol degradation by O₃ and to facilitate the identification of by-products. O₃ reactions in solutions can be easier to perform and could provide a first indication of possible heterogeneous reactions between thymol and O₃ on leaves. Water can also be present on leaf surface and could participate in the reaction mechanisms. Following this feasibility test, additional experiments on thyme leaves were carried out to mimic realistic conditions and to investigate the heterogeneous reactivity of thyme volatiles with O₃.

Reaction of thymol with ozone in solution. We prepared a 20 mL solution of thymol (2×10^{-4} M) in ACN and O₃ at a concentration of 4 ppm was bubbled into it for almost 6 h. Results were monitored by HPLC-DAD analysis that showed that 50% of thymol was degraded. The percentage of degradation is related to ozone and thymol concentrations. According to a study on the catalytic ozonation of thymol, the simplified proposed degradation mechanism is the following: the *para* and *ortho* positions of the hydroxyl on thymol are attacked by O₃ and hydroxyl radical. This leads to diols with a backbone of cymene (Fig. 6.). Several reactions then can take place prompting mineralization [25].

The GC-MS analysis of an experiment conducted on thymol and O₃ revealed the production of Thymoquinone which corroborates the proposed mechanism.

Reaction of thyme VOCs with ozone. Two samples of detached thyme leaves (2 g) were introduced into Pyrex flow-reactors, under irradiation with visible light. To monitor the effect of O₃, the first sample (S1) was not exposed to O₃ while the second (S2) was exposed to O₃ (153 ppbv). In both cases, the production of VOC was monitored via sampling on sorbent tubes followed by ATD-GC-MS analysis.

Table 3 shows the four major terpenes emitted in addition to thymol. After 1 h of ozonation, their levels decreased drastically as expected since terpenes are known to undergo oxidation by O₃. This was associated with the identification of various oxidation products such as linalool-oxide, keto-limononaldehyde and thymoquinone. This finding confirms the role that plays thyme VOC metabolites in the observed good performance for the removal of O₃. However, while the uptake of ozone can be enhanced by the emission of terpenes, one should consider the consequences of O₃ reactions with terpenes since it can lead to the formation of secondary organic aerosols (SOA) [31]. Unfortunately, this was not confirmed here but future experiments are needed to measure the possible emission of ultrafine particles due to reaction of O₃ with thyme volatiles, and to estimate its impact on air pollution.

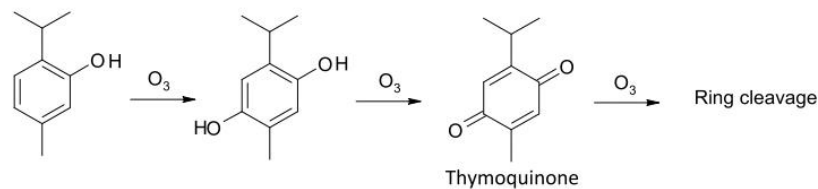


Fig. 6. Thymol degradation pathway via the reaction with O_3 .

Table 3

Major VOC products identified in S1 and S2.

Sample	VOC collected mass (ng)				
	Cymene	Limonene	Thymol	Eucalyptol	Linalool
S1 (no O_3)	12.6	8.5	22.5	13.2	31.3
S2 (with O_3)	0.4	Non detected	Non detected	0.3	1.6

3.2. Depollution capacity of thyme full-size plant

3.2.1. NO_2/O_3 uptakes

These following experiments were conducted using a small thyme plant (with an estimated total leaf area of 500 cm^2) which was pre-conditioned in the big reactor (12 L) with 1 h visible light irradiation while soil was fully covered during experiments to ensure the least interference possible. After 1 h of exposure to NO_2 (50 ppbv) the NO_2 concentration dropped to reach a near-steady state around 10 ppbv. Using eqs. (1) and (2) we calculated a $v_{d(p)}^f$ of 3.84 m/h. In the case of O_3 , same conditions were used as with detached leaves with the exception of O_3 inlet concentration which was increased to 110 ± 3 ppbv to reduce measurement uncertainty. Under these conditions, O_3 concentration dropped by around 91 ppbv to reach 19 ppbv after 1 h of exposure (Fig. SI-4). Assuming a near steady-state condition we obtained a $v_{d(p)}^f$ of 4.65 m/h. These values are comparable with those obtained using detached leaves particularly when considering the uncertainty in the estimation of total leaf area, presence of soil, emission of volatile metabolites and the measurement uncertainty. It is noteworthy that a small production of NO was observed when thyme plant was irradiated which was not detected with detached leaves. NO is a key signaling molecule in plant physiology. However, its production in photosynthetic organisms remains partially unresolved. The best characterized NO production route involves the reduction of nitrite (NO_2^-) to NO via different non-enzymatic or enzymatic mechanisms. To better characterize the role of soil in the production of NO and the uptake of pollutants, additional experiments using soil only were carried out.

- Effect of soil on NO_x production and uptake and of O_3 uptake

Soil, as well, is used on green roofs so its uptake towards NO_2 and O_3 in addition to its NO_x production were studied. In these experiments the same soil used for thyme was studied here.

NO_x production. After 1 h of visible light irradiation, a mixture of N_2 and O_2 (pure synthetic air) was passed through the reactor containing the soil to monitor the NO/NO_2 production. Studied soil was either wet or dry, but the steps were the same in both cases. Only NO was produced at a level of ≈ 20 ppbv in the case of dry soil, and ≈ 10 ppbv in that of wet soil (Fig. SI-5). Irrigation, N-fertilizers, and bacteria are known to be responsible for NO_2 production [32]. In our experiments, the adsorbed NO_2 is probably undergoing reactions producing $NO_{(g)}$ in case of both dry and wet soils; or reacting with water producing ions e.g. NO_2^- and NO_3^- (case of wet soil).

NO_2/O_3 uptake. The same experimental steps were followed as in section 3.2. In the case of O_3 (see Fig. SI-4), the reduction in

concentration (Δ) for exposed soil ranged between 85 (dry) and 88 (wet) ppbv which is very close to that observed with thyme (91 ppbv). This suggests that soil can also be as effective in removing O_3 and could contribute to increase the overall performance of green roofs. On the other hand, soil contributed to the removal of 15 ppbv (wet) to 35 ppbv (dry) of NO_2 as compared with about 40 ppbv for thyme (Fig. SI-6) indicating that the thyme plant is more effective in removing NO_2 . The higher NO_2 uptake by dry soil is likely associated with the higher surface area available for adsorption as compared with wet soil which can be partially saturated with water.

4. Conclusion

Natural air pollution mitigation approaches are needed to help improve air quality especially in urbanized areas. One promising recommended approach is the use of green roofs. In this study, we developed a new NO_2/O_3 bench-scale experimental system to measure the depollution performance of different green roofs species.

After the screening of several species, 3 species were found to be the most efficient for the NO_2/O_3 uptakes: *sedum sexangulare*, *thymus vulgaris*, and *heuchera americana* L. They offer a diversity between being aesthetically pleasant, drought tolerant, climate resilient, and exhibiting good uptakes. NO_2 uptake coefficients ranged from 160 to $523 \mu\text{g}/\text{m}^2/\text{h}$ while that of O_3 varied between 189 and $569 \mu\text{g}/\text{m}^2/\text{h}$. These findings are in accordance with previously reported data using the big-leaf dry deposition models. Nevertheless, values were relatively higher in our experiments possibly due to other mechanisms than dry deposition (adsorption) such as the reactions between the VOCs and O_3 especially in the case of thyme, and between NO_2 and water in the case of the evergreen plant: *sedum* -which are not considered yet in models. If we apply our experimental results using the existing model [16] by taking the average deposition velocity in our experiments ($0.095 \text{ m}/\text{h}$ for NO_2 and $0.084 \text{ m}/\text{h}$ for O_3), the total uptake by the 3 species (*sedum*, *thyme*, and *heuchera*) could reach 9 kg/ha/year of NO_2 and around 13.6 kg/ha/year of O_3 . Assuming that Paris has around 76 ha of green roofs and walls (2016) [33], and if the three species investigated in this study were to be used, one can estimate that 683 kg/year of NO_2 and 1037 kg/year of O_3 can be mitigated.

While our study focused only on the uptake of two air pollutants, additional research should be carried to measure the performance of green roof species towards $PM_{2.5}$ and to investigate the potential formation of SOA. In addition, our experimental design does not consider some important variables such as the effects of humidity, lighting spectrum/intensity changes, nor the diurnal and seasonal cycles of the plant. Field evaluation of laboratory results should also be carried to better understand the effects of seasonality and weather conditions on the depollution performance of green roofs.

Declaration of competing interest

The authors declare that they have no known competing financial interests or personal relationships that could have appeared to influence the work reported in this paper.

Acknowledgements

Y. ARBID thanks Peng CHENG for his technical assistance, Adelina DAVID and Mr. Yann FASCHINETTI for the microscopy analysis, and Mr. Martin LEREMBOURE regarding the LC-MS analysis.

Appendix A. Supplementary data

Supplementary data to this article can be found online at <https://doi.org/10.1016/j.buildenv.2021.108286>.

Funding sources

This work was supported by the University of Clermont Auvergne and the French Ministry of Higher Education and Research.

References

- [1] World Health Organization, Air pollution. <https://www.who.int/health-topics/air-pollution>, 2019.
- [2] J. Zhao, X. Xi, Q. Na, S. Wang, S.N. Kadry, P.M. Kumar, The technological innovation of hybrid and plug-in electric vehicles for environment carbon pollution control, *Environ. Impact Assess. Rev.* 86 (2021), <https://doi.org/10.1016/j.ear.2020.106506>.
- [3] R. Zalakeviciute, Y. Rybarczyk, J. López-Villada, M.V. Diaz Suarez, Quantifying decade-long effects of fuel and traffic regulations on urban ambient PM_{2.5} pollution in a mid-size South American city, *Atmos. Pollut. Res.* 9 (2018) 66–75, <https://doi.org/10.1016/j.apr.2017.07.001>.
- [4] M. Granovskii, I. Dincer, M.A. Rosen, Air pollution reduction via use of green energy sources for electricity and hydrogen production, *Atmos. Environ.* 41 (2007) 1777–1783, <https://doi.org/10.1016/j.atmosenv.2006.10.023>.
- [5] X. Tang, O. Rosseler, S. Chen, S. Houzé de l'Aulnoit, M.J. Lussier, J. Zhang, G. Ban-Weiss, H. Gilbert, R. Levinson, H. Destailats, Self-cleaning and de-pollution efficacies of photocatalytic architectural membranes, *Appl. Catal. B Environ.* 281 (2021) 119260, <https://doi.org/10.1016/j.apcatb.2020.119260>.
- [6] X. Tang, L. Ughetta, S.K. Shannon, S. Houzé de l'Aulnoit, S. Chen, R.A.T. Gould, M. L. Russell, J. Zhang, G. Ban-Weiss, R.L.A. Everman, F.W. Klink, R. Levinson, H. Destailats, De-pollution efficacy of photocatalytic roofing granules, *Build. Environ.* 160 (2019) 106058, <https://doi.org/10.1016/j.buildenv.2019.03.056>.
- [7] J. Chen, C. Poon, Photocatalytic construction and building materials: from fundamentals to applications, *Build. Environ.* 44 (2009) 1899–1906, <https://doi.org/10.1016/j.buildenv.2009.01.002>.
- [8] M. Krichevskaya, S. Preis, A. Moiseev, N. Pronina, J. Deubener, Gas-phase photocatalytic oxidation of refractory VOCs mixtures: through the net of process limitations, *Catal. Today* 280 (2017) 93–98, <https://doi.org/10.1016/j.cattod.2016.03.041>.
- [9] A. Palla, I. Gneco, L.G. Lanza, Unsaturated 2D modelling of subsurface water flow in the coarse-grained porous matrix of a green roof, *J. Hydrol.* 379 (2009) 193–204, <https://doi.org/10.1016/j.jhydrol.2009.10.008>.
- [10] H. Liu, F. Kong, H. Yin, A. Middel, X. Zheng, J. Huang, H. Xu, D. Wang, Z. Wen, Impacts of green roofs on water, temperature, and air quality: a bibliometric review, *Build. Environ.* 196 (2021) 107794, <https://doi.org/10.1016/j.buildenv.2021.107794>.
- [11] J. Mentens, D. Raes, M. Hermy, Green roofs as a tool for solving the rainwater runoff problem in the urbanized 21st century? *Landsc. Urban Plann.* 77 (2006) 217–226, <https://doi.org/10.1016/j.landurbplan.2005.02.010>.
- [12] L.M. Cook, T.A. Larsen, Towards a performance-based approach for multifunctional green roofs: an interdisciplinary review, *Build. Environ.* 188 (2021) 107489, <https://doi.org/10.1016/j.buildenv.2020.107489>.
- [13] Y. He, H. Yu, A. Ozaki, N. Dong, S. Zheng, Long-term thermal performance evaluation of green roof system based on two new indexes: a case study in Shanghai area, *Build. Environ.* 120 (2017) 13–28, <https://doi.org/10.1016/j.buildenv.2017.04.001>.
- [14] T. Van Renterghem, D. Botteldooren, Numerical evaluation of sound propagating over green roofs, *J. Sound Vib.* 317 (2008) 781–799, <https://doi.org/10.1016/j.jsv.2008.03.025>.
- [15] D.B. Rowe, Green roofs as a means of pollution abatement, *Environ. Pollut.* 159 (2011) 2100–2110, <https://doi.org/10.1016/j.envpol.2010.10.029>.
- [16] J. Yang, Q. Yu, P. Gong, Quantifying air pollution removal by green roofs in Chicago, *Atmos. Environ.* 42 (2008) 7266–7273, <https://doi.org/10.1016/j.atmosenv.2008.07.003>.
- [17] D.J. Nowak, D.E. Crane, J.C. Stevens, Air pollution removal by urban trees and shrubs in the United States, *Urban For., Urban Green* 4 (2006) 115–123, <https://doi.org/10.1016/j.ufug.2006.01.007>.
- [18] V. Etyemezian, S. Ahonen, D. Nikolic, J. Gillies, H. Kuhns, D. Gillette, J. Veranth, Deposition and removal of fugitive dust in the arid southwestern United States: measurements and model results, *J. Air Waste Manag. Assoc.* 54 (2004) 1099–1111, <https://doi.org/10.1080/10473289.2004.10470977>.
- [19] N.W. Lepp, Planting green roofs and living walls, *J. Environ. Qual.* 37 (2008) 2408, <https://doi.org/10.2134/jeq2008.0016br>.
- [20] B.A. Currie, B. Bass, Estimates of air pollution mitigation with green plants and green roofs using the UFORE model, *Urban Ecosyst.* 11 (2008) 409–422, <https://doi.org/10.1007/s11252-008-0054-y>.
- [21] A.F. Speak, J.J. Rothwell, S.J. Lindley, C.L. Smith, Urban particulate pollution reduction by four species of green roof vegetation in a UK city, *Atmos. Environ.* 61 (2012) 283–293, <https://doi.org/10.1016/j.atmosenv.2012.07.043>.
- [22] O.A. Abbass, D.J. Sailor, E.T. Gall, Ozone removal efficiency and surface analysis of green and white roof HVAC filters, *Build. Environ.* 136 (2018) 118–127, <https://doi.org/10.1016/j.buildenv.2018.03.042>.
- [23] P. Ramasubramanian, I. Luhung, S.B.Y. Lim, S.C. Schuster, O. Starry, E.T. Gall, Impact of green and white roofs on air handler filters and indoor ventilation air, *Build. Environ.* 197 (2021) 107860, <https://doi.org/10.1016/j.buildenv.2021.107860>.
- [24] G. Pérez, C. Chocarro, A. Juárez, J. Coma, Evaluation of the development of five Sedum species on extensive green roofs in a continental Mediterranean climate, *Urban For. Urban Green.* 48 (2020) 126566, <https://doi.org/10.1016/j.ufug.2019.126566>.
- [25] L. Wang, A. Liu, Z. Zhang, B. Zhao, Y. Xia, Y. Tan, Catalytic ozonation of thymol in reverse osmosis concentrate with core/shell Fe₃O₄@SiO₂/Yb₂O₃ catalyst: parameter optimization and degradation pathway, *Chin. J. Chem. Eng.* 25 (2017) 665–670, <https://doi.org/10.1016/j.cjche.2016.10.017>.
- [26] U. Weerakkody, J.W. Dover, P. Mitchell, K. Reiling, Quantification of the traffic-generated particulate matter capture by plant species in a living wall and evaluation of the important leaf characteristics, *Sci. Total Environ.* 635 (2018) 1012–1024, <https://doi.org/10.1016/j.scitotenv.2018.04.106>.
- [27] D. Palma, Y. Arbid, M. Sleiman, P. De Sainte-Claire, C. Richard, New route to toxic nitro and nitroso products upon irradiation of micropollutant mixtures containing imidacloprid: role of NO_x and effect of natural organic matter, *Environ. Sci. Technol.* 54 (2020) 3325–3333, <https://doi.org/10.1021/acs.est.9b07304>.
- [28] D. Poppendieck, H. Hubbard, M. Ward, C. Weschler, R.L. Corsi, Ozone reactions with indoor materials during building disinfection, *Atmos. Environ.* 41 (2007) 3166–3176, <https://doi.org/10.1016/j.atmosenv.2006.06.060>.
- [29] O.A. Abbass, D.J. Sailor, E.T. Gall, Effectiveness of indoor plants for passive removal of indoor ozone, *Build. Environ.* 119 (2017) 62–70, <https://doi.org/10.1016/j.buildenv.2017.04.007>.
- [30] B. Grant, I. Vatnick, Environmental correlates of leaf stomata density, teaching issues and experiments in ecology, *TIEE* 1 (2004) 1–6. Ecological Society of America, www.tiee.ecoed.net.
- [31] X. Chen, P.K. Hopke, W.P.L. Carter, Secondary organic aerosol from ozonolysis of biogenic volatile organic Compounds: chamber studies of particle and reactive oxygen species formation, *Environ. Sci. Technol.* 45 (2011) 276–282, <https://doi.org/10.1021/es102166c>.
- [32] C.H. Jaeger, R.K. Monson, M.C. Fisk, S.K. Schmidt, Seasonal partitioning of nitrogen by plants and soil microorganisms in an alpine ecosystem, *Ecology* 80 (1999) 1883–1891, [https://doi.org/10.1890/0012-9658\(1999\)080](https://doi.org/10.1890/0012-9658(1999)080).
- [33] M.A. Kleiber, A Paris, quel est l'impact réel de la végétalisation des toits. <https://www.lejdd.fr/JDD-Paris/a-paris-quel-est-l-impact-reel-de-la-vegetalisation-des-toits-3798761>.

Supporting Information

Towards an experimental approach for measuring the removal of urban air pollutants by green roofs

Yara Arbid, Claire Richard, Mohamad Sleiman*

University Clermont Auvergne, CNRS, Clermont Auvergne INP, Institut de Chimie de Clermont-Ferrand
F-63000 Clermont-Ferrand, France

Mohamad.sleiman@sigma-clermont.fr

Figure SI-1. VOCs of thyme obtained by headspace-GC-MS.

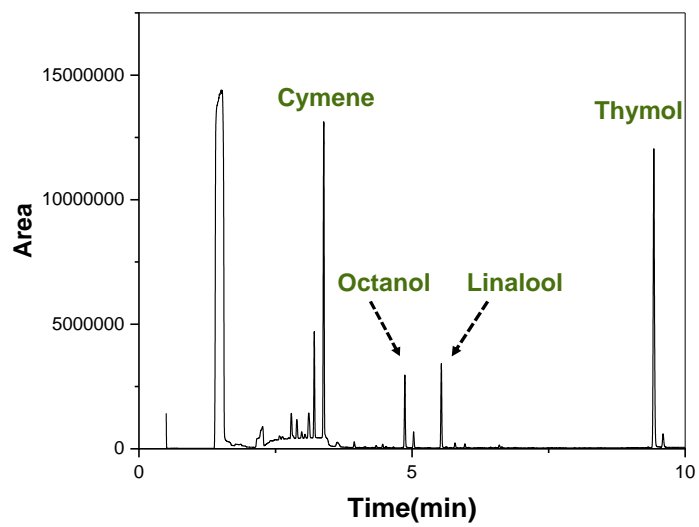


Figure SI-2. The small and the big reactors used in our experiments.



Figure SI-3. Light spectrum emitted by the 2x55W Starlite tubes used in the developed experimental setup.

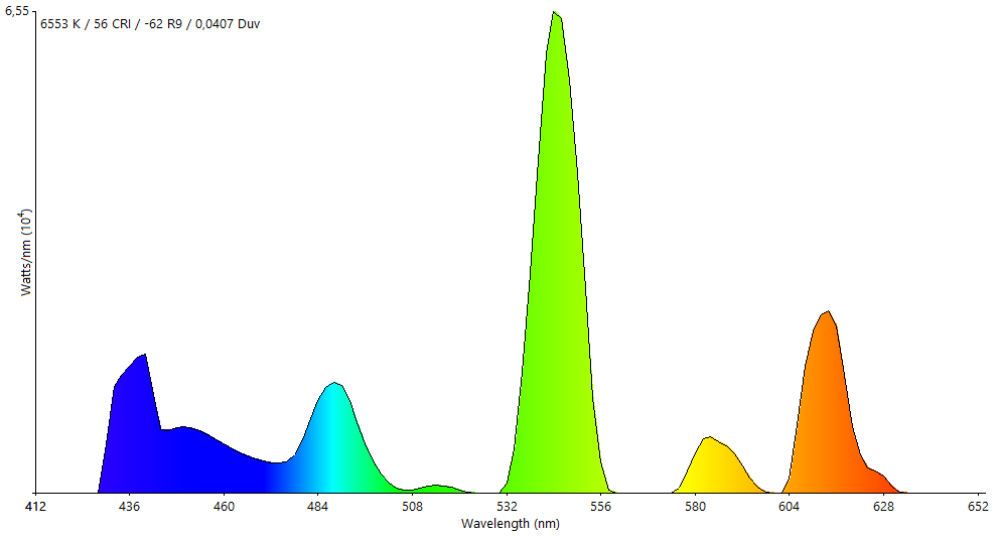


Figure SI-4. The O₃ uptakes of thyme and soil (wet and dry) after 1 h of visible light irradiation.

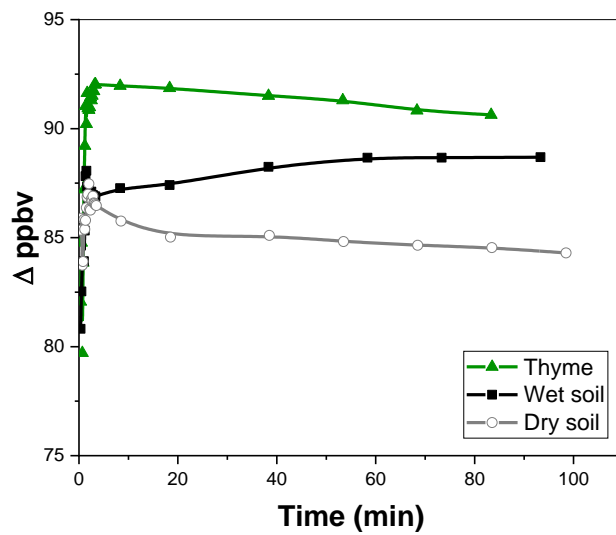


Figure SI-5. NO production by dry and wet soils after 1 h of visible light irradiation.

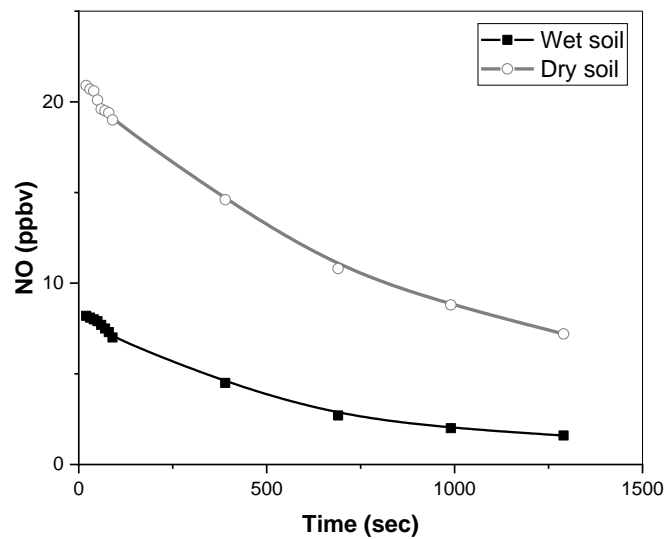
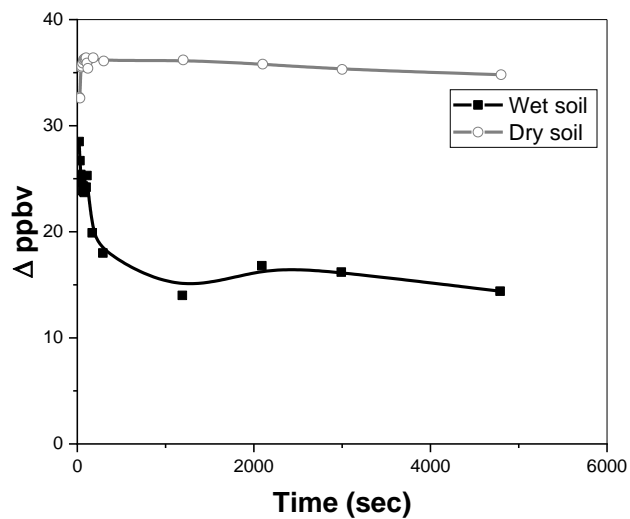


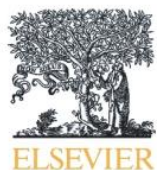
Figure SI-6. NO₂ uptakes of dry and wet soils after 1 h of visible light irradiation. The y-axis shows the difference in the NO₂ values of IMD and that ‘passing through the reactor containing soil’ read on the analyzer.



Manuscript 3

Photochemical interactions between pesticides and plant volatiles

Date of acceptance: September 27, 2021



Photochemical interactions between pesticides and plant volatiles

Yara Arbid, Mohamad Sleiman, Claire Richard*

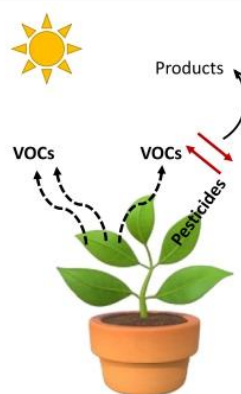
Université Clermont Auvergne, CNRS, ICCF, F-63000 Clermont-ferrand, France



HIGHLIGHTS

- Pesticides and thyme's volatiles undergo photochemical interactions.
- Chlorothalonil is photoreduced while thymol and terpenes are photooxidized.
- Imidacloprid photoinduces the oxidation and the nitration of thymol.
- These reactions were observed when pesticides are applied on thyme's leaves.
- They generate by-products with high to moderate concern levels.

GRAPHICAL ABSTRACT



ARTICLE INFO

Article history:

Received 23 June 2021

Received in revised form 27 September 2021

Accepted 27 September 2021

Available online 6 October 2021

Editor: Yifeng Zhang

Keywords:

Chlorothalonil

Imidacloprid

thyme's leaves

Photoreduction

Photooxidation

Photonitration

ABSTRACT

Among the numerous studies devoted to the photodegradation of pesticides, very scarce are those investigating the effect of plant volatiles. Yet, pesticides can be in contact with plant volatiles after having been spread on crops or when they are transported in surface water, making interactions between the two kinds of chemicals possible. The objectives of the present study were to investigate the reactions occurring on plants. We selected thyme as a plant because it is used in green roofs and two pesticides: the fungicide chlorothalonil for its very oxidant excited state and the insecticide imidacloprid for its ability to release the radical NO_2 under irradiation. Pesticides were irradiated with simulated solar light first in a solvent ensuring a high solubility of pesticides and plant volatiles, and then directly on thyme's leaves. Analyses were conducted by headspace gas chromatography-mass spectrometry (HS-GC-MS), GC-MS and liquid chromatography-high resolution mass spectrometry (LC-HRMS). In acetonitrile, chlorothalonil photosensitized the degradation of thymol, α -pinene, 3-carene and linalool with high quantum yields ranging from 0.35 to 0.04, and was photoreduced, while thymol underwent oxidation, chlorination and dimerization. On thyme's leaf, chlorothalonil was photoreduced again and products arising from oxidation and dimerization of thymol were detected. Imidacloprid photooxidized and photonitrated thymol in acetonitrile, converting it into chemicals of particular concern. Some of these chemicals were also found when imidacloprid was irradiated dispersed on thyme's leaves. These results show that photochemical reactions between pesticides and the plants secondary metabolites can take place in solution as on plants. These findings demonstrate the importance to increase our knowledge on these complex scenarios that concern all the environmental compartments.

© 2021 Elsevier B.V. All rights reserved.

* Corresponding author.

E-mail address: Claire.richard@uca.fr (C. Richard).

1. Introduction

Pesticides undergo degradation processes in surface waters (Pehkonen and Zhang, 2002), on the surface of soil and of leaves (Katagi, 2004) yielding breakdown chemicals. The potential effects of these chemicals on wildlife and human health have attracted numerous studies aiming for identification and to improve knowledge on their physico-chemical, biological and toxicological properties (Martínez Vidal et al., 2009, de Souza et al., 2020).

Pesticides are generally photodegraded when they absorb solar light (Burrows et al., 2002; Mathon et al., 2021) or when they are irradiated in the presence of natural chromophoric species acting as sensitizers (natural organic matter) or photoinducers (nitrate ions, ferric species...) (Remucal, 2014; Ossola et al., 2021; Marussi and Vione, 2021; Brand et al., 1998). Photochemical reactions between two pesticides can also take place. In our group, we have demonstrated that mixing mesotrione and nicosulfuron (ter Halle et al., 2010) or chlorothalonil and cycloxydim (Monadjemi et al., 2011) enhances the rate of photodegradation of each of them. Thiophanate-methyl was also shown to favor the photodegradation of methyl-bifenazate (Hamdache et al., 2018). These results were explained by the capacity of chlorothalonil and the primary photoproduct of thiophanate-methyl to generate oxidant triplet excited states and singlet oxygen capable of oxidizing other pesticides. In addition, reactions can be drastically affected by the medium. This was illustrated in the case of the insecticide methyl-bifenazate, the photodegradation of which was measured to be 70-fold faster on green pepper skin than on a film of paraffinic wax (Hamdache et al., 2018). This behaviour was rationalized by the presence of water from pepper. These results bring evidence that the fate of pesticides can be affected by the presence of other chemicals present in the medium apart from the well-known sensitizers or photoinducers.

Volatile compounds emitted by plants are the subject of intense research because of their implication in atmospheric chemistry, air pollution and defense of plants against pathogens (Atkinson and Arey, 2003; Mellouki et al., 2015; Wannaz et al., 2003; Hammerbacher et al., 2019). However, to the best of our knowledge, scenarios in which they could interact with pesticides were rarely considered in the literature. These potential reactions concern all the environmental compartments. When a pesticide is dispersed on the crop leaves just after been applied, it is surrounded by plant's volatiles facilitating reactions between each group of chemicals at the solid gas interface. Moreover, pesticides and plant volatiles can be transported to surface water after their solubilization in the run off water and can interact in the aquatic compartment. Plant volatiles correspond to a large group of chemicals: mono, di and triterpenes/terpenoids, phenols (Dudareva et al., 2006, Abbas et al., 2017, Mochizuki et al., 2020). They bear functionalities such as H-atoms, double bonds and aromatic rings giving them possibilities to be involved in a lot of photochemical reactions.

Here, we investigated the photochemical reactivity of two pesticides: the fungicide chlorothalonil (CT) and the insecticide imidacloprid (IMD) in the presence of the main thyme volatiles: thymol (T), linalool, 3-carene, α -pinene. These terpenes and thymol are common to other plant species (Petrović et al., 2019; Salehi et al., 2018). Both pesticides are susceptible to have an effect on the plant volatiles: CT shows photooxidant properties *via* its triplet excited state or the formation of singlet oxygen (1O_2) (Bouchama et al., 2014; Monadjemi et al., 2011) while IMD releases NO and NO₂ under irradiation making it a potential nitrosating/nitrating agent (Palma et al., 2020). Out of nitrogen oxides, NO and NO₂ are considered toxic (Skalska et al., 2010). Experiments were first conducted in solution to evidence the reactions. Acetonitrile was chosen for its ability to ensure a high solubility of all the studied chemicals. Then, pesticides were directly irradiated on leaves of thyme to approach the real conditions closely.

2. Experimental part

2.1. Chemicals and standards

IMD (C₉H₁₀ClN₅O₂) and CT (C₈Cl₄N₂) were purchased from Sigma Aldrich (Pestanal™, analytical standard, $\geq 98.0\%$). T (C₁₀H₁₄O, $\geq 98.5\%$), α -pinene (C₁₀H₁₆, 98%), 3-carene (C₁₀H₁₆, 90%), linalool (C₁₀H₁₈O, $\geq 97.0\%$ GC area %), thymoquinone (TQ, C₁₀H₁₂O₂, $\geq 98\%$) were all purchased from Sigma Aldrich. Thymohydroquinone (TQH₂, C₁₀H₁₄O₂, 95%) was purchased from Enamine, Ukraine. All were used without further purification. Water was produced using a reverse osmosis RIOS 5 and Synergy (Millipore) device (resistivity 18 M Ω cm, DOC < 0.1 mg L⁻¹). Acetonitrile (ACN) was purchased from Carlo Erba Reagents (HPLC Plus Gradient grade-ACS-Reag). Thyme (*Thymus vulgaris*) was freely grown under natural sunlight in a garden for seven years in Beaumont (France) and regularly watered. In the case of IMD, we undertook a comparative set of experiments on a thyme plant (*Thymus vulgaris*) bought in a garden center.

2.2. Samples preparation

All stock solutions were prepared in ACN and kept in the dark at 4 °C before use. Final solutions were prepared by diluting stock solutions with ACN. For the experiments on thyme leaves, twigs were cut using scissors. Each twig contained 30 leaves (average area of each leaf of 0.03 cm²) for a total area of 1.8 cm² considering the two faces. Twigs were dipped in IMD or CT solution (7.5×10^{-4} M) for 30 s, left to dry freely for an hour, and then put in hermetically sealed headspace (HS) vials to be either used for control experiments in the dark or irradiated. Dark controls in the absence of pesticides were conducted with twigs directly put in HS vials. The surface concentration of IMD and CT on twigs was evaluated as follows: twigs covered by CT were immersed and agitated in 2 mL of acetonitrile for 2 min while those covered by IMD in 5 mL of acetonitrile. Solutions were then analyzed by high performance liquid chromatography coupled to a photodiode-array detector (HPLC-DAD) to determine the CT's and IMD's concentrations.

2.3. Irradiation

Solar UV radiations reaching the earth's surface contain UVA (315–400 nm) and a part of UVB (295–315 nm). The absorption spectrum of CT and IMD overlapping the radiations reaching the earth's surface within the wavelength range 295–350 nm (Fig. S1-A), we used the following irradiation devices to simulate solar light. The first one (device 1) was used to calculate the quantum yield of CT photodegradation in the presence of thyme's volatiles. Solutions containing CT (10^{-4} M) + volatiles (10^{-3} M) were put in a cuvette and irradiated at 313 nm (UVB) in parallel beam using a high pressure mercury lamp equipped with an Oriel monochromator. A radiometer QE65000 from Ocean optics was used to measure the photon flux I_0 : $(3.0 \pm 0.2) \times 10^{14}$ photons cm⁻² s⁻¹ at 313 nm. Samples were taken at chosen irradiation times and directly analyzed by HPLC-DAD to follow the degradation profile of CT. To monitor the disappearance of CT or IMD (10^{-4} M) in ACN alone or in the presence of volatiles (10^{-3} M) and detect new photoproducts we needed to use a device delivering a more intense photon flux. Solutions (20 mL) were placed in a cylindrical Pyrex reactor (1.4 cm internal diameter) sealed with an air-tight silicon cap surrounded by 3 polychromatic tubes simulating UVB (Philips, TL20W/01-RS, $\lambda_{max} = 313$ nm) installed inside a custom-made cylindrical irradiation device (device 2). Aliquots were sampled at chosen irradiation times and directly analyzed by HPLC-DAD to monitor the degradation profiles of CT or IMD and UHPLC coupled to high resolution mass spectrometry (LC-HRMS) and gas chromatography coupled to mass spectrometry (GC-MS) to identify photoproducts. The third device (device 3) was a solar simulator CPS Atlas equipped

with a xenon arc lamp, a filter cutting off wavelengths shorter than 290 nm and a cooling system maintaining the bottom of the device at 10 °C. The global irradiance in the range of 300–800 nm was set at 500 W m⁻². It represents a medium value at 40°N latitude in summer. This device was used to irradiate the HS vials containing thyme twigs alone or covered with IMD or CT. In the case of IMD, 2 h of irradiation were enough to detect significant amounts of nitro derivatives of thymol. For CT, due to the difficulty to demonstrate the interaction between CT and thyme's volatile, we extended the irradiation until 6 h. Vials were then analyzed directly by Headspace gas chromatography coupled to mass spectrometry (HS-GC-MS) or chemicals contained in and on twigs were extracted by ACN as previously explained and analyzed by LC-HRMS or GC-MS. Irradiation experiments in solution were duplicated and on twigs duplicated or triplicated.

2.4. Analyses

UV-Vis absorption spectra of volatiles, CT, IMD, TQ, and TQH₂ were recorded using a Varian Cary 3 spectrophotometer. CT and IMD degradation profiles were tracked by HPLC-DAD using a NEXERA XR HPLC-DAD apparatus. The analytical column was a Phenomenex-kinetex C₁₈ (100 mm × 2.1 mm, 2.6 μm particle size) for CT experiments and EC 150/4.6 NUCLEODUR C₁₈ endcapped column for IMD analyses. The eluent was a mixture of ACN and water and the flow rate was set at 0.2 and 1 mL min⁻¹ for CT and IMD, respectively. The HPLC conditions for CT were as follows: the elution gradient started with 30% ACN maintained for 2 min and then linearly increased to reach 80% after 13 min; while that for IMD started with 30% ACN which was maintained for 10 min. Photoproducts were analyzed and quantified using HRMS on an Orbitrap Q-Exactive (ThermoScientific) coupled to an ultra-high performance liquid chromatography (UHPLC) instrument Ultimate 3000 RSLC (ThermoScientific). The column was a Kinetec EVO C₁₈ (100 × 2.1 mm), particle size of 1.7 μm (Phenomenex). The elution gradient started with 15% acetonitrile maintained for 5 min, then the percentage of acetonitrile was linearly increased to reach 55% after 5 min. The flow was set at 0.45 mL min⁻¹. Analyses were made in positive (ESI⁺/ESI⁻) electrospray mode. Identification of the major constituents was carried out using the Xcalibur software and when necessary by matching retention times with those of authentic standards. The *m/z* of proposed structures differed by less than 5 ppm from the theoretical mass. Standard solutions of TQ were analyzed immediately after have been prepared. The limit of detection LOD in the case of TQ was estimated to 10⁻⁶ M by analyses of authentic solutions.

Photoproducts were also analyzed using an Agilent 6890 GC coupled to an Agilent 5973 MS. The separation was carried out using a HP-5 μs column (25 m × 0.25 mm × 0.25 μm) operating initially at 80 °C over 1 min, followed by a 10 °C min⁻¹ ramp to reach 200 °C and then a 30 °C min⁻¹ ramp to reach 260 °C maintained for 1 min (to calculate the degradation of terpenes) in the case of CT experiments, while the analysis was operated initially at 70 °C followed by a 10 °C min⁻¹ ramp to reach 160 °C for 5 min and then a 30 °C min⁻¹ ramp to reach 250 °C maintained for 2 min in the case of IMD. The flow rate was 1 mL min⁻¹ with an injection volume of 1 μL in both cases. T and some of its photoproducts were quantified after derivatization with N, O-bis (trimethylsilyl)trifluoroacetamide (BSTFA). The derivatizing solution (2 mL) was prepared by mixing 60 μL of BSTFA with 1.4 mL sample. Separation was achieved as previously described for CT experiments.

To determine the volatile metabolites produced by the plant, HS-GC-MS (Shimadzu HS-20 coupled with QP2010SE) was used. Twigs of 0.2 g alone or after dipping in CT solution were transferred into a 20 mL headspace glass vial, then left in the dark or irradiated and incubated for 5 min at 80 °C. The analytical column (Mega 5-MS 30 m × 0.25 mm) was operated initially at 50 °C for 1 min, followed by an 8 °C min⁻¹ ramp to reach 170 °C and held for 4 min, and then a 15 °C min⁻¹ ramp to reach 275 °C maintained for 1 min. The mass

spectrometer source was heated to 200 °C, and signals were detected between mass to charge ratios (*m/z*) of 50 and 350.

Identification of the major constituents was carried out using the NIST 17 database and when necessary by matching retention times and ion fragments with those of authentic standards. For calibration, a stock solution of T was prepared in ethanol at a concentration of 1 g L⁻¹. Quantification of T was performed by means of 5-point calibration curve for which the concentrations of standards ranged from 2 to 100 mg L⁻¹. All standard solutions were stored in dark at 2–8 °C in amber glass vials with Teflon-lined caps. They were found to be stable under short-term (48 h) storage conditions. A linear response was obtained with a correlation coefficient (*R*²) of 0.997. Selectivity was evaluated by analyzing a set of blank samples and monitoring the absence of interferences with *S/N* ratios higher than 3. No significant interfering peaks were observed in the ion chromatogram time window monitored for T. The precision of the method was determined by calculating the relative standard deviation (RSD) of six replicate measurements of diluted T solution (10 mg L⁻¹). All RSDs were acceptable and less than 7% indicating a good precision. The limit of detection LOD was calculated from the standard deviation (*σ*) of multiple measurements (*n* = 7) of diluted T solutions within a factor of 5 of the background signal. LOD was set equal to 3*σ* which resulted in a value of 13 pg. The limit of quantification (LOQ) was defined as 10*σ* or 43 pg. In all cases, LOD and LOQ were significantly below the levels determined in the thyme extracts (0.07 to 2.7 mg).

2.5. Quantum yields of CT photodegradation in the presence of terpenes in acetonitrile

The quantum yield of CT photodegradation (*Φ*_{CT}) was determined using Eq. (1):

$$\Phi_{CT} = \Delta c / (I_a \times \Delta t) \quad (1)$$

where $\Delta c / \Delta t$ was the rate of CT consumption expressed in M s⁻¹ and *I_a* was the rate of photon absorption by CT at 313 nm expressed in Einstein L⁻¹ s⁻¹. *I_a* was obtained using Eq. (2):

$$I_a = I_0 \times \left(1 - 10^{-\epsilon \times \ell \times [CT]_0} \right) \times 1000 / \ell \quad (2)$$

where ϵ = 1760 M⁻¹ cm⁻¹, [CT]₀ = 10⁻⁴ M, and ℓ = 1 cm.

2.6. Laser flash photolysis

Laser flash photolysis experiments were carried out using an Applied Photophysics LKS.60 apparatus equipped with a Nd³⁺:YAG laser Quanta-Ray GCR-130 used in a right-angle geometry with respect to the monitoring light beam. Samples were irradiated using the fourth harmonic (266 nm, 9 ns pulse duration) in a quartz cuvette. ³CT* was generated by irradiating CT (5 × 10⁻⁵ M in aerated ACN) and its decay monitored at 330 nm. The reactivity of ³CT* with thyme's volatiles was measured within the concentration range 10⁻⁴–2 × 10⁻³ M. In the case of IMD, no transient species were detected.

2.7. Photoproducts toxicity

The toxicity of photoproducts formed during the irradiations was estimated using the freely available ECOSAR (Ecological Structure-Activity Relationship) computer program (v 2.0). It predicts the toxicity of a molecule using a structure-activity approach. The acute (LC50, the concentration that is lethal to half of fish after 96 h of exposure to a certain molecule) and chronic toxicities (ChV) of CT, IMD, and formed photoproducts on fish in fresh waters as well as logKow were obtained. The program (v 2.0) is available from the website: epa.gov/tscsa-screening-tools/ecological-structure-activity-relationships-ecosar-predictive-model.

3. Results

3.1. Characterization of the thyme's constituents

This first objective was to determine what are the main volatile compounds in thyme's twigs, to estimate the amount of T in thyme's twig and to identify and quantify the chemicals related to T. Volatile compounds released from thyme's twigs after 2 h in the dark in the HS vials were analyzed by HS-GC-MS (Fig. SI-2). T, linalool, 3-carene and α -pinene were the main detected compounds. T is a phenolic compound while linalool, 3-carene and α -pinene are terpenes (Scheme 1). The amount of extractable T from thyme's twigs by ACN was measured by GC-MS. Based on several replicates using twigs containing 30 leaves (weight 0.2 g), it could be estimated to range between 0.35 and 2.7 mg per g of wet twigs. After that, we analyzed the non-volatile chemicals. For this, two vials containing two twigs each were left in the dark for 4 h, extracted in 2 mL of ACN and analyzed by UHPLC-HR-MS and GC-MS. Several peaks directly connected to T were found (Table 1). By UHPLC-HR-MS, one got a peak at $m/z = 165.0901$ in ES^- corresponding to $[M + O - H^+]^-$ and named TO. By MS-MS, TO gave two main fragments at 149.0593 and 135.0443 corresponding to the loss of O and CH_2O , respectively (Fig. SI-3). The oxidation of T can take place on the isopropyl group, on the methyl group or on the ring. No loss of H_2O was observed ruling out an oxidation of the isopropyl carbon atoms. The oxidation of the ring would lead to thymolhydroquinone. However, TO was not assigned to thymolhydroquinone because the two compounds had different retention times in HPLC (3.3 min for TO against 4.5 min for thymolhydroquinone), and different maximum of absorption (278 nm for TO against 290 nm for thymolhydroquinone). We therefore concluded that TO was the benzyl alcohol derivative (Table 1). The peak detected at $m/z = 165.0901$ in ES^+ (Fig. SI-4) corresponded to $[M + O - 2H + H^+]^+$ and was assigned to the quinonic derivative TQ (Table 1). Its maximum of absorption at 250 nm was fully in line with this assignment. The other peak at $m/z = 179.0704$ in ES^- corresponding to $[M + 2O - 2H - H^+]^-$ was attributed to the quinonic derivative of TO, TQO (Fig. SI-5). The two peaks showing $m/z = 313.1806$ and 329.1754 in ES^- were assigned to dimers, T-TO and

TO-TO respectively (Figs. SI-6 and 7). By GC-MS, TO, TQ and several isomers of TO-TO were also detected.

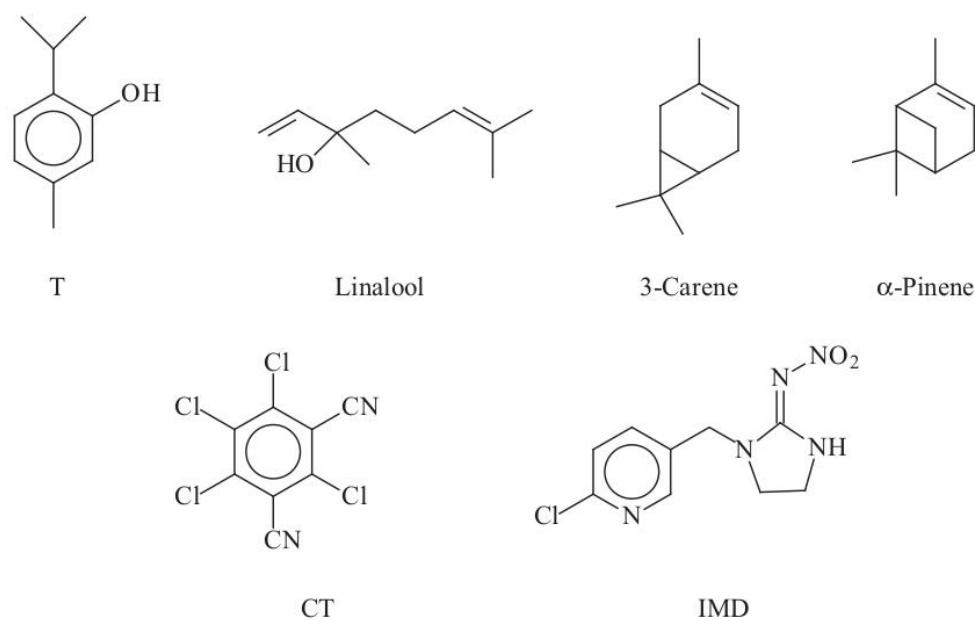
The second objective was to investigate the effect of irradiation on the formation of these compounds. For this, two vials containing two twigs each were irradiated in the solar simulator for 4 h and extracted using ACN. The same compounds were detected and the effect of irradiation on their formation can be seen in Table 2. The peak areas were between 15 and 100-fold higher after irradiation than in the dark showing the drastic effect of light.

3.2. Interactions between CT and thyme's volatiles

3.2.1. Irradiation of CT and thyme's volatiles in acetonitrile solution

Neither T, 3-carene, linalool and α -pinene nor CT underwent significant photodegradation when irradiated alone in ACN solution. Thyme's volatiles do not absorb the radiations emitted by the tubes (Fig. SI-1B), while CT absorbs the radiations (Fig. SI-1A) but yields a triplet excited state $^3CT^*$ efficiently deactivated by oxygen ($7.8 \times 10^8 M^{-1} s^{-1}$, Monadjemi et al., 2011) (Fig. 1A). In contrast, the irradiation of CT ($10^{-4} M$) in the presence of each of these volatiles ($10^{-3} M$) led to the fast disappearance of CT (Fig. 1A) and the thyme's volatiles (Fig. 1B). As shown in Fig. 1A, the CT photodegradation increased in the order $T > \alpha$ -pinene $>$ 3-carene $>$ linalool. In accordance, the quantum yield of CT photodegradation (Φ_{CT}) was equal to 0.35, 0.20, 0.15, 0.04 for T, α -pinene, 3-carene and linalool, respectively against <0.001 for CT alone. Concerning the thyme's volatiles loss, T was the fastest to disappear, followed by α -pinene, 3-carene, and linalool (Fig. 1B).

To confirm the ability of thyme's volatiles to react with $^3CT^*$ and measure the bimolecular rate constant of the reaction (k_r), we undertook laser flash photolysis experiments. CT was irradiated in the presence of each of these chemicals added at a concentration comprised between 3×10^{-4} and $2 \times 10^{-3} M$ while the decay of $^3CT^*$ was monitored at 330 nm (Fig. 1). Alone, in air-saturated ACN, $^3CT^*$ disappeared by an apparent first order kinetic with $k = 1.6 \times 10^6 s^{-1}$ corresponding to the sum $k_d + k_{O_2}[O_2]$, where k_d is the rate constant of deactivation by collision with the solvent molecules, k_{O_2} the rate constant of reaction



Scheme 1. Structure of chlorothalonil (CT), imidacloprid (IMD), thymol (T), linalool, 3-carene and α -pinene.

Table 1
Structures of by-products arising from T and CT detected in the different conditions.

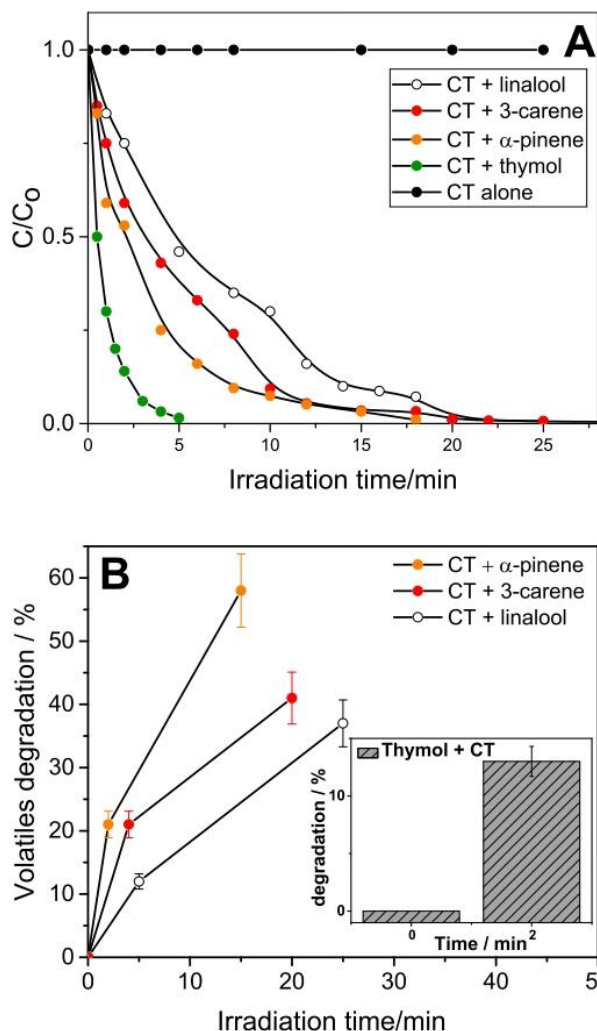
Label	UHPLC-MS m/z (m/z of DNPH adduct)	GC-MS m/z
T		
TO	165.0910 in ES ⁻	150, 135, 117 166, 151, 139
TQ	165.0910 in ES ⁺ (343.1049 in ES ⁻)	164, 149, 136, 93
TQO	179.0704 (359.1000 in ES ⁻)	
TCl	183.0571/185.0542 in ES ⁻	184/186, 169/171, 149/151
TO-TO	329.1754 in ES ⁻ several isomers	298, 284 298, 241 298, 283, 241 298, 283, 149
T-TO	313.1806 in ES ⁻ several isomers	
CT		
CT-Cl		266, 229, 194 230/232/234/236
CT-2Cl		196/198/200

with oxygen and [O₂] the concentration of oxygen in the solution. In the presence of T, ³CT* disappeared faster than alone showing that a reaction between ³CT* and T took place (Fig. 1A). This reaction might be an energy transfer or an electron/H atom transfer reaction. The energy level of ³CT* was previously estimated to lay at 275 kJ mol⁻¹ based on phosphorescence measurements at 77 K in pentane (Porras et al., 2014). This is lower than the energy level reported for phenol ~314–334 kJ mol⁻¹ (Becker, 1969) making the energy transfer from ³CT* to T unlikely. Moreover, given the ability of ³CT* to oxidize phenols (Monadjemi et al., 2011), an electron or H atom transfer from T to ³CT* with formation of the reduced CT radical (CT^{-•}/CTH[•]) and the phenoxyl radical (T_H[•]) (Scheme 2) looks more probable.

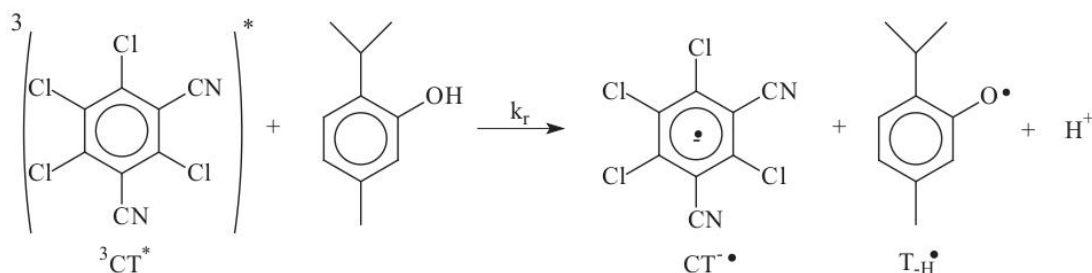
Table 2

Recovered mass of T (GC-MS) and UHPLC-MS areas of CT photoproducts extracted from thyme's twigs. SD are given in brackets; d: detected by GC-MS.

By-product	Thyme dark (4 h)	Thyme hν (4 h)	Thyme + CT dark (4 h)	Thyme + CT hν (4 h)
T	0.07 mg (14%)	0.54 mg (39%)	0.07 mg (14%)	0.54 mg (39%)
TO	7.8 × 10 ⁷ (14%)	1.3 × 10 ⁹ (15%)	3.1 × 10 ⁷ (10%)	1.1 × 10 ⁹ (25%)
TQ	6.0 × 10 ⁵ (40%)	2.2 × 10 ⁷ (20%)	7.0 × 10 ⁵ (10%)	1.7 × 10 ⁷ (10%)
TQO	Traces	3.2 × 10 ⁷ (20%)	3.0 × 10 ⁵ (10%)	2.7 × 10 ⁷ (15%)
TCl	-	-	-	-
TO-TO	2.0 × 10 ⁸ (10%)	2.2 × 10 ⁹ (30%)	1.2 × 10 ⁸ (10%)	2.3 × 10 ⁹ (10%)
T-TO	1.0 × 10 ⁸ (10%)	1.5 × 10 ⁹ (15%)	5.0 × 10 ⁷ (20%)	1.6 × 10 ⁹ (20%)
CT-Cl	-	-	-	d
CT-2Cl	-	-	-	d

**Fig. 1.** Irradiation of CT (10⁻⁴ M) alone and in the presence of thyme's volatiles (10⁻³ M). A: Decay profile of CT and B: percentages of thyme's volatiles loss.

The shape of the time-resolved absorption spectrum of Fig. 2A revealed the formation of a secondary species that could be therefore either the reduced CT radical or T_H[•]. Its significant absorption measured at 330 nm matches more with the reduced CT radical (Bouchama et al., 2014) than with T_H[•] that shows maxima at 390 and 410 nm (Venu et al., 2013). Due to the overlapping of the two species absorption, a numerical analysis of the differential equations was necessary to determine the k_t value. The best fit of the experimental

Scheme 2. Reaction of ${}^3\text{CT}^*$ with thymol

data was obtained by taking $k_r = 7.0 \times 10^9 \text{ M}^{-1} \text{ s}^{-1}$, $\epsilon_{\text{CT}^*}/\epsilon_{\text{phenoxyl}} = 2.0$, and a first order decay rate constant of $5 \times 10^5 \text{ s}^{-1}$ for the reduced CT radical in air-saturated medium (Bouchama et al., 2014). Individual evolution of these species is shown in the inset of Fig. 1A.

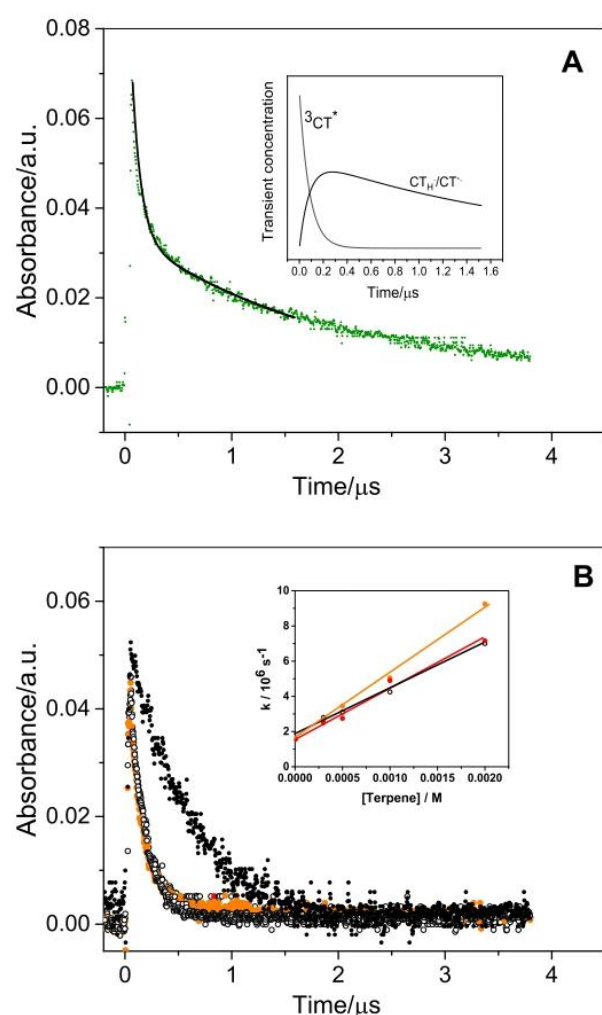
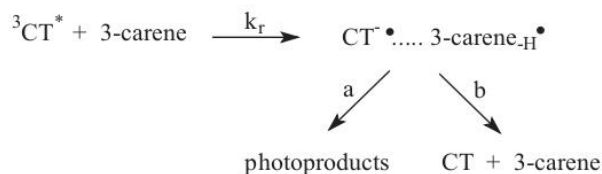


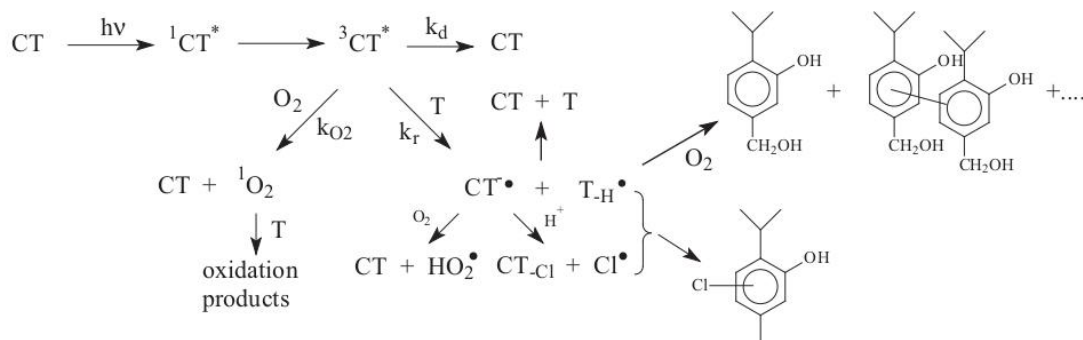
Figure 2. Laser flash photolysis of CT ($5 \times 10^{-5} \text{ M}$) in the presence of thyme's volatiles. A: absorbance variation vs time in the mixture CT + T (●). The black line is the fitted curve. Inset: Absorption profiles of ${}^3\text{CT}^*$ and the reduced CT radical; B: absorbance variation vs time for CT alone (●) in the mixtures CT + α -pinene (●), CT + 3-carene (●) and CT + linalool (●); inset: Plot of k vs [terpene]. Air-saturated ACN, detection at 330 nm.

In the case of α -pinene, 3-carene and linalool, the absorbance at 330 nm completely decayed within 1 μs with the flash (Fig. 1B). This result demonstrated the reaction of ${}^3\text{CT}^*$ with terpenes. However, with these compounds, the formation of the reduced CT radical was not observed (Fig. 1B). Values of k_r could be deduced from the linear plot of k , the observed first order rate constant, vs [terpene] (inset of Fig. 1B). Assuming $k = k_d + k_{\text{O}_2}[\text{O}_2] + k_r[\text{terpene}]$, one got $k_r = 2.6 \times 10^9$, 2.8×10^9 and $3.9 \times 10^9 \text{ M}^{-1} \text{ s}^{-1}$ for α -pinene, 3-carene, and linalool, respectively. The oxidation of terpenes by ${}^3\text{CT}^*$ was likely due to the presence of labile H atoms in their structures and the non-observation of the 330 nm radical could be tentatively explained by an in-cage reaction between the reduced CT radical and the oxidized terpene leading directly to photoproducts (Scheme 3 in the case of 3-carene). If one admits that the relative importance of process a that yielded photoproducts and process b in which CT was regenerated depended on the structure of the terpene, then one can also explain why Φ_{CT} varied from 0.20 for α -pinene to 0.04 for linalool whereas the k_r values laid in a very narrow range for these two compounds. Finally, we found that all four thyme's volatiles readily reacted with ${}^3\text{CT}^*$. The higher reactivity of T compared to that of α -pinene, 3-carene, and linalool is in line with the presence of an easily abstractable phenolic H atom.

Product studies were also undertaken by GC-MS and UHPLC-HRMS. For the CT + T mixture, we detected a new photoproduct showing $m/z = 183.0571$ and 185.0542 in ES^- along with TO, TQ, TQO, T-TO_{2H}} and TO-TO_{2H}}. This compound corresponded to $[\text{T}-\text{H}+\text{Cl}-\text{H}^+]^-$ and was named TCl (Table 1). By GC-MS, we detected TCl again, CT_{Cl} and CT_{2Cl} . The formation of dechlorinated CT confirmed that photoreduction took place. CT_{Cl} was also detected upon the irradiation of CT + 3-carene, but no other photoproducts were found by GC-MS and no photoproducts at all were detected with α -pinene and linalool.

Based on these data and on the known CT photoreactivity, the reaction pathways shown in Scheme 4 can be proposed to explain the reaction between CT and T. In neat acetonitrile, ${}^3\text{CT}^*$ is generated with a quantum yield close to unity and trapped by O_2 ($k_{\text{O}_2} = (1 \pm 0.1) \times 10^9 \text{ M}^{-1} \text{ s}^{-1}$) to yield ${}^1\text{O}_2$ with a quantum yield equal to 0.85 ± 0.06 (Bouchama et al., 2014). T will therefore compete with O_2 for the reaction with ${}^3\text{CT}^*$. Taking $k_r = 7.0 \times 10^9 \text{ M}^{-1} \text{ s}^{-1}$ and $[\text{O}_2] = 1.9 \times 10^{-3} \text{ M}$ in air-saturated acetonitrile solution at 24 °C (Murov et al., 1993), one can estimate that T (10^{-3} M) could trap 79% of ${}^3\text{CT}^*$ while 21% of O_2 . In our experimental conditions, T was thus mainly photooxidized through a direct reaction with ${}^3\text{CT}^*$, however, given the

Scheme 3. Reaction of ${}^3\text{CT}^*$ with 3-carene.



Scheme 4. Mechanism of CT photolysis in the presence of T.

known good reactivity of singlet oxygen with phenolic compounds (Wilkinson and Brummer, 1981), a part of the loss of T may be attributable to the reaction $T + {}^1O_2$. Once formed, T_{-H}^{\bullet} should be further oxidized into TO, TQ and yield dimeric species. The detection of TCl demonstrates that CT can also photoinduce the chlorination of other chemicals. A possible explanation is the release of chlorine atoms from CT^{\bullet} followed by their recombination with T_{-H}^{\bullet} (Scheme 4). Such a reaction also rationalizes the formation of dechlorinated CT.

The values of k_r for terpenes were 1.8 to 2.7-fold lower than for T. Therefore, the percentage of ${}^3CT^*$ trapped by terpenes at 10^{-3} M should be consequently lower than for T and the amount of singlet oxygen generated higher. The photooxygenation of terpenes bearing double bonds such as α -pinene, linalool and 3-carene is therefore likely in our conditions, given their reactivity with singlet oxygen (Chiron et al., 1997).

Similar reactions can take place in water or in media enriched in water because ${}^3CT^*$ was also detected in water/acetonitrile (90:10, v/v) with a quantum yield of formation also close to unity (Bouchama et al., 2014). However, changing the solvent is expected to induce some changes in the pathway ratios. For instance, the percentage of ${}^3CT^*$ trapped by O_2 will decrease significantly from acetonitrile to water because the O_2 concentration is reduced by a factor of about 7 (from 1.9×10^{-3} M to 2.7×10^{-4} M in air-saturated solutions at 24 °C). This may favor the direct reaction between ${}^3CT^*$ and the two volatiles T and linalool for which the water solubility is good and thus the CT photoreduction. In contrast, for 3-carene and α -pinene that show a very low water solubility, CT photoreduction should be insignificant and ${}^3CT^*$ could mainly lead to singlet oxygen. However, the lifetime of singlet oxygen is shorter in water (4 μ s, Rodgers and Snowden, 1982) than in acetonitrile (61–68 μ s, Hurst et al., 1982) which will affect negatively the rate of terpenes photooxidation. Last, the higher polarity of water compared to acetonitrile may increase k_r , although it is already quite high in acetonitrile.

3.2.2. Irradiation of CT on thyme's leaves

We started the experiments on thyme's leaves by estimating the amount of CT deposited on two twigs after their dipping in a solution of CT (7.5×10^{-4} M). In the 2 mL of ACN used for the extraction, the CT concentration was of 3.4×10^{-5} M. Based on a total leaves area of 3.6 cm², we finally got a CT concentration of 5 ± 1 μ g/cm², which is in the range of the surfacic concentrations calculated for typical CT application rates of 0.5–1 kg ha⁻¹.

Then, CT was irradiated for 6 h in the solar simulator on thyme's leaves or deposited on a glass dish chosen as an inert support and ACN extracts analyzed by GC–MS (Fig. 3). While no CT photodegradation was observed on dishes, an almost full loss of CT on thyme's leaves was measured. CT_{-Cl} and CT_{-2Cl} were formed (Inset of Fig. 2) confirming the photoreduction of CT when applied on thyme's leaves. T that was present in high amounts in the thyme's twigs was

the candidate to induce this photoreduction, even though its involvement in the reaction cannot firmly demonstrated.

Moreover, the GC–MS area of T peak increased similarly after 4 h of irradiation for thyme's twigs irradiated in the absence of CT and for thyme's twigs irradiated in the presence of CT from $(2.8 \pm 0.4) \times 10^6$ to $(2.3 \pm 0.9) \times 10^8$ (Table 2). The presence of CT did not affect the nature of T byproducts (TO, TQ, TQO, T-TO and T-TO_{-2H}) and their peak area measured after 4 h of irradiation and in the dark (Table 2). The only evidence of an interaction between CT and T came from the analyses of the gaseous phase of irradiated vials by HS-GC–MS. Indeed, in this case, a drastic loss of T was observed (Fig. SI-8). The apparent discrepancy between the HS-GC–MS analyses conducted directly on the volatiles present in the vials and the GC–MS analyses that required extraction of chemicals by ACN can be explained as follows. CT deposited on leaves consumed T present in the gaseous phase, and the weak volatility of T limited any reequilibration through remission from leaves allowing to detect the T loss by HS-GC–MS. However, this T consumption was not measurable after extraction by ACN because extraction allowed the recovering of the great part of T present in the leaves while the loss of T that was related to the initial concentration of CT on the twigs laid below the measurement uncertainties. Indeed, we estimated that 5.7×10^{-7} mol of T could be extracted while 6.7×10^{-8} mol of CT were present on twigs. As 1 mol of CT was expected to oxidize 1 mol of T at its best, the amount of T consumed was less than 12% of T extracted, thus negligible.

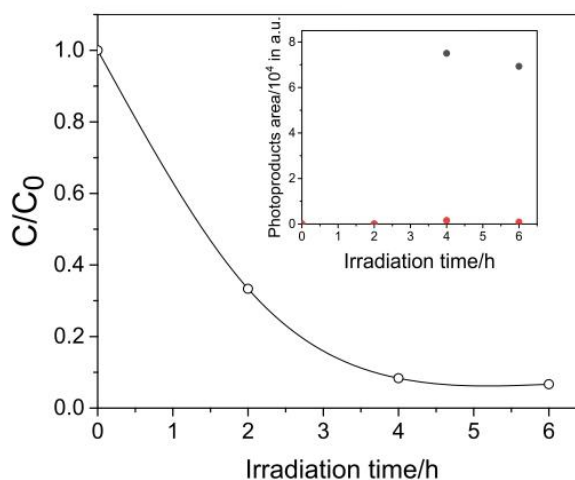
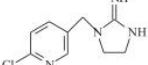
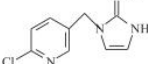
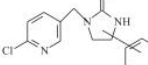
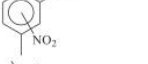
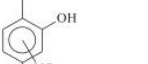
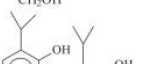


Fig. 3. Decay profile of CT upon irradiation on thyme's twigs ●. Inset: Formation of CT_{-Cl} (●) and CT_{-2Cl} (●).

Table 3
Structures of T and IMD by-products detected in the different conditions.

Label	Structure ^a	UHPLC-MS m/z
IMD		254.0445/256.0414
IMD-NO ₂ +H		211.0742/213.0710
IMD-HNO		223.0385/225.0356
IMD-IMD-N ₂ O ₃		432.0744/434.0715/436.0689
TO		165.0910
TNO ₂		194.0812
TONO ₂		210.0761
TO-TNO ₂		358.1649

^a All the chemicals are detected in ES⁻ except IMD-NO₂+H in ES⁺.

To conclude, we demonstrated that in solution photochemical reactions between CT and thyme's volatiles, in particular T, took place with photoreduction of CT and photooxidation/photochlorination of T. On thyme's leaves, photoreduction of CT was also observed. The involvement of T in this reaction was likely based on the data obtained in solution, but could not be firmly confirmed.

3.3. Interactions between IMD and thyme's volatiles

3.3.1. Irradiation of IMD and T in acetonitrile solution

After 30 min of irradiation alone in device 2, IMD (10⁻⁴ M) disappeared by 6.5 × 10⁻⁵ M (65%). Three photoproducts were identified (Table 3). The main one gave a peak at m/z = 211.0742/213.0710 in ES⁺ (Fig. SI-9) and corresponded to [M-NO₂+H+H⁺]⁺, it was assigned to the imino derivative IMD-NO₂+H. Two other minor peaks

were detected at m/z = 223.0385/225.0356 in ES⁻ (Fig. SI-10) corresponding to [M-NO-H-H⁺]⁻ and at m/z = 432.0744/434.0715/436.0689 (Fig. SI-11) corresponding to [2M-N₂O₃-H⁺]⁻. They were named IMD-HNO and IMD-IMD-N₂O₃, respectively.

In the presence of T (10⁻³ M), IMD disappeared by 3.0 × 10⁻⁵ M (30%) after 30 min of irradiation (Table 4), i. e. less than alone. On the other hand, the T loss was of 7% after 2 h, yielding a consistent consumption of around 1.7 × 10⁻⁵ M after 30 min (Table 4). IMD-NO₂+H, IMD-HNO and IMD-IMD-N₂O₃ were detected again but in much smaller amounts than in the absence of T (Table 4). In addition, we detected along TO, a peak at m/z = 194.0812 in ES⁻ (Fig. SI-12) corresponding to [M+NO₂-H-H⁺]⁻ and assigned to nitrothymol TNO₂, a second peak at m/z = 210.0761 in ES⁻ (Fig. SI-13) corresponding to [M+O+NO₂-H-H⁺]⁻ assigned to nitrated TO, as well as traces of a peak at m/z = 358.1649 in ES⁻ corresponding to the dimer [2M+O+NO₂-H-2H-H⁺]⁻ and labelled TO-TNO₂. Although solutions were carefully handled in the dark, traces of TNO₂ were detected in the non-irradiated solutions. It seemed therefore that IMD was also able to release some NO₂ molecules, spontaneously.

These results showed that T inhibited the IMD photodegradation and the photoproducts formation, in particular that of IMD-HNO and IMD-IMD-N₂O₃ while undergoing nitration. This inhibition strongly suggests that competition between T and IMD took place.

As shown in scheme 5, the excitation of IMD released NO₂ by the cleavage of the N-NO₂ bond and led to the formation of the radical IMD-NO₂ that is further converted into IMD-NO₂+H after the abstraction of an H atom (Palma et al., 2020). The formation of TNO₂ could be explained by the oxidation of T by NO₂ into the corresponding phenoxyl radical followed by the addition of NO₂ onto it (Marussi and Vione, 2021). Similarly, the nitration of TO into TONO₂ should involve the oxidation of TO by NO₂ followed by the addition of NO₂ on the corresponding phenoxyl radical. The lower rate of IMD loss in the presence of T was in favor of a competition between IMD and T for the reaction with NO₂ and suggests that NO₂ reacted with IMD, for example, by H atom abstraction.

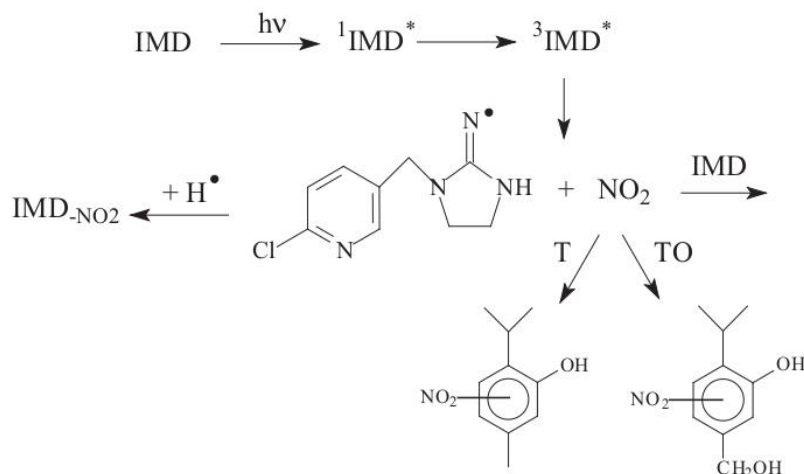
3.3.2. Irradiation of IMD on thyme's leaves

As for CT, we estimated the amount of IMD deposited on two twigs after their dipping in a solution of IMD (7.5 × 10⁻⁴ M). In the 5 mL of ACN used for the extraction, we measured a IMD concentration of 3.9 × 10⁻⁵ M. Based on a total leaves area of 3.6 cm², we finally got a IMD concentration of 14 ± 2 μg/cm² that is enough to observe reactions.

Vials containing twigs covered with IMD were irradiated in the solar simulator for 2 h, and in parallel other vials were left in the dark for the control. The ACN extracts were then analyzed by UHPLC-HR-MS. In the samples left in the dark, we detected TO, TNO₂, TONO₂ and TO-TNO₂ (Table 4), confirming that the NO₂ release from IMD could also take place in the dark. As shown in Table 4, upon irradiation of IMD on twigs, TNO₂ and TO-TNO₂ were detected in amounts equivalent to those observed in the dark. However, for TONO₂ a 50-folds enhancement was measured. The presence of IMD little increased the formation of TO compared to thyme irradiated in the absence of IMD. Another set

Table 4
Decay of T and IMD (HPLC-DAD) and formation of T and IMD by-products (UHPLC-HRMS) vs experimental conditions. UHPLC-HRMS area with SD in brackets, nd = not determined.

By-product	IMD alone in ACN hv (0.5 h)	IMD + T in ACN dark (0.5 h)	IMD + T in ACN hv (0.5 h)	Thyme hv (2 h)	Thyme + IMD dark (2 h)	Thyme + IMD hv (2 h)
IMD	Δ = 6.5 × 10 ⁻⁵ M	<10 ⁻⁶ M	Δ = 3.0 × 10 ⁻⁵ M	-	-	Δ = 6.8 × 10 ⁻⁵ M
IMD-NO ₂ +H	2.4 × 10 ⁹	Traces	1.8 × 10 ⁹	-	Traces	Traces
IMD-HNO	7.7 × 10 ⁷	Traces	7.4 × 10 ⁶	-	Traces	Traces
2 × IMD-N ₂ O ₃	6.9 × 10 ⁷	Traces	7.3 × 10 ⁶	-	Traces	Traces
T	-	<10 ⁻⁶	Δ = 1.7 × 10 ⁻⁵ M	nd	nd	nd
TO	-	4.0 × 10 ⁶ (5%)	2.0 × 10 ⁸ (5%)	3.4 × 10 ⁹ (25%)	2.3 × 10 ⁸ (25%)	4.9 × 10 ⁹ (25%)
TNO ₂	-	1.5 × 10 ⁷ (5%)	4.7 × 10 ⁹ (5%)	-	3.3 × 10 ⁶ (20%)	2.6 × 10 ⁶ (20%)
TONO ₂	-	<10 ⁶	5.4 × 10 ⁸ (5%)	-	9.4 × 10 ⁵ (20%)	4.3 × 10 ⁷ (20%)
TO-TNO ₂	-	<10 ⁶	2.4 × 10 ⁶ (10%)	-	1.0 × 10 ⁵ (20%)	2.0 × 10 ⁴ (20%)



Scheme 5. Mechanism of IMD photolysis in the presence of T.

of experiments was undertaken on the same variant of thyme just bought in a garden center and thus much younger and much less exposed to solar light. In this case also, nitration reactions were observed under irradiation but they yielded TNO₂ and not TONO₂ as for the older thyme. Accordingly, the young thyme contained much less TO than the older one.

Therefore, we conclude that IMD generated nitrocompounds when it was in contact with T, with an increase of the phenomenon under light exposure. The reaction involved the radical NO₂ that was released in the medium mainly photochemically but also spontaneously. T had also an effect of the fate of IMD: by quenching NO₂, it increased its lifetime.

3.4. Estimation of the photoproducts toxicities

Using the ECOSAR computer program (version 2.0), we estimated the potential acute (LC₅₀) and chronic toxicity (ChV) of the starting chemicals and their degradation products (Table 5). CT is classified as a moderate toxic chemical. Its photoreduction by T and terpenes in CT_{-Cl} and CT_{-2Cl} decreases the acute and chronic toxicity on fish from 6.98 to 74.40 mg L⁻¹ and 0.81 to 7.57 mg L⁻¹, respectively and also the bioaccumulation, but these compounds are still classified as moderately toxic compounds. On the other hand, TO is less toxic on fish than T with LC₅₀ of 20.90 against 1.86 mg L⁻¹ and ChV of 2.08 against 0.21 mg L⁻¹ and less bioaccumulated. In contrast, TQ, T-TO, TO-TO and TCl are more toxic than T with LC₅₀ ≤ 1.12 mg L⁻¹ and ChV ≤ 0.16. TQ, T-TO and TCl are classified as highly toxic. TCl was not

detected in the experiments on thyme's leaves, this might be due to a high value of K_{ow} and a diffusion of this compounds inside the cuticle preventing its extraction by ACN. In the case of IMD, T inhibited the pesticide degradation rate and any new chemical deriving from IMD was formed. Other good H-donor chemicals such as phenolic compounds contained in plants may have the same effect and therefore increase the lifetime of IMD and lengthen its insecticidal effect. T and TO underwent nitration. TONO₂ is moderately toxic as T with higher LC₅₀ but lower ChV, while TNO₂ is classified as highly toxic with LC₅₀ = 1.39 mg L⁻¹ and ChV = 0.15. Therefore, chemicals that are more toxic than the starting compound can be formed during these reactions.

4. Conclusion

In this work, we investigated the photochemical reactions between pesticides and plant's volatiles in solution and leaf surfaces and we demonstrated that interactions take place in both media. The interactions modified the fate and the transformation pathways of the chemicals and depended on the chemicals structure and the matrix. This was illustrated by the examples of the fungicide chlorothalonil and the insecticide imidacloprid chosen as pesticides and thymol, α-pinene, 3-carene and linalool as plant's volatiles. Studying these reactions is relevant for several reasons. First, they can occur in the real conditions on plants and in surface waters and affecting the fate of the chemicals, these reactions can also alter the phytosanitary treatments shortening the lifetime of the pesticide for example, and lead to repeated and/or increased treatments. These are therefore important factors to consider in the

Table 5
Estimation of the compounds toxicities.

Compound	Acute toxicity (LC ₅₀) on fish concentration (mg L ⁻¹)	Chronic toxicity (ChV) on fish concentration (mg L ⁻¹)	Log Kow (estimated)	Bioaccumulation	Concern level
CT	6.98	0.81	3.66	+	Moderate
CT _{-Cl}	23.00	2.52	3.02	-	Moderate
CT _{-2Cl}	74.40	7.57	2.37	-	Moderate
T	1.86	0.21	3.51	+	Moderate
TO	20.90	2.08	2.05	-	Moderate
TQ	0.05	0.003	2.25	-	High
TCl	0.82	0.10	4.16	+	High
T-TO	0.12	0.02	5.27	+	High
TO-TO	1.12	0.16	4.21	+	Moderate
TNO ₂	1.29	0.15	3.91	+	High
TONO ₂	14.20	1.47	2.44	-	Moderate
IMD	5.13	5.21	0.55	-	Moderate

design of pesticides. Secondly, the interactions can potentially generate toxic by-products leading to the pollution of water bodies and of air. The air pollution may be observed in particular in the cities where green roofs are installed. Indeed, their growth in many urban zones in the world could be accompanied by increased possibilities of reactions between plant's volatiles and other chemicals such as the pesticides used to protect the roof plants which might finally lead to an enhanced formation of by-products. For all these reasons, it seems necessary to get a better insight into these overlooked reactions often referred to as "cocktail effect".

The novelty statement

This work investigated whether pesticides could interact with plant's volatiles under solar light. These reactions were studied in solution and with the pesticide being directly applied on plant's leaves. Such scenarios were rarely considered, the great majority of studies being devoted to the photolysis of pesticides and to their fate when irradiated in the presence of natural sensitizers.

We demonstrate that the two chosen pesticides (fungicide chlorothalonil and insecticide imidacloprid) actually react with thyme's volatiles through oxidation and nitration.

These reactions may increase water bodies and air pollution and we think that this study may initiate other works in this field.

Declaration of competing interest

The authors declare that they have no known competing financial interests or personal relationships that could have appeared to influence the work reported in this paper.

Acknowledgments

This research was supported by a PhD fellowship from the University Clermont-Auvergne/French Ministry of Higher Education and Research. The authors would like to thank Martin Lereboure (Engineer CNRS) and Frédéric Emmenegger (Tech CNRS) for UHPLC-MS analyses, and Guillaume Voyard (Engineer CNRS) for HPLC-DAD analyses.

Appendix A. Supplementary data

Supplementary data to this article can be found online at <https://doi.org/10.1016/j.scitotenv.2021.150716>.

References

- Abbas, F., Ke, Y., Yu, R., Yue, Y., Amanullah, S., 2017. Volatile terpenoids: multiple functions, biosynthesis, modulation and manipulation by genetic engineering. *Planta* 246, 803–816. <https://doi.org/10.1007/s00425-017-2749-x>.
- Atkinson, R., Arey, J., 2003. Atmospheric degradation of volatile organic compounds. *Chem. Rev.* 103 (12), 4605–4638. <https://doi.org/10.1021/cr0206420>.
- Becker, R.S., 1969. *Theoretical and Interpretation of Fluorescence and Phosphorescence*. Wiley-Interscience, New-York.
- Bouchama, S., de Sainte-Claire, P., Arzoumanian, E., Oliveros, E., Boulkamh, A., Richard, C., 2014. Photoreactivity of chlorothalonil in aqueous solution. *Environ Sci Process Impacts* 16 (4), 839–847.
- Brand, N., Mailhot, G., Bolte, M., 1998. Degradation photoinduced by Fe(III): method of alkylphenol ethoxylates removal in water. *Environ. Sci. Technol.* 32, 2715–2720. <https://doi.org/10.1021/es980034v>.
- Burrows, H.D., Canle, M.L., Santaballa, J.A., Steenken, S., 2002. Reaction pathways and mechanisms of photodegradation of pesticides. *J. Photochem. Photobiol. B* 67, 71–108. [https://doi.org/10.1016/S1011-1344\(02\)00277-4](https://doi.org/10.1016/S1011-1344(02)00277-4).
- Chiron, F., Chalchat, J.C., Garry, R.P., Pilichowski, J.F., Lacoste, J., 1997. Photochemical hydroperoxidation of terpenes I. synthesis and characterization of α -pinene, β -pinene and limonene hydroperoxides. *J. Photochem. photobiol. A Chem* 111, 75–86. [https://doi.org/10.1016/S1010-6030\(97\)00184-6](https://doi.org/10.1016/S1010-6030(97)00184-6).
- Dudareva, N., Negre, F., Nagegowda, D.A., Orlova, I., 2006. Plant volatiles: recent advances and future perspectives. *Crit. Rev. Plant Sci.* 25, 417–440. <https://doi.org/10.1080/07352680600899973>.
- ter Halle, A., Lavielle, D., Richard, C., 2010. The effect of mixing two herbicides mesotrione and nicosulfuron on their photochemical reactivity on cuticular wax film. *Chemosphere* 79, 482–487. <https://doi.org/10.1016/j.chemosphere.2010.01.003> Get rights and content.
- Hamdache, S., Sleiman, M., de Sainte-Claire, P., Jaber, F., Richard, C., 2018. Unravelling the reactivity of bifentazate in water and on vegetables: kinetics and byproducts. *Sci. Tot. Environ.* 636, 107–114. <https://doi.org/10.1016/j.scitotenv.2018.04.219>.
- Hammerbacher, A., Coutinho, T.A., Gershenzon, J., 2019. Roles of plant volatiles in defence against microbial pathogens and microbial exploitation of volatiles. *Plant Cell Environ.* 42, 2827–2843. <https://doi.org/10.1111/pce.13602>.
- Hurst, J.R., McDonald, J.D., Schuster, Gary B., 1982. Lifetime of singlet oxygen in solution directly determined by laser spectroscopy. *J. Am. Chem. Soc.* 104, 2065–2067.
- Katagi, T., 2004. Photodegradation of pesticides on plant and soil surfaces. *Rev. Environ. Contam. Toxicol.* 182, 1–195. https://doi.org/10.1007/978-1-4419-9098-3_1.
- Martinez Vidal, J.L., Plaza-Bolaños, P., Romero-González, R., Garrido Frenich, A., 2009. Determination of pesticide transformation products: a review of extraction and detection methods. *J. Chromat. A* 1216, 6767–6788. <https://doi.org/10.1016/j.chroma.2009.08.013>.
- Marussi, G., Vione, D., 2021. Secondary formation of aromatic nitroderivatives of environmental concern: photoneitration processes triggered by the photolysis of nitrate and nitrite ions in aqueous solution. *Molecules* 26, 2550. <https://doi.org/10.3390/molecules26092550>.
- Mathon, B., Ferréol, M., Coquery, M., Choubert, J.-M., Chovelon, J.-M., Miège, C., 2021. Direct photodegradation of 36 organic micropollutants under simulated solar radiation: comparison with free-water surface constructed wetland and influence of chemical structure. *J. Hazard. Mat.* 407, 124801. <https://doi.org/10.1016/j.jhazmat.2020.124801>.
- Mellouki, A., Wallington, T.J., Chen, J., 2015. Atmospheric chemistry of oxygenated volatile organic compounds: impacts on air quality and climate. *Chem. Rev.* 115, 3984–4014. <https://doi.org/10.1021/cr500549n>.
- Mochizuki, T., Ikeda, F., Tani, A., 2020. Effect of growth temperature on monoterpene emission rates of *Acer palmatum*. *Sci. Tot. Environ.* 745, 140886. <https://doi.org/10.1016/j.scitotenv.2020.140886>.
- Monadjemi, S., el Roz, M., Richard, C., ter Halle, A., 2011. Photoreduction of chlorothalonil fungicide on plant leaf models. *Environ. Sci. Technol.* 45, 9582–9589. <https://doi.org/10.1021/es202400s>.
- Murov, S.L., Carmichael, I., Hug, G.L., 1993. *Handbook of Photochemistry*. Second edition. Marcel Dekker, NY.
- Ossola, R., Jönsson, O.M., Moor, K., McNeill, K., 2021. Singlet oxygen quantum yields in environmental waters. *Chem. Rev.* 121, 4100–4146. <https://doi.org/10.1021/acs.chemrev.0c00781>.
- Palma, D., Arbid, Y., Sleiman, M., De Sainte-Claire, P., Richard, C., 2020. New route to toxic nitro and nitroso products upon irradiation of micropollutant mixtures containing imidacloprid: role of NOx and effect of natural organic matter. *Environ. Sci. Technol.* 54, 3325–3333. <https://doi.org/10.1021/acs.est.9b07304>.
- Pehkonen, S.O., Zhang, Q., 2002. The degradation of organophosphorus pesticides in natural waters: a critical review. *Crit. Rev. Environ. Sci. Technol.* 32, 17–72. <https://doi.org/10.1080/10643380290813444>.
- Petrović, J., Stojković, D., Soković, M., 2019. Chapter eight – terpene core in selected aromatic and edible plants: natural health improving agents. *Adv. Food Nutr. Res.* 90, 423–451. <https://doi.org/10.1016/bs.afnr.2019.02.009>.
- Porras, J.J., Fernandez, J., Torres-Palma, R.A., Richard, C., 2014. Humic substances enhance chlorothalonil phototransformation via photoreduction and energy transfer. *Environ. Sci. Technol.* 48, 2218–2225. <https://doi.org/10.1021/es404240x>.
- Remual, C.K., 2014. The role of indirect photochemical degradation in the environmental fate of pesticides: a review. *Environ. Sci. Process. Impacts* 16, 628–653. <https://doi.org/10.1039/C3EM00549F>.
- Rodgers, M.A.J., Snowden, P.T., 1982. Lifetime of $(^1O_2)$ in liquid water as determined by time-resolved infrared luminescence measurements. *J. Am. Chem. Soc.* 104, 5541–5543.
- Salehi, B., Mishra, A., Prakash, Shukla, I., Sharifi-Rad, M., del Mar Contreras, M., Segura-Carretero, A., Fathi, H., Nasrabadi, N., Nasri, 2018. Thymol, thyme, and other plant sources: Health and potential uses. *Phytoter. Res.* 32, 1688–1706. <https://doi.org/10.1002/ptr.6109>.
- Skalska, K., Miller, J.S., Ledakowicz, S., 2010. Trends in NOx abatement : a review. *Sci. Tot. Environ.* 408, 3976–3989. <https://doi.org/10.1016/j.scitotenv.2010.06.001>.
- de Souza, R.M., Seibert, D., Quesada, H.B., Bassetti, F.J., Fagundes-Klen, M.R., Bergamasco, R., 2020. Occurrence, impacts and general aspects of pesticides in surface water: a review. *Process Saf Environ Prot* 135, 22–37. <https://doi.org/10.1016/j.psep.2019.12.035>.
- Venu, S., Naik, D.B., Sarkar, S.K., Aravind, U.K., Nijamudheen, A., Aravindakumar, C.T., 2013. Oxidation reactions of thymol: a pulse radiolysis and theoretical study. *J. Phys. Chem. A* 117, 291–299. <https://doi.org/10.1021/jp3082358>.
- Wannaz, E.D., Zygadlo, J.A., Pignata, M.L., 2003. Air pollutants effect on monoterpenes composition and foliar chemical parameters in *Schinus arica* L. *Sci. Tot. Environ.* 305, 177–193. [https://doi.org/10.1016/S0048-9697\(02\)00466-7](https://doi.org/10.1016/S0048-9697(02)00466-7).
- Wilkinson, F., Brummer, J.G., 1981. Rate constants for the decay and reactions of the lowest electronically excited singlet state of molecular oxygen in solution. *J. Phys. Chem. Ref. Data* 10, 809–999. <https://doi.org/10.1063/1.555965>.

Supporting Information

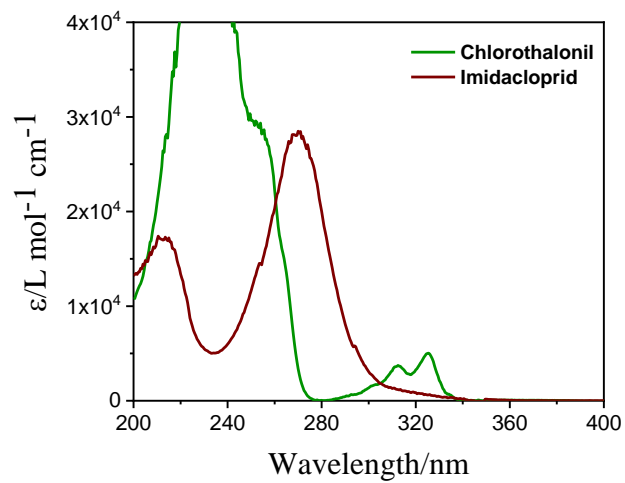
Photochemical interactions between pesticides and plant volatiles

Yara Arbid, Mohamad Sleiman, Claire Richard *

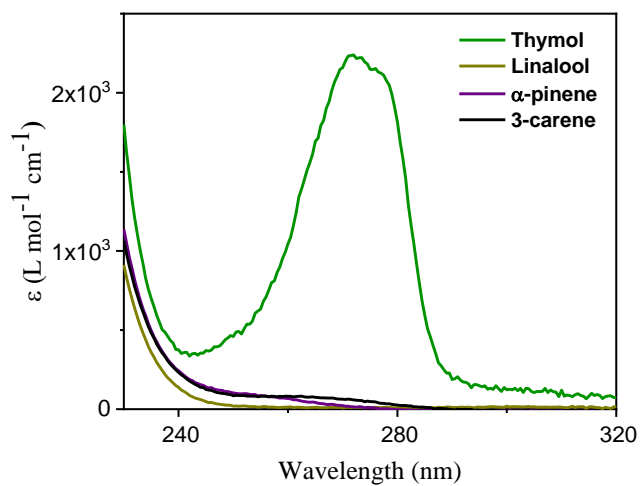
University Clermont Auvergne, CNRS, Clermont Auvergne INP, Institut de Chimie de Clermont-Ferrand
F-63000 Clermont-Ferrand, France

Claire.richard@uca.fr

Figure SI-1: UV spectrum of chlorothalonil and imidacloprid (A) and thymol, linalool, 3-carene and α -pinene (B)



A)



B)

Figure SI- 2: HS-GC-MS of thymol, linalool, 3-carene and α -pinene

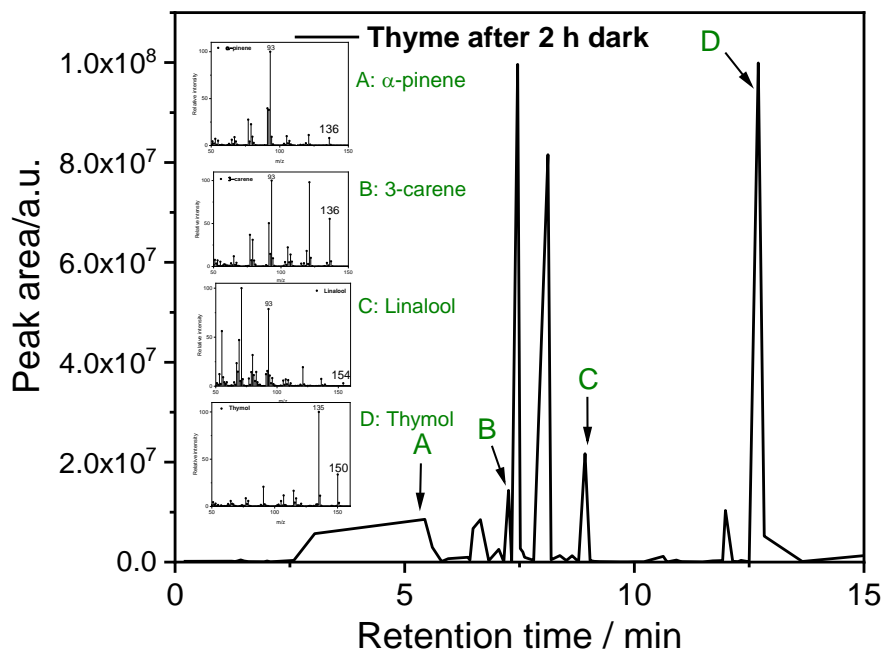


Figure SI- 3: MS-MS spectrum of TO at $m/z = 165.0910$ in ES^-

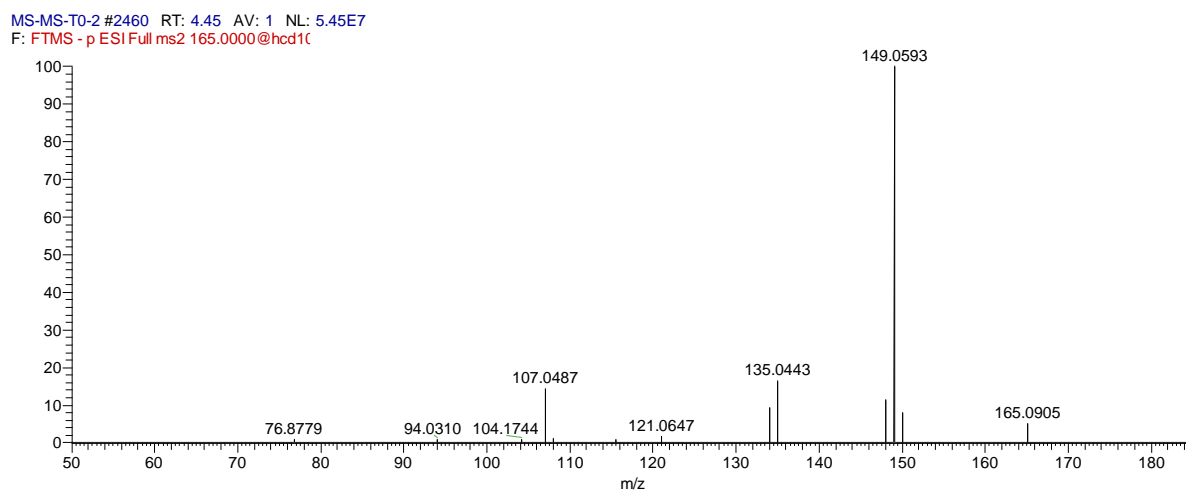


Figure SI- 4: MS spectrum of TQ ($m/z = 165.0910$ in ES^+)

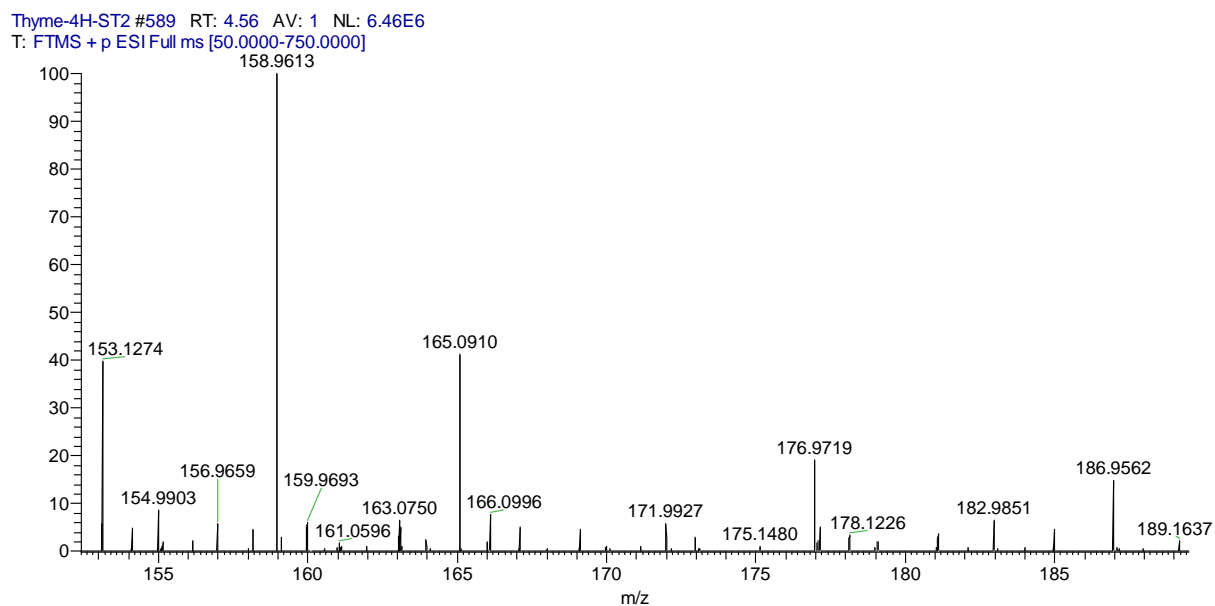


Figure SI- 5: MS spectrum of TQO ($m/z = 179.0702$ in ES^-)

Thyme-4H-ST2 #532 RT: 4.12 AV: 1 NL: 1.20E7
T: FTMS - p ESI Full ms [50.0000-750.0000]

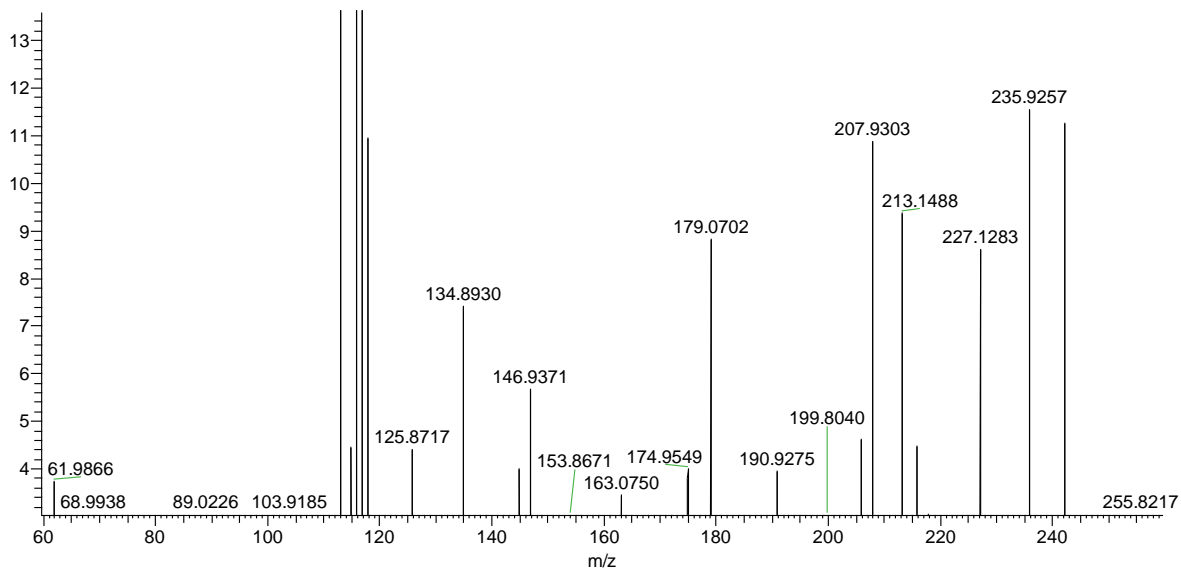


Figure SI- 6: MS spectrum of T-TO_{2H} ($m/z = 313.1805$ in ES^-)

Thyme-CT-4H-ST2 #796 RT: 6.18 AV: 1 NL: 1.25E8
T: FTMS - p ESI Full ms [50.0000-750.0000]

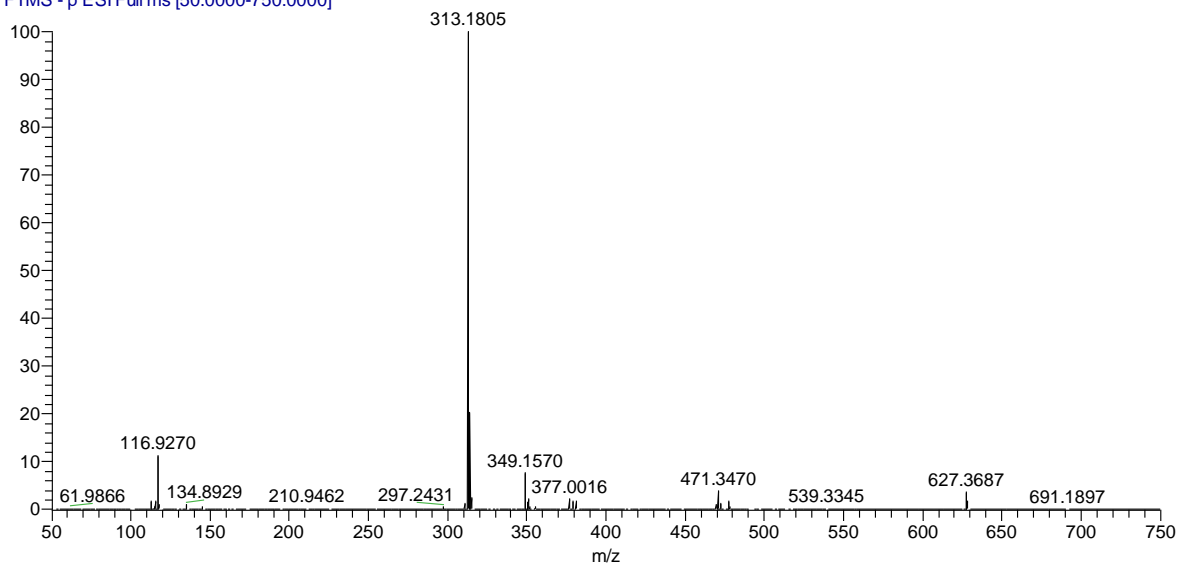


Figure SI- 7: MS spectrum of TO-TO_{2H} (m/z = 329.1753 in ES⁻)

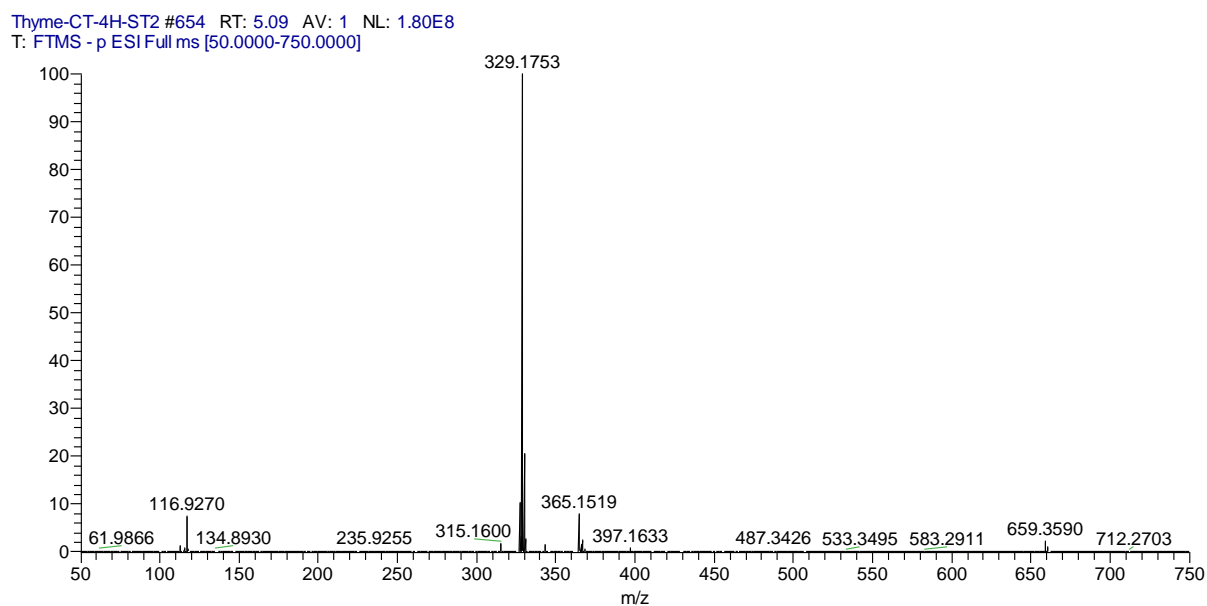


Figure SI-8: Analysis by HS-GC-MS of the gaseous phase of vials containing two thyme's twigs covered with CT. Analyses were performed before irradiation (dark) and after 2, 4 and 6 h of irradiation.

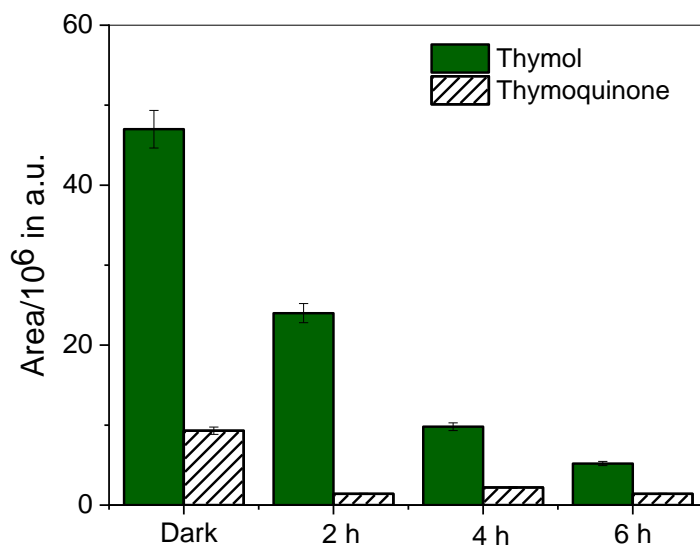


Figure SI- 9: MS spectrum of IMD-NO₂+H (m/z = 211.0742 in ES⁺)

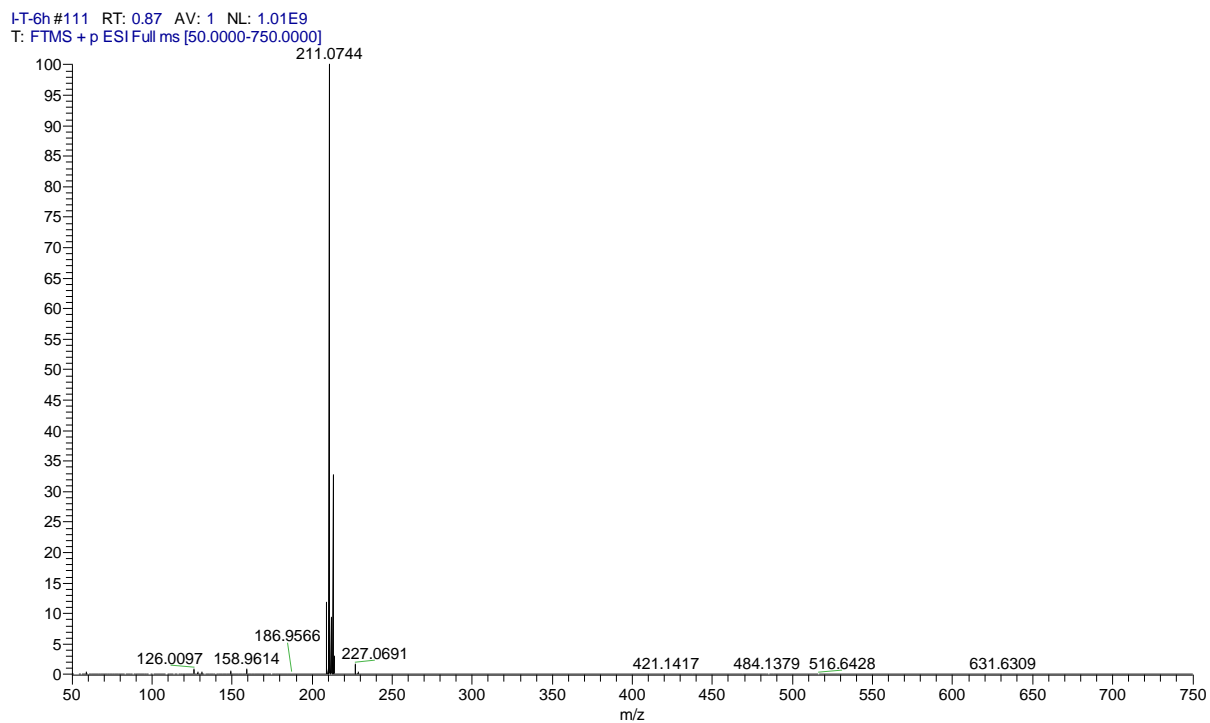


Figure SI- 10: MS spectrum of IMD-HNO (m/z = 223.0385/225.0356 in ES⁻)

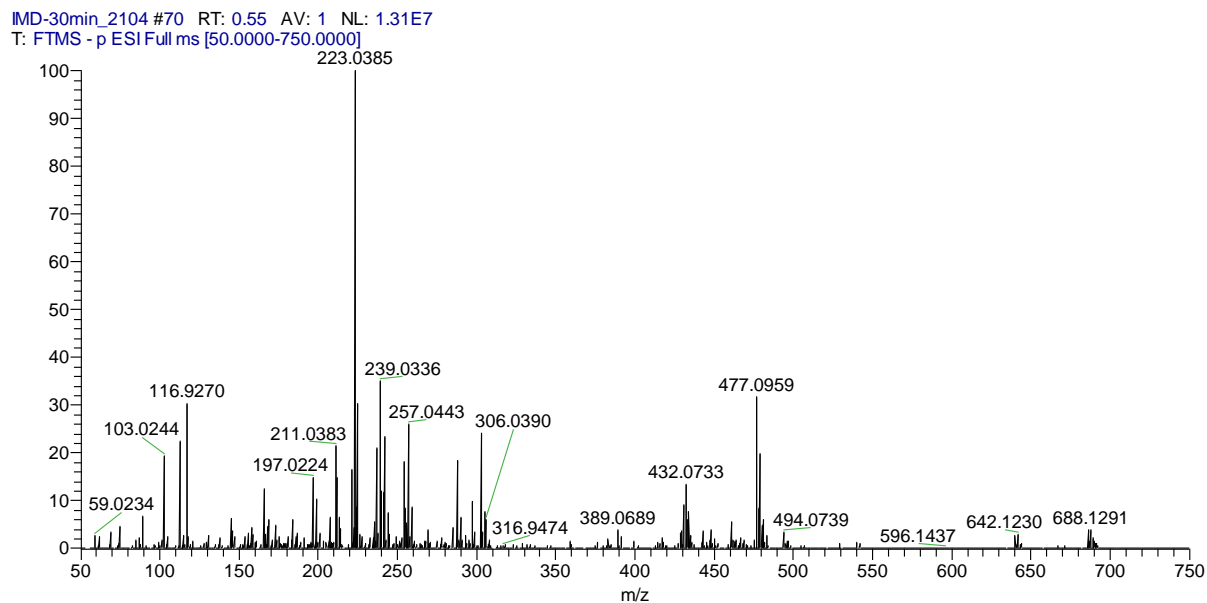


Figure SI- 11: MS spectrum of IMD-IMD-N₂O₃ (m/z = 432.0744/434.0715/436.0689 in ES⁻)

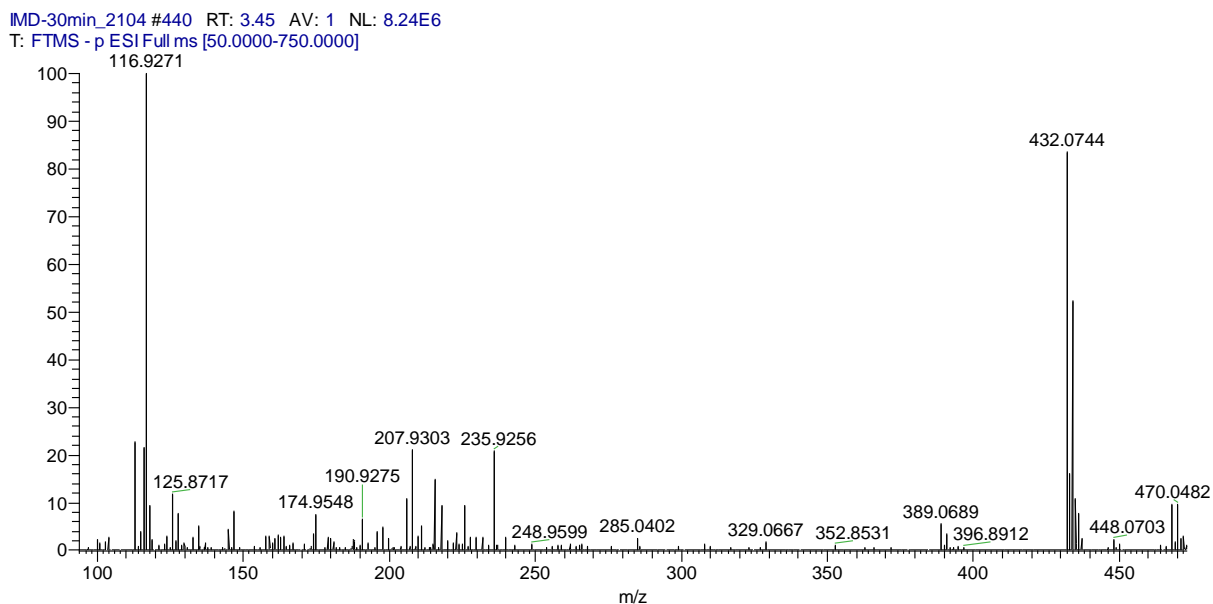


Figure SI- 12: MS spectrum of TNO₂ (m/z = 194.0812 in ES⁻)

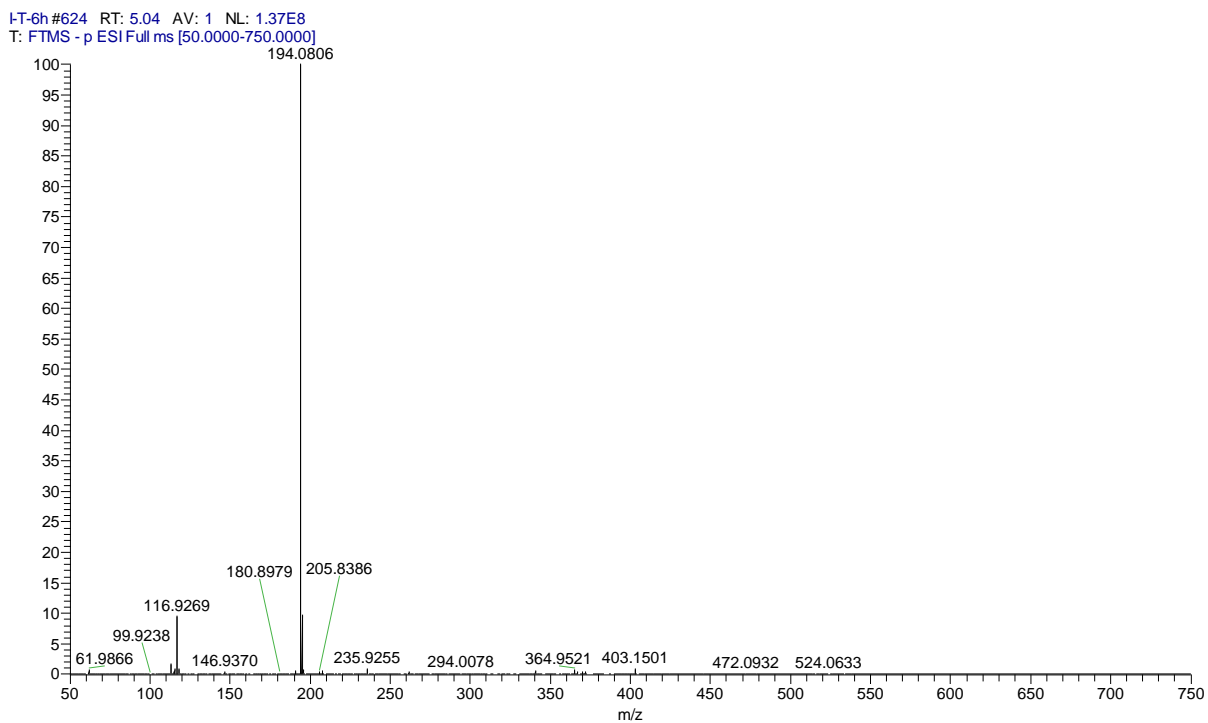
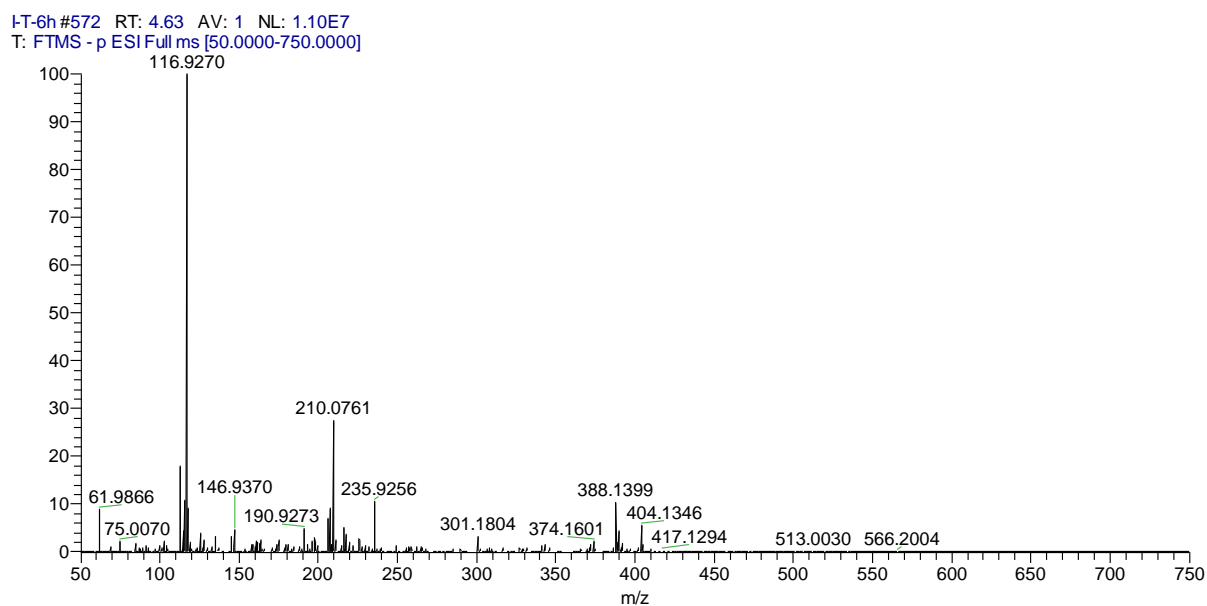


Figure SI- 13: MS spectrum of TONO₂ (m/z = 210.0761 in ES⁻)



4. General conclusions

CO₂, NO_x, O₃, and other air pollutants are being enormously emitted into the atmosphere leading to health problems, urban heat island effect, and climate change. Fortunately, different solutions to decrease the impact of air pollution on the environment exist. Among them, green roofs have shown promising results in removing prevalent air pollutants besides being aesthetically pleasing, enhancing the building thermal performance, and managing stormwater. Research concerning green roofs and their air pollution removal capacity were predicted or estimated using models holding many uncertainties. This renders quantitative data a necessity to exactly measure their depollution performance towards specific pollutants. Our objective was to get a better insight into the depolluting potential of green roof plant species, in particular, their uptake capacity towards air pollutants, and their behavior in the presence of pesticides and solar light. Air pollutants chosen were NO_x and O₃ being chief ones emitted abundantly while pesticides were CT and IMD since they are reactive upon solar irradiation. This led to different questions to be solved: How can we quantitatively measure the depollution capacity of plant species used on green roofs? Which plants are efficient in removing pollutants and what are the mechanisms taking place? Do plants treated with pesticides undergo interactions with the latter through their volatiles under irradiation? What are the photoproducts formed and are they toxic?

To answer those questions, a setup was first built –after carefully considering the sources– consisting of different components that enabled us to monitor the change in concentrations of NO_x and O₃. Then, we started with our experimentation by calculating, measuring quantitatively, as well as understanding the depollution performances and mechanisms of green roof plant species. In addition, interactions between a volatiles-emitting plant and two pesticides were investigated while noting the toxicity of the formed photoproducts.

Our setup was modular that allowed us to measure both NO_x and O₃ uptakes of plants. An O₃ generator produced O₃ while IMD was the source of NO₂. Both sources were stable, continuous, and the amount of O₃ and NO₂ generated (90 ppbv and 50 ppbv respectively) are close to the recommended exposure limit. The insecticide, IMD, showed a production of NO₂ in solution and on solid (petri dishes) with different yields. Hence, this setup permits the measurement of NO₂/O₃

uptakes of both leaves and full-size plant, the study of interactions between VOCs and O₃, the production of HONO through the HONO trap present before the NO_x analyzer, and can enable future research to study the possible reaction between NO_x and VOCs.

Screening of 13 plants -using their leaves- utilizing the setup led to the choice of the 3 best performant plant species: *sedum sexangulare* (sedum), *thymus vulgaris* (thyme), and *heuchera Americana L* (heuchera). Experiments showed that thyme had the best NO₂ uptake followed by sedum and then heuchera. SEM analysis revealed that thyme had the largest stomatal area which explained its good performance in removing NO₂ whereas the HONO trap installed before the analyzer confirmed the surface reaction between NO₂ and water, case of sedum. Heuchera retained NO₂ due to its big hairy leaves. Moreover, the same trend was found with the O₃ uptake where thyme had the highest one followed by sedum and then heuchera. ATD-GC-MS explained thyme's performance which showed that its VOCs have the ability to react with O₃. Consequently, thyme can be a good solution for urban environments polluted with O₃ and NO₂. It can be used on all types of green roofs (intensive, semi-intensive, and extensive). However, with pesticides being often sprayed on these roofs, thyme's emission of volatiles, and the presence of light, a photochemical interaction can take place probably producing toxic compounds.

Further experiments dealt with two pesticides: IMD and CT, and thyme: an odorous plant under irradiation (mimicking real irradiation conditions). Manuscript 1 revealed that IMD releases NO₂ under irradiation that photoinduces the nitration/nitrosation of phenol and resorcinol. This suggests the possible nitration/nitrosation of phenolic metabolites released by plants. In our experiments, we confirmed this by irradiating thymol and IMD in solution as well as real thyme leaves dipped in IMD. The LC-MS and GC-MS analyses showed the formation of nitrated thymol, nitrated TO, and nitrated dimers. Nonetheless, IMD alone underwent degradation faster than in the presence of thymol which inhibited the process due a competition between the two. In addition to that, photoproducts detected in solution of volatiles (thymol, α -pinene, 3-carene, and linalool) + CT and thyme leaves dipped in CT showed the dechlorination of CT and chlorination of volatiles especially thymol which had the highest disappearance yield. Nevertheless, in the case of CT, this pesticide didn't undergo degradation when present alone but disappeared in the presence of the volatiles especially thymol. In general, thymol was oxidized and CT reduced. The formed photoproducts in both cases showed an important toxicity.

As a final conclusion, this thesis revealed the depollution capacity of green roofs towards NO_2 and O_3 . Thyme significantly removed both pollutants, sedum uptook NO_2 , while heuchera retained the pollutants due to its hairy leaf structure. In an urban environment extremely polluted with O_3 and NO_x , choosing sedum and thyme to be implemented on green roofs would be very efficient and beneficial. However, interactions happening on the roof between the sprayed pesticides and volatiles emitted can lead to toxic photoproducts. In our case, IMD produced nitrated/nitrosated compounds while CT acted as a strong oxidant in the presence of volatiles. Hence, the careful choice of pesticides to be sprayed on a specific plant is compulsory. Nonetheless, even if IMD, for example, wasn't directly sprayed on an odorous plant, its presence in the environment will lead to the spontaneous formation of NO_2 . The latter can further react with the thymol naturally emitted by thyme or undergo other photochemical reaction worsening the already-present air pollution problem. Future experiments should consider the validation of results on real green roofs to understand the uptake capacity of selected plants towards target pollutants on the larger scale. Simulations can be first done to have an insight before directly moving to experiments on green roofs. Nevertheless, seasonality, plant physiology, concentration of pollutants in the specific urban area, and temperature are factors to be noted. In this PhD, we studied the ability of green roof plants to remove NO_x and O_3 ; nonetheless, other pollutants should be studied as $\text{PM}_{2.5}$ which has adverse health effects or SO_2 . This should be done by considering other possible mechanisms, the presence of microorganisms on leaves, or the secondary pollutants formed as SOA. Since the leaves of plants are a reaction site, further research must examine deeply this complex system. An example is the effect of plant cuticles on the uptake and possible stress factors affecting the opening of stomata. Naturally, plants respond to stress by emitting VOCs, our results revealed the possible interactions between sprayed pesticides and the latter; nevertheless, the fate of formed products should be studied more systematically and these interactions on other plant species can be investigated. This might help optimize the choice of plants and pesticides in a specific urban environment.

Annex 1

Description of the setup used for the IMD experiments

To investigate the IMD behavior under irradiation (with two fluorescent tubes emitting light with a wavelength range of 300-450 nm with $\lambda_{\text{max}}=365$ nm) and identify the possible products generated, IMD aqueous solutions were put in a cylindrical Pyrex gas flow reactor (**Fig.A1**).

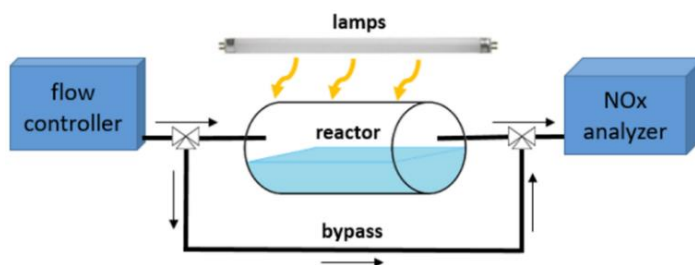


Figure A 1. Setup used to monitor NOx formation upon irradiation of IMD solutions.

The setup consists of flow controllers that control the flow of both N_2 and O_2 (flow rate to 0.7 L min^{-1}) which mix to reach the Pyrex gas flow-reactor (0.65 L, length 27 cm, and diameter 5.7 cm) containing IMD (10^{-4} M , 200 ml). The solution was irradiated from the top with two fluorescent tubes (Sylvania F15W/BL 368, 438 mm \times 26 mm, 300–450 nm, and $\lambda_{\text{max}}=365$ nm) placed at 5 cm above the reactor. The reactor was connected to a NOx chemiluminescence analyzer (Thermo Scientific i-42 NOx analyzer). A bypass connecting the flow controllers directly to the analyzer was present to measure the background levels of NOx in the gas inlet (negligible). After irradiation, the light was turned off, and the outlet of the reactor was connected to the NOx analyzer. NOx levels were measured every 10 s initially and then at larger intervals for a period of up to 2 h.

Annex 2

Description of the setup used for the NO₂/O₃ uptake experiments

The setup is illustrated by **Fig.A2**.

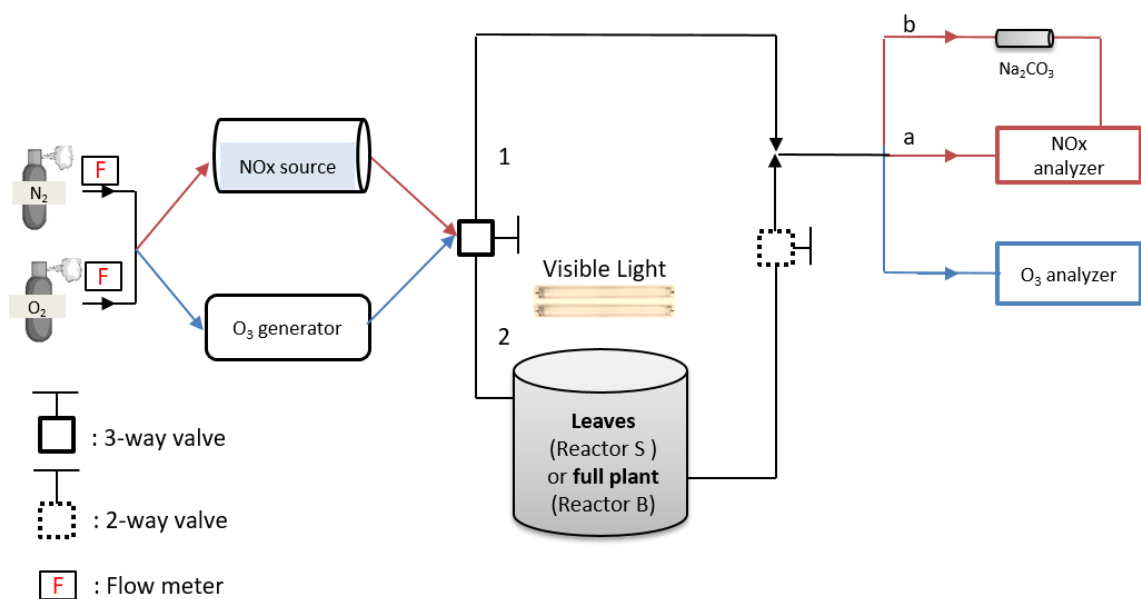


Figure A 2. The NO_x (red) and O₃ (blue) setups.

Set up configuration for experiments on NO_x/HONO. The setup includes two flow meters, an NO_x source, stainless steel reactors, and an NO_x analyzer. Two stainless steel reactors were used. The sizes ranged from 0.6-12 L. The small stainless-steel reactor had a Pyrex cover, and the leaves were introduced from the bottom and the reactor was tightened with screws; while with the big stainless-steel reactor, plants were introduced from the top and the cover was rotated for tightening. In both cases, Teflon lined gaskets were used to seal the reactor and avoid gas leakage. Inlet and outlets were present in both reactors and placed on opposite sides but at different height locations to ensure optimum flow path. The flow meters were used to regulate the flow of oxygen and nitrogen simultaneously, i.e., 500 L/min for nitrogen and 300 L/min for oxygen resembling the percentage of those gases in real air. They were added together in a T-like shaped union and passed

through the cylindrical glass Pyrex gas flow-reactor containing 200 mL of pure IMD. A 3-way valve was present where it either fed the NO_x analyzer directly with the carried gas (path 1) or passed it through small/big stainless-steel reactors. Without irradiation, IMD (10⁻⁵ M) was able to produce ~ 50 ppbv of NO₂ which was sufficient to perform experiments

The reactors contained freshly cut leaves or the full plant size/soil in it (path 2). When path 2 was undertaken, NO_x entered the stainless reactor, part of it was removed, then left the reactor to a switch valve that either directs the flow to the NO_x analyzer or to the room exhaust. Before reaching the NO_x analyzer, the gas flow can either then be directed through a HONO trap or not (with HONO trap (a) or without (b)) depending on whether we want to measure the HONO formation in the overall NO₂ concentration measured by the analyzer. Tubes used were all made Teflon (PTFE) and all connection components (fittings, ferrules, unions, and valves) were from Swagelok. The temperature in the room was regulated to 23°C by an air conditioner. Experiments were performed in dark or light conditions. Valves before the stainless-steel reactor containing the plant were closed for a certain time. Before opening the valves connecting the stainless-steel reactor to the analyzer, measurements were taken to report the exact concentration of the NO_x produced by IMD. It was done every 10 seconds for a period of several minutes (path 1); to ensure that the NO₂ produced concentration is stable. Control experiments were also performed to measure the uptake due to the empty reactor (without plants) in order to evaluate any possible interference.

Set up configuration for experiments with O₃. This setup resembles the previous one in mostly all parts. The difference was the presence of an ozone generator rather than a solution of IMD. Path 1 and path 2 were also present. O₃ was generated by turning on the UV pen-ray lamp found inside the generator. Dioxygen bond is broken due to UVC light (185 nm) producing 2 radicals which will react with the O₂ and produce a continuous flow of O₃. The setup was assembled in a way enabling us to measure both NO_x and O₃ concentrations by just changing some tube connections.